NASA Contractor Report 3810

Synoptic Scale Wind Field Properties From the SEASAT SASS

Willard J. Pierson, Jr.,
Winfield B. Sylvester,
and Robert E. Salfi

NASA

NASA Contractor Report 3810

Synoptic Scale Wind Field Properties From the SEASAT SASS

Willard J. Pierson, Jr.,
Winfield B. Sylvester,
and Robert E. Salfi

*CUNY Institute of Marine and Atmospheric
Sciences at the City College
New York, New York*

NASA

TABLE OF CONTENTS

INTRODUCTION

The ability to determine the winds in the planetary boundary layer
over the oceans of the Earth by a radar scatterometer called the SASS on
SEASAT has been demonstrated. The objectives of the SASS program were met,
and perhaps exceeded, as described by Lame and Born (1982). A problem was
identified when it was recognized that errors in the conventional data need
to be better understood. The sources for the differences between a SASS-1
winds, a conventionally measured wind, and a wind derived from a planetary
boundary layer analysis using conventional data are many and varied. Yet to
be produced are planetary boundary layer analyses of the winds based on the
SEASAT SASS-1 data only, augmented by a minimum amount of conventional data
such as atmospheric pressures at the sea surface and air sea temperature
differences. The purpose of this investigation is to prepare and analyse
wind fields from the SASS data.

The three most important applications of SEASAT-SASS-like data in the
future will be (1) the correct description of the winds over the entire global
ocean at an appropriate resolution, (2) the use of these data to produce
vastly improved initial value updates for computer based synoptic scale
numerical weather predictions and (3) as shown, by O'Brien, et al. (1982),
the specification of the wind stress field and the curl of the wind stress at
the sea surface for oceanographic applications. In this investigation, synoptic
scale vector wind fields with a known error structure will be produced at a
one degree resolution from the SEASAT SASS-1 GOASEX data. These synoptic
scale wind fields will be used to compute fields for the horizontal divergence
of the winds in the planetary boundary, the vertical velocity at 200 meters,
and to determine the error structure of the resulting fields. The vector wind
stress fields can then be found from the vector wind fields, and the errors in
these fields can be computed. Finally, the curl of the wind stress can be
computed, with a specified error structure.

Certain assumptions need to be made concerning the accuracy of the present
SASS-1 model function and the wind recovery algorithm. Also the drag
coefficient that relates wind stress to the wind at ten meters is a matter of
some uncertainty. If any of these assumptions need modification and updating

1

for future systems, the main results of this study will still be applicable.

As a first effort, the atmosphere will be assumed to be neutrally stratified. An application of the Monin-Obukhov theory for non-neutral stability as in Large and Pond (1981) would provide an improved wind field at 19.5 (or 10) meters for the computation of divergence. The field for the air-sea temperature difference would be needed to an accuracy comparable to the neutral stability wind field.

Technical reports concerned with the accuracy of the SASS winds have been written by Weller, et al. (1983) and Wentz and Thomas (1983). The former, if read too quickly, seems to suggest that the meteorologically measured winds used to calibrate the SASS-I model function from 4 to 16 m/s were 10% too high compared to their true value. Closer study suggests perhaps 5 to 7 percent, and in our opinion, a closer analysis of Figs. 8 and 9 of their paper and of Tables 2 and 3 indicate poor data analysis methods and suggest that the SASS-1 meteorological winds were close to the mark. The SOS-SASS-1 wind recovery algorithm is questionable (Pierson 1983c) because it tends to give too high a wind for the 2 solution case and the "Y" base of the three solution case, which is the reason for the deletion of some of the data provided by the NASA Langley Research Center (page 13).

Wentz and Thomas (1983) derive what is claimed to be a model function superior to SASS-1 for which the wind speed "seems to be biassed about 1 m/s too high". The SASS-1 model function can probably be improved outside the range from 4 to 16 m/s. The SOS SASS-1 recovery algorithm is possibly the reason for part of these differences. Calibration over a greater range of wind speeds and aspect angles will be difficult, but much of the GOASEX data fall within the range from 4 to 16 m/s.

A quotation from Guymer (1983a) summarizes the situation prior to Weller, et al. (1983). "The absolute accuracy of the measurements has proved difficult to ascertain, and even subsequent calibrations and intercomparisons on land have failed to resolve the question (Weller, personal communication)".

Woiceshyn, et al. (1983) have provided the most convincing evidence that there are difficulties for both V pol and H pol pairs for both very low and very high winds when these are compared with each other. The situation needs further study along the lines outlined by Pierson (1983c). The difficulties

2

brought to light by this study show that the S.O.S. wind recovery algorithm, Jones, et al. (1982), is the major source of the discrepancy between co-located winds from V pol pairs and H pol pairs for low winds, especially for high incidence angles. The incorrect assumption that backscatter in either decibels (or bels) is normally distributed about its expected value as given by the model function in decibels, or bels, requires the determination of an equivalent variance that cannot be recovered if K_p is greater than one. SASS backscatter values were discarded for three reasons; namely, (1) $K_p > 1$, (2) received power negative, and (3) $\sigma^o < -50$ db. Since H pol is much weaker than V pol at high incidence angles, a large fraction of the H pol measurements were discarded for low winds and the winds that were recovered were biassed high.

The analyses to follow may have winds that are too high in areas of light winds so that gradients in such areas will be increased. For winds above 8 or 9 m/s, the effects will not be too important. The methodology described in this paper can be re-applied to corrected wind fields by means of the use of MLE's as in Pierson and Salfi (1982).

3

DATA

The data used in this investigation were provided by the NASA Langley Research Center. They consist of the de-aliased SASS-1 vector winds produced as the final product of the analysis of the SASS data for the SEASAT orbit segments chosen for intensive study during the Gulf of Alaska SEASAT Experiment (GOASEX). Preliminary results for this experiment are described by Jones, et al. (1979). Two workshop reports, Born, et al. (1979) and Barrick, et al. (1979), plus a summary of conventional data analyses, Woiceshyn (1979), give additional details.

The SASS-1 model function was based on the JASIN data with results summarized by Jones, et al. (1982), Schroeder, et al. (1982) Moore, et al. (1982) and Brown, et al. (1982). As described by Jones, et al. (1982), the GOASEX data were reprocessed by means of the SASS-1 model function. De-aliasing was accomplished by selecting that wind direction closest to the planetary boundary layer wind fields obtained from conventional data. The model function recovers the effective neutral stability wind at 19.5 meters.

The winds recovered from the SASS are very densely concentrated over the swath scanned by that instrument on SEASAT. Examples can be found for the raw data density in Wurtele, et al. (1982). Only pairs of backscatter measurements $90°$ apart were used to obtain winds with all combinations of vertically (V) and horizontally (H) polarized measurements (i.e. V with V, H with H, V with H and H with V). For this study, no distinction has been made for possible effects of polarization. The communication noise errors could be quite different for the different polarization combinations.

A sample of a data listing for a particular GOASEX pass is shown in Table 1a and 1b. The data for a north bound pass of revolution 1141 are shown. The central part of the full table is repeated in both 1a and 1b.

In order, the values tabulated in the twenty one columns (as numbered with 11, 12 and 13 repeated) are as follows:

(1) Revolution Number,
(2) the latitude of the mid point of the line connecting the centers of the two cells used in the calculation,
(3) the longitude as above,

(4) the wind speed in meters per second from a boundary layer model,
(5) the neutral stability wind speed from the SASS,
(6) the from which wind direction in degrees from a boundary layer model clockwise from north,
(7) the closest alias wind direction from the SASS,
(8) a quality code for the accuracy of the boundary layer wind,
(9) a code for the estimate of the precipitation in the area,
(10) the distance between the two SASS cells,
(11) the average of the values in the next two columns,
(12) the incidence angle in degrees of the forward beam,
(13) the incidence angle of the aft beam,
(14) the pointing direction of the forward beam in degrees clockwise from north,
(15) the pointing direction of the aft beam,
(16) the backscatter in decibels measured by the forward beam,
(17) the backscatter for the aft beam,
(18) the noise standard deviation for the forward beam in per cent (multiply the antilog of the backscatter by this number divided by 100 to get the standard deviation of the measurement),
(19) the NSD for the aft beam,
(20) the polarization of the forward beam $(0 = H, 1 = V)$ and
(21) the polarization of the aft beam.

In this investigation, only the elements of the data vector corresponding to LAT, LONG, WSP, WDR and FOR AZ were used to derive the results. For some portions of some of the SASS swaths, the boundary layer conventional winds differed substantially from the SASS winds. The data base for the conventional fields will be discussed later. Future scatterometer systems may eliminate the need to remove aliases as in Pierson and Salfi (1982), for example. Wind fields produced by the methods described herein would then be independent of conventional data sources, except sea surface atmospheric pressure and, perhaps, air temperatures. Sea temperature is remotely sensed and does not vary rapidly.

The GOASEX data set provided by NASA Langley contained the results of the analysis of nine passes over the North Pacific. These were portions of revolutions 825, 826, 1141, 1183, 1212, 1226, 1227, 1298 and 1299. Extensive depictions of conventional data are available for those four orbit segments underlined above (Woiceshyn (1979)).

5

TABLE 1a. Sample Data Listing from Rev. 1141, Left Side

1 REV NO.	2 LAT	3 LON	4 AWSP	5 WSP	6 AWDR	7 WDR	8 QUAL	9 PRECIP	10 CELL SEP DIST	11 THETA	12 FOR THETA	13 AFT THETA
1141	53.10	207.27	21.5	19.8	278.5	260.2	1	4	24.0	34.60	34.40	34.80
1141	53.14	207.19	21.5	21.5	278.7	284.2	1	4	32.0	34.50	34.40	34.60
1141	53.57	207.26	21.5	19.0	279.3	267.6	1	4	21.0	36.50	34.60	38.40
1141	53.60	207.18	21.5	19.0	279.5	259.9	1	4	20.0	36.40	34.30	38.40
1141	53.65	207.10	21.4	22.0	279.7	288.8	1	4	23.0	36.30	34.30	38.20
1141	53.82	207.92	21.5	19.8	278.8	268.3	1	4	15.0	40.40	39.10	41.70
1141	53.85	207.84	21.5	20.6	278.9	259.2	1	4	7.0	40.30	38.80	41.70
1141	53.89	207.75	21.4	22.6	279.1	289.3	1	4	18.0	40.20	38.80	41.50
1141	53.02	208.63	22.0	19.6	276.5	264.2	1	3	17.0	40.40	39.20	41.70
1141	53.05	208.55	22.0	20.6	276.7	254.4	1	3	6.0	40.30	38.90	41.70
1141	53.09	208.46	22.0	22.4	276.9	276.6	1	3	19.0	40.20	38.90	41.50
1141	53.41	208.27	21.9	19.4	277.6	268.2	1	3	16.0	40.40	39.20	41.70
1141	53.44	208.19	21.9	20.1	277.8	260.3	1	3	6.0	40.30	38.90	41.70
1141	53.49	208.11	21.9	22.1	278.0	289.6	1	3	19.0	40.20	38.90	41.50
1141	53.69	208.85	21.9	21.4	276.9	250.8	1	3	15.0	43.90	43.10	44.80
1141	53.74	208.76	21.8	23.8	277.1	290.3	1	3	27.0	43.80	43.10	44.50
1141	53.20	209.60	22.3	20.5	274.9	270.3	1	4	18.0	45.30	43.40	47.20
1141	53.29	209.20	22.2	20.7	275.8	250.9	1	4	16.0	43.90	43.10	44.70
1141	53.39	209.45	22.3	20.1	275.3	244.2	1	4	27.0	45.30	43.10	47.50
1141	53.33	209.11	22.2	22.3	276.0	273.8	1	4	29.0	43.80	43.10	44.50
1141	53.61	209.26	22.1	21.5	275.9	277.0	1	4	19.0	45.30	43.40	47.20
1141	53.80	209.10	21.9	21.0	276.5	245.9	1	4	27.0	45.30	43.10	47.50
1141	53.87	209.90	21.9	21.1	274.6	269.1	1	4	17.0	48.50	47.30	49.70
1141	53.07	210.58	22.3	21.4	272.6	273.1	1	3	18.0	48.50	47.30	49.70
1141	53.16	210.81	22.4	20.4	272.0	265.5	1	3	27.0	49.60	47.30	51.90
1141	53.24	210.43	22.4	19.6	273.0	237.2	1	3	10.0	48.50	47.00	50.00
1141	53.47	210.24	22.3	21.2	273.5	273.0	1	3	18.0	48.50	47.30	49.70
1141	53.57	210.48	22.3	20.6	272.9	268.6	1	3	27.0	49.60	47.30	52.00
1141	53.65	210.09	22.2	20.6	273.9	234.8	1	3	11.0	48.50	47.00	50.00
1141	53.98	210.15	21.8	21.2	274.0	270.2	1	3	30.0	49.60	47.30	52.00
1141	53.91	210.75	22.0	20.3	272.2	233.5	1	3	22.0	51.50	50.60	52.30
1141	53.04	211.76	22.4	19.7	269.4	266.3	1	3	7.0	52.50	51.00	54.00
1141	53.06	211.67	22.4	20.8	269.7	249.1	1	3	16.0	52.30	50.70	54.00
1141	53.09	211.40	22.4	19.7	270.4	233.5	1	3	25.0	51.50	50.70	52.20
1141	53.44	211.44	22.4	20.2	270.1	266.5	1	3	7.0	52.50	51.00	54.00
1141	53.39	211.55	22.4	17.9	269.8	246.9	1	3	23.0	52.70	51.00	54.30

TABLE 1b, Sample Data Listing from Rev. 1141, Right Side

11 THETA	12 FOR THETA	13 AFT THETA	14 FOR AZ	15 AFT AZ	16 NRCS, FOR	17 NRCS, AFT	18 NSD, FOR	19 NSD, AFT	20 POL, FOR	21 POL, AFT
34.60	34.40	34.80	18.91	109.34	-10.84	-6.66	6.5	5.5	0	1
34.50	34.40	34.60	18.91	109.57	-10.84	-8.41	6.5	5.6	0	0
36.50	34.60	38.40	19.13	109.57	-9.62	-8.32	6.5	4.4	1	1
36.40	34.30	38.40	18.65	109.57	-10.84	-8.32	6.5	4.4	0	1
36.30	34.30	38.20	18.65	109.76	-10.84	-10.18	6.5	4.5	0	0
40.40	39.10	41.70	19.65	110.05	-11.19	-9.27	4.9	3.6	1	1
40.30	38.80	41.70	19.21	110.05	-13.16	-9.27	5.0	3.6	0	1
40.20	38.80	41.50	19.21	110.21	-13.16	-11.83	5.0	3.8	0	0
40.40	39.20	41.70	20.16	110.47	-11.01	-9.54	4.9	3.6	1	1
40.30	38.90	41.70	19.73	110.47	-13.00	-9.54	5.0	3.6	0	1
40.20	38.90	41.50	19.73	110.66	-13.00	-12.17	5.0	3.8	0	0
40.40	39.20	41.70	19.92	110.27	-11.39	-9.47	4.9	3.6	1	1
40.30	38.90	41.70	19.48	110.27	-13.47	-9.47	5.0	3.6	0	1
40.20	38.90	41.50	19.48	110.44	-13.47	-11.94	5.0	3.8	0	0
43.90	43.10	44.80	20.04	110.74	-14.76	-10.38	3.8	3.2	0	1
43.80	43.10	44.50	20.04	110.89	-14.76	-12.94	3.8	3.5	0	0
45.30	43.40	47.20	20.66	111.75	-12.35	-16.07	3.6	4.1	1	0
43.90	43.10	44.70	20.28	110.96	-15.12	-10.71	3.9	3.2	0	1
45.30	43.10	47.50	20.28	111.42	-15.12	-12.15	3.9	3.4	0	1
43.80	43.10	44.50	20.28	111.11	-15.12	-13.81	3.9	3.6	0	0
45.30	43.40	47.20	20.45	111.55	-12.22	-15.35	3.7	3.9	1	0
45.30	43.10	47.50	20.04	111.22	-14.76	-11.61	3.8	3.3	0	1
48.50	47.30	49.70	21.00	112.00	-13.02	-16.98	3.1	5.0	1	0
48.50	47.30	49.70	21.44	112.39	-13.11	-16.71	3.1	4.9	1	0
49.60	47.30	51.90	21.44	112.82	-13.11	-18.37	3.1	6.7	1	0
48.50	47.00	50.00	21.06	112.08	-17.02	-13.44	3.7	4.0	0	1
48.50	47.30	49.70	21.23	112.19	-13.23	-16.84	3.1	5.0	1	0
49.60	47.30	52.00	21.23	112.63	-13.23	-18.21	3.1	6.6	1	0
48.50	47.00	50.00	20.83	111.89	-16.40	-13.11	3.6	4.0	0	1
49.60	47.30	52.00	21.00	112.44	-13.02	-17.84	3.1	6.4	1	0
51.50	50.60	52.30	21.40	112.36	-18.01	-13.75	4.6	5.0	0	1
52.50	51.00	54.00	22.19	113.42	-14.21	-19.49	3.7	8.5	1	0
52.30	50.70	54.00	21.82	113.42	-18.36	-19.49	4.7	8.5	0	0

7

THEORETICAL CONSIDERATIONS

The objectives of this analysis of the SASS data are to recover the
synoptic scale wind at a one degree resolution on a spherical coordinate
grid and to derive synoptic scale fields for divergence, vertical velocity,
the vector wind stress, and the curl of the wind stress from these winds.
For use in a synoptic scales analysis at some initial time, the requirement
is for the winds to be specified as east-west and north-south components at
integral intersections of latitude and longitude in the form of values as
close as possible to $U_s(\lambda_o,\theta_o)$ and $V_s(\lambda_o,\theta_o)$, where the subscript, s,
designates an error free synoptic scale measurement with synoptic scale
gradients accounted for and their effects removed and with mesoscale fluctua-
tions and instrument errors reduced.[*]   The SASS winds were not measured
at the location, λ_o,θ_o.   They contain the effects of mesoscale variability,
and there are errors (sampling variability as an effect of communication
noise and cell location inaccuracies), in the measurement of the backscatter
that in turn result in errors in the calculated winds.

The locations of the SASS measurements are more or less randomly
distributed in an area around the desired location, λ_o,θ_o, but the gradients
in the wind are systematic and need to be considered. If the SASS-1 wind
vector recovery algorithm and model function have no systematic bias, the
mesoscale fluctuations and the effects of communication noise will also be
random and have the same probabilistics and statistical properties within an
area around λ_o,θ_o.

The individual SASS winds can be combined in such a way that the effects
of gradients can be greatly reduced as a source of error in finding the wind
at λ_o,θ_o. Also the random errors introduced by mesoscale variability and
communication noise, can be modeled probabilistically, interpreted statistically
and greatly reduced by means of the application of small sample theory.

It is not necessary to separate the combined effects of mesoscale varia-
bility and communication noise. Their effects can, however, be considered in

---

[*]An appendix defines the notation, except were noted.

the interpretation of the results that are obtained. Often the effects of communication noise stand out above the effects of mesoscale variability, especially as a function of aspect angle relative to the pointing angles of the radar beams of the SASS.

Consider a number of measurements, all of the same geophysical quantity such as some kind of a wind represented by u, made in the same area, that all ought to be nearly equal to the same value. These values will not be equal for numerous reasons. Conceptually there is some correct (or true) value and the actual values will scatter in a random way about this correct value. The measurements can be described as having a probability density function (pdf), $f(u)$, with the usual properties of a pdf, namely,

$$f(u) \geq 0 \tag{1}$$

$$\int_{-\infty}^{\infty} f(u) \, du = 1 \tag{2}$$

and
$$\int_{-\infty}^{\infty} u f(u) \, du = u_1 \tag{3}$$

which is the first moment of the pdf and can be associated with the correct value.

Moments about u_1 as in

$$u' = u - u_1$$

yield
$$\int_{-\infty}^{\infty} (u - u_1) \, f(u) \, du = 0 \tag{4}$$

and
$$\int_{-\infty}^{\infty} (u - u_1)^2 \, f(u) \, du = (\Delta u)^2 \tag{5}$$

Now let
$$u = u_1 + t\Delta u \tag{6}$$

or
$$t = (u - u_1)/\Delta u \tag{7}$$

so that $f(u)$ is transformed into $f(t)$. The pdf, $f(u)$, is transformed into

$$f(u_1 + t\Delta u)\Delta u \, dt = f^*(t) \, dt \tag{8}$$

9

and $f^*(t)dt$ has the properties that

$$\int_{-\infty}^{\infty} f^*(t)dt = 1 \qquad (9)$$

$$\int_{-\infty}^{\infty} t \, f^*(t)dt = 0 \qquad (10)$$

$$\int_{-\infty}^{\infty} t^2 f^*(t)dt = 1 \qquad (11)$$

The concept can be generalized if various reasons for the variability of the measurements can be identified. Suppose that there are, say, two causes for the variability that many differ from one set of measurements to another such that

$$(\Delta u)^2 = (\Delta u_1)^2 + (\Delta u_2)^2 \qquad (12)$$

Then the pdf can be generalized to the product of two independent pdf's, $f(t_1) \cdot f(t_2)$, and (7) becomes

$$u = u_1 + t_1 \Delta u_1 + t_2 \Delta u_2 \qquad (13)$$

with obvious extentions, if needed, such as, for example, conditions such that t_1 and t_2 are not independent and covariances are needed.

Small sample theory can be applied under the assumption that all of the measurements are for the purpose of learning more about u_1. Suppose that M measurements are made as in

$$u_i = u_1 + t_{1i} \Delta u_1 + t_{2i} \Delta u_2 \qquad (14)$$

where the t_{1i} and t_{2i} are from (not necessarily the same) pdf's with properties defined by (10), (11) and (12). ($f^*(t)$ is the convolution of $f(t_1)$ and $f(t_2)$).

The average value of the u_i is given by (16) from (11)

$$\bar{u} = \frac{1}{M} \sum_1^M u_i$$

$$= u_1 + \frac{1}{M} \sum t_{1i} \, \Delta u_1 + \frac{1}{M} \sum t_{2i} \, \Delta u_2$$

$$= u_1 + \frac{1}{M} \sum t_i \, \Delta u = u_1 + \frac{1}{M} \sum t \left[(\Delta u_1)^2 + (\Delta u_2)^2 \right]^{\frac{1}{2}} \qquad (15)$$

and the expected value of the average is (16).

$$\mathcal{E} \, (\bar{u}) = u_1 \qquad (16)$$

The random variable

$$t_1^* = \frac{1}{M} \sum t_{1i} \qquad (17)$$

has a mean of zero and a second moment of

$$M_2 \, (t_1^*) = 1/M \qquad (18)$$

so that $\bar{u}$ can be represented by

$$\bar{u} = u_1 + t_1^* \, (M^{-\frac{1}{2}} \, \Delta u_1) + t_2^* (M^{-\frac{1}{2}} \, \Delta u_2)$$

$$= u_1 + t^* \left[M^{-1} ((\Delta u_1)^2 + (\Delta u_2)^2) \right]^{\frac{1}{2}} \qquad (19)$$

The expected value of $\bar{u}$ is u_1 and the expected value of $(\bar{u}-u_1)^2$ is

$$\mathcal{E} \, (\bar{u} - u_1)^2 = M^{-1} \left[(\Delta u_1)^2 + (\Delta u_2)^2 \right] \qquad (20)$$

From a given sample, it is possible to estimate the mean, $\bar{u}$, the standard deviation, Δu, and to use the fact that $\bar{u}$ has a standard deviation with reference to the desired true value given by $M^{-\frac{1}{2}} \, \Delta u$ where M is the sample size.

A number of SASS individual wind values can be combined in such a way as to recover a single estimate with a greatly reduced variability. When these estimates are then combined to form fields, this greatly reduced variability, which is known, can be used to find the variability of various derived fields.

It is well known that the mean of a sample from almost any typical, but unknown, pdf will be nearly normally distributed by virtue of the central limit theorem so that although the pdf's of t, t_1, and t_2 may not be known, the pdf's of t^*, t_1^* and t_2^* will be close to a unit variance zero mean normal pdf for most of the values of M that occur in what follows.

As in any statistical procedure the moments of a pdf, such as u_1, always remain unknown. The statistics only provide a way to put bounds on the estimate of u_1, that is $\bar{u}$, that are made narrower because of the sample size. In (15), $\bar{u}$, M, $(\Delta u_1)^2 + (\Delta u_2)^2 = (\Delta u)^2$ are all known statistics, where $(\Delta u_1)^2 + (\Delta u_2)^2$ is an estimate of the variance from the sample. Thus (15) can be rewritten as

$$u_1 = \bar{u} - t^* M^{-\frac{1}{2}} \Delta u \qquad (21)$$

where all is known on the RHS except t^* (the minus sign is not too relevant). The values of u_1 when found at a grid of points form a field consisting of values of $\bar{u}$ plus a quantity that provides information on the variability of $\bar{u}$.

As an example, if $\bar{u}$ is 10.73 m/s, Δu is 2 m/s, and M is 25, then about two thirds of the time it would be expected that the interval 10.33 to 11.13 m/s would enclose the true value, u_1. If sampling variability quantities are kept track of in the finite difference calculations of properties of the wind field, they provide estimates of the sampling variability of these properties.*

---

*See also, pg. 46.

12

PRELIMINARY DATA PROCESSING

The first data processing step was to sort the data shown as an example in Table 1 for each revolution into overlapping two degree by two degree sets centered on the one degree integer values of latitude and longitude. The vector winds found from combining many individual SASS winds around a grid point of a model have been called superobservations. A given SASS wind could be found in four different sets. As in Figure 1, a given set of SASS winds would have latitudes and longitudes that varied from $\lambda_o - 1$ to $\lambda_o + 1$ and $\theta_o - 1$ to $\theta_o + 1$.

A preliminary investigation suggested that the two solution cases and the base of the "Y" in three solution cases gave both directions and speeds that were systematically different from the other directions and speeds within a given two degree square. Since the original data set gives the pointing direction of beam 1, say, χ_o, dealiased winds were checked to see if the directions were within $\chi_o \pm 1^o$, χ_o plus 89° to 91°, χ_o plus 179° to 181°, and χ_o plus 269° to 271°. If they were, those particular data vectors were removed from the set. In Table 1a, for example, the data corresponding to SASS directions of 288.8, 289.3, 289.6 and 290.3, were deleted.

When centered on λ_o and θ_o, the latitudes and longitudes can be transformed by subtracting λ_o and θ_o from each element in the set. The locations of each SASS wind will then be defined by values of $\Delta\lambda$ and $\Delta\theta$ that both range between plus and minus one.

13
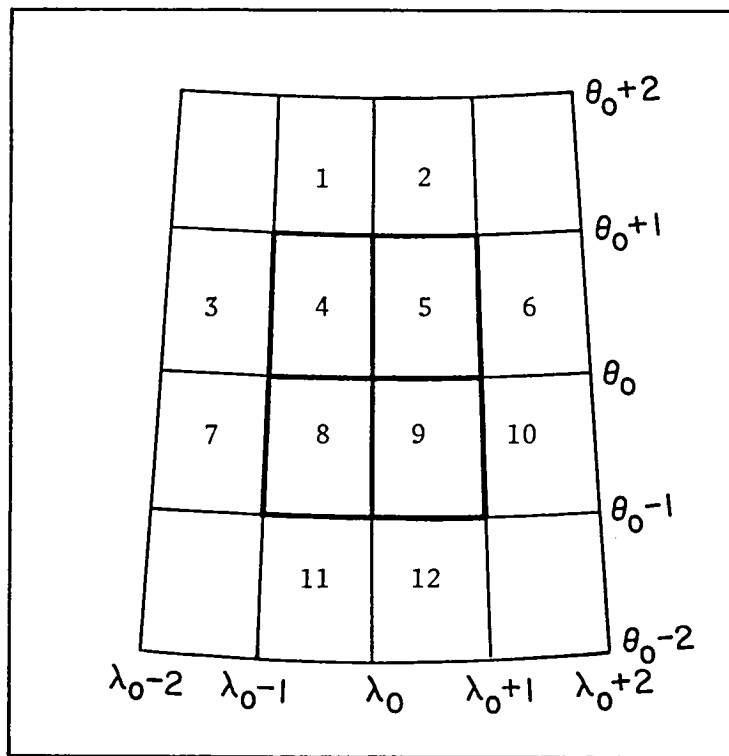
Fig. I The 2° by 2° Overlapping Spherical Coordinate Grid Centered on Integer Values of Latitude and Longitude.

14

The average latitude and longitude for the data set will be equations (22) and (23) for the N + n values in the 2 degree square.

$$\lambda_o + \overline{\Delta\lambda_1} = \lambda_o + \frac{1}{N+n} \sum_1^{N+n} \Delta\lambda_j \tag{22}$$

$$\theta_o + \overline{\Delta\theta_1} = \theta_o + \frac{1}{N+n} \sum_1^{N+n} \Delta\theta_j \tag{23}$$

The values of $\overline{\Delta\lambda}$ and $\overline{\Delta\theta}$ will usually be close to, but not exactly, zero. The location of this point will be in one of the four quadrants of the heavy square in Figure 1. By selectively removing n of the data vectors in the set based on the location of $\overline{\Delta\lambda}$ and $\overline{\Delta\theta}$, it is possible to reduce both $\overline{\Delta\lambda}$ and $\overline{\Delta\theta}$ for the remaining subset below some preassigned minimum as in equations (24) and (25).

$$\lambda_o + \overline{\Delta\lambda} = \lambda_o + \frac{1}{N} \sum_1^N \Delta\lambda_i \tag{24}$$

$$\theta_o + \overline{\Delta\theta} = \theta_o + \frac{1}{N} \sum_1^N \Delta\theta_i \tag{25}$$

This subset of data for each two by two degree square was processed further to obtain the results to follow. Also needed for later use will be the average values of $(\Delta\lambda_i)^2$, $(\Delta\theta_i)^2$ and $(\Delta\lambda_i \cdot \Delta\theta_i)$.

WIND VECTORS

The N value for the winds in each data set consisted of a speed and a (from which) direction (meteorological convention, clockwise from north). The directions were averaged to obtain a value for the average direction as in (26) where the summation notation is abbreviated.

$$\overline{\chi} = \frac{1}{N} \sum \chi_i \tag{26}$$

Each wind was then resolved into a component in the direction of $\overline{\chi}$ and a component normal to $\overline{\chi}$ as in (27) and (28).

$$V_{Pi} = |V|_i \cos(\chi_i - \overline{\chi}) \tag{27}$$

$$V_{Ni} = |V|_i \sin(\chi_i - \bar{\chi}) \tag{28}$$

These components were averaged to obtain (29) and (30).

$$\bar{V}_P = \frac{1}{N} \sum V_{Pi} \tag{29}$$

$$\bar{V}_N = \frac{1}{N} \sum V_{Ni} \cong 0 \tag{30}$$

In all cases $\bar{V}_N$ was essentially zero. The standard deviations of $\bar{V}_P$ and $\bar{V}_N$ about their sample means were also computed as in (31) and (32).

$$\Delta u = SD(V_P) = \left(\frac{1}{N} \sum (V_{Pi} - \bar{V}_P)^2 \right)^{\frac{1}{2}} \tag{31}$$

$$\Delta v = SD(\bar{V}_N) = \left(\frac{1}{N} \sum V_{Ni} - \bar{V}_N)^2 \right)^{\frac{1}{2}} \tag{32}$$

The processed data at this point consist of the sample size, N, the mean direction, $\bar{\chi}$, the mean component in the mean direction, $\bar{V}_P$ and the values of Δu and Δv as located at a point given by $\lambda_o + \overline{\Delta \lambda}$ and $\theta_o + \overline{\Delta \theta}$ with the values located very close to the integer values of latitude and longitude over the ocean plus the average values of $(\Delta \lambda_j)^2$, $(\Delta \theta_j)^2$ and $\Delta \lambda_j \Delta \theta_j$ (i.e. VAR $(\Delta \lambda)$, VAR $(\Delta \theta)$ and COV $(\Delta \lambda \Delta \theta)$).

The "from which" meteorological convention can be converted to a "toward which" vector by adding 180° (mod 360°). The new direction, clock angle, is needed for use in analyzing the wind field. The east-west, U_λ, (abbreviated as U), and the north-south, V_θ, (abbreviated as V) components of the three non-zero vectors given by (29), (31), and (32) are next found.

The mean east-west and north-south components are given by (33) and (34).

$$\bar{U} = \bar{V}_P \sin(\bar{\chi} + 180^o) = -\bar{V}_P \sin \bar{\chi} \tag{33}$$

$$\bar{V} = \bar{V}_P \cos(\bar{\chi} + 180^o) = -\bar{V}_P \cos \bar{\chi} \tag{34}$$

The components of Δu and Δv from (31) and (32) in the east-west direction according to the convention shown in Figure 2 are (35) and (36).

$$\Delta u_1 = -\Delta u \sin \bar{\chi} \qquad (35)$$

$$\Delta u_2 = - \Delta v \cos \bar{\chi} \qquad (36)$$

The components in the north-south direction are given by (37) and (38).

$$\Delta v_1 = - \Delta u \cos \bar{\chi} \qquad (37)$$

$$\Delta v_2 = \Delta v \sin \bar{\chi} \qquad (38)$$

The vectors $(V_p, \bar{\chi})$, $(\Delta U, \bar{\chi})$ and $(\Delta V, \bar{\chi} + 90^o)$, can be used to form two orthogonal vectors, as in (39) and (40).

$$V_{PS} = \bar{V}_P - t_1 \Delta u \qquad (39)$$

$$V_{Ns} = \bar{V}_N - t_2 \Delta v = 0 - t_2 \Delta v \qquad (40)$$

and $\bar{\chi} = \chi_s$. The subscript, s, represents the desired synoptic scale value.

The orthogonal coordinate system has one axis parallel to the direction, $\bar{\chi}$, and t_1 and t_2 are independent random variables with zero means and unit standard deviations as in equation (9) to (11). When resolved into north-south and east-west components, east-west variability is correlated with north-south variability so as to confine the scatter of points to the form of ellipses such as the one shown by the dashed line in Figure 2. The variability of $\bar{U}$ and $\bar{V}$, where U_s and V_s are the desired synoptic scale components, analogous to u_1 in equation (7), can be represented by (41) and (42). The calculated values, $\bar{U}$ and $\bar{V}$, equal the true values U_s and V_s, plus the effects of gradients and the random errors.

$$\bar{U}(\lambda_o + \overline{\Delta\lambda}, \theta_o + \overline{\Delta\theta}) = U_s(\lambda_o + \overline{\Delta\lambda}, \theta_o + \overline{\Delta\theta})$$

$$+ t_1 \Delta u_1 + t_2 \Delta u_2 \qquad (41)$$

$$\bar{V}(\lambda_o + \overline{\Delta\lambda}, \theta_o + \overline{\Delta\theta}) = V_s(\lambda_o + \overline{\Delta\lambda}, \theta_o + \overline{\Delta\theta})$$

$$+ t_1 \Delta v_1 + t_2 \Delta v_2 \qquad (42)$$

Following these transformations, the data for each integer value of latitude and longitude for each point in the SASS swath consists of λ_o,

17
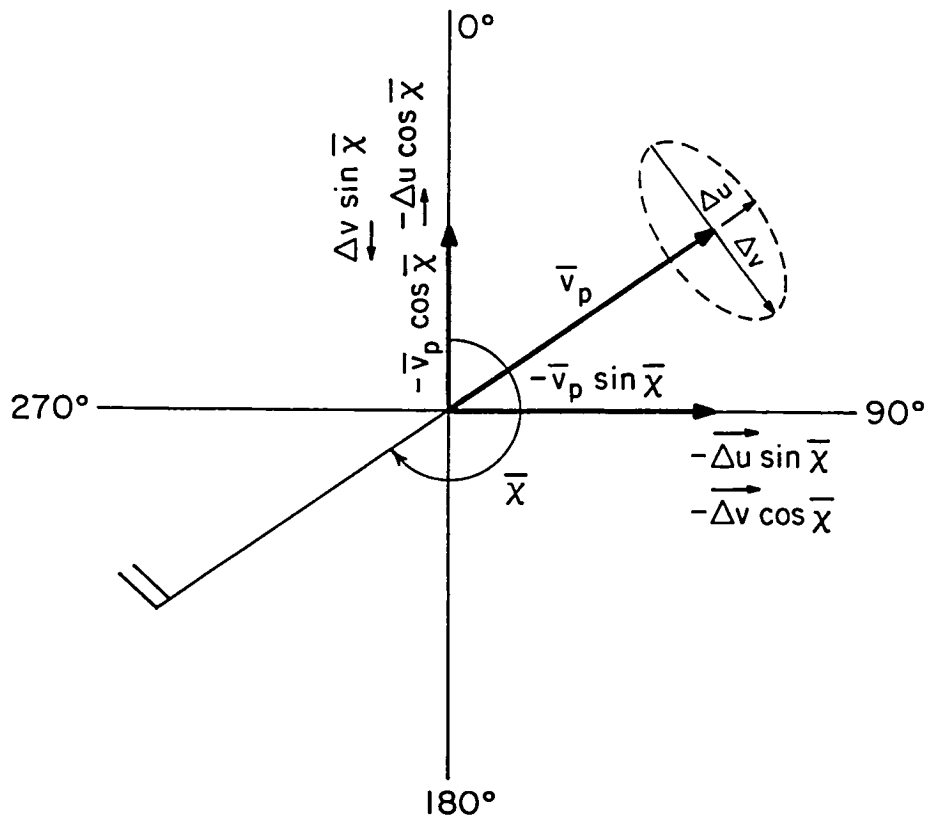
Fig. 2 Conventions for the Conversion of $\overline{v}_p$, $\overline{\chi}$, Δu, and Δv to $\overline{u}$, $\overline{v}$, Δu_1, Δu_2, Δv_1 and Δv_2.

18

θ_o, $\overline{\Delta\lambda}$, $\overline{\Delta\theta}$, $\bar{U}$, Δu_1, Δu_2, $\bar{V}$, Δv_1, Δv_2, VAR($\Delta\lambda$), VAR($\Delta\theta$), COV($\Delta\lambda\Delta\theta$) and N. The following steps process the $\bar{U}$ and $\bar{V}$ components of the processed SASS data to determine the best possible field for the synoptic scale wind.

Consider the east-west component of the wind at a point where it was estimated by the SASS somewhere within the two degree square. The value could be described by equation (43).

$$U(\lambda_i, \theta_i) = U_s(\lambda_o, \theta_o) + \frac{\partial U_s(\lambda_o, \theta_o)}{\partial \lambda}(\lambda_i - \lambda_o)$$

$$+ \frac{\partial U_s(\lambda_o, \theta_o)}{\partial \theta}(\theta_i - \theta_o) + t_i \Delta U' \qquad (43)$$

where $\Delta U'$ is to be defined later.

The average value of the N values of $U(\lambda_i, \theta_i)$ is

$$\bar{U} = \frac{1}{N}\sum (U(\lambda_i, \theta_i)) = \bar{U}(\lambda_o + \overline{\Delta\lambda}, \theta_o + \overline{\Delta\theta})$$

$$= U_s(\lambda_o, \theta_o) + \frac{\partial U_s(\lambda_o, \theta_o)}{\partial \lambda}\overline{\Delta\lambda} + \frac{\partial U_s(\lambda_o, \theta_o)}{\partial \theta}\overline{\Delta\theta} + \frac{1}{N}\sum t_i \Delta U' \qquad (44)$$

Everything except $U_s(\lambda_o, \theta_o)$ is known, or can be estimated, and the two other terms on the right hand side are usually small because $\overline{\Delta\lambda}$ and $\overline{\Delta\theta}$ are small. For points in the interior of the swath, it is possible to estimate a correction from the gradients of $\bar{U}$ as in (45) where uncorrected values near the grid points are used to find approximate gradients,

$$\bar{U}(\lambda_o, \theta_o) = \bar{U}(\lambda_o + \overline{\Delta\lambda}, \theta_o + \overline{\Delta\theta})$$

$$- \tfrac{1}{2}(\bar{U}(\lambda_o + 1 + \overline{\Delta\lambda}, \theta_o + \overline{\Delta\theta}) - \bar{U}(\lambda_o - 1 + \overline{\Delta\lambda}, \theta_o + \overline{\Delta\theta}))\overline{\Delta\lambda}$$

$$- \tfrac{1}{2}(\bar{U}(\lambda_o + \overline{\Delta\lambda}, \theta_o + 1 + \overline{\Delta\theta}) - \bar{U}(\lambda_o - 1\overline{\Delta\lambda}, \theta_o - 1 + \overline{\Delta\theta}))\overline{\Delta\theta} \quad (45)$$

subject to the conditions that appropriate inequalities hold, namely

either $\bar{U}(\lambda_o + 1 + \overline{\Delta\lambda}, \theta_o + \overline{\Delta\theta}) > \bar{U}(\lambda_o + \overline{\Delta\lambda}, \theta_o + \overline{\Delta\theta}) > \bar{U}(\lambda_o - 1 + \overline{\Delta\lambda}, \theta_o + \overline{\Delta\theta})$ (46)

or $\bar{U}(\lambda_o + 1 + \overline{\Delta\lambda}, \theta_o + \overline{\Delta\theta}) < \bar{U}(\lambda_o + \overline{\Delta\lambda}, \theta_o + \overline{\Delta\theta}) < \bar{U}(\lambda_o - 1 + \overline{\Delta\lambda}, \theta_o + \overline{\Delta\theta})$ (47)

and either $\bar{U}(\lambda_o + \overline{\Delta\lambda}, \theta_o + 1 + \overline{\Delta\theta}) > \bar{U}(\lambda_o + \overline{\Delta\lambda}, \theta_o + \overline{\Delta\theta}) > \bar{U}(\lambda_o + \overline{\Delta\lambda}, \theta_o - 1 + \overline{\Delta\theta})$ (48)

or $\bar{U}(\lambda_o + \overline{\Delta\lambda}, \theta_o + 1 + \overline{\Delta\theta}) < \bar{U}(\lambda_o + \overline{\Delta\lambda}, \theta_o + \overline{\Delta\theta}) < \bar{U}(\lambda_o + \overline{\Delta\lambda}, \theta_o - 1 + \overline{\Delta\theta})$ (49)

If sets of these inequalities are not satisfied, then $U(\lambda_o, \theta_o)$ is near a maximum or a minimum, in one or both directions, (or a saddle point) and the correction is simply to set $U(\lambda_o, \theta_o)$ equal to $U(\lambda_o + \overline{\Delta\lambda}, \theta_o + \overline{\Delta\theta})$.

The expected value of the square of $U(\lambda_i, \theta_i) - \bar{U}(\lambda_o, \theta_o)$ is given from (43) by (50).

$$
\mathcal{E} \left(\frac{1}{N} \sum (U(\lambda_i, \theta_i) - \bar{U}(\lambda_o, \theta_o)) \right)^2
$$

$$
= \left(\frac{\partial U_s(\lambda_o, \theta_o)}{\partial \lambda} \right)^2 \text{VAR}(\Delta\lambda) + \left(\frac{\partial U_s(\lambda_o, \theta_o)}{\partial \theta} \right)^2 \text{VAR}(\Delta\theta)
$$

$$
+ 2 \frac{\partial U_s(\lambda_o, \theta_o)}{\partial \lambda} \frac{\partial U_s(\lambda_o, \theta_o)}{\partial \theta} \text{COV}(\Delta\lambda \, \Delta\theta) + (\Delta U')^2
$$ (50)

In (50), the first three terms represent the effects of gradients of the east-west component of the wind. These and similar terms contribute to the variability of U and V in (31) and (32) and of Δu_1, Δu_2, Δv_1 and Δv_2 in (41) and (42). These effects need to be removed so that the effects of sampling variability can be found.

The contribution of the variability of the values of $U(\lambda_i, \theta_i)$ and $V(\lambda_i, \theta_i)$ from gradients in the synoptic scale wind is the first three terms in (45). For SASS values uniformly scattered over a particular two degree by two degree square, the average values of $(\Delta\lambda_i)^2$ and $(\Delta\theta_i)^2$ will be about one third and the average value of $\Delta\lambda_i, \Delta\theta_i$ will be close to zero. SASS winds concentrated in diagonally opposed quadrants would yield a non-zero value for this third term. The synoptic scale contribution to the variability of the estimate of $U_s(\lambda_o, \theta_o)$ can be estimated by (51) where the values corrected by (45) have been used.

$$
\text{VAR (SYNOPTIC)} = \frac{1}{4} (\bar{U}(\lambda_o + 1, \theta) - \bar{U}(\lambda_o - 1, \theta))^2 \text{ VAR } \Delta\lambda
$$

$$
+ \frac{1}{4} (\bar{U}(\lambda_o, \theta_o + 1) - \bar{U}(\lambda_o, \theta_o - 1))^2 \text{ VAR } \Delta\theta
$$

$$
+ \frac{1}{2} (\bar{U}(\lambda_o + 1, \theta_o) - \bar{U}(\lambda_o - 1, \theta_o))(\bar{U}(\lambda_o, \theta_o + 1) - \bar{U}(\lambda_o, \theta_o - 1)) \text{ COV } \Delta\lambda\Delta\theta \quad (51)
$$

The variability of the estimate, $\bar{U}(\lambda_o, \theta_o)$, that is the result of mesoscale variability of the winds from one SASS cell to the other and of the effects of communication noise is found by means of (52).

VAR (MESO   PLUS COMMUNICATION NOISE)
$$= (\Delta u_1)^2 + (\Delta u_2)^2 - \text{VAR (SYNOPTIC)}$$

$$= (\Delta U')^2 \tag{52}$$

where $(\Delta U')$ is now defined in (43) by equation (52). Since VAR(SYNOPTIC) is an estimate, it may exceed $(\Delta u_1)^2 + (\Delta u_2)^2$ in which case $(\Delta U')^2$ is set to zero. The analyses of superobservations by Pierson (1982a, 1983b), assumed that gradients of the synoptic scale wind could be neglected in the study of superobservations. For some parts of the wind fields obtained from the SASS, the assumption is not justified, and this correction needs to be made. Often it is small. Specific examples will be given later.

A parallel set of equations for the north-south components of the synoptic scale winds can also be obtained. The final results of processing the data in this way produces values of $\bar{U}(\lambda_o, \theta_o)$, $\bar{V}(\lambda_o, \theta_o)$, $\Delta U'$ and $\Delta V'$ at the integer values of λ and θ in the main part of the SASS swath where $\overline{\Delta\lambda}$ are $\overline{\Delta\theta}$ small. Near the edges of the SASS swath, which will be discussed separately, other methods are needed because of the smaller number of values in the superobservation, the location of the data fairly far from the desired latitude and longitude and the lack of values for all of the quantities needed in the above equations.

The elliptical scatter of the winds that form a superobservation is an important aspect of the sampling variability of the measurements. From (52), and its equivalent for V and from (35), (36), (37) and (38), reduced values of Δu_1 and Δu_2 may prove useful in studying the effects of mesoscale variability and communication noise.

Let
$$K = \left[(\Delta U')^2 + (\Delta V')^2 \right] \left[(\Delta u_1)^2 + (\Delta u_2)^2 + (\Delta v_1)^2 + (\Delta v_2)^2 \right]^{-1} \tag{53}$$

21

Then let
$$\Delta U_1' = K^{\frac{1}{2}} \Delta u_1 \tag{54}$$

$$\Delta U_2' = K^{\frac{1}{2}} \Delta u_2 \tag{55}$$

$$\Delta V_1' = K^{\frac{1}{2}} \Delta v_1 \tag{56}$$

$$\Delta V_2' = K^{\frac{1}{2}} \Delta v_2 \tag{57}$$

This change effectively reduces the elliptical scatter of the original data by an amount attributable to the removal of synoptic scale variability over the two degree by two degree square.

The final result of the steps taken so far is to make it possible to represent the east-west and north-south components of the synoptic scale wind at λ_o, θ_o in forms similar to equations (19) and (21). They are equations (58) and (59) and equations (60) and (61).

$$\bar{U}(\lambda_0, \theta_o) = U_s(\lambda_o, \theta_o) + t_1 N^{-\frac{1}{2}} \Delta U_1' + t_2 N^{-\frac{1}{2}} \Delta U_2' \tag{58}$$

$$\bar{V}(\lambda_o, \theta_o) = V_s(\lambda_o, \theta_o) + t_1 N^{-\frac{1}{2}} \Delta V_1' + t_2 N^{-\frac{1}{2}} \Delta V_2' \tag{59}$$

$$U_s(\lambda_o, \theta_o) = \bar{U}(\lambda_o, \theta_o) - t_1 N^{-\frac{1}{2}} \Delta U_1' - t_2 N^{-\frac{1}{2}} \Delta U_2' \tag{60}$$

$$V_s(\lambda_o, \theta_o) = \bar{V}(\lambda_o, \theta_o) - t_1 N^{-\frac{1}{2}} \Delta V_1' - t_2 N^{-\frac{1}{2}} \Delta V_2' \tag{61}$$

For an analysis of (58) and (59), the same values for t_1 and t_2 must be used in both equations. This shows that $\bar{U}$ and $\bar{V}$ are not independent and for example that

$$\mathcal{E} \left(\left[\left(\bar{U}(\lambda_o, \theta_o) - U_s(\lambda_o, \theta_o) \right) \right] \left[\bar{V}(\lambda_o, \theta_o) - V_s(\lambda_o, \theta_o) \right] \right) \tag{62}$$

$$= N^{-1} (\Delta U_1' \, \Delta V_1' + \Delta U_2' \, \Delta V_2') \tag{63}$$

Equations (60) and (61) put all of the known statistics on the right hand side. It needs to be interpreted with care. There is, conceptually, only one correct value for U_s, and only one, for V_s. Picking t_1 and t_2 at random generates many values of U_s and V_s, one of which may be the correct one. If t_1 and t_2 are constrained to lie on a circle and are normally

distributed then

$$P(t_1^2 + t_2^2 < r^2) = \frac{1}{2\pi} \int\!\!\!\int_{t_1^2 + t_2^2 = r^2} e^{-(t_1^2 + t_2^2)/2}\ dt_1\ dt_2$$

$$= \frac{1}{2\pi} \int_o^r \int_o^{2\pi} e^{-\zeta^2/2}\zeta d\zeta d\theta$$

$$= 1 - e^{-r^2/2}$$

so that if $r = 2$, the ellipse generated in the $U_s V_s$ plane will have a probability of 0.865 of enclosing the true value of U_s and V_s.

In the analysis of superobservations, each SASS wind in the four degree square is given equal weight in contrast to some of the present analysis techniques that weight wind and pressure reports from ships as a function of how far away they are from the grid point being analysed. For conventional data and conventional analysis procedures, the same report will influence a grid point from distances as far away as five or ten degrees of latitude or longitude. Other sources of error dominate the analysis of conventional data and maximum use must be made of each oceanic observation because of the poor spacing and sparceness of the data.

For SASS data the error sources are different and the dominant ones are essentially random. Equally weighted observations are the most effective way to reduce the variability inherent in the SASS data.

THE FIELD OF HORIZONTAL DIVERGENCE

For constant density at a fixed height above the sea surface, the equation of continuity in spherical coordinates is given by equation (64).

$$\frac{1}{R^2}\left[\frac{\partial}{\partial R}(R^2\ W)\right] + \frac{1}{R\cos\theta}\frac{\partial U}{\partial\lambda} + \frac{1}{R\cos\theta}\frac{\partial\ (V\cos\theta\ )}{\partial\theta\ \partial\ \theta} = 0 \tag{64}$$

The divergence of the horizontal wind at 19.5 meters for a neutral atmosphere is given by equation (65).

$$\text{div}_2\ W_h = \frac{1}{R\cos\theta}\left(\ \frac{\partial U}{\partial\lambda} + \cos\ \theta\ \frac{\partial V}{\partial\theta} - V\sin\ \theta\right) \tag{65}$$

A finite difference estimate of the divergence at a one degree resolution requires values of U at $\lambda_o + 1$, θ_o and $\lambda_o - 1$, θ_o and values of V at $\lambda_o, \theta + 1$; λ_o, θ_o and λ_o, $\theta_o - 1$. We neglect also the ellipticity of the Earth, and use $R = 2 \cdot 10^7 (\pi)^{-1}$. The equations are in the form of (60) and (61).

The finite difference value for the horizontal divergence of the wind is given by equation (66) where the various ΔU_1, and so on, are associated with the appropriate latitude and longitude.

$$\begin{aligned}
\left(\text{div}_2\ W_h\right)_s = \frac{4\cdot 5\cdot 10^{-6}}{\cos\theta_o}&\left[\left(\bar{U}(\lambda_o + 1,\ \theta_o) - t_1\ \Delta U_1' - t_2\ \Delta U_2' - \bar{U}(\lambda_o - 1,\ \theta_o)\right.\right.\\
&\left. + t_3\Delta U_1' + t_4\ \Delta U_2'\right) + \cos\ \theta_o\left(\bar{V}(\lambda_o,\ \theta_o + 1) - t_5\ \Delta V_1' - t_6\ \Delta V_2'\right.\\
&\left. - \bar{V}(\lambda_o, \theta_o - 1) + t_7\ \Delta V_1' + t_8\ \Delta V_2'\right) - 0.0349065\left(\sin\ \theta(\bar{V}(\lambda_o, \theta_o))\right.\\
&\left.\left. - t_9\ \Delta V_1' - t_{10}\ \Delta V_2'\right)\right]
\end{aligned} \tag{66}$$

The expected value of $(\text{div}_2\ W_h)_s$ simplifies to equation (67).

$$\begin{aligned}
\mathcal{E}\ (\text{div}_2\ W_h)_s = \frac{4\cdot 5\cdot 10^{-6}}{\cos\theta_o}&\left(\bar{U}(\lambda_o + 1,\ \theta_o) - \bar{U}(\lambda_o - 1,\ \theta_o)\right.\\
&+ \cos\ \theta_o(\bar{V}(\lambda_o,\ \theta_o + 1) - \bar{V}(\lambda_o,\ \theta_o - 1))\\
&\left. - 0.0349065\ (\sin\ \theta_o\ \bar{V}(\lambda_o,\ \theta_o))\right) = \overline{\text{div}_2\ W_h}
\end{aligned} \tag{67}$$

The expected value of the variance of the divergence is given by equation (68)

$$\mathcal{E}\left[(div_2 \, W_h)_s - (\overline{div_2 \, W_h}) \right]^2 = VAR \, (div_2 \, W_h)$$

$$= \frac{2.025 \cdot 10^{-11}}{(\cos \theta_o)^2} \left[(\Delta U_1' \, (\lambda_o + 1, \, \theta_o))^2 + (\Delta U_2'(\lambda_o + 1, \theta_o))^2 + (\Delta U_1'(\lambda_o - 1, \theta_o))^2 \right.$$

$$+ (\Delta U_2'(\lambda_o - 1, \, \theta_o))^2 + (\cos \theta_o)^2 \, ((\Delta V_1'(\lambda_o, \, \theta_o + 1))^2 + (\Delta V_2'(\lambda_o, \, \theta_o + 1))^2$$

$$+ (\Delta V_1'(\lambda_o, \theta_o - 1))^2 + (\Delta V_2'(\lambda_o, \, \theta_o - 1))^2)$$

$$\left. + 1.2184 \cdot 10^{-3} \, (\sin \theta_o)^2 \, ((\Delta V_1' \, (\lambda_o, \theta_o))^2 + (\Delta V_2'(\lambda_o, \, \theta_o))^2) \right] \qquad (68)$$

The divergence at one of the grid points in the SASS swath where sufficient data are available is thus given by equation (69) where t by the central limit theorem is approximately a normally distributed random variable with a zero mean and a unit variance.

$$(div_2 \, W_h)_s = \overline{div_2 \, W_h} + t \, (VAR(\overline{div_2 \, W_h}))^{\frac{1}{2}} \qquad (69)$$

The wind in the layer of air near the ocean surface can be expressed as a function of height, h, given the wind profile for the first few hundred meters. Given the friction velocity, (u^*), the divergence can be expressed as a function of height for neutral stability and integrated from the surface upward. This will be done after the fields for the wind stress and the curl of the wind stress are found.

The Monin-Obukhov theory and the concept of the drag coefficient given by equation (70) for a neutral atmosphere

$$C_{D10} = u_*^2/\bar{U}_{10}^2 \tag{70}$$

where $\quad u_*^2 = \tau/\rho = - <u'w'> \tag{71}$

have been the methods used to try to understand the turbulent boundary layer over the ocean. Many different sets of measurements have been made in order to try to determine the relationship between wind stress and the wind at 10 meters.

It is not relevant to this particular investigation to review the great many papers that have been written that describe the results of these many investigations. Reviews of some of these studies are given by Phillips (1977) and Neumann and Pierson (1966).

More recent results using more modern and more carefully calibrated instrumentation that cover a large range of wind speeds are those of Davidson, et al. (1981), Dittmer (1977), Smith (1980) and Large and Pond (1981). Low winds are covered by Davidson, et al. (1981), low and moderate winds, by Dittmer (1977) and moderate and high winds, by Smith (1980) and Large and Pond (1981).

Smith and Large and Pond used methods that measured $<u'w'>$ directly as well as the dissipation in the Kolmogorov range which was then correlated with $<u'w'>$ and $\bar{U}_{10}$. All of the data obtained to determine the relationship between wind stress and $\bar{U}_{10}$ scatter when plotted either as τ/ρ versus $\bar{U}_{10}$ or as C_{10} versus $\bar{U}_{10}$.

To investigate the problem in still one more way, an analysis was made as a term paper[*], by Vera, of the data provided by W. G. Large and extracted from the publications of Davidson, et al. and Dittmer. For neutral stability, the data were of the form n_i, $(\tau/\rho)_i$, $\bar{U}_{10i}$, for a data set that ranged from light winds of 1 m/s to winds of 27 m/s. The higher winds have smaller values

---

[*] Vera, Emilio E., A Study of Curve Fitting Procedures for the Wind Versus Wind Stress Relationship. Term paper for an Oceanography Course, The City College of New York.

26

for n_i (where n_i represented the number of individual runs in a restricted range of wind speeds that were averaged to produce the u_*^2 and $\bar{U}_{10}$ values) and weight the fit less strongly than moderate and low winds.

The need is for the most accurate possible prediction of the wind stress given the wind at ten meters. Instead of first finding C_{10}, it seems that it would be more direct to minimize the error in predicting the wind stress from the wind speed from the available data as in equation (72).

$$Q = \sum_1^N (n_i ((\tau/\rho)_i - A \bar{U}_{10i} - B \bar{U}_{10i}^2 - C \bar{U}_{10i}^3)^2 \tag{72}$$

This is accomplished by finding those values of A, B and C that minimize Q by requiring that $\partial Q/\partial A = 0$ $\partial Q/\partial B = 0$ and $\partial Q/\partial C = 0$ which yields equations (73).

$$\begin{vmatrix} \sum n_i \bar{U}_{10i}^2 & \sum n_i \bar{U}_{10i}^3 & \sum n_i \bar{U}_{10i}^4 \\ \sum n_i \bar{U}_{10i}^3 & \sum n_i \bar{U}_{10i}^4 & \sum n_i \bar{U}_{10i}^5 \\ \sum n_i \bar{U}_{10i}^4 & \sum n_i \bar{U}_{10i}^5 & \sum n_i \bar{U}_{10i}^6 \end{vmatrix} \begin{vmatrix} A \\ B \\ C \end{vmatrix} = \begin{vmatrix} \sum n_i \bar{U}_{10i} (\tau/\rho)_i \\ \sum n_i \bar{U}_{10i}^2 (\tau/\rho)_i \\ \sum n_i \bar{U}_{10i}^3 (\tau/\rho)_i \end{vmatrix} \tag{73}$$

A good fit was found for the data that were used in terms of equation (74).

$$u_*^2 = \tau/\rho = 10^{-3} (2.717 \bar{U}_{10} + 0.142 \bar{U}_{10}^2 + 0.0761 \bar{U}_{10}^3) \tag{74}$$

Graphs of τ/ρ versus $\bar{U}_{10}$ for the averaged data of Large and as extracted from the two other sources are plotted on linear scales in Figure 3 and on logarithmic scales in Figure 4. Figure 4 shows how the slope of the τ/ρ versus $\bar{U}_{10}$ relationship varies from one to almost three as the wind speed increases.

Vera also investigated the possibility that some power law as in equation (75) might fit the data better.

$$\tau/\rho = \alpha \bar{U}^\beta \tag{75}$$

It was found that no power law did as well as equation (74). As shown in

27

Figure 4 power laws can only be made to fit a portion of the data and fail outside of a restricted range. Equation (74) will consequently be used in this investigation subject to the comment made in the introduction. Given any equation that relates wind stress and the wind at ten meters, the analysis that follows can still be applied.

The SASS data are for winds at 19.5 meters. To calculate the stress it is necessary to know the wind at 10 meters. The wind at 10 meters is

$$\bar{U}(10) = \frac{u_*(\bar{U}_{10})}{\kappa} \ \ell n \ (10/z_o) \tag{76}$$

,since $u_*(\bar{U}_{10})$ is known as a function of $\bar{U}_{10}$, which implies z_o, and at 19.5 meters it is

$$\bar{U}(19.5) = \frac{u_*(\bar{U}_{10})}{\kappa} \ \ell n \ (19.5/z_o) \tag{77}$$

so that

$$\bar{U}(19.5) = \bar{U}(10) + \frac{u_*(\bar{U}_{10})}{\kappa} \ \ell n \ (19.5/10) \tag{78}$$

When $\bar{U}(10)$ is varied in convenient increments, a table of $\bar{U}(19.5)$ versus $\bar{U}(10)$ can be generated. Given a value of $\bar{U}(19.5)$, interpolation yields a value of $\bar{U}(10)$ to be used in the calculation of τ/ρ and if ρ is known τ. The values are given on page 71 in Table 2. (See footnote, pg. 71).
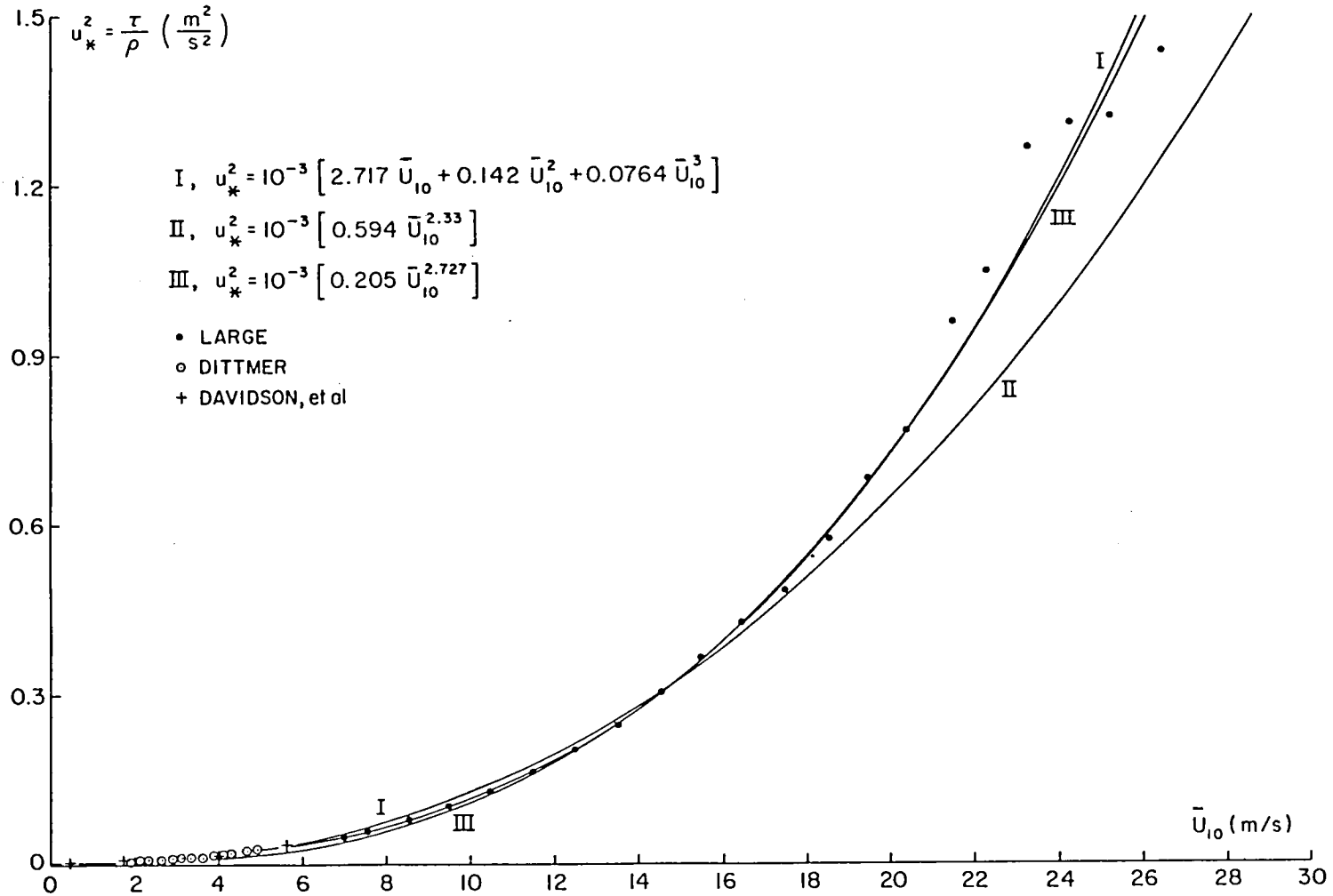
FIGURE 3 u_*^2 Versus $\bar{U}_{10}$ on Linear Scales.
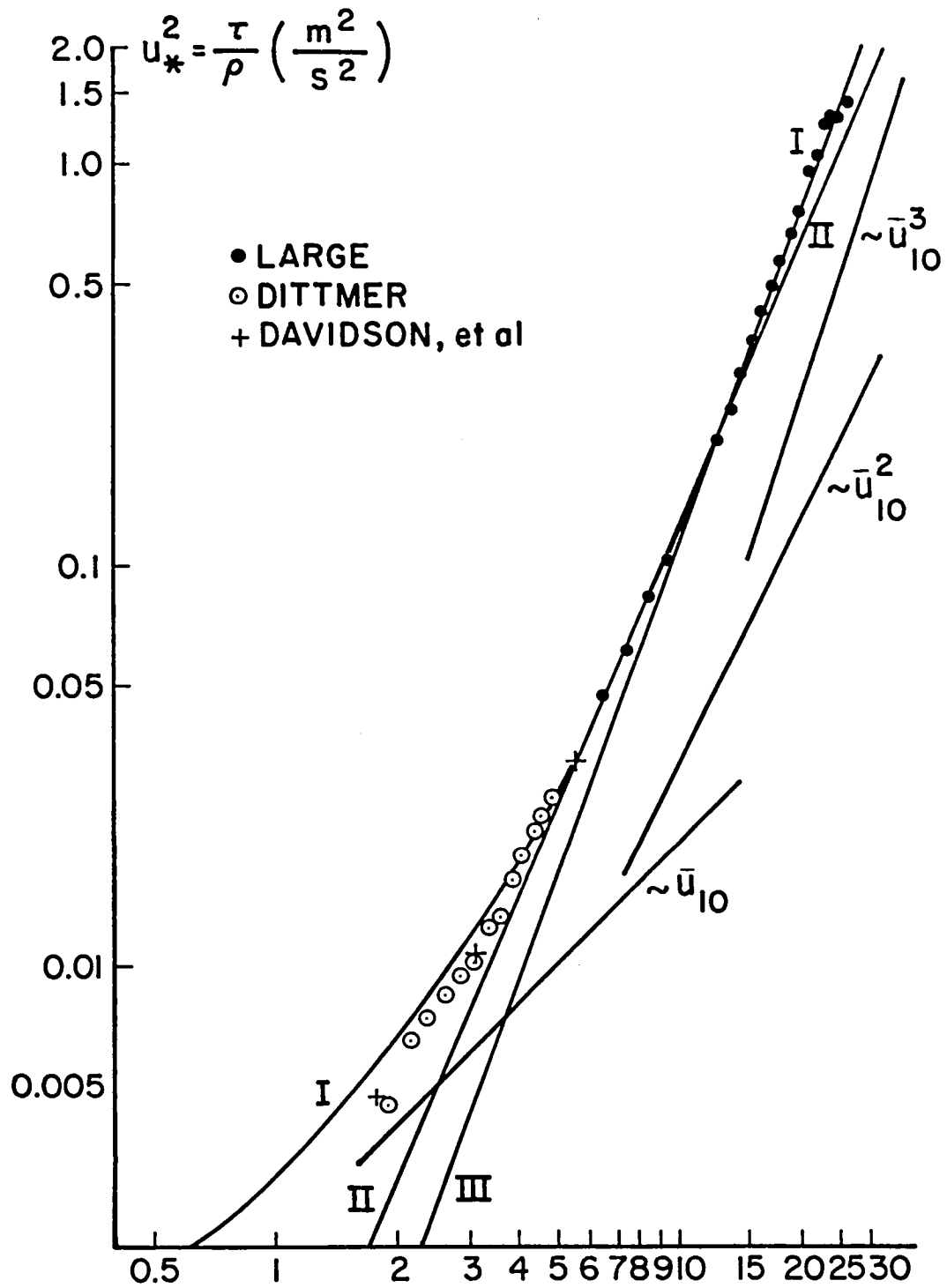
FIGURE 4 u_*^2 Versus $\overline{U}_{10}$ on logarithmic Scales.

THE CALCULATION OF THE STRESS

Given the individual SASS winds scattered over a SEASAT swath, one might consider taking the basic data, reducing the wind to 10 m., calculating the stress and deriving such quantities as the curl of the stress at whatever resolution is available. For many reasons, this line of analysis will lead to dubious results.

Aspects of the difficulty can be illustrated by calculating a super-observation wind stress two different ways. The first is by calculating the stress at each SASS point averaging the stresses, and analysing the statistics, and the second is by using the results of equations (26) to (32) reinterpreting them and calculating the stress and its statistics from the vector averaged winds.

A new coordinate system is needed as a first step. Let two great circles intersect at λ_o, θ_o with one in the direction $\bar{\chi}$ from (26) and the other at right angles to it, and let distance along the first be given by G_1 (degrees) and along the second by G_2 (degrees). A coordinate transformation would be possible as in the divergence analysis as a last step when needed.

The wind from the SASS at any point in the two degree by two degree square would then be represented by (79) and (80).

$$V_{Pi} = U_P(\lambda_i, \theta_i) + \Delta U_i \tag{79}$$

$$V_{Ni} = V_N(\lambda_i, \theta_i) + \Delta V_i \tag{80}$$

where in turn

$$\Delta U_i = \frac{\partial U(\lambda_o, \theta_o)}{\partial G_1} \Delta G_{1i} + \frac{\partial U(\lambda_o, \theta_o)}{\partial G_2} \Delta G_{2i}$$

$$+ t_{1i} \Delta U_m + t_{2i} \Delta U_c \tag{81}$$

and

$$\Delta V_i = \frac{\partial V(\lambda_o, \theta_o)}{\partial G_1} \Delta G_{1i} + \frac{\partial V(\lambda_o, \theta_o)}{\partial G_2} \Delta G_{2i}$$

$$+ t_{3i} \Delta V_m + t_{4i} \Delta V_c \tag{82}$$

In (81) and (82), any residuals from the gradients of the wind from the average values of ΔG_{1i} and ΔG_{2i} can be removed for superobservations as shown by equation (44). The terms ΔU_m, ΔU_c, ΔV_m and ΔV_c have a new meaning and must be interpreted in terms of the analysis given by Pierson (1983a) The terms, ΔU_m and ΔV_m, represent the contribution to a particular SASS wind of the mesoscale variability of the wind for each SASS cell. The terms, ΔU_c and ΔV_c, represent the communication noise error in the measurement made by SASS for each pair of cells. They are in the form of standard deviations to be multiplied by random numbers, t_{1i}, t_{2i}, t_{3i}, and t_{4i}, from zero mean unit variance probability density functions. This random error is a not too well known function of incidence angle, aspect angle, polarization and neutral stability wind speed. For winds near upwind, downwind and cross wind, the communication noise error can be substantial and the mesoscale contribution is a strong function of wind speed. If finite differences are used to calculate divergences over smaller distances with the original SASS winds, the last two terms in (81) and (82) dominate the calculation of the gradients to find differences as opposed to the analysis given previously for a superobservations. The SASS GOASEX data do not provide a way to separate these two effects. Even more discouraging results are obtained when these individual observations are used to obtain wind stress and wind stress curl.

From (79) and (80), the magnitude of the wind at $\lambda_i \theta_i$ is

$$|V_i| = ((U_p(\lambda_i,\theta_i) + \Delta U_i)^2 + (\Delta V_i)^2)^{\frac{1}{2}} \tag{83}$$

and so the magnitude of τ/ρ is

$$\tau/\rho\,(\lambda_i,\ \theta_i) = A|V_i| + B|V_i|^2 + C|V_i|^3 \tag{84}$$

When expanded to second order in ΔU_i and ΔV_i, this becomes (85)

$$\tau/\rho(\lambda_i,\theta_i) = AU_p(\lambda_i,\theta_i) + B(U_p(\lambda_i,\theta_i))^2 + C(U_p(\lambda_i,\theta_i))^3$$

$$+ (A + 2BU_p(\lambda_i,\theta_i) + 3C(U_p(\lambda_i,\theta_i))^2)\Delta U_i$$

$$+ (B + 3CU_p(\lambda_i,\theta_i))\,(\Delta U_i)^2$$

$$+ (B + \frac{3}{2}CU_p(\lambda_i,\theta_i))(\Delta V_i)^2 \tag{85}$$

The squares of ΔU_i and ΔV_i involve terms of the form,

$$t_{1i}^2 \, (\Delta U_m)^2 + t_{2i}^2 \, (\Delta U_c)^2$$

that do not fluctuate about zero and that do not average to zero. Moreover they are amplified at high winds by the wind speed. Individual values of the wind stress calculated from the SASS data thus appear to be somewhat untrustworthy.

If the N winds used to generate the superobservation wind are each used separately, N values of τ/ρ can be obtained and these N magnitudes of τ/ρ can be averaged. The expected value of this average is given by (86) where $U = U(\lambda_o, \theta_o)$.

$$
\begin{aligned}
\mathcal{E}\ (\tau/\rho(\lambda_i, \theta_i)) = {}& A\bar{U}_P + B\bar{U}_P^2 + C\bar{U}_P^3 \\[4pt]
& + (A + 2B\bar{U}_P + 3C\bar{U}_P^2)(\frac{\partial \bar{U}_P}{\partial G_1}\overline{\Delta G_1} + \frac{\partial \bar{U}_P}{\partial G_2}\overline{\Delta G_2}) \\[4pt]
& + (B+3C\bar{U}_P)^2\ ((\frac{\partial \bar{U}_P}{\partial G_1})^2\ \mathrm{VAR}\ \Delta G_1 + (\frac{\partial \bar{U}_P}{\partial G_2})^2\ \mathrm{VAR}\Delta G_2 + 2\frac{\partial \bar{U}_P}{\partial G_1}\frac{\partial \bar{U}_P}{\partial G_2}\ \mathrm{COV}\ \Delta G_1\ \Delta G_2) \\[4pt]
& + (B+\frac{3}{2}C\bar{U}_P)^2\ ((\frac{\partial \bar{V}_P}{\partial G_1})^2\ \mathrm{VAR}\ \Delta G_1 + (\frac{\partial \bar{V}_P}{\partial G_2})^2\ \mathrm{VAR}\Delta G_2 + 2\frac{\partial \bar{V}_P}{\partial G_1}\frac{\partial \bar{V}_P}{\partial G_2}\ \mathrm{COV}\ \Delta G_1\ \Delta G_2) \\[4pt]
& + (B+3C\bar{U}_P)(B+\frac{3}{2}C\bar{U}_P)(\frac{\partial \bar{U}_P}{\partial G_1}\frac{\partial \bar{V}_P}{\partial G_2}\ \mathrm{VAR}\Delta G_1 + \frac{\partial \bar{U}_P}{\partial G_2}\frac{\partial \bar{V}_P}{\partial G_2}\ \mathrm{VAR}\ \Delta G_2 + \frac{\partial \bar{U}_P}{\partial G_1}\frac{\partial \bar{V}_P}{\partial G_2} \\[4pt]
& + \frac{\partial \bar{U}_P}{\partial G_2}\frac{\partial \bar{V}_P}{\partial G_1})\ \mathrm{COV}\ \Delta G_1\ \Delta G_2 \\[4pt]
& + (\Delta U_m)^2 + (\Delta U_c)^2 + (\Delta V_m)^2 + (\Delta V_c)^2 \qquad\qquad (86)
\end{aligned}
$$

Although the average can in theory be corrected by various estimates of the numerous terms that produce a bias, the errors of various kinds in the original SASS data are quite large. Additional terms to third order would introduce even larger effects since the cube of the wind speed is involved. Variability in direction produces even more intricate results.

The variance of the data would be found from $\mathcal{E}(\tau/\rho(\lambda_i, \theta_i) - \mathcal{E}\ \tau/\rho(\lambda_i, \theta_i))^2$ and yields terms involving the squares of ΔU_m, ΔU_c, ΔV_m and ΔV_c multiplied

functions of U, A, B and C. This variance would be reduced by N^{-1} when used in calculations involving the wind stress field but proceeding in this way leads to intricate correction procedures and the need to correct for large effects.

In contrast consider the average wind for the N values around λ_o, θ_o as given by (29) and (30) which could be corrected for the effects of a gradient by finding (45) and its counterpart for $\bar{V}(\lambda_o, \theta_o)$. The standard deviations caused only by the combined effects of mesoscale effects and communication noise could be found from (54) through (57) and returning to vectors parallel and normal to the direction $\bar{\chi}$.

The result would be four numbers at λ_o, θ_o, namely $\bar{\chi}$, and

$$\bar{V}_P = \bar{U}_P(\lambda_o, \theta_o) + t_5 N^{-\frac{1}{2}} \Delta U_{mc} \qquad (87)$$

$$\bar{V}_N = t_6 N^{-\frac{1}{2}} \qquad (88)$$

where the combined residual effects of mesoscale variability and communication noise have been reduced by $N^{-\frac{1}{2}}$ to describe the sampling variability of the mean. Failure to correct for the contribution from the synoptic scale gradients and using the values found at $\lambda_o + \overline{\Delta\lambda}$, $\theta_o + \overline{\Delta\lambda}$ with standard deviations reduced by $N^{-\frac{1}{2}}$ would also give much more stable results.

For a superobservation, substitute (87) and (88) into (85) and the result is (89).

$$\tau/\rho(\lambda_o, \theta_o)_s = A\bar{U}_P + B\bar{U}_P^2 + C\bar{U}_P^3$$

$$+ (A + 2B\bar{U}_P + 3C\bar{U}_P^2) t_5 N^{-\frac{1}{2}} \Delta U_{mc}$$

$$+ (B + 3C\bar{U}_P) t_5^2 N^{-1} (\Delta U_{mc})^2$$

$$+ (B + \frac{3}{2} C\bar{U}_P) t_6^2 N^{-1} (\Delta V_{mc})^2 \qquad (89)$$

Over a two degree field the uncertainty in the value of $\tau/\rho(\lambda_o, \theta_o)$ is greatly reduced by the factor $N^{-\frac{1}{2}}$ and the bias is even more strongly reduced by N^{-1}. Similar effects occur for direction.

It appears to suffice to process the data in an even simpler way for the center of the swath. The superobservation wind data can be reduced to 10 meters instead of the individual winds. The value of $u_*^2 = \tau/\rho(\lambda_o, \theta_o)$ can be found from

$$\bar{\tau}/\rho \ (\lambda_o, \ \theta_o; \ \bar{U}_p) = A \ \bar{U}_p + B \ \bar{U}_p^2 + C \ \bar{U}_p^3 \qquad (90)$$

The variability of the stress in the direction $\bar{\chi}$ can be found from (27), (31) and (30) after correction by (54) to (57) and after correction to 10 meters,

$$\Delta_p(\tau/\rho) = \tau/\rho \ (\bar{U}_p + N^{-\frac{1}{2}} \Delta U_{mc}) - \tau/\rho \ (\bar{U}_p) \qquad (91)$$

The variability normal to $\bar{\chi}$ that would give a vector stress with the same direction as the vector sum of (87) and (88) with $t_5 = 0$ and $t_6 = 1$ is given by (92)

$$\Delta_N(\tau/\rho) = \tau/\rho(\bar{U}_p) \ (\frac{N^{-\frac{1}{2}} \Delta V_{mc}}{\bar{U}_p}) \qquad (92)$$

The stress is represented by

$$\tau/\rho_1(\lambda_o, \theta_o)_{Ps} = \tau/\rho(\bar{U}_p) + t_7 \ \Delta_p(\tau/\rho) \qquad (93)$$

$$\tau/\rho(\lambda_o, \theta_o)_{Ns} = t_8 \ \Delta_N(\tau/\rho) \qquad (94)$$

with orthogonal components in the direction, $\bar{\chi}$ and normal to $\bar{\chi}$. These in turn can be resolved into east-west and north-south components and processed in the same way as the winds.

The curl of the horizontal vector wind stress is found by first multiplying equations (93) and (94) by $\rho(\lambda_o, \theta_o)$ which can be found from the virtual temperature and the atmospheric pressure at the sea surface and then computing the north-south and east-west components of the stress plus the appropriate $\Delta\tau$'s. Values of $\rho(\lambda_o, \theta_o)$ vary about 1.25 kg/m^3. In spherical coordinates,

$$\text{CURL}(\vec{\tau}_h) = \frac{1}{R\cos\theta} \left(\frac{\partial\tau_{(\theta)s}}{\partial\lambda} - \frac{\partial(\cos\theta\,\tau_{(\lambda)s})}{\partial\theta} \right)$$

$$= \frac{1}{R\cos\theta} \left(\frac{\partial\tau_{(\theta)s}}{\partial\lambda} - \cos\theta\,\frac{\partial\tau_{(\lambda)s}}{\partial\theta} + \sin\theta\,\tau_{(\lambda)s} \right) \tag{95}$$

where $\tau_{(\theta)s}$ and $\tau_{(\lambda)s}$ are the north-south and east-west vector components of $\vec{\tau}_s$. If for example

$$\tau_{(\theta)s}(\lambda_o, \theta_o) = \bar{\tau}_{(\theta)}(\lambda_o, \theta_o) + t_9\,\Delta\tau_1 + t_{10}\,\Delta\tau_2 \tag{96}$$

$$\tau_{(\lambda)s}(\lambda_o, \theta_o) = \bar{\tau}_{(\lambda)}(\lambda_o, \theta_o) + t_{11}\,\Delta\tau_3 + t_{12}\,\Delta\tau_4 \tag{97}$$

and so on, the finite difference value of (95) is

$$\text{CURL }(\vec{\tau}_h)_s = \frac{4.5\cdot 10^{-6}}{(\cos\theta_o)} \Bigg(\tau_{(\theta)s}(\lambda_o+1, \theta_o) - \tau_{(\theta)s}(\lambda_o-1, \theta_o)$$

$$- \cos\theta_o\,(\tau_{(\lambda)s}(\lambda_o, \theta_o+1) - \tau_{(\lambda)s}(\lambda_o, \theta_o-1))$$

$$+ 0.0349065\,\sin\theta_o\,\tau_{(\lambda)s}(\lambda_o, \theta_o)) \Bigg\} \tag{98}$$

with dimensions of (newtons m^{-2}) m^{-1}.

Ten different random effects are found in the calculation. The expected value of the curl and the expected value of the variance of the curl are given by (99) and (100) where ten different $\Delta\tau$'s from the five different stresses that are used are needed for (100).

$$\mathcal{E}\ (\mathrm{CURL}\ (\vec{\tau}_h))_s = \frac{4.5 \cdot 10^{-6}}{(\cos\ \theta_o)}\ \left[\ \bar{\tau}_{(\theta)}\ (\lambda_o + 1,\ \theta_o) - \bar{\tau}_{(\theta)}\ (\lambda_o - 1,\ \theta_o)\right.$$

$$- \cos\ \theta_o\ (\bar{\tau}_{(\lambda)}\ (\lambda_o, \theta_o + 1) - \bar{\tau}_{(\lambda)}\ (\lambda_o, \theta_o - 1))$$

$$\left. + 0.0349065\ \sin\ \theta_o\ \bar{\tau}_{(\lambda)}\ (\lambda_o, \theta_o)\right]$$

$$= \overline{\mathrm{CURL}\ (\vec{\tau}_h)} \qquad\qquad (99)$$

$$\mathrm{VAR}\ (\overline{\mathrm{CURL}(\vec{\tau}_h)}) = \frac{2.025 \cdot 10^{-11}}{(\cos\ \theta_o)^2}\ \left[\ (\Delta\tau(\lambda_o + 1,\ \theta_o)_1)^2 + \cdots\right.$$

$$+ (\Delta\tau(\lambda_o - 1,\ \theta_o)_1^2 + (\Delta\tau(\lambda_o - 1,\ \theta_o)_2^2$$

$$+ (\cos\ \theta)^2\ ((\Delta\tau(\lambda_o, \theta_o + 1)_3)^2 + \cdots\ )$$

$$\left. + 1.2184 \cdot 10^{-3}\ (\sin\ \theta_o)^2\ ((\Delta\tau(\lambda_o, \theta_o)_1)^2 + \cdots)\right] \qquad (100)$$

,where $\cdots$ the represents the additional terms needed to complete the full equation,

so that

$$(\mathrm{CURL}\ \vec{\tau}_h)_s = \overline{\mathrm{CURL}(\vec{\tau}_h)}\ + t(\mathrm{VAR}(\mathrm{CURL}(\vec{\tau}_h)))^{\frac{1}{2}} \qquad (101)$$

If the neutral wind profile is assumed to extend to the height, h_2, equation (65) can be rewritten and the result integrated from h_1, very near the sea surface where $W(R_o + h_1)$ is nearly zero at the synoptic scale, to h_2. In the limit, h_1 can be set to zero and the subcript, 2, can be omitted.

$$\int_{R_o + h_1}^{R_o + h_2} \frac{\partial}{\partial R} (R^2 W (R)) dR = - \int_{R_o + h_1}^{R_o + h_2} R \, div_2 \, W_h \, dR \tag{102}$$

Many of the terms that arise and that enter into the finite difference calculation are negligable. Two turn out to be important and are effectively multiplied by terms that are constants as far as the integration is concerned. One is of the form given by equation (103),

$$\int_{h_1}^{h_2} (const_1) \, dz = const_1 \, (h_2 - h_1) \tag{103}$$

and the other is (104)

$$\int_{h_1}^{h_2} const_2 \, \ell n(z/10) \, dz = const_2 (h_2 \, \ell n \frac{h_2}{10} - h_2 - h_1 \, \ell n \frac{h_1}{10} + h_1) \tag{104}$$

By means of equations similar to (27), and following, with the wind reduced to 10 meters and with the standard deviations of the means, values for $\bar{V}_p$, ΔU and ΔV can be found at λ_o, θ_o.

Define

$$u_* = (A\bar{V}_p + B\bar{V}_p^2 + C\bar{V}_p^3)^{\frac{1}{2}} \tag{105}$$

$$\Delta u_{*P} = u_*(\bar{V}_p + \Delta U) - u_*(\bar{V}_p) \tag{106}$$

and $\quad \Delta u_{*N} = u_*(\bar{V}_p) \cdot (\Delta V/V_p) \tag{107}$

Then $\quad V_p(z)_s = \bar{V}_p + \dfrac{u_* \, \ell n \, z/10}{\kappa} + t_1 \, (\Delta U + \dfrac{\Delta u_* \, \ell n \, z/10}{\kappa}) \tag{108}$

$$V_N(z)_s = t_2(\Delta V + \dfrac{\Delta u_{*N} \, \ell n \, z/10}{\kappa}) \tag{109}$$

The terms analogous to (33) to (40) are

$$U(z) = -(\bar{V}_P + \frac{u_* \ell n\ (z/10)}{\kappa})\ \sin\ \bar{\chi}$$

$$= \bar{U}(10) + \delta_1 U)\ \ell n\ z/10 \tag{110}$$

$$\bar{V}(z) = -(\bar{V}_P + \frac{u_* \ell n\ (z/10)}{\kappa})\ \cos\ \bar{\chi}$$

$$= \bar{V}(10) + (\delta_1 V)\ell n\ (z/10) \tag{111}$$

$$\Delta U_1(z) = \Delta U_1 - \frac{\sin\ \bar{\chi}\ \Delta u_{*P}\ \ell n\ (z/10)}{\kappa}$$

$$= \Delta U_1 + (\delta_2 U_1)\ \ell n\ (z/10) \tag{112}$$

$$\Delta U_2(z) = \Delta U_2 - \frac{\cos\ \bar{\chi}\ \Delta u_{*N}\ \ell n\ (z/10)}{\kappa}$$

$$= \Delta U_2 + (\delta_2\ U_2)\ell n\ (z/10) \tag{113}$$

$$\Delta V_1(z) = \Delta V_1 - \frac{\cos\ \bar{\chi}\ \Delta u_{*P}\ \ell n\ (z/10)}{\kappa}$$

$$= \Delta V_1 + (\delta_2 V_1)\ \ell n\ (z/10) \tag{114}$$

$$\Delta V_2(z) = \Delta V_2 + \frac{\sin\ \bar{\chi}\ \Delta u_{*N}\ \ell n\ (z/10)}{\kappa}$$

$$= \Delta V_2 + (\delta_2 V_2)\ \ell n\ (z/10) \tag{115}$$

The appropriate terms, all of which can be found for each grid point in the field, can be substituted into (71). After integration of (102) and simplification by the results implied by (103) and (104), the final result is equation (116), where the subscript on h_2 has been dropped. The ΔU's and so on, need to be found at the correct latitudes and longitudes.

$$w(h)_s = \frac{-4.5 \cdot 10^{-6} h}{\cos\ \theta_o}\left[\bar{U}_{10}(\lambda_o + 1,\ \theta_o) + \delta_1 U(\lambda_o + 1, \theta_o) \cdot (\ell n \frac{h}{10} - 1)\right.$$

$$\left. - \bar{U}_{10}(\lambda_o - 1, \theta_o) - \delta_1 U(\lambda_o - 1, \theta_o) \cdot (\ell n \frac{h}{10} - 1) + t_1(\Delta U_1 + \delta_2 u_* (\ell n \frac{h}{10} - 1))\right)$$

39

$$+ t_2(\Delta U_2 + \delta_2 U_2(\ln\frac{h}{10} - 1)) - t_3(\Delta U_1 + \delta_2 U_1(\ln\frac{h}{10} - 1))$$

$$- t_4(\Delta U_2 + \delta_2 U_2(\ln\frac{h}{10} - 1))$$

$$+ \cos\theta_o(\bar{V}_{10}(\lambda_o, \theta_o + 1) + \delta_1 V(\lambda_o, \theta_o + 1)(\ln\frac{h}{10} - 1)$$

$$- \bar{V}_{10}(\lambda_o, \theta_o - 1) - \delta_1 V(\lambda_o, \theta_o - 1)(\ln\frac{h}{10} - 1) + \cdots)$$

$$+ 0.0349065 \sin\theta_o(\bar{V}_{10}(\lambda_o, \theta_o) + \cdots) \Bigg] \tag{116}$$

At h = 200 meters, $\ln\frac{h}{10} - 1$ is 2.0 and (117) becomes (118) in ms^{-1}.

$$w(200)_s = \frac{-9 \cdot 10^{-4}}{\cos\theta_o} \Bigg[\bar{U}_{10}(\lambda_o + 1, \theta_o) + 2(\delta_1 U(\lambda_o + 1, \theta_o)) + \cdots$$

$$+ \cos\theta_o(\bar{V}_{10}(\lambda_o, \theta_o + 1) + 2(\delta_1 V(\lambda_o, \theta_o + 1) + \cdots$$

$$+ 0.0349065 \sin\theta_o(\bar{V}_{10}(\lambda_o, \theta_o) + 2\delta_1 V(\lambda_o, \theta_o))$$

$$+ \cdots) \Bigg] \tag{117}$$

As in preceding analyses,

$$w(200)_s = \bar{w}(200) + t \Delta\bar{w}(200) \tag{118}$$

which can be evaluated in a way exactly similar to previous results.

As a note in passing, there is not much difference between (105), (106) and (107) and (90), (91) and (92). The computation of errors for the specific application is made simpler by the choice that was made. From

$$u_* + \Delta u_* \cong (u_*^2 + (\Delta u_*^2))^{\frac{1}{2}} = u_*(1 + (\Delta u_*^2)/u_*^2)^{\frac{1}{2}}$$

$$\cong u_*(1 + (\Delta u_*^2)/2u_*^2) = u_* + (\Delta u_*^2)/2u_* \tag{119}$$

it can be seen that two different ways to find Δu_* yield nearly the same quantity.

INDEPENDENCE AND COVARIANCES

The reasons for the variability of one SASS pair of backscatter values compared to another pair are basically uncorrelated and random. The mean wind speed and the mean direction for a superobservation are perturbed by two independent and uncorrelated random effects, one parallel to the wind and one normal to it. A correlation becomes evident when resolving the super-observation into east-west and north-south components. A superobservation has been based on data from a 2° by 2° square, and once the effect of synoptic scale gradients are removed (which involves SASS values scattered randomly over the square from as far away as $\lambda_0 \pm 2$ and $\theta_0 \pm 2$), the estimate of the standard deviation of the mean is based on a sample of independent random variables. The choice of grid point spacing for superobservations for future systems remain a matter to be investigated and is a function of the model to be used and of the scatterometer that obtained the data. A very coarse resolution model in the horizontal would require a more careful treatment of gradients.

The use of overlapping squares at a one degree resolution introduces correlations between the estimates of the winds and the standard deviation of the variability simply because the same values are used in different estimates. Every other grid point in the east-west or north-south direction is independent and those located diagonally (for example, λ_0, θ_0 to λ_0+1, θ_0+1) are weakly correlated. Smoothness in the wind field can be judged by inspecting every other point in the grid.

For the calculation of the divergence, the vertical velocity at h and the curl of the wind stress, the analysis becomes more complex. Some particular SASS speeds and directions can make contributions to the means plus standard deviations of three of the five terms that enter into the calculation. (The additional complexity introduced by (45) is not considered).

Equations (69) and (118) are essentially statistics formed from a linear weighted combination of the original data. Equation (100) is a pseudo-linearized plus non linear weighted combination of the original data.

Correlations do not do much damage in the estimation of means, but they can affect estimates of variances and standard deviations. The contribution of a particular SASS value to the final estimate of the divergence can be traced through the entire analysis. The value for the difference between two estimates of the east-west component so as to find $\partial U/\partial\lambda$ is calculated from completely different east-west components of the SASS values and thus the numbers on which the estimate is based are independent. The north-south difference so as to find $\partial V/\partial\theta$ is based on completely different north-south components of the SASS values weighed by a cosine and are also found from completely different values and thus the estimate is based on independent data.

For the calculation of the divergence as in (69) and quantities such as (101) and (119), the full expression is, however, somewhat more complicated and merits a more complete analysis. In Figure 1, the one degree squares that contain SASS values that enter into the evaluation of (74) are numbered from one to twelve. The values of $\bar{U}$ (λ_o, θ_o) and $\bar{V}$ (λ_o, θ_o) (and so on) are partially obtained from SASS values in squares 4, 5, 8, and 9. The wind for the point, λ_o, θ_o, was represented by equations (60) and (61). Let N equal $N = N_4 + N_5 + N_8 + N_9$, and then the term $\sum_1^N t_i \, \Delta U_i'$ can be represented by (120).

$$\sum_1^N t_i \, \Delta U_1 \approx \sum_1^{N_4} t_{i,4} \, \Delta U_{1,4} + \sum_1^{N_5} t_{i,5} \, \Delta U_{1,5} + \sum_1^{N_8} t_{i,8} \, \Delta U_{1,8} + \sum_1^{N_9} t_{i,9} \Delta U_{1,9} \quad (120)$$

where the t's on the RHS are independent and the second subscript represents the one degree square containing the SASS value. The expected value of each side is zero and the expected value of the square of each side is

$$\mathcal{E} \left(\sum_1^{N_4} t_{1,4} \, \Delta U_{1,4} + \sum_1^{N_5} t_{1,5} \, \Delta U_{1,5} + \sum_1^{N_8} t_{1,8} \, \Delta U_{1,8} + \sum_1^{N_9} t_{1,9} \, \Delta U_{1,9} \right)^2$$

$$\approx 4 \left(\frac{N}{4} \, (\Delta U_1') \right)^2 \quad (121)$$

where the assumption that the error properties are the same in all four squares is made.

All of the contributions from each of the squares numbered in Figure 1 can be identified by a double subscript notation as above. The analysis can

42

be carried through keeping track of the dependence of $\Delta U_1'$ and $\Delta V_1'$ and of $\Delta U_2'$ and $\Delta V_2'$ throughout the finite difference calculation.

The contribution to the divergence from squares, 4, 5, 8 and 9 come from terms involving the gradients of U_s and V_s and the value of V_s at λ_o, θ_o. For the $\Delta U_1'$ and $\Delta V_1'$ terms in (60) and (61) a part of their contribution can be represented by (122) where α' is the coefficient of the sine term in (67).

$$
\begin{aligned}
\text{Contribution} = \ & t_{1,5} \, N_5^{-\frac{1}{2}} \, (\Delta U_{1,5}' + \cos \theta_o \, \Delta V_{1,5}' + \alpha' \sin \theta_o \, \Delta V_{1,5}') \\[6pt]
& + t_{1,4} \, N_9^{-\frac{1}{2}} \, (\Delta U_{1,9}' - \cos \theta_o \, \Delta V_{1,9}' + \alpha' \sin \theta_o \, \Delta V_{1,9}') \\[6pt]
& + t_{1,4} \, N_4^{-\frac{1}{2}} (-\Delta U_{1,4}' + \cos \theta_o \, \Delta V_{1,4}' + \alpha' \sin \theta_o \, \Delta V_{1,4}') \\[6pt]
& + t_{1,8} \, N_8^{-\frac{1}{2}} \, (-\Delta U_{1,8}' - \cos \theta_o \, \Delta V_{1,8}' + \alpha' \sin \theta_o \, \Delta V_{1,8}') \qquad (122)
\end{aligned}
$$

The expected value of this contribution to the divergence is zero. The expected values of $t_{1,5}^2$, $t_{1,9}^2$, $t_{1,4}^2$ and $t_{1,8}^2$ are one. The squares of the terms in parentheses give the terms found in (73) subject to the reasonable assumption of (121), and what it implies, plus six cross product terms. The signs of the cross products terms are such that one of two similar terms has a positive sign and one has a negative sign. The cross correlation between $\bar{U}$ and $\bar{V}$ when estimated from scattered SASS values will consequently cancel out and be close to zero in the estimate of the variability of the divergences as in (73). Although the terms in (71) as identified by t_1 to t_{10} are not strictly independent, this analysis shows that (68) and consequently (69), is essentially correct. The same conclusions are also valid for (99), (100), (101), (116), (117) and (118).

The SASS data clustered around a value for λ_o, θ_o at the edge of the swath would usually have a smaller number of observations and values of $\overline{\Delta\lambda}$ and $\overline{\Delta\theta}$ that could not be reduced to small values of typically $\pm$ 0.07 by the methods described by (22) to (24). If $|\Delta\lambda|$ and $|\Delta\theta|$ were not both less than 0.5, the data were discarded. Moreover the precedures given in (44) and (51) for removing the effects of gradients and of transferring the values at $\lambda_o + \overline{\Delta\lambda}$ and $\lambda_o + \overline{\Delta\theta}$ to λ_o, θ_o cannot be applied unless the data for a point also have data for the four points to the north, south, east and west.

The recovery of these points for use in the finite difference calculation of the divergence and wind stress curl, even if some accuracy is lost, is worthwhile. This is accomplished by the use of two points toward the interior of the swath to form a triangle in the local λ, θ plane, say, for example,

Point 1, $\quad (\lambda_o + \Delta\lambda_o, \quad \lambda_o + \Delta\theta_o) = (\Delta\lambda_o, \Delta\theta_o)$

Point 2, $\quad \lambda_o + 1 + \Delta\lambda_1, \quad \theta_o + \Delta\theta_1 \quad = (1 + \Delta\lambda_1, \Delta\theta_1)$

Point 3, $\quad \lambda_o + 1 + \Delta\lambda_2, \quad \theta_o - 1 + \Delta\theta_2 = (1 + \Delta\lambda_2, - 1 + \Delta\theta_2)$

where point one is the edge point.

Associated with each point is an east-west and north-south component of the averaged wind at each point, say U_1, U_2, U_3 for the east-west components. $U = U(\lambda,\theta) + C_1 + C_2\lambda + C_3\theta$ can be found to fit the three values of U at the three points, and then C_1 at λ_o, θ_o is the desired value for the east-west component at the edge point. Similar results can be found for V. The result is a vector wind for an edge point. The standard deviations for V_p and V_N, or the four components, are transferred without an attempt at correction for gradient effects to the integer latitude longitude edge point.
These points with associated value can then be used in (44) and (51) for interior points of the swath, and the desired fields for divergence and curl for the interior points. The penalty is a larger value for the standard deviations of the estimates near the swath edges (no corrections for gradients and smaller values of N). The gain is a wider swath.

SUMMARY OF DATA PROCESSING METHODS

The moving two degree by two degree overlapping "square" on the sphere of the Earth is a somewhat smoothed two dimensional "box car" window in the spatial domain. It is not quite "square" because of the deletion of values near the edges, especially the corners, so as to make $\overline{\Delta\lambda}$ and $\overline{\Delta\theta}$ closer to zero. Since the data points are unevenly scattered over the "square", the statistical properties of the scatter in the location of the points are needed so as to be able to make the final corrections to the estimates of the synoptic scale properties.

This data processing procedure effectively suppresses most of the errors that result from communication noise and mesoscale variability effects by mean of two-dimensional wave number filters because both of these contributions are white noise for wavenumbers higher than that corresponding to twice the grid spacing. East-west wavelengths shorter than 2° of longitude at a given latitude and north-south wave lengths shorter than 222 km are effectively removed in much the same way as an average over time removes the higher frequencies in a signal.

Both the mesoscale variability and the errors of the SASS estimate itself vary from one part of the field to the other, and it is not possible to separate one from the other, except to note that for some wind directions the SASS estimate can be highly variable, especially in direction as a result of the form of the model function.

The final estimates of the synoptic scale winds at the desired grid locations still have sampling variability errors, but much of the non-synoptic scale two dimensional noise has been removed by spatial filtering. The final wind at each grid point is very close to being the "true" synoptic scale wind at that grid point, and the synoptic scale gradients in the values of the wind components have been preserved by the process.

Moreover, the steps in the analysis of the data carry along the statistical properties of the scatter of the individual SASS winds in terms of estimates of the variances that result from mesoscale and communication noise. As derived, these values become especially important in the finite difference calculation of the divergence and the wind stress curl. Differences between two large

45

and nearly equal quantities, each with a fairly large standard deviation, can result in estimates of gradients that are small at some places in the field and that have such large standard deviations that even the sign of the difference may not be known.

There is one weakness in the preceding derivations that should be pointed out. Equations (1) through (21) are results available from any text on probability and statistics. However, (21) is correct only if the true population parameter value of Δu is known. In our analysis, to proceed at all, the estimates of these variances and standard deviations have replaced the unknown population parameters.

The difficulty is that these estimates are not as close as one would like to the desired population parameter. They are themselves random variables with considerable scatter.

For very small samples from a normal pdf (and normality is not a necessary assumption for this analysis), roughly under 30, the mean has a student t pdf and the estimate of the variance is Chi Square distributed with N-1 degrees of freedom. When large volumes of data are processed such as for the SASS, and its successors, an average of one out of ten variance estimates will be outside the 90% Chi Square confidence interval. Pierson (1983a) has treated aspects of this part of the analysis of superobservations (See page 1703) with the further assumption that the random variability is normally distributed.

Since these unknown variances are themselves variable from one part of the field to another, it is not presently possible to proceed to more complex levels of statistical data analysis in the study of SASS winds. The analysis is, in a sense, closed at one level of complexity by the replacement of the unknown population parameter by its estimate. The results to follow are internally consistent insofar as the various fields that are obtained. They also yield some rather surprizing results from the point of view of synoptic scale analyses.

To illustrate the variability of sample size for a superobservation, Figure 5 shows a bar graph with sample size on the horizontal axis and number of occurrences on the vertical scale for the data for REV 1141, which is typical. Sample sizes range from a low of 6 to a high of 48. The distribution,
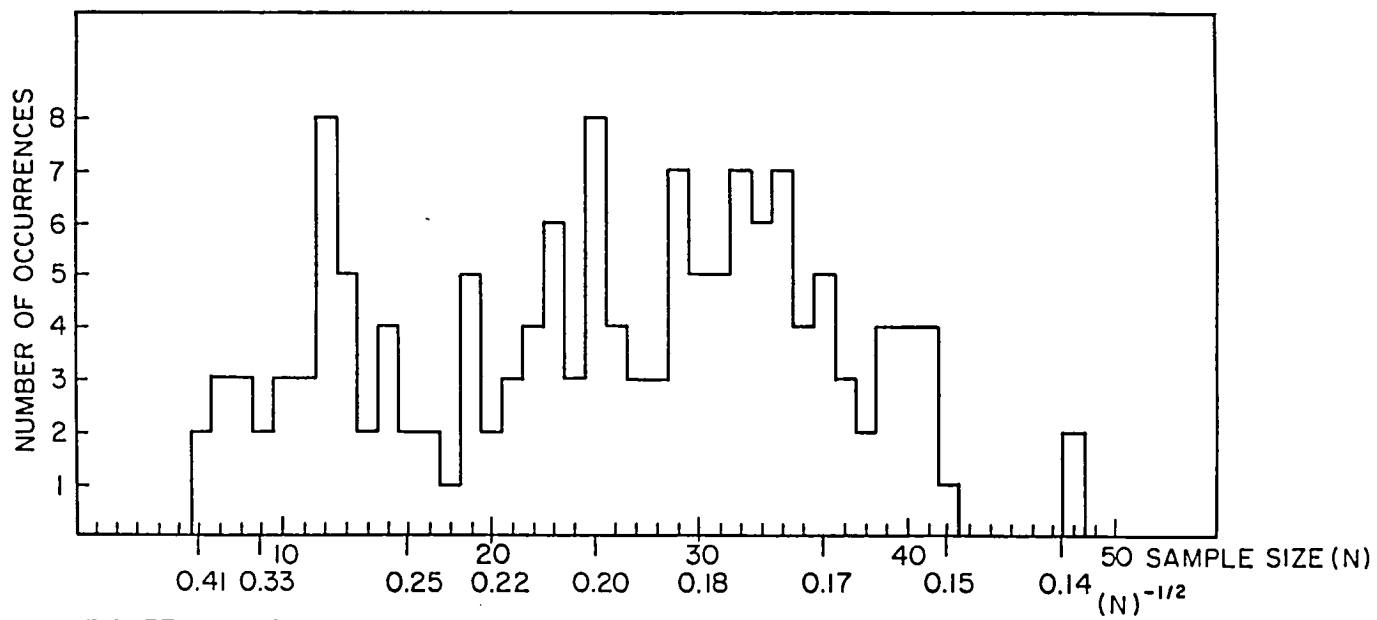
FIGURE 5. HISTOGRAM OF SAMPLE SIZES FOR REV 1141

47

with some imagination, appears to be bi-modal with one group ranging from 6 to 18 and the second from 19 to 48. The first group is associated with the edges of the swath (and the other complications introduced by edges), whereas the second group is associated with the central part of the swath.

Also shown below the value of N is the value of $N^{-\frac{1}{2}}$. As assumed, a sample size greater than 16 reduces the standard deviation of the mean to 25% of the standard deviation of the sample of SASS winds.

The results obtained above, and derived in particular for the study of the SEASAT SASS data, can, in principle, be applied to any set of wind estimates (measurements) with the properties that (1) there are many more measurements than needed to define the winds for a given resolution, (2) that the measurements all have the same underlying causes for their "errors" and sampling variability effects, and (3) there are no biasses in the measurements that were the result of calibration errors for the measurement system. These procedures will perform in much the same way for any future scatterometer systems, including the one planned for NROSS.

The GOASEX experiment attempted to compare the SEASAT-SASS data with its inherent sources of variability, which result from communication noise and mesoscale variations in the winds, with conventionally measured winds that form an inhomogeneous data set with (1) a large number of different sources for actual errors and biasses (2) a usually much larger contribution from mesoscale variability and (3) large separations between the relatively few available measurements from which to try to obtain an analysis at the desired scale.

Procedures for the use of conventional synoptic scale observations have been developed by many different meteorological centers for the purpose of preparing the initial value update for a synoptic scale computer based numerical weather prediction at various resolutions, depending on the available resources and the area of the earth covered by the model. A global synoptic scale model at a one degree horizontal resolution with, say, comparable vertical resolution is not quite within the capability of present systems. However, such a resolution is conceivable within the next decade.

Whether or not a model with such a resolution would give improved forecasts in the one to three day range given only the conventional data is a debatable point. The sparceness of the conventional data, especially over the ocean, plus their wide variation in accuracy, when combined with the present procedures for initial value specification all combine to produce such large errors in the initial value specification that it is very much to be doubted that any noticeable improvement would be found at two to three days.

A single isolated ship report in a oceanic area five degrees of longitude by five degrees of latitude with all of its inherent sources of error (Pierson (1983a)) can influence a very large area of the ocean, even outside of the five degree by five degree area. If the report is so much in disagreement with the first guess initial value specification (a forecast from a past initial value update) that it is disregarded, it does no good (or harm) at all. If it differs from the first guess, and is wrong and is used to correct the first guess, the update is wrong. If it is wrong and agrees with the update, the update is, nevertheless, still wrong. Given the sources of error introduced by Beaufort reports and the conventional two minute averages for transient ships discussed by Pierson (1983a), one can hardly dare to hope that a given planetary boundary layer initial value specification is correct to within the limits described by Brown et al. (1982). With an incorrect wind field, an incorrect specification of the sea surface atmospheric pressure field, and probably the thermal wind for the first few kilometers, the correct specif- ication of the entire atmospheric column, even with remote soundings from spacecraft, becomes doubtful.

The analyses of four GOASEX orbit segments that extend, for northbound passes, from about 30° N to landfall demonstrate in a most convincing way the value of scatterometer data for producing highly accurate synoptic scale values by means of superobservations. The results are so different from what would be deduced from the presently available procedures for the analysis of sparce conventional surface data that one wonders whether or not the present conventional methods come close to representing what actually happens over the oceans. The discussion of the results obtained for these "REVS" will highlight the differences that are evident compared to conventional analyses.

Within the coming decade, remote sensing systems can become capable of providing the information needed for improved meteorological forecasts, a start at understanding and predicting the ocean circulation, and a better data base for air-sea interaction effects in their widest sense. The entire atmospheric column affects the oceans, if for no other reasons than the presence or absence of clouds at their full range of heights above the sea surface, their thicknesses and their importance in the tropics for raising water vapor to great heights in maritime tropical air masses.

50

The sea surface temperature through cloud free skies can now be measured accurately by infrared methods (Strong and McClain (1984)). There may be ways that atmospheric sounding systems can be improved so as to, perhaps, identify inversions and measure the temperature of the air in contact with the ocean. Passive microwave methods, despite all of their inherent difficulties may provide sea surface temperatures for ocean areas nearly always cloud covered.

Scatterometers will measure the winds (with essentially no ambiguities) at resolutions far in excess of those needed for the synoptic scale. Such measurements will most of the time have errors because of communication noise that will obscure the mesoscale variations. Over most of the ocean most of the time, there will be no need to resolve the mesoscale variability. Only its correct incorporation into the model as a contribution from turbulence will be needed. Meteorologists and oceanographers may cease to be so rigid as to what defines either a meteorological spacecraft or an oceanographic spacecraft, and some future system may carry both a scatterometer and an atmospheric sounding system to the mutual advantage of both.

Improved models will be needed to supercede the present Monin-Obukhov (1953) theories. Tchen (personal communication) has identified some incorrect assumptions in that theory, and an improved theory is possible. Turbulence is treated inadequately in the present numerical forecasting models for the higher layers of the atmosphere. Here again improvements are possible, (Tchen, personal communication).

Measurements of the winds, even with fairly large communication errors, at the mesoscale will be useful near fronts over the ocean, in extratropical cyclones, where wind gradients will be so large that the communication noise error will be relatively less important, around islands and land sea boundaries with complex shapes, and for the first several hundred kilometers offshore from land where the solenoidal field is particularly strong and favors frontogenesis and cyclogenesis.

Brown (1983) has shown how well the SEASAT-SASS could locate fronts over the JASIN area. In our study, no attempt to treat the possibility of the presence of a front in a two degree by two degree square was made. For winds with ambiguities removed, and a front correctly located, our procedures would yield a compromise direction, depending on the location of the front within

the square, and larger values for the variability about the mean.

Most numerical forecasting systems ignore fronts, probably to their detriment. Present integration schemes for prediction would obliterate them even if they were put into the initial value specification. The sloping frontal surface in the atmosphere is also usually lost because of the coarse vertical resolution. Fairly elementary techniques for the location of fronts by means of scatterometer winds at 25 to 50 km resolution such that the front could be located as a curved line within a distance of five to twenty kilometers normal to the line could be developed. The basis would be to define a line crossing a two degree "square" and making "yes-no" tests of whether or not the wind direction changed by more than that indicated by the analysis described above as a result of sampling variability, when compared to an area known to be on one or the other side of the front.

Strictly, divergence should be found only within an air mass and not calculated across a front. The curl of the wind stress across a front may be considerably larger than any of the values found in our analysis for much the same reason.

Conventional observations will still be needed. The developing global data buoy network can provide improved winds by obtaining ten minute averages six times an hour, measuring the atmospheric pressure at the time of the spacecraft passage, and reporting air and sea surface temperatures. Various parameters related to turbulence could also be of value to more modern boundary layer theories. Air temperature and sea surface atmospheric pressure will still be of great value from transient ships. The effort involved to get them to measure winds correctly and to calibrate each ship would be extensive.

Inexpensive drifting buoys that reported only water temperature and sea surface atmospheric pressure, along with their location, proved to be of great value in the Southern Hemisphere for somewhat improved meteorological forecasts and for the study of ocean currents. A sufficient number of these buoys located in oceanic data sparce areas would be of great value in a total system, especially if their reports were made to a spacecraft carrying a scatterometer and an atmospheric sounder as it passes near-by as well as at synoptic times.

The volume of data that would be available from the systems described

above is large even for a scatterometer alone. (Boggs (1982)). However, it can be processed and used on a real time basis.

One very difficult problem, nevertheless, remains. It is the problem of asynoptic four dimensional data assimilation in a real time system. Until it is solved remote sensing from spacecraft such as SEASAT will not reach its full potential. Sylvester (1983) has identified the kinds of errors that result from using a plus or minus three hour data window so as to force remotely sensed data into the six hourly synoptic report straight jacket.

Asynoptic data assimilation methods have been used experimentally and are under development for further experiments. Examples of recent papers on this subject are those of Atlas (1981), Atlas, et al. (1981), Cane, et al. (1981) Ghil, et al. (1979), and Pierson (1979).

Operational models (that we know about) do not presently have the four-dimensional data assimilation ability. One reason seems to be that the new initial value specification excites unwanted and incorrect internal gravity wave modes that take many hours (real time) to dissipate. The belief seems to be that asynoptic assimilation will enhance even more these unwanted modes and cause the model to behave unrealistically. The possibility that the new kinds of data could produce initial value specifications at the end of a twelve hour cycle that would be so nearly correct that these internal wave modes would be greatly reduced has not been investigated.

The difficulties that may arise with the use of the newer spherical harmonic procedures for specifying constant pressure surfaces, although conceptually an improvement at a synoptic time, have not been considered with reference to asynoptic data assimilation. Such representations seem to be at cross purposes insofar as the use of remotely sensed data is concerned.

PROGRAMS, DATA TAPES, DATA LISTINGS AND
CONTOURED RESULTS

The de-aliases SASS winds, as mentioned before, are available from
the NASA Langley Research Center. The format and a sample from one of
the orbit segments are given at the start of this report. The programs
that were used and a listing of the final results for this study are
given in an appendix. A data tape has also been prepared that gives the
final results at each latitude and longitude for each of the four "REVS"
that were analysed. These were REVS 1141, 1183, 1212 and 1298. The data
tape and the programs used are the primary source for anyone wishing to
study these results in other ways. They can be made available. The
listings are a secondary source and can be used for numerous studies.
The figures to follow are a tertiary source.

The analyses have been made from data plotted by hand, analysed and
contoured by hand, and drafted by hand. Other analyses would be possible
if done by another analyst. The various objective computer based contouring
procedures, especially if the known uncertainties for each value were used
to smooth and/or refine the contouring procedure, might each reveal other
interesting features.

RESULT FROM THE PRELIMINARY DATA PROCESSING PROCEDURES

The next 11 figures, Figures 6 through 17, show examples of results obtained after the data had been processed up to a certain point. All projections are more or less polar stereographic, but they are not necessarily true scale at some particular latitude. They are based on the analysis of superobservations located at $\lambda_o + \overline{\Delta\lambda}$, $\theta_o + \overline{\Delta\theta}$ consisting of vector wind fields, and $\vec{u}_*^2$ fields, plus associated statistics. The values have not been moved to integer values of latitude and longitude, the effects of gradients have not been taken out of either the winds or the $\vec{u}_*^2$ values. Values at the edges have not been relocated at integer latitude-longitude values. The results at this stage are consequently not quite ready for the calculation of the divergence and the wind stress curl.

Figures 6 through 8 are for REVS 1141, 1183 and 1298. The winds are plotted as the feathers of wind vectors (from which in the conventional meteorological way) except that the length of the barb is fractionally related to wind speed. One full barb corresponds to 10 m/s. Circled points are for less than 2 m/s. The dots represent the location ($\lambda_o + \overline{\Delta\lambda}$, $\theta_o + \overline{\Delta\theta}$) of each superobservation. They are clearly not exactly at integer values of latitude and longitude. They are a few values north of 55° N for 1141, which are not shown. Especially at the edges of the swath, the departures from the integer latitude-longitude values are substantial.

The SEASAT-SASS swath had many peculiarities. It is widest toward the poles and narrowest near the Equator. The distance along a latitude circle at 55° N for a one degree longitude change is about 64 km. whereas at 35° N it is about 91 km. Moreover blank areas can frequently cut across a swath during a calibration cycle. The combined effect for a latitude-longitude grid can produce a narrow width as at 38° N and about 5 superobservations along 32° N contrasted to seven at 54° N as in Figure 6 (REV 1141).

Figure 7 for REV 1183 is the only one of the four GOASEX passes analysed in this set that merited the analysis of the results obtained by switching to a V pol mode for both sides of the spacecraft. East north easterly winds south of 35° N are shown in the easternmost swath which continue in the westernmost portion, turn to south westerly and then southerly winds by the time the field reaches 40° N.
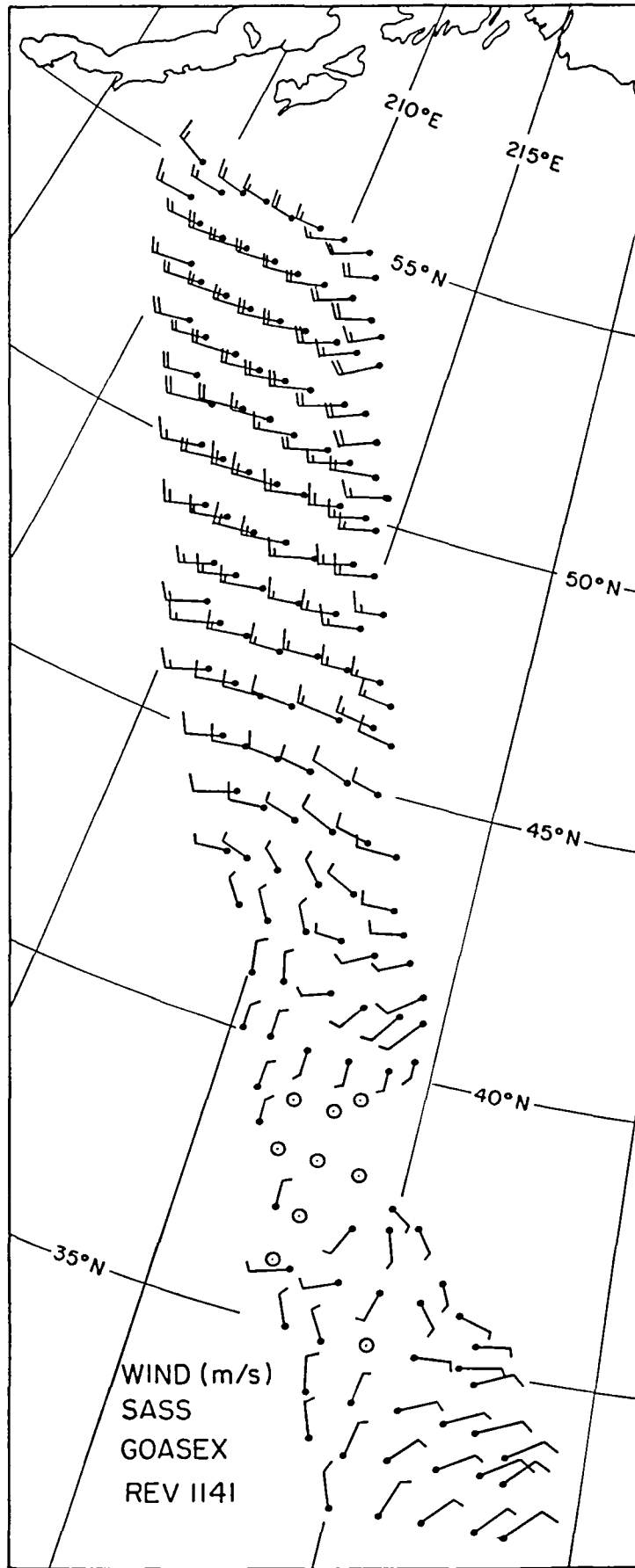
FIG. 6 Preliminary Analysis of REV 1141. Full Barb
is 10 m/s. Circles less than 2 m/s.
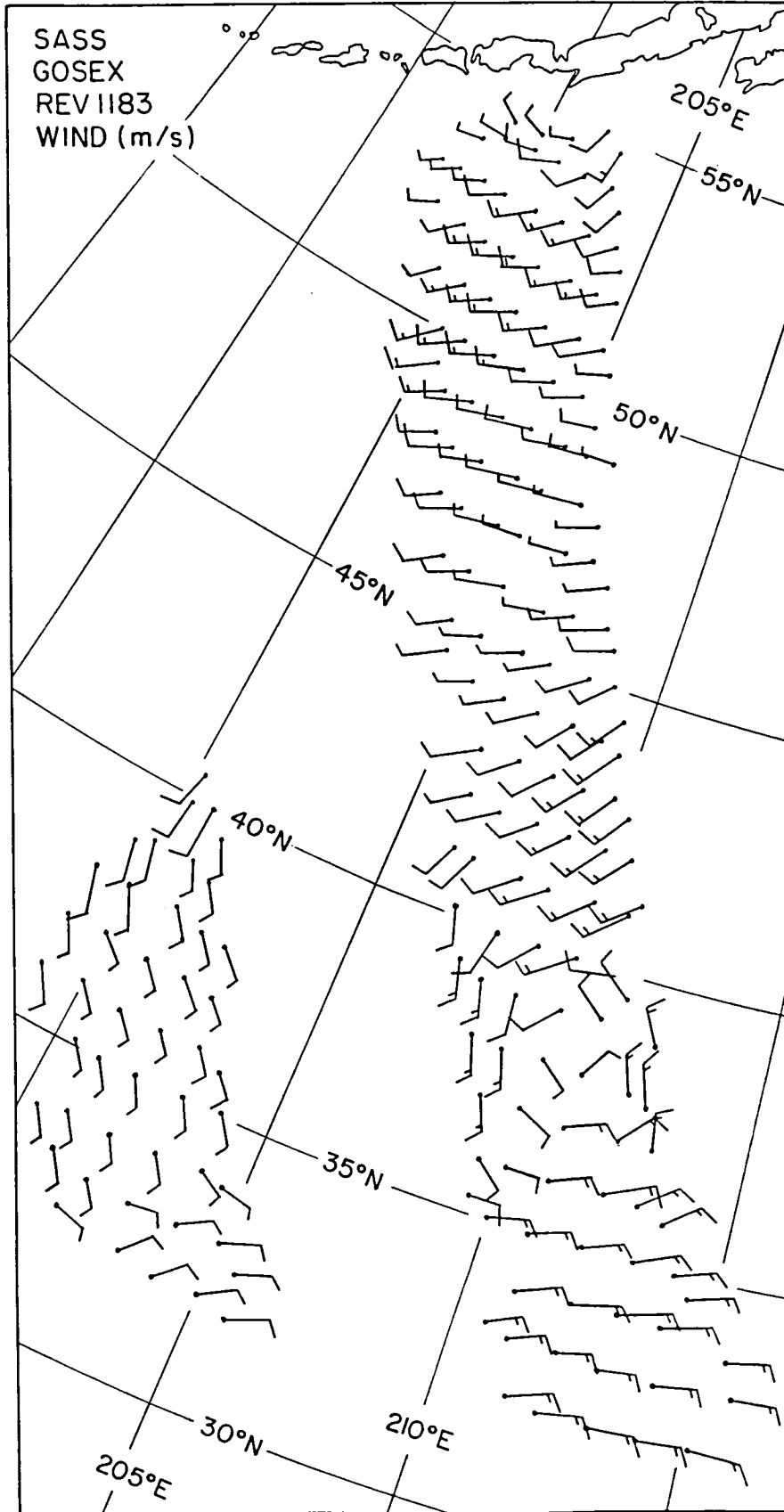
FIG 7 Preliminary Analysis of REV 1183. Full Barb is 10 m/s. Circles less than 2 m/s.
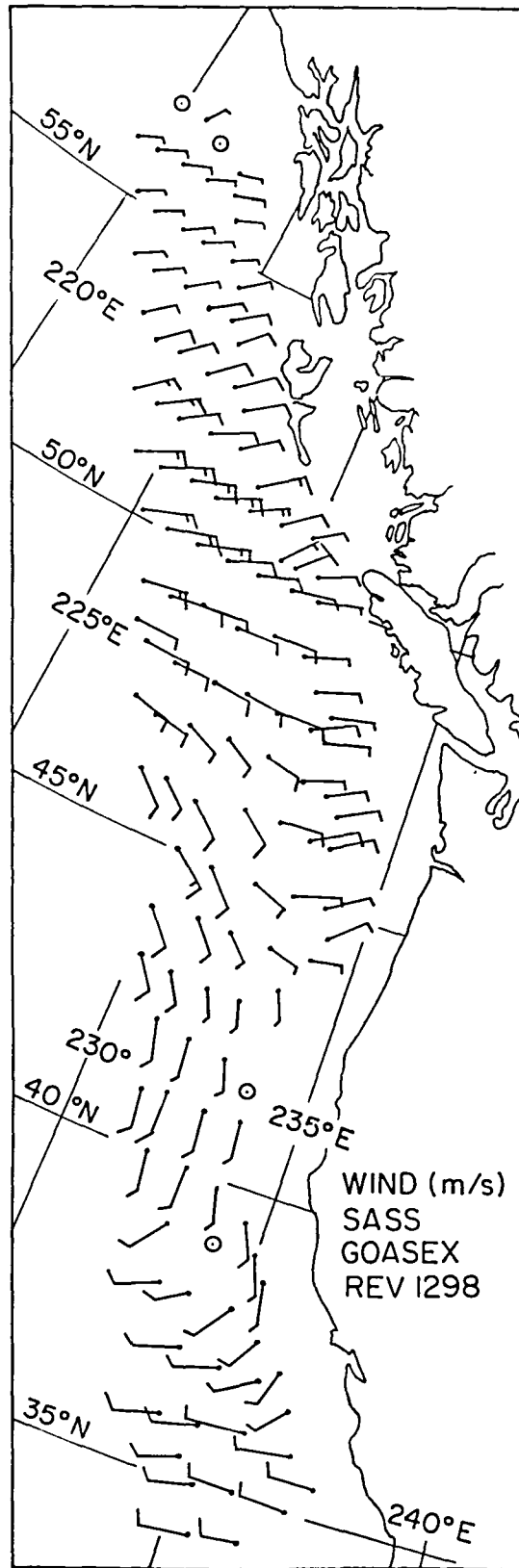
Fig. 8   Preliminary Analysis of REV 1298.   Full Barb
is 10 m/s.   Circles less than 2 m/s.

In Figure 8, the winds are all easterly to southerly north of 40° N. The light winds and the two circled dots near the **center** north of 55° N are near a high pressure center. This is an interesting field of flow for what are supposedly the prevailing westerlies.

Figures 9, 10 and 11 show expanded areas of the previous swaths (1141, 1183 and 1298) so as to illustrate the value of even uncorrected super-observations. Although drafted in slightly different ways, each figure shows the vector toward which direction of the wind plus four numbers. The first is the number (N) of SASS winds averaged to find the super-observation. The second is the magnitude of the wind vector in the direction shown. The length of the drafted vector is proportional to the wind speed. The third is the standard deviation of the individual SASS winds in the direction of the wind vector for the (N) SASS values that were combined to produce the superobservation. The last number is the standard deviation of the individual (N) SASS winds normal to the direction that is shown. The vector averages in these examples all form a smooth field of flow.

At 55° N 210° E in Figure 9 (REV 1141), 25 SASS winds were combined to obtain a superobservation that shows the air moving toward the east northeast (directions are drawn to the nearest degree) at a velocity of 18.1 m/s. The standard deviation in the direction of the superobservation of the 25 SASS winds is 4.5 m/s and the standard deviation normal to the direction of the SASS winds is 8.8 m/s. A plot such as Figure 2 would show an ellipse with a major axis perpendicular to the wind direction and a length of about one half the length of the wind vector. The minor axis would be in the direction of the wind vector and about one quarter of its length. About two thirds of the 25 SASS winds ought to fall within this ellipse. The values shown need to be divided by five to describe the properties of the superobservation (with gradients not considered).

The superobservation then has a speed of 18.1 ± 0.9 m/s in the direction shown with a variability normal to the indicated direction of ± 1.76 m/s. The variability in direction is roughly ± $\tan^{-1}$ (1.76/18.1) (or ± $\tan^{-1}$ 0.097) or 5.6°. Large values such as these propagate through the analysis and finally result in large standard deviations for the estimates of the divergence and the curl of the wind stress.

For contrast, consider the values near 51° N 209° E in Figure 9 for a
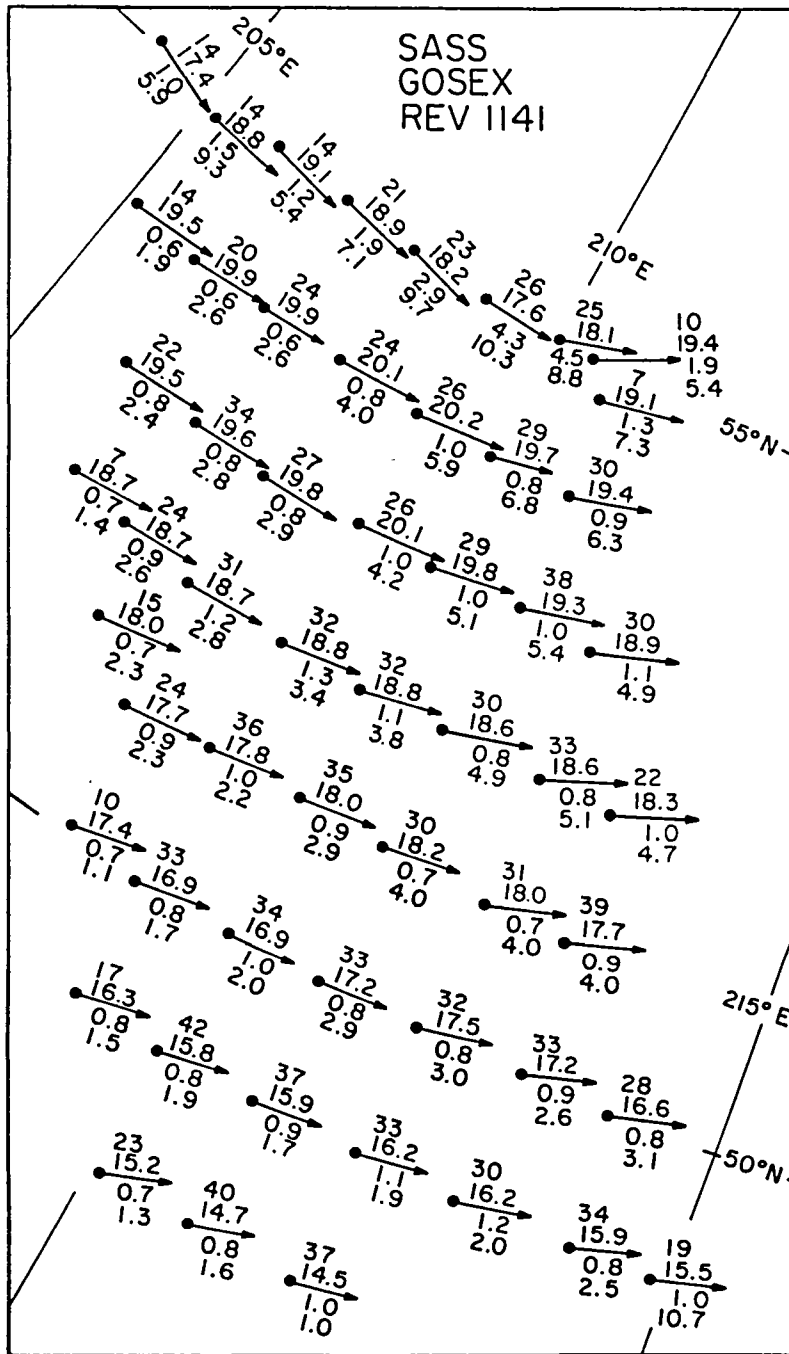
Fig. 9 Statistics from Preliminary Analysis of REV
        1141.(See Text).
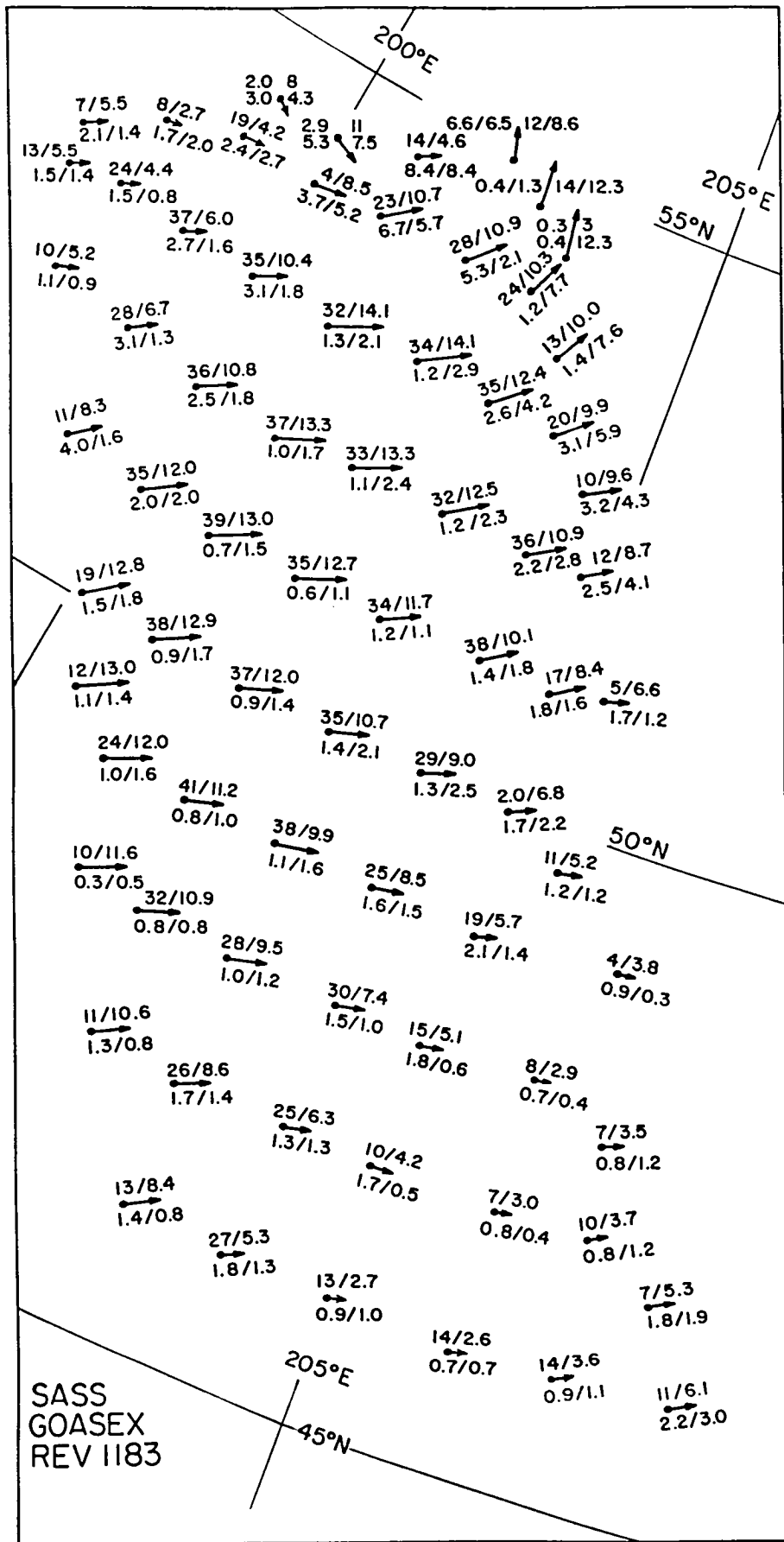
Fig. 10   Statistics from Preliminary Analysis of REV 1183.
(See Text).

61
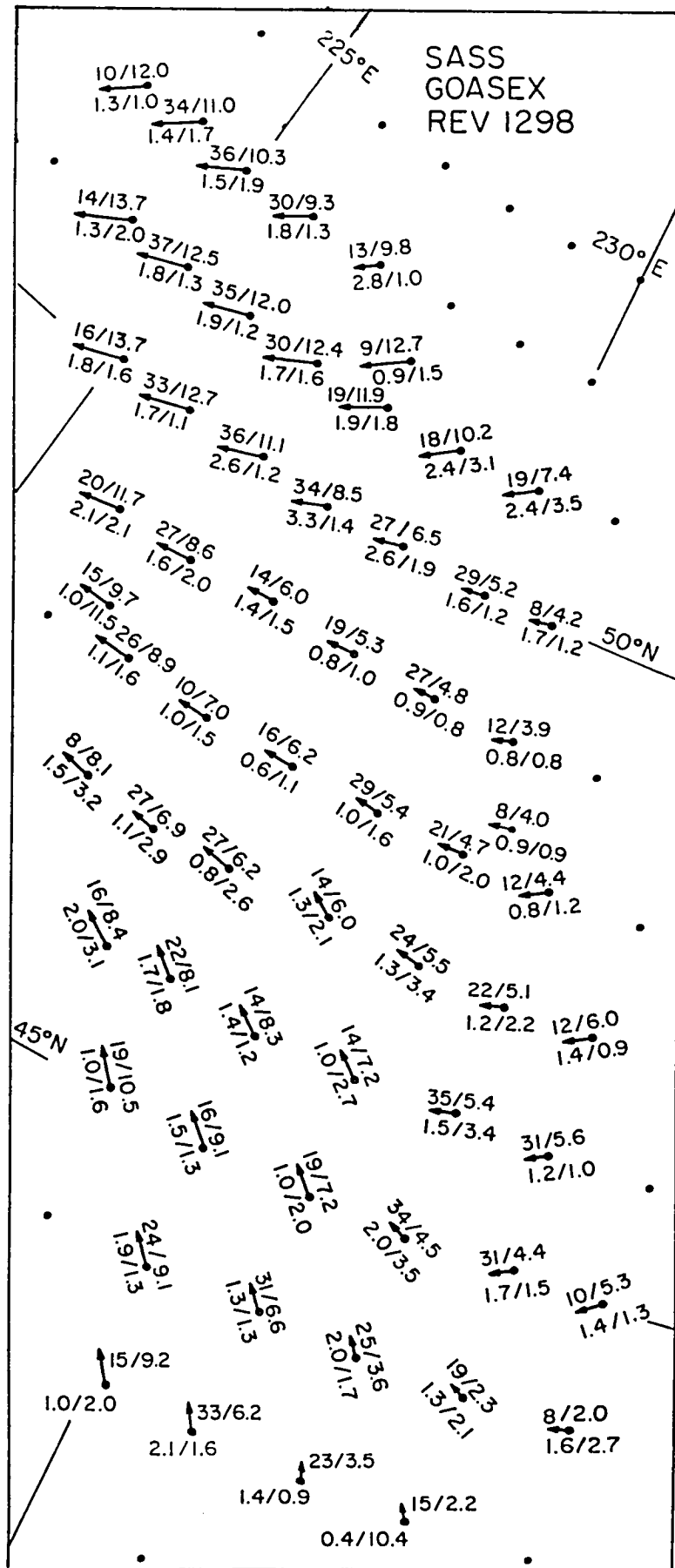
Fig. 11 Statistics from Preliminary Analysis of
REV 1298. (See Text).

62

sample size (N) of 36. An ellipse plotted in the same way as the one described above would be quite small. The superobservations wind would be toward the direction shown with a value of 17.8 ± 0.17 m/s in the wind direction and a variability normal to this of ± 0.37 m/s. The variability in direction would be $\pm 1.2^{\circ}$.

The sample size, because of peculiarities of the swath varies from a low of 7 to a high of 42. Small sample sizes even after further corrections, especially at the swath edges, propagate through the model to increase the standard deviations of the estimates of the divergence and the wind stress curl.

The segment of REV 1141 (Figure 9) selected for illustration can be used to judge the smoothness of the wind field. Adjacent values are correlated because two degree by two degree overlapping squares were used, but every other point in the north-south or east-west direction is based upon completely independent SASS values. Diagonal points are almost independent. One fourth of their data is common. The field in Figure 6 is obviously quite smooth and the standard deviations for the superobservations could be used judiciously in a contouring scheme to produce an even smoother field at the synoptic scale.

The rather large differences in the sampling variability values for the two selected examples are representative of what was found for all of the REVS that were studied. There are numerous reasons why this happens. If the forward pointing SASS beam was pointing in such a direction that the winds were close to upwind, crosswind or downwind, the cosinusoidal variation of back-scatter would be present for the measurements made by both beams and present for each of the two SASS cells that were paired to recover the wind. Since the cells did not fall exactly one on the other, mesoscale variability would be different for each of the two cells and the communication noise and attitude error effects would also be different. Variations in the estimated backscatter for the paired cells can cause false two solution results (which were discarded) or large variations in the recovered wind directions as described in Pierson and Salfi (1982) for the now canceled NOSS SCATT and in Pierson (1983b).

Conversely, if the forward pointing SASS beam is at 45°, 135° 225° or 315° to the wind direction, the model function backscatter changes most rapidly as a function of aspect angle. The same amount of mesoscale variability plus communication noise sampling variability will result in

63

relatively much smaller changes in wind direction and wind speed.

As the SEASAT progressed from the Equator to landfall on a northbound pass as in these four examples, the pointing direction of the forward beam changed continuously. At times it was close to upwind, downwind or crosswind, which resulted in the large standard deviations shown in the figures. For winds 30° to, say, 60° past upwind and those corresponding to the above plus 90°, 180° and 270°, smaller standard deviations would be expected.

Figure 10 (REV 1183) shows much the same thing as Figure 9 with a somewhat more complex field near the top of the figure. A cursory inspection suggests a rather smoothly varying wind field, but there are some surprises for synoptic meteorologists hidden in this relatively simple plot which will be described when Figure 12 is discussed.

Figure 11 shows again more of the same except that the winds all have a component toward the west. The sample size ranges from a low of 8 to a high of 36. There are no noticeably large values for the two standard deviations of the SASS samples.

Figures 12, 13 and 14 are the streamline isotach analyses of the data plotted in Figures 9, 10, and 11. The wind speeds increase from 15 m/s near 48° N to 20 m/s near 54° N, 209° E for REV 1141 in Figure 12. As a more detailed discussion of the fully analysed data to follow will show, this kind of a wind field is to be expected for the area shown for the synoptic scale conditions that were present.

Figure 13 for REV 1183 is the first of several results to be obtained that should cause concern for synoptic meteorologists and those accustomed to using conventional data from buoys and transient ships. Suppose that only one ship report is available between 50° N and 55° N and that it is located somewhere along 53° N. Also suppose that west of 198° E, east of 205° E, north of 55° N and south of 50° N the usual conventional data are available.

Also suppose that the ship report has no errors whatsoever and reports the true synoptic scale wind (a doubtful assumption for reasons given
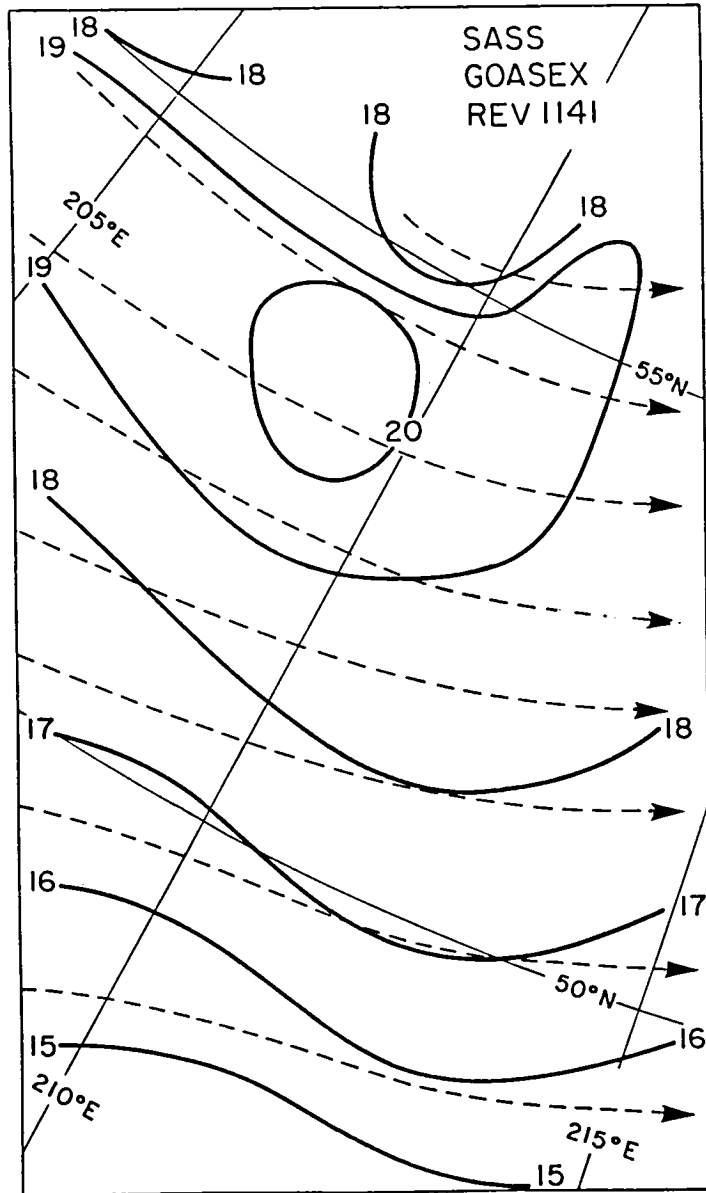
FIG. 12   Preliminary Streamline (Dashed) Isotach (Solid)
          Analysis of Part of REV 1141.
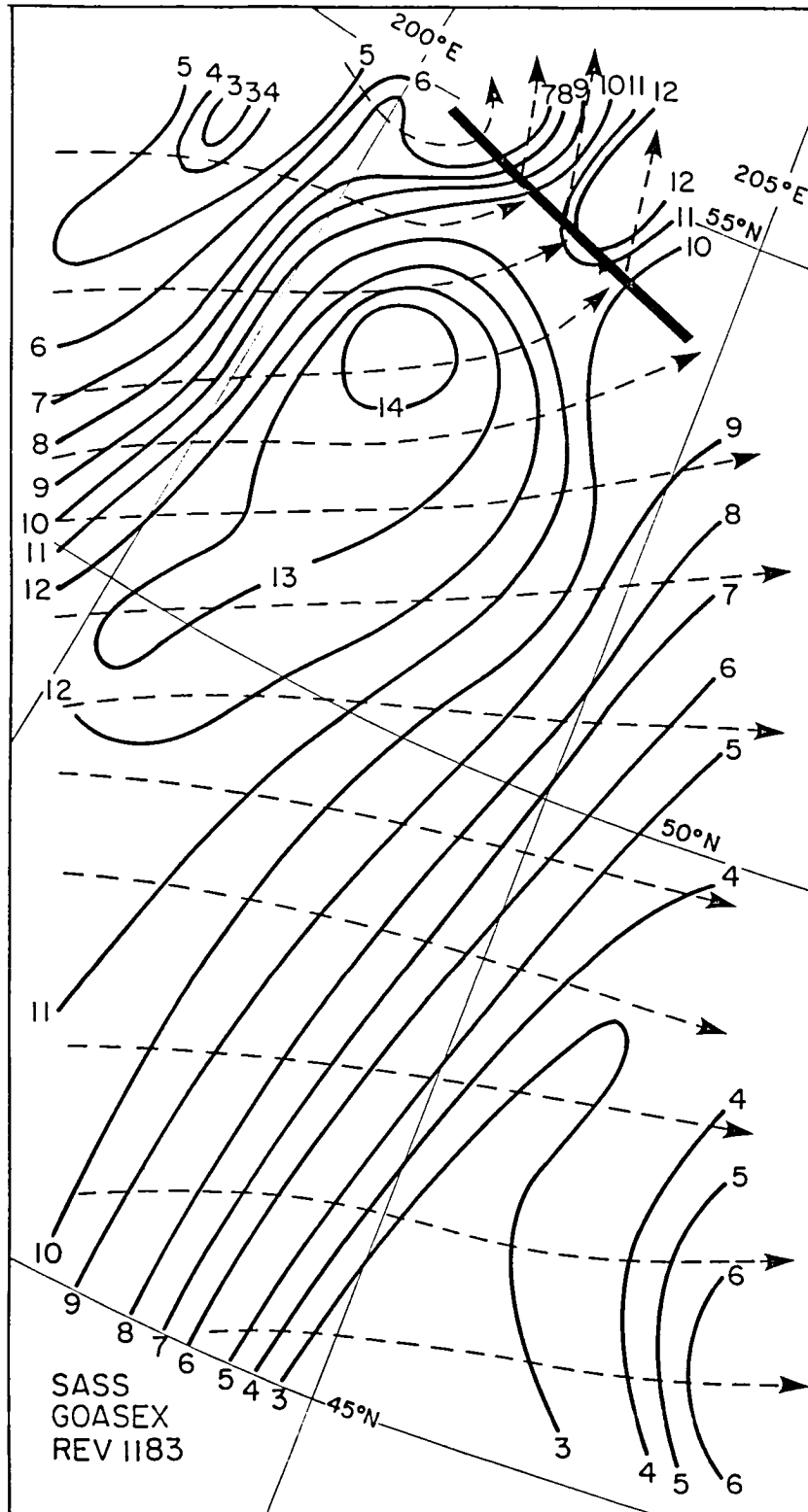
FIG. 13 Preliminary Streamline (Dashed) Isotach (solid)
Analysis of Part of REV 1183.
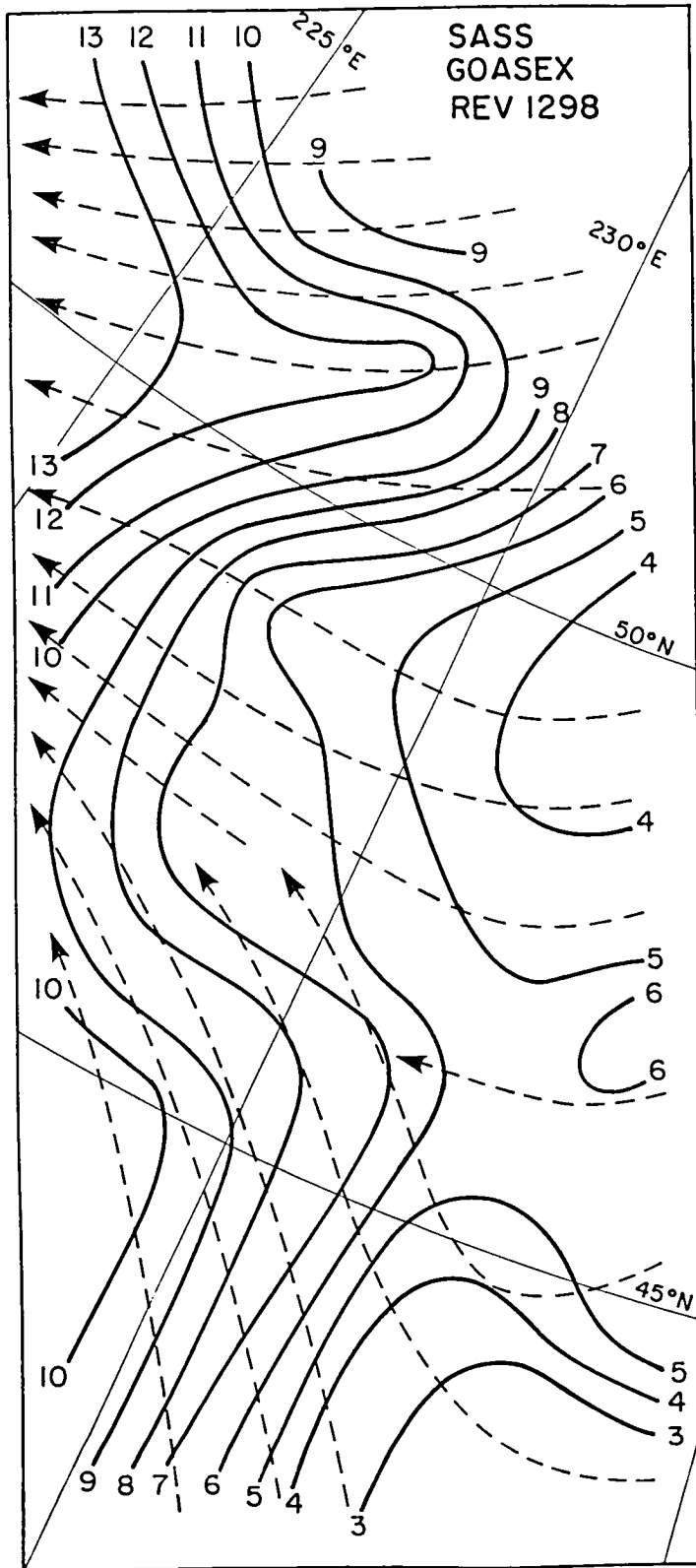
FIG 14   Preliminary Streamline   (Dashed) Isotach (Solid)
Analysis of Part of REV 1298.

elsewhere) and also suppose that the SASS superobservations are the synoptic scale winds. With a slight counter clockwise wind shift, on proceeding from the west toward the east the wind speed reported by this one lonely ship would vary from 5 to 4.5 m/s and then increase through values of 6, 7, 8, 9, 10, 11, 12, 13 and 14 m/s followed by a decrease through 13, 12, 11 and 9 m/s. The gradient of wind speed along 200° E is particularly strong.

Six or seven examples might be constructed with this one ship report "bogused" in at various locations and with all other conventional reports the same. Those adept at "manuscript" synoptic scale analyses and those organizations that do computor analyses would be told that this one report was to be treated as absolutely correct. How different would these six or seven analysis be with this single report representing this large area? As will be shown later, how deep would the low be to the north for each analysis? Would the analyses come anywhere near representing the wind field shown in the figure?

A similar problem could be formulated near 45° N where the superobservations show wind speeds decreasing from 10 to 3 m/s over about 2.5^{o} of longitude. An even more intriguing study might be made by finding the actual ships that were located in the area analysed (or for that matter the results from the full swath to follow) using the superobservation winds everywhere possible, and making the usual synoptic analysis, either by "manuscript" methods or by a computor forced to fit the winds as closely as possible.

Figure 14 (REV 1298) shows a rather wild pattern for the streamlines and isotachs, quite unlike the work of art shown as an analysis of conventional data in Woiceshyn, et al. (1979) for REV 1298 in terms of streamlines and isotachs found from conventional data. Further discussion will be deferred until the full swath is treated later.

Figure 15 for REV 1298 shows the vector values of $\vec{u}_*^2$ calculated from equations (74) and (90) through (94). The sample size, the value of $u_*^2(\tau/\rho)$, and the east-west and north-south standard deviations of the vector components (reduced by $N^{-\frac{1}{2}}$ from the superobservations) are shown to two significant figures except when rounding yielded 0.00. The value of u_*^2 varies from 0.23 ($u_* = 0.48$ m/s) to 0.01 ($u_* = 0.1$ m/s) over the field.

SASS
GOASEX
REV 1298
u_*^2 $(M/S)^2$

225°E

10/.16
.01/.00 34/.13
.01/.00 36/.11
.01/.00

14/.22 30/.09
.01/.01 .01/.00

37/.18 13/.10
.01/.00 .02/.00

230°E

35/.16
.01/.00

50°N

16/.23 30/.17 9/.18
.02/.01 .01/.00 .01/.01

33/.18 19/.16
.01/.00 .01/.01

36/.13 18/.11
.01/.00 .01/.01

34/.07 19/.05
20/.14 .01/.00 .01/.01
.01/.01 27/.04
27/.07 .01/.00

29/.03 8/.02
15/.10 14/.03 50°N
.01/.00 26/.08 19/.03
10/.05 27/.02

16/.04 12/.02

8/.06
.01/.01 29/.03
27/.05 21/.02
.00/.00 27/.04
12/.02

14/.03
16/.07 24/.03
.01/.01 22/.06
.01/.00 14/.07 22/.02
.00/.00 14/.05
45°N 12/.03
19/.12 .00/.01
.01/.00 35/.03
16/.08 31/.03
.01/.00 19/.05
34/.02
24/.08 31/.02
.01/.00 10/.03
31/.04
15/.08 25/.01
.01/.00 19/.01
33/.04 8/.01

23/.01

15/.01

FIG. 15 $\vec{u}_*^2$ for REV 1298. (See Text).

Figures 16 and 17, within the limitations described above, are the "first cut" analyses of the vector $\vec{u}_*^2$ fields for REVS 1141 and 1298. Equation (74) has been used along with the assumption that the wind stress is in the same direction as the wind. Since neutral stability has been assumed there are one to one relationships between $\bar{U}_{10}$, $\bar{U}_{19.5}$, u_* and u_*^2. These values are given in Table 2 below. Those who prefer some other relationship between u_*^2 and $\bar{U}_{10}$ can compute the comparable values for $\bar{U}_{19.5}$ and u_*^2 and relable the contours. It will be found that the differences between $\bar{U}_{19.5}$ and $\bar{U}_{10}$ will be small, but that the total range of u_*^2 values, if five or six different proposed relationships are used, can differ by a factor of two, or so, for the same value of $\bar{U}_{10}$. Based on the kinds of data that were used to obtain (74) the relationship used is probably one of the better ones. The isotachs in preceeding and subsequent figures could simply be relabled with values of u_*^2 based on Table 2, but equal increments would not be the result.

Figures 6 through 14 combine to illustrate three important effects when a sample of N SASS winds are combined to attempt to produce a superobservation at integer values of latitude and longitude plus appropriate statistics on the sampling variability of the winds either in natural coordinates (i.e. parallel and normal to the average direction) or as east-west and north-south components in a spherical coordinate system. They are (1) that even deleting selected values at the outer edges of a two degree square cannot yield an average latitude and longitude exactly at an integer value, (2) that the superobservations at the edges of the swath have a smaller sample size and are frequently displaced by large distances from the desired latitude and longitude. (If there are no data at all in one or two of the four quadrants of Figure 1, it is hardly possible to get an average latitude and longitude near the desired value). and (3) that strong gradients over the two degree square can be falsely interpreted as a part of the variance of the super-observation winds.

For points in the interior of the swath, corrections for these effects are not too difficult to first order. Some kind of interactive scheme might do better. The only somewhat surprizing result is equation (51). If all of the SASS samples were concentrated on a line, if they all had the same direction (whatever that means on a sphere) and speed and if the line, more or less, went from $\lambda_o - 1$, $\theta_o - 1$ to $\lambda_o + 1$, $\theta_o + 1$, then, for example, COV $\Delta\lambda\Delta\theta$ would be positive and fairly large and the signs of the various

TABLE 2. Values of $\bar{U}_{19.5}$, $\bar{U}_{10}$, u_*^2 and u_* from Equations (74) and (78) (in meters/sec except for u_*^2).[†]

$\bar{U}_{19.5}$	$\bar{U}_{10}$	u_*^2	u_*
1.	0.9	0.003	0.052
2.	1.9	0.006	0.078
3.	2.8	0.011	0.103
4.	3.8	0.016	0.128
5.	4.7	0.024	0.156
6.	5.7	0.034	0.185
7.	6.6	0.047	0.216
8.	7.6	0.062	0.249
9.	8.5	0.081	0.284
10.	9.5	0.103	0.321
11.	10.4	0.130	0.360
12.	11.3	0.160	0.400
13.	12.3	0.196	0.442
14.	13.2	0.236	0.486
15.	14.1	0.281	0.531
16.	15.0	0.333	0.577
17.	16.0	0.390	0.624
18.	16.9	0.453	0.673
19.	17.8	0.524	0.724
20.	18.7	0.601	0.775
21.	19.6	0.685	0.828
22.	20.5	0.777	0.881
23.	21.4	0.876	0.936
24.	22.3	0.984	0.992
25.	23.2	1.100	1.049
26.	24.2	1.225	1.107
27.	25.1	1.359	1.166
28.	26.0	1.502	1.225
29.	26.9	1.655	1.286
30.	27.7	1.817	1.348

[†] Here, and on pages 26 to 30 and 70 and 71 (and elsewhere), $\bar{U}_{10}$, $\bar{U}_{19.5}$, $\bar{U}(10)$ and $\bar{U}(19.5)$ denote the height above the sea surface and the time averaged wind in the mean wind direction. z_o is the roughness length.
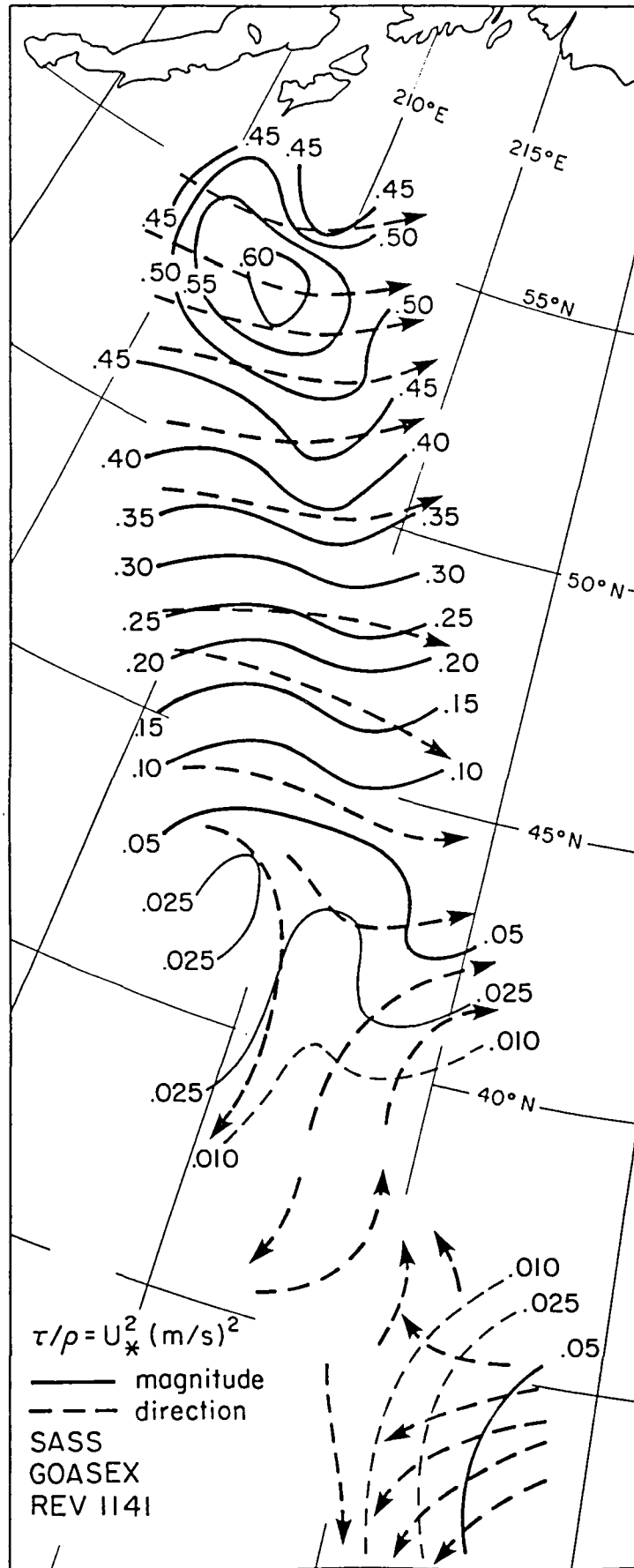
FIG. 16 Preliminary $\vec{u}_*^2$ Streamline (Dashed)
Isopleth (Solid) Analysis for REV 1141.

72
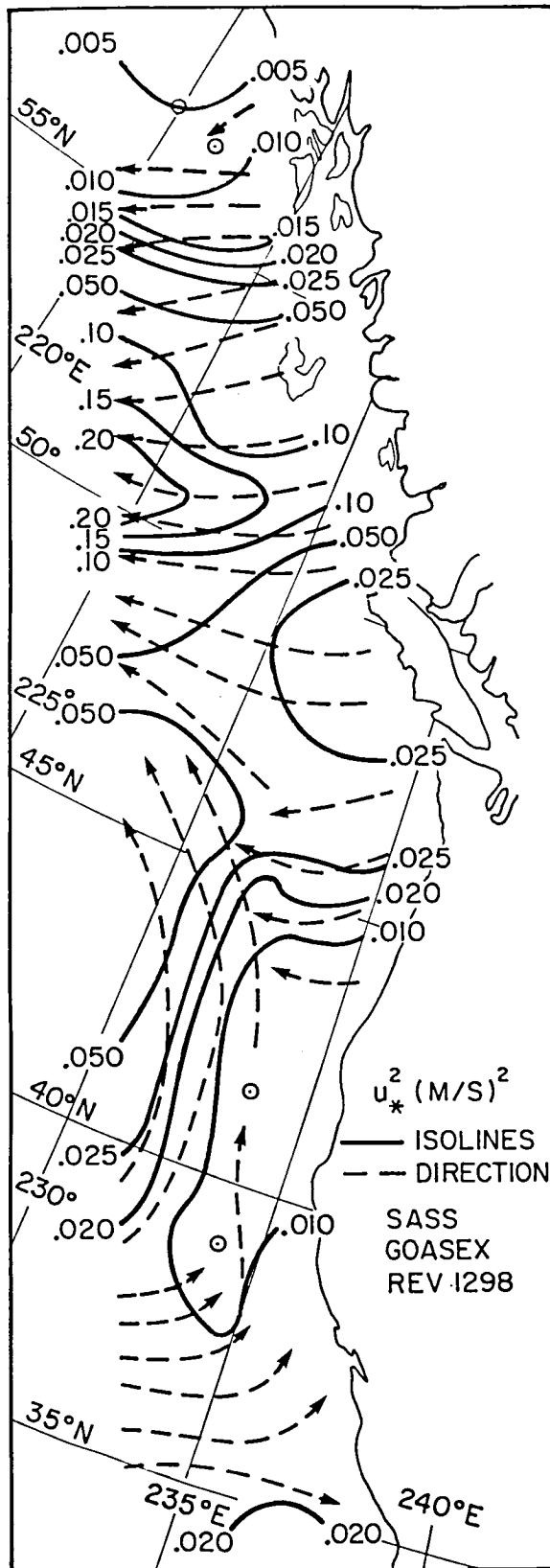
FIG. 17 Preliminary $\vec{u}_*^2$ Streamline (Dashed)
Isopleth (Solid) Analysis for REV 1298.

terms would effectively cancel out the contributions to the variances of the east-west and north-south components from gradients in the wind.

The edges are more difficult because not enough information is available. The way that this difficulty was overcome is described in the section entitled "Edges". Again there might be better ways to do it.

COMPARISON CONVENTIONAL DATA AND THEIR ANALYSES

The four portions of the SEASAT REVS that were processed both for GOASEX and for this study were REVS 1141, 1183, 1212, 1298.

They were chosen for the GOASEX I and II Workshops for the first attempt to relate scatterometer winds to conventional data because large variations in wind speed were indicated by the conventional data, they happened close to a synoptic time and they passed near some of the data buoys, Weather Ship Papa and (or) the *Oceanographer*, where special observations were made by conventional methods.

According to Schroeder, et al. (1982), there were two GOASEX Workshops as cited therein. A basic product of the GOASEX I Workshop edited by P. M. Woiceshyn (1979, April) with the full title "SEASAT GULF OF ALASKA WORKSHOP: Volume II., Comparison Data Base: Conventional Marine Meteorological and Sea Surface Temperature Analysis; Appendixes A and B".

This volume (JPL Document 622-101) is dated April 1979 on the cover but the results contained therein were mostly available in January 1979. The results were assembled, analysed, and presented by R. Brown, V. Cardone, G. Cunningham, J. Ernst, J. Overland, P. Woiceshyn and M. Wurtele with acknowledgements for the help of S. Schoenberg, S. Ghan, J. DeVault (NOAA-PMEL), J. Wilkerson (NOAA-NESS) and J. Pedigo, J. Patterson and E. Vander Wyk (JPL). The ship and buoy data are tabulated in a report by Wilkerson and McNutt (1979).

This report is an example of the best that can be done in an analysis of the meteorological conditions over the eastern half of the North Pacific, north of about 30° N by means of conventional data. The results contained in that report will be contrasted with the results we obtained in this study of the de-aliased winds from four GOASEX passes.

The 159 page report contains the usual front matter, which describes which authors contributed what sections. Section A-2 shows the GOES cloud imagry for the eastern North Pacific westward to about the international date line and eastward to Lousiana and the Gulf of Mexico. The cloud imagry

almost from the Equator to at least 60° N in the Gulf of Alaska is well resolved. There is one cloud image from GOES for a time near the SEASAT pass that was studied.

In this same section, the conventional sea surface isobaric analyses and frontal systems are shown for the six hourly synoptic time closest to the SEASAT pass along with the ship reports that were used to make the analyses. Both the cloud imagry and the synoptic charts will be reproduced in our study.

REVS 1141, 1183, 1212, and 1298 were all northbound passes. As listed, they crossed 30° N at about 1849 GMT, 1721 GMT, 1803 GMT and 1828 GMT. Thus they are not quite synoptic with either the 1800 GMT surface analysis or the cloud imagry for the time shown on each GOES image.

The four synoptic charts to be used for these four REVS cover an area from about 30° N to 60° N and from 135° W (225° E) to 170° W (190° E). There are 54 regions bounded by latitude circles and longitude lines 5 degrees apart within this area, of which four should be deleted as mostly land. There are thus about 50 5° latitude by 5° longitude "squares" for the area analysed. There are also consequently about 1250 one degree by one degree "squares" for the area analysed. At 45° N, a 1° by 1° square has an area of about 8700 square kilometers so that the total oceanic area involved is somewhere around 10 million square kilometers, plus or minus a million, or so.

For REV 1140 (and 1141) there were about 68 ship and buoy reports at 1800 GMT, and for 1183, 1212 and 1298 there were about 47, 69 and 65 respectively. This averages to 1¼ ship reports per 5 by 5 degree square, or 0.05 reports per one degree square.

For the 50 five degree squares, there were about one third without a single report so that there were almost two ships per 5° square where there were data.

The analysts undoubtedly used every skill available to the synoptician including judgements as to whether or not to ignore a ship reported wind. Also cloud imagry was used to locate fronts, and the alternative analysis for 1140 (1141) used it to advantage.

Section A-3 shows sea surface temperature. Section A-4 shows air temperatures and air sea temperature difference fields for some, but not all of the passes. Section A-5 shows dew point temperatures fields, so that more modern Monin Obukhov theories might be used. Section A-6 analyses cloud cover and precipitation data because of the scatterometer attenuation problem for precipitation. (See Moore, et al. (1982)). Only REVS 1140 (1141) and 1298 were done.

Section A-7 shows kinematic wind field analyses for REVS 1134 (1135), 1140 (1141), 1292, and 1298. Section A-8 uses three planetary boundary layer models to derive surface wind fields from the available ship reports and synoptic scale analyses. These are available for 1140 (1141), 1183, 1212 and 1298.

The pressure fields in these planetary boundary layer analyses do not agree with the synoptic analyses very well. Three model results are shown, each for the same pressure field, but yielding different winds. One model is too simple to be believed and is used only as a straw man. These fields will be compared with the SEASAT superobservation fields where appropriate.

There follows some statistics and a delightful cartoon that shows a cold front with a loop in it, the location of the "Pressure Modification and Emission Laboratory", the East Pacific High Dragon (which eats ship reports), the "Sea of arrows" and Typhoon "Peter", which apparently never slowed down enough to be seen during a SEASAT pass. A closing appendix describes the computer programs used to generate the PBL analyses.

The planetary boundary layer (hereinafter PBL) models used in this appendix had only one major objective, which was to produce vector wind fields over the ocean, especially in the area of a GOASEX pass, that would define the wind at 19.5 meters as both the effective neutral wind and the actual wind. The directions are the same but the speeds differ. Properties of these models are given by Brown and Liu (1982). How well they succeeded as a basis for comparison with the SEASAT SASS winds can be found from a study of numerous papers in the two JGR SEASAT special issues. Other aspects are given by Pierson (1983b, 1983c).

Any PBL analysis is only as good as the data that go into it. Whether or

not the 1200 GMT analysis plus a six hour projection was used is not clear. About 50 ships for about 10 million square km is not a very sound basis for analysis.

These PBL models account to a greater or lesser extent for thermal wind effects and various amounts of cross isobar flow from high to low pressure. The friction drag of the moving air over the water is an additional component of the balance of forces involved such that one expects the PBL to produce a greater inflow of air into low pressure centers with, consequently, upward vertical motions. A corresponding outflow from high pressure centers with downward vertical motions for the same reasons is to be expected.

With this friction drag as an added important effect in the PBL, which is absent at higher elevations, one might expect that the PBL would play an important role in determining vertical velocities in the atmosphere with a consequent release of latent heat for ascending air and adiabatic heating for descending air.

For atmospheric levels (in various forecasting models) above the PBL there is more nearly a geostrophic or gradient balance and more nearly non-divergent flow at the synoptic scale.

The PBL models for the presently available computor based numerical forecasting models are, as of our latest review of the subject, much cruder than the PBL models used to try to define the winds for GOASEX. For these models, the grid point values for the winds have to accomplish too much with too little. Much of the vertical velocity field of the PBL is consequently lost in such models. Combined with inadequate data over the ocean, these inadequate models can be part of the reason for poor numerical weather forecasts.

The month of September 1978 was not an unusual month from the climato-logical aspect. The winds over the Eastern North Pacific were not particularly high and the extratropical cyclones that traversed the areas were not very deep. During more recent years, the high surf and extensive beach errosion on the California Coast were the result of much higher winds over the Pacific than those experienced in September 1978. To obtain some idea of what might have happened, compared to what did happen, Pierson (1982b) shows a sequence

of 24 hourly Fleet Numerical Oceanography Center wind field analyses and wave height specifications for October 1977 that show winds of 25 to 35 m/s and hindcast significant wave heights of 19 meters in the same areas that were traversed by the GOASEX passes. The month by month variability of winds and waves does not follow the same annual cycle from one year to the next.

For Revolution 1141, Seasat passed the equator on a northbound pass at 1840 GMT, (Klose (1979)) reached 30° N 9 minutes later and 60° N 18 minutes after crossing the equator on 14 September 1978. Plus or minus several minutes are required to measure the two backscatter values at the outer edge of the swath. The GOES cloud imagry is shown in Figure 18. The SASS swath that was analysed provided data around the question mark cloud pattern, across the weak cold front, on through the scattered cumulus clouds to the south of the low and northward to an area just to the west of the low center shown to the east of Kodiak Island, Alaska.

The synoptic scale analysis that is to be compared to the superobservation data is the alternative analysis provided by Woiceshyn, et al. (1979) as shown in Figure 19. It differs from the other analysis that was provided in that the high to the south of the cold front has been split in two parts as an attempt to account for the hooklike cloud pattern in Figure 18. The alternative analysis is to be preferred to the original analysis in that the conventional winds to the south of the front no longer blow from low pressure toward high pressure.

Interesting features of Figure 19 are winds that blow from low to high pressure between 40° N and 45° N near 155° W (205° E). For 50° to 55° N and 140° W (220° E) to 135° W (225° E), two ship reports give wind directions that differ by about 90°. Otherwise the ship reports are relatively consistent with the isobaric analysis.

The first row of superobservations that were recovered began at 33° N for longitudes from 219° E to 223° E. The swath extended north westerly and ended up with Kodiak Island near its center. Three superobservations were recovered at 57° N (208° E to 210° E), five at 56° N (207° E to 211° E), and eight at 55° (204° E to 211° E). There were a total of 149 superobservations of the vector wind for a neutral atmosphere (and consequently 149 vector $\vec{u}_*^2$ values). Because of edge effects, this allowed 92 values of the divergence and the curl to be found for a narrower swath. There was a total of 1,534 individual SASS winds that were used to generate the superobservations for an average of 10.3 SASS winds per superobservation, or more correctly, four

FIG. 18 GOES Cloud Imagry for REV 1141. (From Woiceshyn,
         et al. (1979)).*

---

*Infrared images for all four Revs. plus details of visible
 images for REVS 1183 and 1212 are described in an appendix.

18Z 14 SEPT 1978   **REV 1140**

FIG. 19 Conventional Analysis Associated with REV 1141. One Full Barb for a
Ship Report Represents 10 Knots. (From Woiceshyn, et al. (1979)).

times that for many values with many of the SASS winds used four times. Twenty five latitude circles had superobservations ranging from 3 to 9, as the latitude varied, with an average of nearly 6. The 149 superobservations are more or less the equivalent of six 5° by 5° squares completely resolved with 25 winds per 5° square for 6/50 (12%) of the area covered by Figure 18. For a two sided swath in an operational mode, the area covered would be doubled to about 24% at the expense (perhaps) of a reduced number of samples. All of the statistics change considerably for NROSS.

For this one sided swath the raw data have been reduced from 1534 winds to 149 winds, yet the data density of the superobservations within the swath is still at least 12.5 times greater than the data density of conventional reports.

The other charts in Woiceshyn, et al. (1979) show that the air sea temperature difference was within $\pm 1^{o}$ C of zero degrees C over the swath with air 2° to 4° C colder than the water moving in behind the low but not reaching the swath. Dew points were reasonable, given the air temperatures so that the atmosphere may have been close to a neutral stratification.

Figure 20 shows the streamline isotach analysis of the superobservation wind field. The northernmost portion of the field is rather complex with tight gradients and sharp wind shifts to the southeast of Kodiak Island. An isotach maximum of 20 m/s is determined by 3 speeds in excess of 20 m/s at 53° N 209° E and at 54° N, 208° E and 209° E. Farther to the south (45° to 50° N), there is a wavelike pattern in the isotachs not found in the streamlines. Still farther to the south the streamlines show anticyclonic curvature (40° to 43° N, 215° E).

Near the question mark, the de-aliased winds have produced a small cyclonic vortex. At the southernmost part of the swath, east north east and north east trades (perhaps) show up with speeds of 6 to 8 m/s.

The kinematic analysis for the area covered by REV 1141 and the two alternative PBL analyses for REV 1141 all differ from the streamline isotach analysis of the superobservations. The 40 knot isotach in the kinematic analysis covers a much larger area both eastward and westward. The isotachs run east-west near Kodiak whereas Figure 20 shows a wavy perturbation north

of 55° N. The center of the low is indicated at about 58° N 145° W (215° E)
beyond the area covered by the SEASAT swath. The kinematic analysis was
probably used to select the nearest SASS wind direction especially near the
question mark cloud pattern. The winds though light are realistic for
direction near the question mark cloud pattern.

The two PBL analysis place the low as in Figure 19 but yield nearly zero
wind speeds where a ship reported 20 knots north of the low center. High winds
are shown south of Kodiak, but it is difficult to judge whether or not they
reach 20 m/s. Point for point, the PBL analyses seem to show winds shifted
slightly clockwise compared to Figure 20 suggesting that the cross isobar
flow in Figure 20 is stronger than in the models. These models both give
negligable winds in the area between the two highs to the south of the front.

Figure 21 shows the vector values of $\vec{u}_*^2$ in $m^2 sec^{-2}$. This figure could
have been avoided by simply co-labeling the isotachs of Figure 20 by means of
Table 2. However the analysis was done independently for values in steps of
0.1 units to a low of 0.1 and then contours for 0.05 and 0.025 were added
for areas of light winds.

The required data to compute the air density were not easily available.
Since $\rho = P/RT$ (where the virtual temperature to account for water vapor
should be used), three fields would be needed to find ρ. Based on the air
temperature and the pressure as calculated at a few points, the effects of
high pressure and high absolute temperature and low pressure and low absolute
temperature seemed to cancel most of the time and produce values of ρ of
1.25 ±0.03 kilograms per cubic meter. The contours in Figure 21 can be
multiplied by 1.25 to obtain a fairly close value for the stress in newtons
per square meter.

Figure 22 shows a composite of a sketch of the cloud patterns along the
REV 1141 swath based on Figure 18, the fronts from Figure 19 and the values
of $\overline{div_2 W_h}$ calculated from the 92 superobservations. Smoothing that would
be possible by taking into account the standard deviations of the estimates
has not been used. It is virtually impossible to transfer the detail (there
really are a finite number of pixels) of a GOES image to a polar stereographic
projection without some simplification. The cloud analysis, as suggested by
the arrow , for the frontal clouds has not been extended much beyond the

84

FIG. 20 Final Streamline Isotach Analysis for REV 1141.
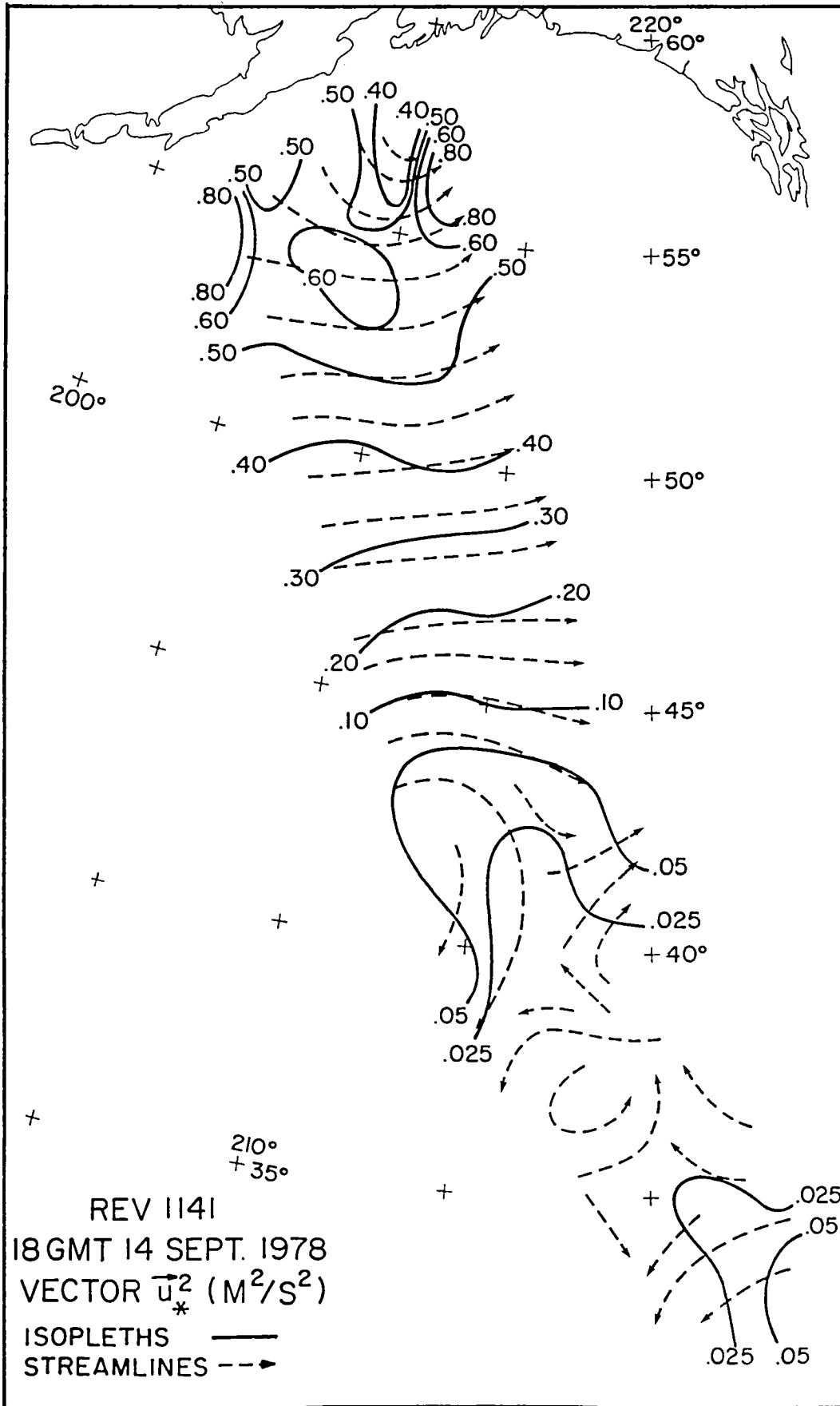
FIG. 21 Final Streamline Isopleth Analysis for $\vec{u}_*^2$ for REV 1141.

SEASAT swath except for the clouds near 45° N 210° E.

An area of strong convergence with a maximum of $-7.3 \times 10^{-5} \sec^{-1}$ is shown near 55° N under the clouds associated with the occluded front with a secondary area of -3×10^{-5} near 53° N 213° E. The northern portion of the zero divergence line is close to the boundary between the scattered cumulus south of the low and the clear skies north of the front.

The zero and -1×10^{-5} divergence lines trend north-south from 44° N to 53° N. These values seem to be anticipating the arrival of the clouds to the west. There is weak divergence under the clouds associated with the front, even weaker convergence near the front and divergence in the clear skies south of the front. The question mark cloud pattern shows an area of convergence of -3×10^{-5}. The fronts and the clouds may have moved some during the time interval between the synoptic chart, the cloud image and the SEASAT pass. All in all, the $\overline{\mathrm{div}_2 W_h}$ field is fairly consistent with known meteorological facts and the cloud patterns.

Values of the divergence between $\pm 1 \times 10^{-5}$ imply virtually non divergent flow at the synoptic scale. For values within this range, 16 values could have changed sign within one standard deviation. For 26 values, the sign would be unchanged.

If the divergence were constant for the first 200 m above the sea surface, the upward vertical velocity for a value of -7.3×10^{-5} would be 1.46 cm/s at 200 m. At 200 m within the $-6 \times 10^{-5} \sec^{-1}$ contour 43 cubic meters of air pass upward through the 200 m surface per square meter of the sea surface per hour. A one degree square bounded by 53° N and 56° N has an area of 7×10^{9} square meters so that 3×10^{11} cubic meter of air pass upward over a one degree square at this location in one hour (if the system moves slowly enough). The -3×10^{5} contour far to the south has a 40% larger area for a one degree square, but the area covered by the contour is about equal to the area of a one degree square at 55.5° N. Thus only about 1.5×10^{11} cubic meters are ascending at 200 m in this area per hour.

Figure 23 shows the curl of the vector wind stress over the swath. Contoured values range from a high of 15×10^{-7} newtons per square meter per meter to a low of -10×10^{-7}. The value tabulated at 56° N 210° E has been
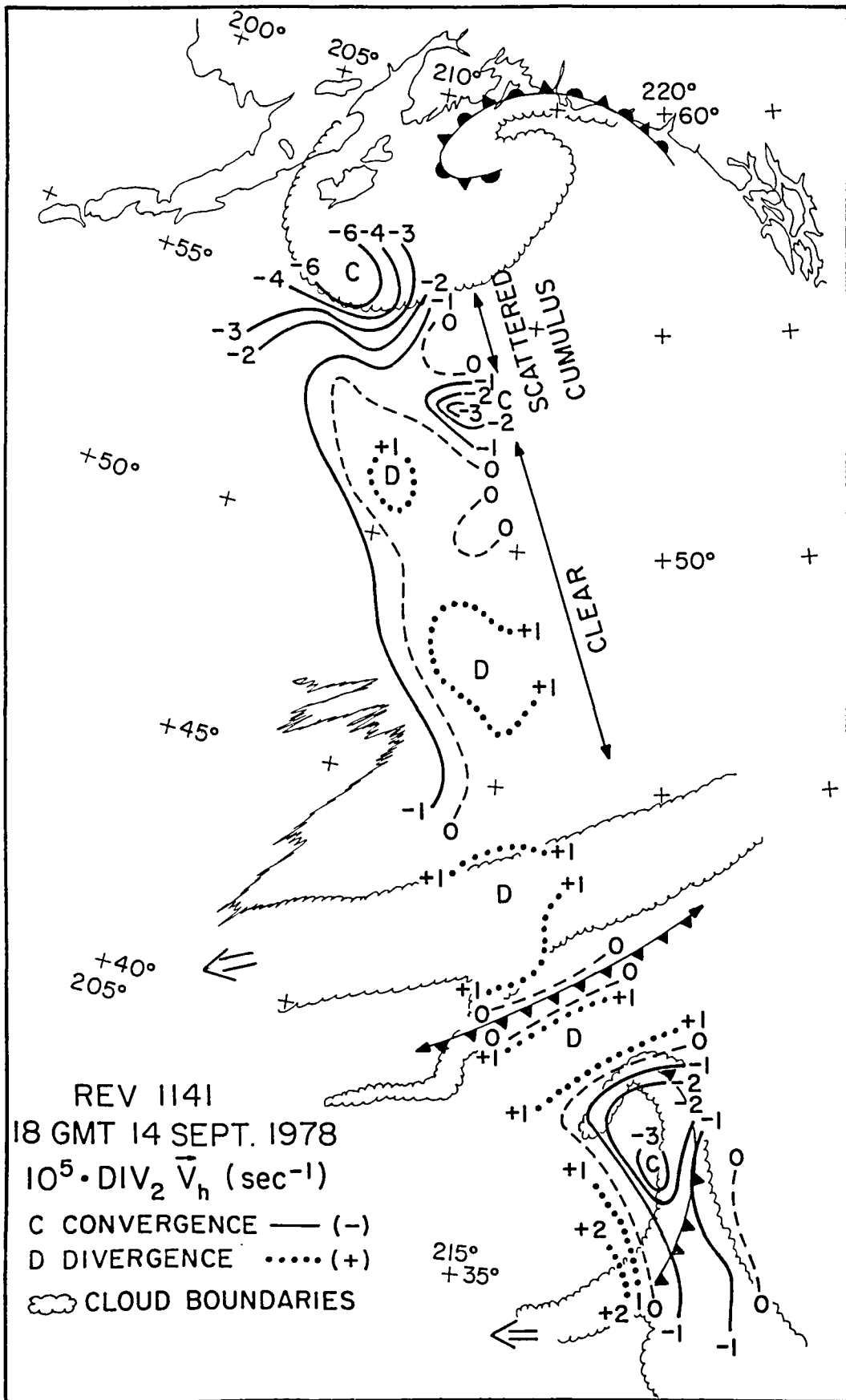
FIG. 22 A Composite Analysis of the Divergence of the Horizontal
Wind, GOES Clouds, and Synoptic Scale Frontal Analysis for
REV 1141.

88
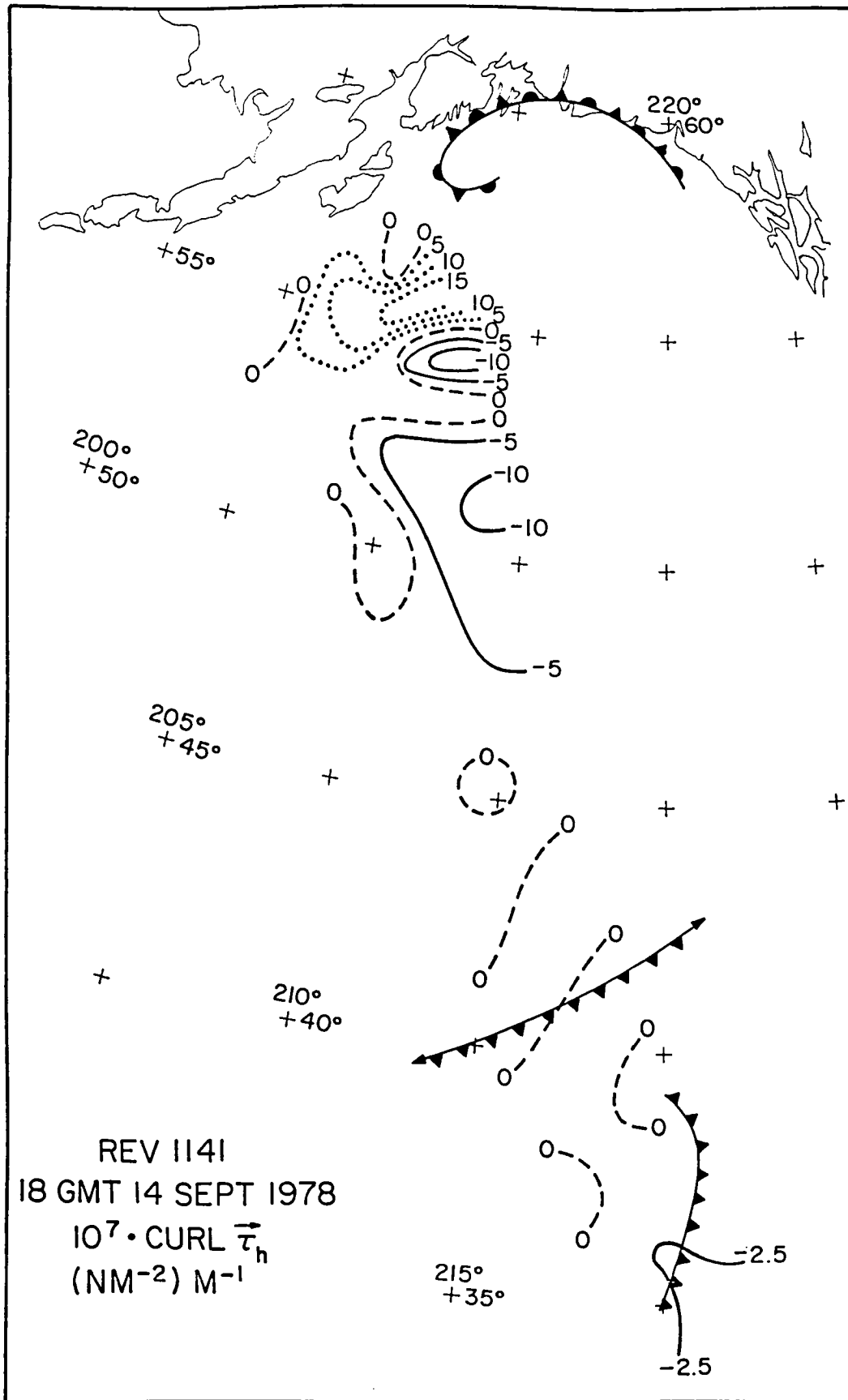
FIG. 23 The Curl of the Wind Stress for REV 1141.

ignored. For the southerly portion of the swath to 48° N, values range from -5×10^{-7} to $+4.2 \times 10^{-7}$. With values close to zero over large areas, of the 91 remaining values, only ten were such that the estimate minus one standard deviation differed in sign from the estimate plus one standard deviation.

The wind stress on the ocean and the curl of the wind stress are believed to be important quantities for the study of the wind driven part of the ocean circulation. Further interpretation of Figures 21 and 23 will be deferred until the results for all four REVS are available.

Revolution 1183 crossed the equator on a northbound pass at about 1712 GMT on 17 September 1978. It reached 30° N 9 minutes later and 60° N 18 minutes later. At the start of the pass, the SASS was in the V pol both sides mode, but it switched to the right side near 40° N. Superobservations were available from 33° N to 55° N. There were 173 superobservations (38 for the left swath portion) and 102 values for the divergence and the curl. There were 1267 original SASS winds for an average of 7.3 SASS values (X4 near the center of each swath) per superobservation.

Figure 24 shows the GOES clouds. The top left hand quarter of the cloud pattern is involved with the pass. The pass, where data were available, starts just to the south of the clear band running east-west below the numbers (35A 0051). The western piece covers the scattered cumulus below the front and under SE78 35A. The eastern piece continues northward past the band of towering cumulus, highlighted by the rising sun and embedded in the cold frontal cloud structure, on over the thinning clouds near the bend in the jet stream. The heavy line with cone shaped arrows is the jet stream. To the right of the thinning clouds and to the north of the jet stream is a band of bright clouds.

To the north of the broad frontal cloud band, a dark streak, meaning clear skies, can be seen. It turns westward below the 5 in 35A at the top of the image. The cloud patterns to the far west and north are difficult to resolve because of perspective effects.

Figure 25 shows the synoptic scale analysis. Only that part to the west of 215° E (145° W) is involved with the swath. The easternmost swath passes mostly to the west of the occlusion and the low center. The frontal analysis is based, probably on continuity, on seven ship reports and three not particularly useful land reports. The two ship reports near 45° N 115° W and 160° W would give cause to move the primary cold front westward by several hundred kilometers.

Figure 26 shows the streamline isotach analysis with isotachs every 2 m/s except for the 3 m/s and the 13 m/s isotach, the latter in the lower right corner. The high winds according to this analysis are west of the occlusion and the cold front. The warm front is barely in the swath. The differences

FIG. 24   GOES Cloud Imagry for REV 1183 .   (From Woiceshyn,
          et al. (1979)).
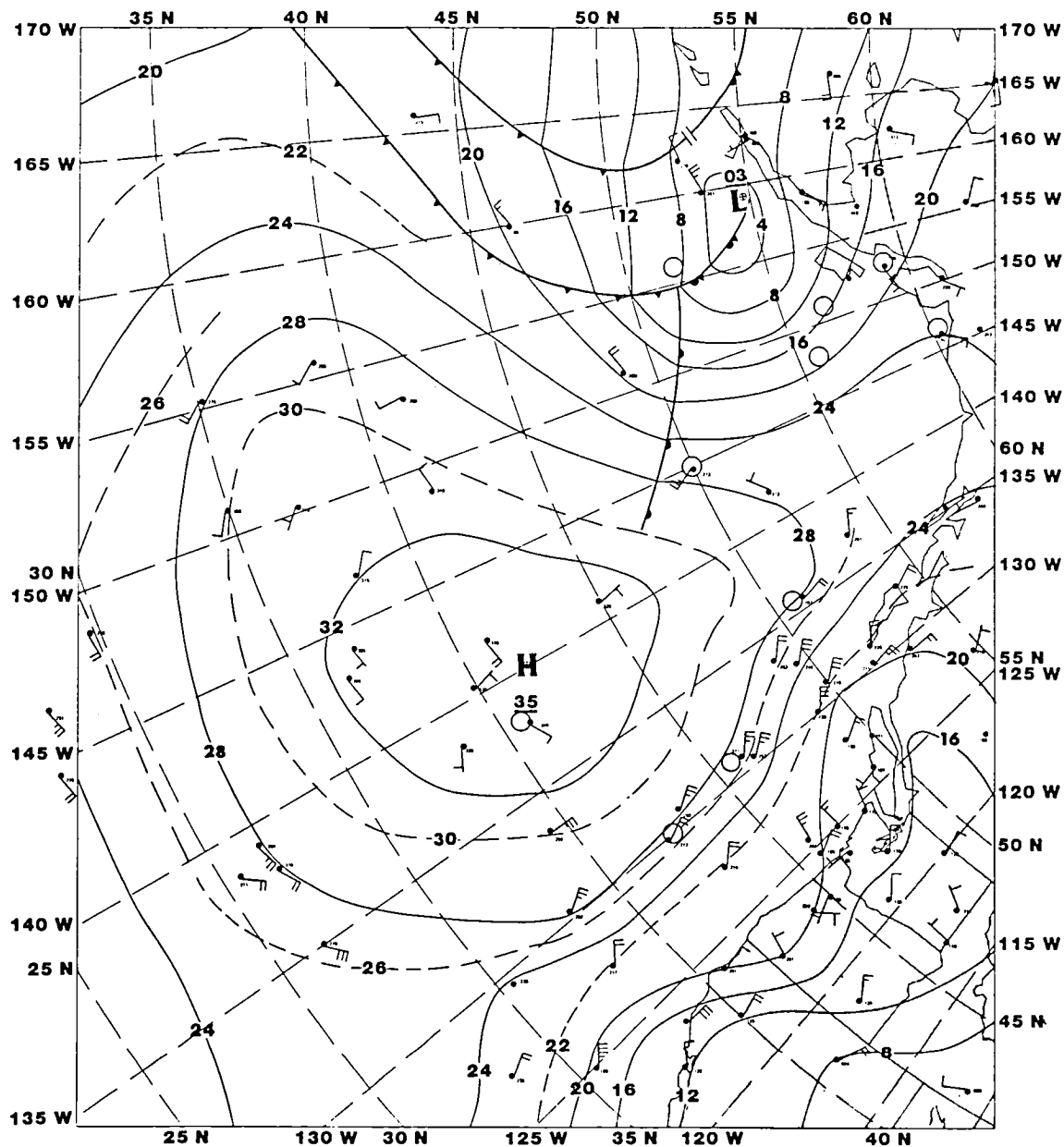
18Z 17 SEPT 1978   **REV 1183**

FIG. 25 Conventional Analysis Associates with REV 1187. One Full Barb for
a Ship Report Represents 10 Knots. (From Woiceshyn, et al. (1979)).

between this figure and the earlier one for REV 1183 (Fig 13) are the result of moving the edges to grid points and the various steps taken to correct for gradients. The data in the appendix can be compared to the preceding figure (Figure 10) to see what changes occurred. They were small and in the correct sense. The diverging streamline pattern near 210° E 39° N is not reflected in the isobaric pattern. There is the strong temptation to continue both the streamlines and the isotachs across the gap, which locates the subsatellite track, especially for the 6, 4, 3, 3, 4, 6 and 8 isotachs. There is a ship report at about 53° N, 200° E of 25 knots. A second ship at about 52.5° N 198° E reports, perhaps, 10 knots. The superobservations give 10.6 m/s (about 21 knots) for the first and 4.3 to 5 m/s (about 8.6 to 10 knots depending on exact location). The agreement is a bit of a surprise, when Brown, et al. (1982) and Brown (1983) are used to suggest the size of ship report errors. The isobaric pattern in Fig. 25 does not reflect the strong gradients in the area behind the occlusion. A ship at 49° N 151° W (209° E) reported about 20 knots. It lies just to the north-east of the 4 m/s isotach. Some stronge convolutions in the streamline isotach analysis would be needed if this ship report were included in the analysis.

There is no kinematic analysis for REV 1183. The PBL analyses provide a smoother version of the isobaric field of Fig. 25, with a low not as deep. There is no indication of the strong southwesterly flow in the 5° square 50° - 55° N, 160° - 155° W (200° - 205° E). The ship report at 160° W 53° N N is not reproduced in either speed or direction as in Fig. 25. The band of light winds (205° E, 45° N) with isotachs running south south westerly from north to south does not appear in the PBL's. There are numerous other discrepancies between the pressure fields of Fig. 25, and of the PBL's, and what they would imply for the winds of the PBL's, and the wind field given by the superobservations. There is in general a stronger cross isobar flow shown by the superobservations, plus much stronger gradients, than would be shown by present conventional data analyses and theoretical PBL analyses.

Figure 27 shows $\vec{u}_*^2$ which varies over the field from 0.30 to 0.025. The values of u_* exceeds 0.40 m/s over an area just inside the 0.15 isopleth so that the drag of the air over the water is substantial over a large area behind the occluded front to the north, in areas near the high pressure center and in what may be the trade winds. The air sea temperature difference
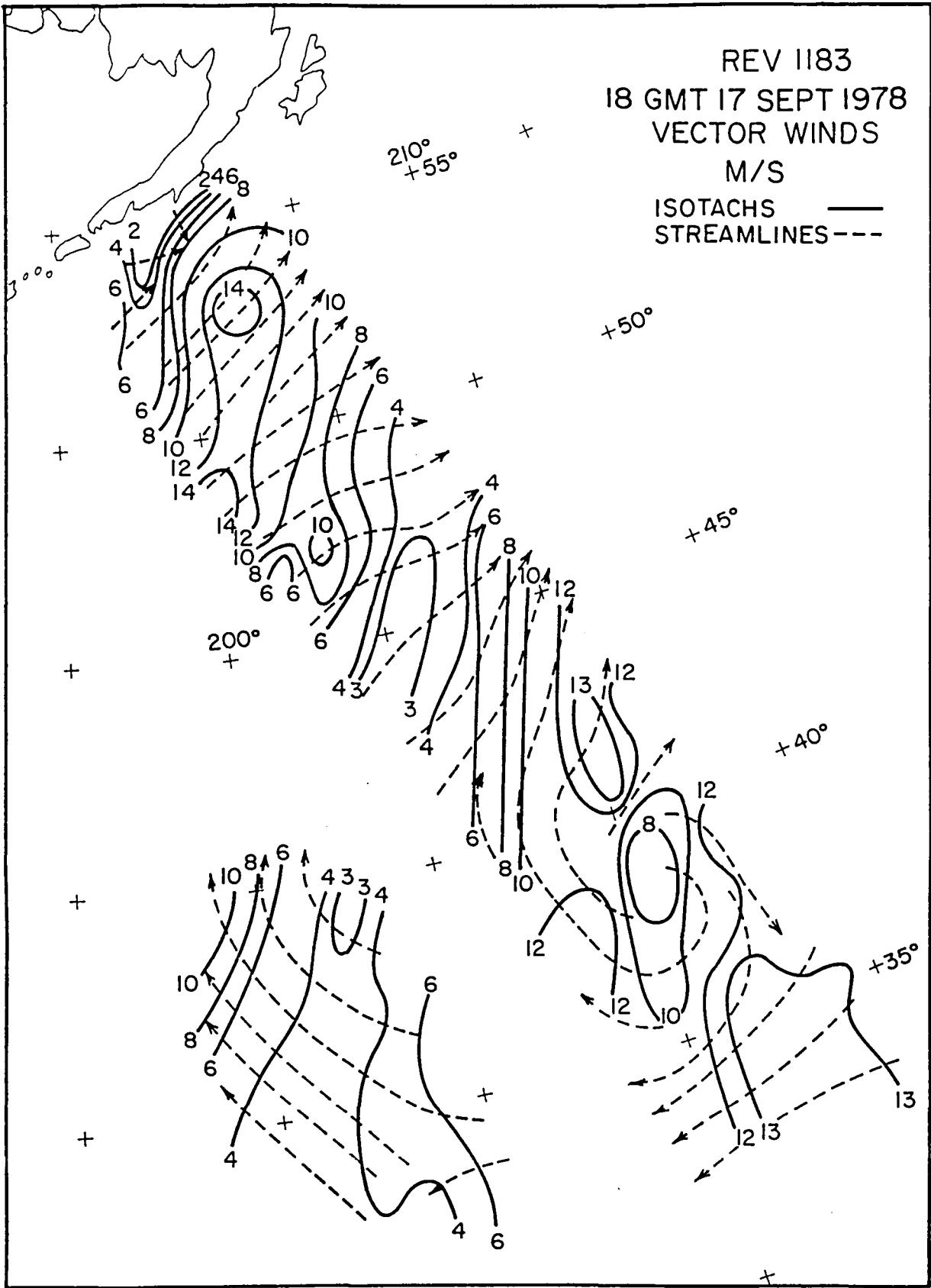
FIG. 26   Final Streamline Isotach Analysis for REV 1183.

charts show values from zero to minus one and do not reflect the presence of a front.

Figure 28 is a composite, as before, of the cloud imagry from Fig. 24, the frontal analysis from Fig. 25 and the horizontal field of divergence from the superobservations. From those GOES images that showed latitude longitude lines, transparent overlays were made and relocated by means of coastal landmarks so as to map the clouds to the polar stereographic projection. The divergence ranges from -4×10^{-5} to 6×10^{-5}.

The clear band in the upper left does not align well with the secondary cold front. With such sparce conventional data, the analysis could be changed to conform to the clear sky band.

At the top of the occlusion there is convergence associated with high bright clouds. To the south, and in advance of the secondary cold front, there is an area of divergence ($4 \times 10^{-5} \sec^{-1}$) located in the area of clearing skies at the bend in the jet stream.

Convergence is associated with the occlusion and the cold front with strong convergence just in advance of the primary cold front (-3×10^{-5}) where the sunlit cumulus peaks can be seen in the cloud images. Had the swath been two sided all the way, perhaps this area of convergence could also have been located farther to the south in advance of the front.

Farther to the south, the main swath just shows negligable divergence over a large part followed by strong divergence just to the north of, and in, the east-west band of clear skies. A time lapse loop might show the clouds to be dissipating to the north of the clear band.

The eastern side of the small westward portion of the swath shows convergence where the scattered cumulus (not drawn individually) occurs in the image and relatively clearer skies west of the zero contour on to the frontal cloud band.

Figure 29 shows the curl of the wind stress which, again, has been computed for a density of 1.25 kg per cubic meter. This figure and Figure 27 will be discussed later.
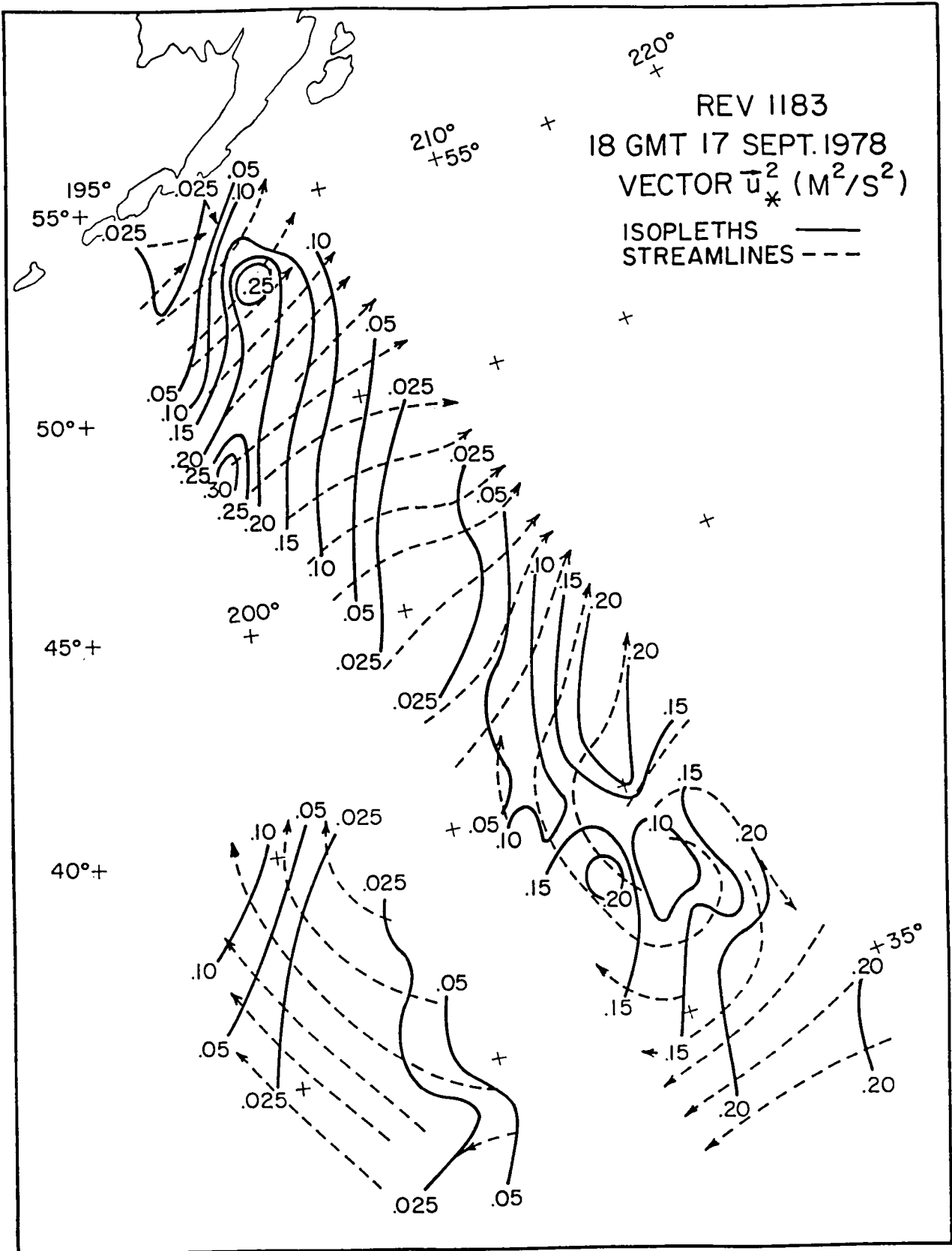
FIG. 27   Final Streamline Isopleth Analysis for $\vec{u}_*^2$ for REV 1183.

POOR CLOUD RESOLUTION
AT HIGH LATITUDES

DIV. = + 4 ASSOCIATED WITH
BROKEN THINNER CLOUDS
BEHIND OCCLUSION

205°
+55°

215°
+50°

SCATTERED
CUMULUS

CLEAR

CLEAR

195°
+45°

HIGH CUMILIFORM TOPS
THROUGH STRATUS

CLR

+40°

CLEAR

REV 1183
18 GMT 17 SEPT 1978
$10^5 \cdot DIV_2 \vec{V}_h$ (sec^{-1})
CONVERGENCE C —— (−)
DIVERGENCE   D ······ (+)
CLOUD BOUNDARIES

CLEAR

+35°

SCATTERED
CUMULUS

DENSE
OVERCAST

COMPLEX
CLOUD PATTERNS
TO SOUTH

FIG. 28   A Composite Analysis of the Divergence of the Horizontal Wind, GOES Clouds,
and Synoptic Scale Frontal Analysis for REV 1183.
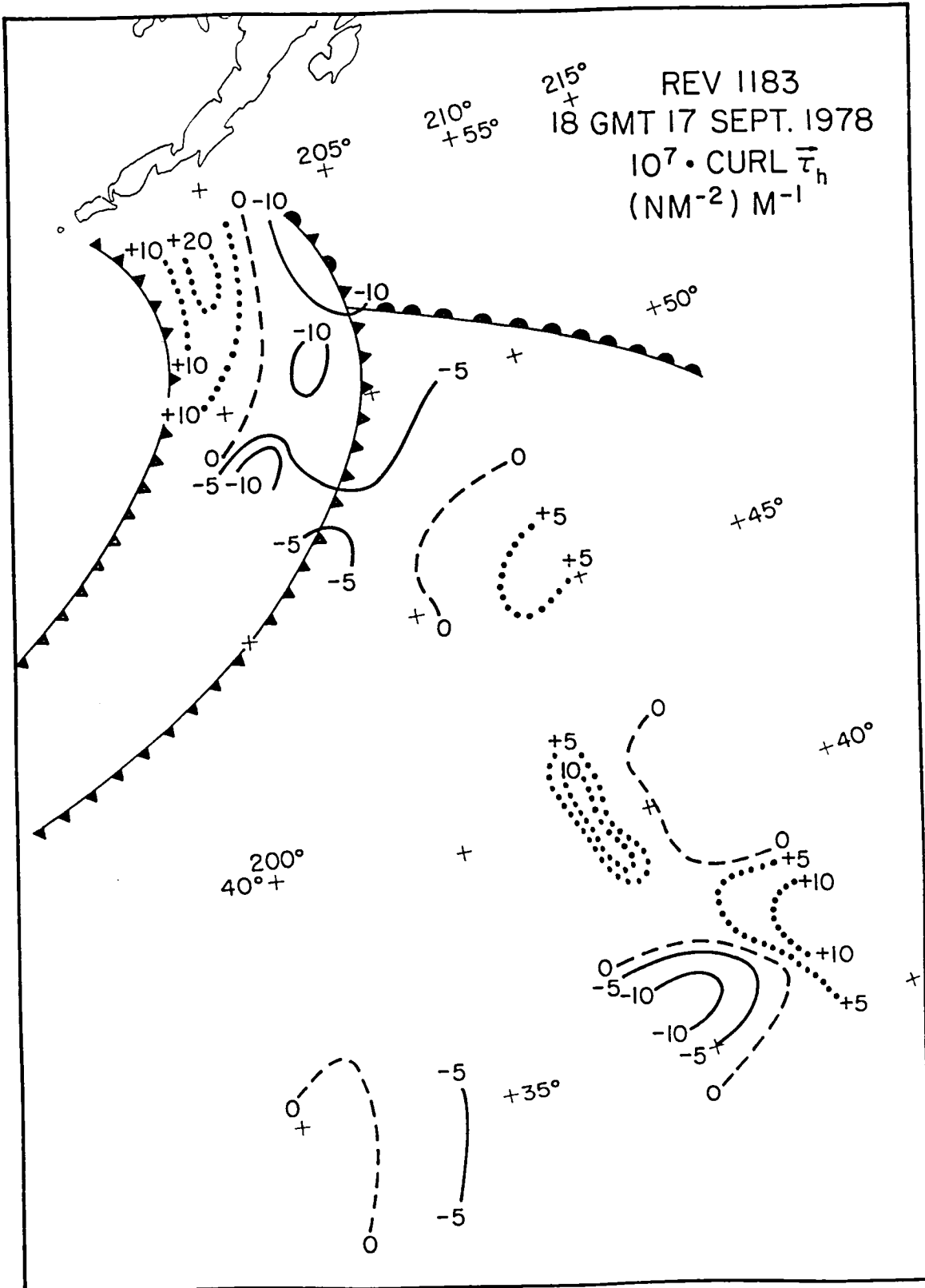
FIG. 29   The Curl of the Wind Stress for REV 1183.

99

Figures 30 and 31 illustrate an almost text book occlusion, cold front and warm front pattern with a low of 990 mb just off the coast of North America at 59° N 143° W. The clouds extend well over the continent almost to the Arctic Ocean and as far south over land as Vancouver Island. SEASAT passed the Equator going north a few second before 1754 GMT on 19 September 1978 and, as usual, passed 30° N about 9 minutes later and 60° N about 18 minutes after crossing the Equator. There were 1081 original SASS winds that gave 120 superobservations for an average of 9 (X 4 near the swath center) SASS values per superobservation. These, in turn, yielded 65 values for the divergence and the curl.

The coastal areas of Washington, Oregon and California are clear, and along much of the United States Coast there are clear skies to the west over the Pacific for 5 or more degrees of latitude. The clouds associated with the system occur on both sides of the front with a slight thinning along longitude 130° W (230° E). Strong winds from the south are shown in advance of a fairly accurately located front. The winds are west to north-west behind the front.

The front in Fig. 31 is essentially located by six ship reports and one land report from the Queen Charlotte Island for the area of interest. There is a rather wide arching zone in which it could be located on the basis of the avaiable data. Two ships in the warm sector report 30 knot (15 m/s) winds.

Figure 32 shows the streamline isotach analysis of the winds. A strong southerly flow from one side of the swath to the other of 15 m/s is shown. Warm air advection is also shown in the temperature field of Woiceshyn, et al. (1979) but the air is not significantly either colder or warmer than the ocean. There is no dew point field. Light winds under 2.5 m/s are found off Oregon. South of about 43° N near the coast the winds are north-east and increase in speed to 12.5 m/s near 35° N.

Figure 33 shows the isopleths and streamlines for $\vec{u}_*^2$. Values contoured range from 0.60 to 0.005 corresponding to u_* values of 0.77 m/s to 0.07 m/s.

18 5 19SE78 35A-2   00271 18911 UC2

FIG. 30 GOES Cloud Imagry for REV 1212. (From Woiceshyn,
et al. (1979)).
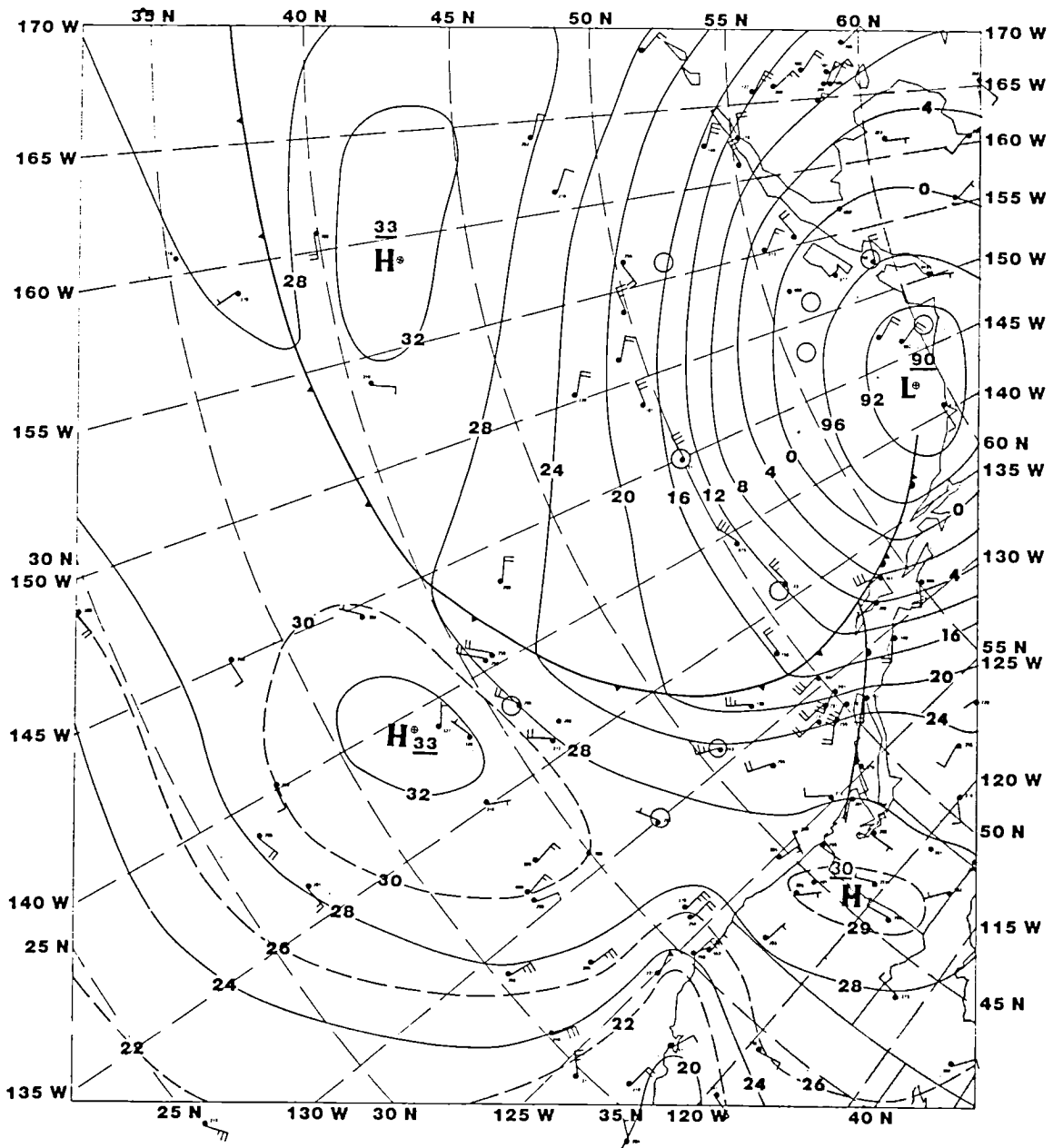
18Z 19 SEPT 1978   **REV 1212**

FIG. 31 Conventional Analysis Associated with REV 1212. One Full Barb for
         a Ship Report Represents 10 Knots. (From Woiceshyn, et al. (1979)).

102
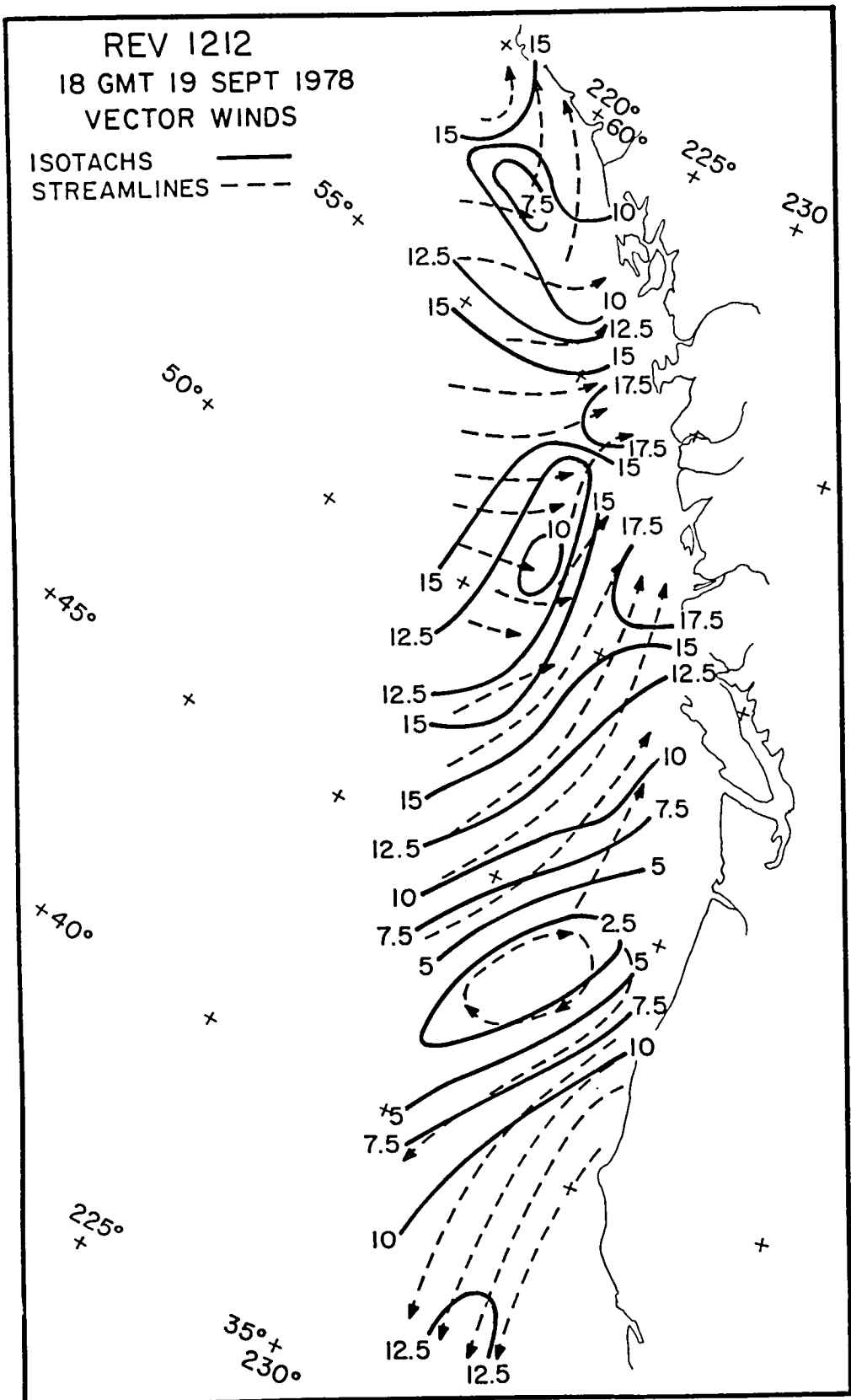
FIG. 32 Final Streamline Isotach Analysis for REV 1212.
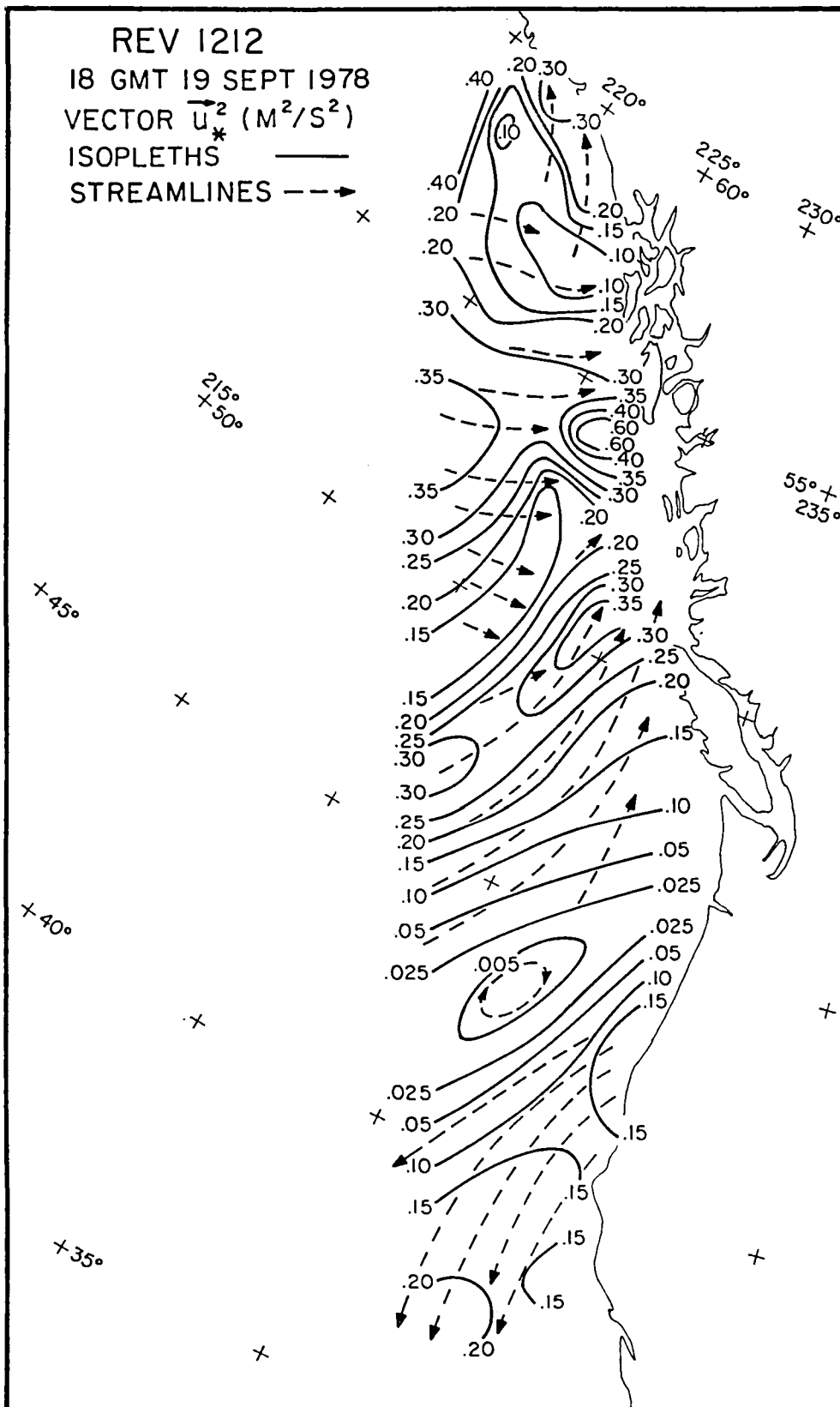
FIG. 33 Final Streamline Isopleth Analysis for $\vec{u}_*^2$ for REV 1212.

104

Figure 34 is the composite similar to those before of the clouds, the fronts and the divergence field. A band of convergence with values less than (i.e. more negative) -2×10^{-5} lies on both sides of the cold front and extends all the way to the low center. The maximum convergence is -8×10^{-5}, which corresponds to a vertical velocity of 1.6 cm/sec at 200 meters at the junction of the cold and warm fronts. The total volume of ascending air moving upward per hour in this area would be rather large. There is also strong convergence in the warm sector just to the west of the warm front. There is a thin band where the divergence is greater than -2×10^{-5} but less than zero associated with the thin clouds mentioned for Fig. 31.

Farther south, the divergence is either negligable or positive. It is associated either with clear skies or nondescript thinning clouds.

Figure 35 shows the curl of the wind stress. It is almost everywhere negative with the most negative value equal to -3×10^{-6}.

FIG. 34 A Composite Analysis of the Divergence of the Horizontal
Wind, GOES Clouds, and Synoptic Scale Frontal Analysis
for REV 1212.
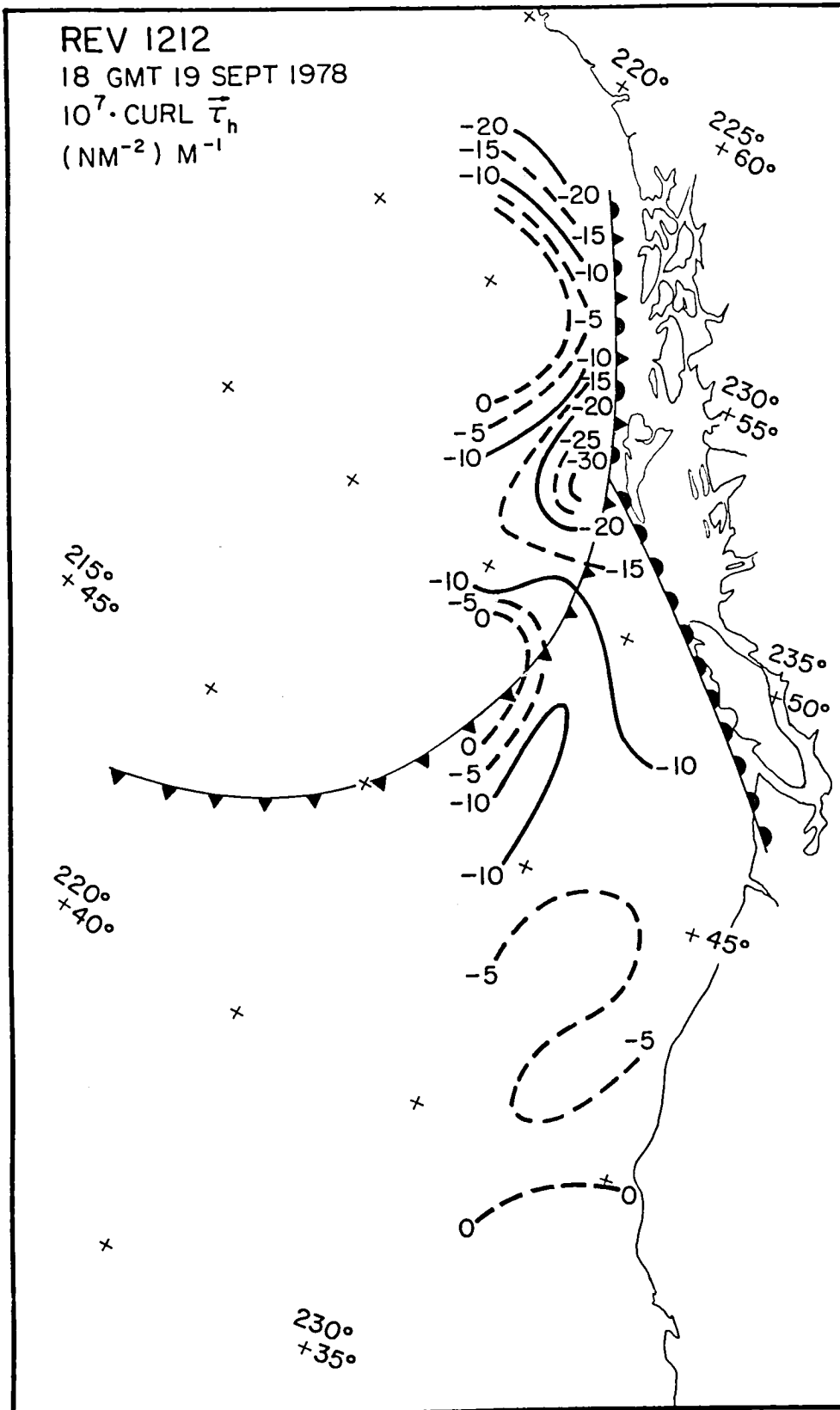
FIG. 35 The Curl of the Wind Stress for REV 1212.

107

Revolution 1298 crossed the Equator northbound about 13 seconds after 1819 GMT. From nine to eighteen minutes later, it had made the backscatter measurements between 30° and 60° N needed to provide the 1056 SASS winds used in this study, where the actual data used began at 35° N. There were 130 superobservations for an average of 8 (X 4 near the swath center) SASS winds per superobservation. These yielded 67 values for the divergence and the curl.

The cloud pattern off the west coast in Fig. 36 suggests three frontal systems with a dominant one in the center associated with the largest and brightest cloud shield to the north. Two closed low centers are identified to the east of 145° W of 994 mb and 1003 mb. The 1012 mb isobar surrounds a vast area of lower pressures in which all three frontal systems are located as in Fig. 37. To the far north in the Gulf of Alaska, a 1025 mb high pressure center is shown. South of the high and north and east of the low nearly all of the ship reported winds have a component from the east.

From east to west, in Fig. 37, the first frontal system is shown as an open wave cold front-warm front, the second as an occlusion changing to a cold front without any associated warm front and the third, as a simple cold front. The air temperatures shown by Woiceshyn, et al. (1979), show a large oscillation of the isotherms. For example, the 14° C isotherm extends southward to 38° N at 145° W and sweeps northward to 51° N at 132° W. Within the SEASAT swath, the air-sea temperature difference is close to zero, and, at most, -1° C.

The wind field for REV 1298, as in Fig. 38, shows west winds near 35° N, turning to south and southeast winds off California and Oregon, and then to dominantly easterly winds the rest of the way north until the high center is reached. The air accelerates as it moves offshore from 4 to 12 m/s along one streamline and from 8 to 14 m/s along another. The PBL analyses for this REV do not agree very well with the pressure field shown in Fig. 37. Nor do the winds increase offshore at a rate indicated by Fig. 38. The values of $\vec{u}_{*}^{2}$ reach as high as 0.25, which corresponds to a u_{*} of 0.50 m/s as shown in Fig. 39.

FIG. 36 GOES Cloud Imagry for REV 1298. (From Woiceshyn,
        et al. (1979)).
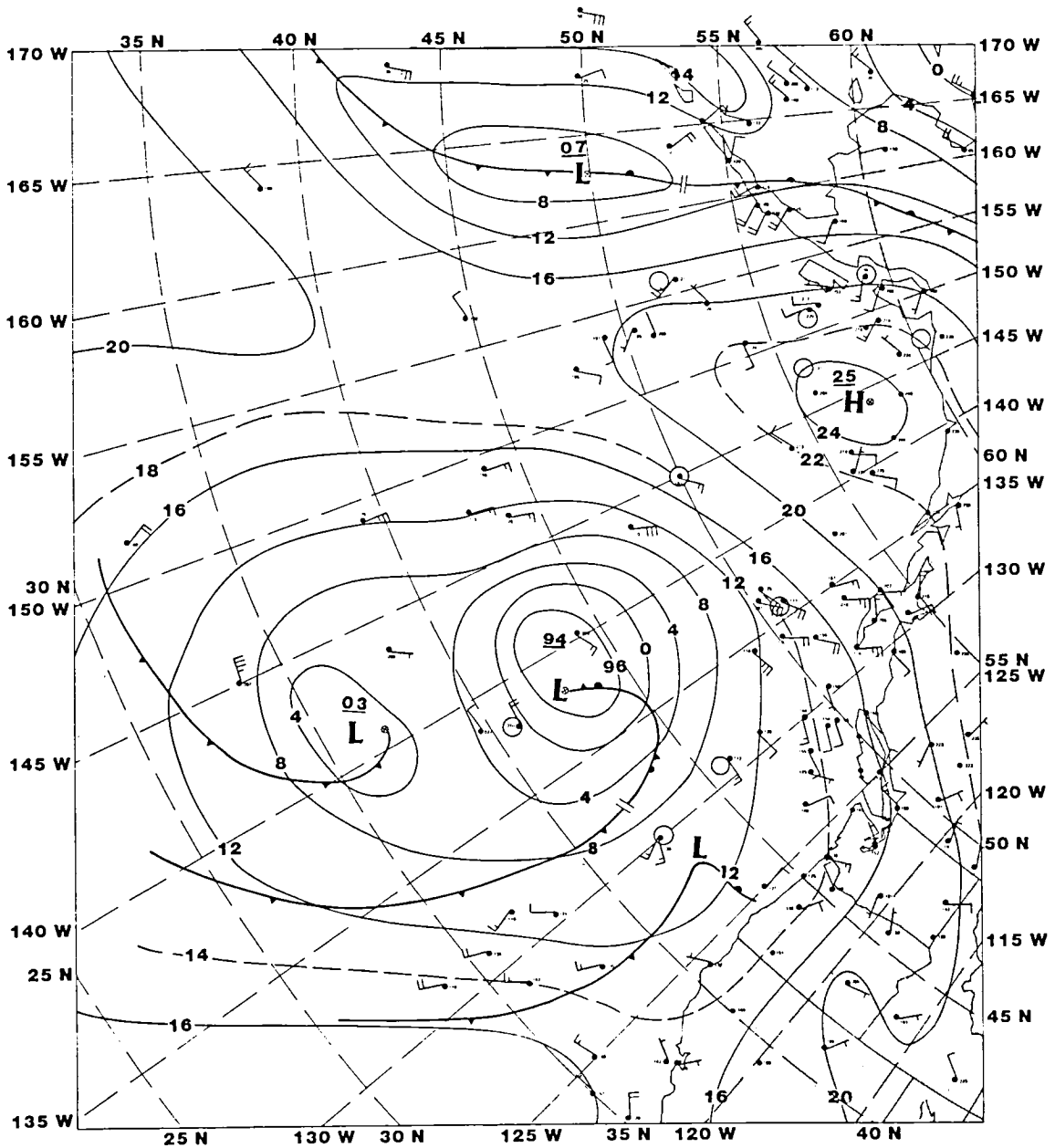
18Z 25 SEPT 1978　　　　　　　　　　**REV 1298**

FIG 37 Conventional Analysis Associated with REV 1298. One Full Barb for
a Ship Report Represents 10 Knots. (From Woiceshyn, et al. (1979)).

FIG. 38 Final Streamline Isotach Analysis for REV 1298.

111

FIG. 39   Final Streamline Isopleth Analysis for $\vec{u}_*^2$ for REV 1298.

The composite of the fronts, clouds, and superobservation divergence
field is not particularly revealing with the values for the divergence
ranging from just over $+2 \times 10^{-5}$ to just under -2×10^{-5}. Divergence is
found between the open wave and the approaching dominant center. Although
the air is being accelerated into the dominant low center, the swath does
not pick up any dominant features.

The pattern for the curl of the wind stress is clearly defined in Fig.
41. The maximum is 1.3×10^{-6}. The use of 1.25 kg/m^3 may not be as accurate
as it could be because of the correlation of high pressure and cold air and
low pressure and warm air.
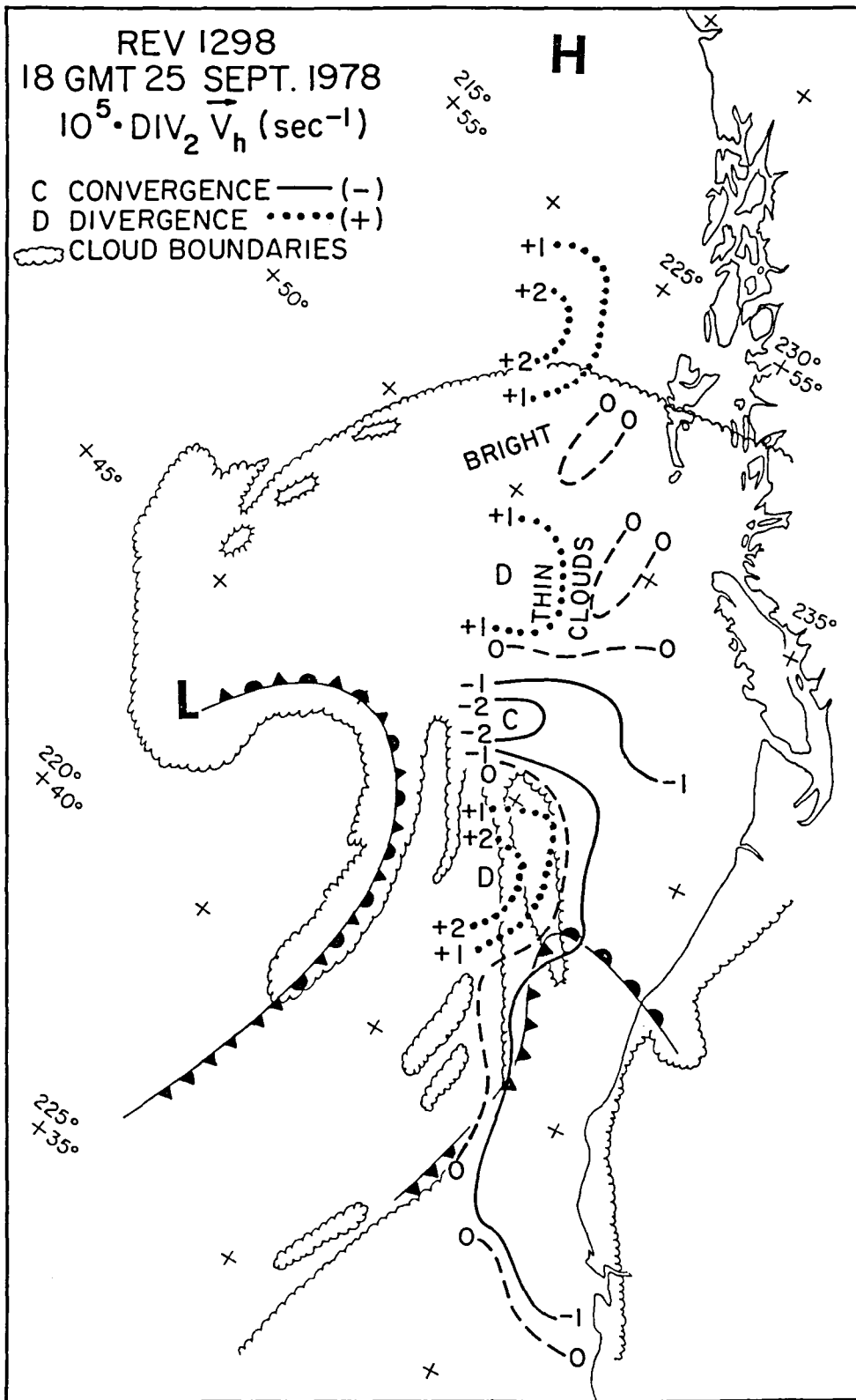
FIG. 40   A Composite Analysis of the Divergence of the Horizontal
   Wind, GOES Clouds, and Synoptic Scale Frontal Analysis
          for REV 1298.

114

REV 1298
18 GMT 25 SEPT. 1978
$10^7 \cdot$ CURL $\vec{\tau}_h$
$(NM^{-2}) M^{-1}$

0

0

-2
-5
-2
-5

-5   -5
-2
0
+2
+5
+10   +2
+13
+13   +2
+10

+5
+2

0
0

0
0

-2
0
-2

0
235°

$2/5°$ ×45°

$220°$ +40°

$225°$ +

$35°$+
$230°$
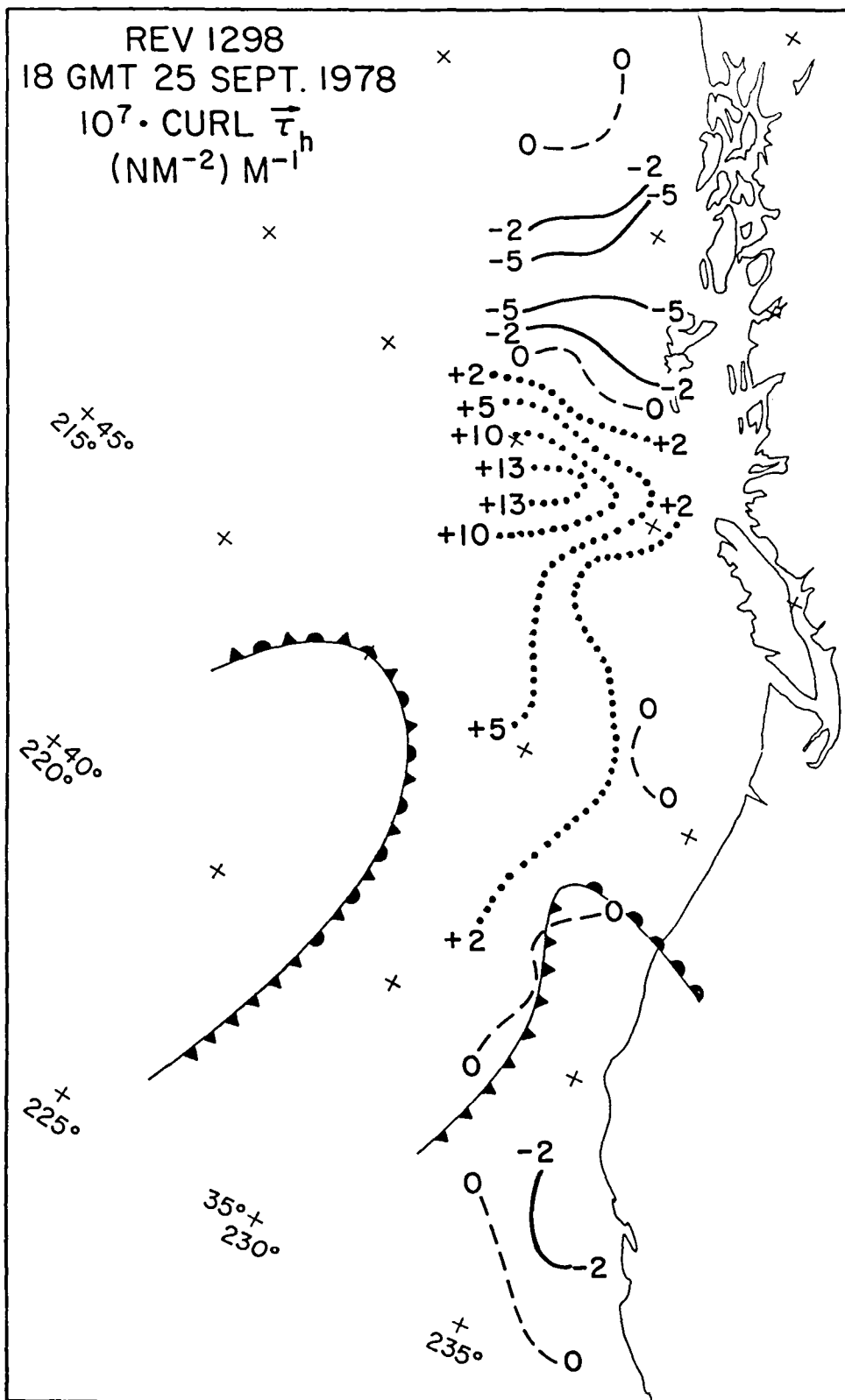
FIG. 41   The Curl of the Wind Stress for REV 1298.

115

WIND STRESS, WIND STRESS CURL AND OCEAN CURRENTS

Figures 21, 23, 27, 29, 33, 35, 39 and 41 provide a tantalizing glimpse of two quantities that are important in the study of ocean currents. Those for $\vec{u}_*^2$ represent the quantity, $\vec{\tau}/\rho = -\langle u'w' \rangle$, for a scale somewhat larger than represented by the time averages of these eddy quantities as measured by Smith (1980) and Large and Pond (1981), except perhaps for westerly (or easterly) winds above about 15 m/s to the north near 55° N to 60° N. The smooth variation from a $\vec{U}_{10}^1$ to a $\vec{U}_{10}^2$ to a $\vec{U}_{10}^3$ power for u_*^2 would fit the data of Large and Pond (1981) because these data were used to obtain equation (74). The dependence for lighter winds is realistic from the point of view that C_{10} should increase as the wind decreases for light winds as required in numerous models.

Present thinking on the subject is that the downward flux of momentum cannot produce a real stress on the sea surface and cannot generate waves. The fluctuations in u'w' must first be converted into pressure fluctuations on the water, which in turn generate the waves. The breaking waves and Stokes drift then produce the surface currents of the oceans. Whether or not a shear wind stress can generate a shear current in the ocean is a matter of some conjecture. The wave induced surface drift can be "of the same order as the surface drift generally attributed to the effect of the wind shear stress" and at roughly the same angle to the wind as the Ekman current (Madsen (1978)). Once the waves produce a surface current, especially if breaking and turbulence are involved, a downward flux of momentum in the water could produce a changing direction of the current with depth as in Ekman theory.

The early history of the theory of ocean currents frequently involved the curl of the wind stress. However, the winds were the climatologically averaged winds, and the stress was often computed by means of a constant times the square of the wind speed measured at a presumed 10 meters above the sea surface. The constant varied from one study to another. Moreover, since the vector averages of the winds squared and directed in the direction of the vectors is not the same as averaged directed squares of the winds (or since $(\vec{u}_*^2)$ averaged at each grid point of the model for, say, on a week, a month or a year is not the same as the value of $\vec{u}_*^2$ computed from $\vec{U}_{10}$ averaged at each grid point for the same time interval), these weekly, or monthly, or annual, wind stress fields are strange quantities indeed.

If, however, the climatological winds are somehow connected to the
climatological oceans in the ways described by various theories through
1966, or so, (see Neumann and Pierson (1966)), then equations such as
equations (123) from Sverdrup (1947), (124) from Stommel (1948) and (125)
from Munk (1950) would apply, and equations for the integrated mass transports
such as those of Welander (1959) and Munk and Carrier (1950) might be
extended and applied to more realistic oceans. There have been efforts to
do so since the cited papers were published.

$$\beta \frac{\partial s}{\partial y} + \frac{\partial \tau_x}{\partial y} - \frac{\partial \tau_y}{\partial x} = 0 \tag{123}$$

$$\beta \frac{\partial \psi}{\partial x} + k \nabla^2 \psi = \text{curl}_z \tau \tag{124}$$

$$A_h \nabla^4 \psi - \beta \frac{\partial \psi}{\partial x} = \text{curl}_z \tau \tag{125}$$

In these equations, $\beta = \partial f / \partial y$ ($f = 2\omega \sin \theta$) where the motions are treated
in terms of the β plane approximation to motions on a sphere (i.e. $\theta = \theta_o + \frac{\partial \theta}{\partial y} d y$).
S in (123) is the integrated mass transport, and the equation does not
hold near the western side of an ocean. In (124), ψ is a stream function, and
the paper in which it first appeared caused quite a stir in oceanographic
circles because it produced a westward intensification of ocean currents for
a rectangular ocean (i.e. something like a Gulf Stream).

Theoretical efforts have continued since these papers, and there are
many scientists still concerned with the details of the curl of the wind
stress as a driving force for the surface circulation of the oceans. The
four figures for the four GOASEX passes of our study (Figs. 23, 29, 35 and
41) are, to our knowledge, the first finite difference calculations of the
curl of the synoptic scale wind stress for a spherical earth with an assignable
error structure made from a synoptic scale wind field.

Drifting buoys drouged to a depth of 30 m by 9.2 m diameter parachutes
were deployed in the eastern North Pacific during parts of 1975, 1976 and 1977
and tracked by the Random Access Measurement System on Nimbus Spacecraft.
Reports on the day to day movements of these buoys by Kirwan, et al. (1978a)
and Kirwan, et al. (1979) have described the paths of these buoys. Supplementary
reports by Kirwan, et al. (1975), Kirwan, et al. (1978b), Kirwan and Chang
(1978), and McNally, et al. (1978), plus other references, have described these
buoys plus other designs, and theoretical aspects of their movement.

The hour by hour and day by day movement of these drogued buoys is very irregular and complex. It is too much to expect that a particular buoy stays with a particular volume of water along its entire path. Any particular portion of the path of a buoy for that particular day and time represents an appreciable percentage of the water motion at 30 m.

Kirwan, et al. (1978a) plotted and interpreted the paths of 22 drifters launched in the North Pacific between about 167° W to 153° W and 35° N to 45° N for the period from 10 September 1976 to 31 August 1977. During this year (approximately) the buoys spread out. One went as far north as 57° N, 137° W, and another went as far south and east as 34° N and 127° W. Some first went northward and then southward. Some followed the cyclonic gyre in the Gulf of Alaska on the average; others got into the California current.

The surface movement of ocean water tends to be in geostrophic balance with the geodynamic topography, that is the slope of the sea surface relative to the geoid. This slope has been measured for areas where it is large and the geoid is well enough known as in Cheney (1982). For this area, Wyrtki (1974) found a slope of 0.6 geodynamic meters relative to the 1000 decibar surface from 30° N to 50° N along 155° W, which is a value that is probably too small to detect with altimetry and our present knowledge of the geoid in this area. The dynamic topography contours spread out upon approaching North America to form the Gulf of Alaska gyre and California current as a part of the North Pacific gyre.

Superimposed on the gradient current would be the tidal currents. A water volume would follow a complicated path made up of various sized ellipses produced by the phase reinforcement and cancellation of those tidal frequencies important to the ocean's response for a particular area.

Also strong local winds could excite inertial oscillations starting out at random times, headed in random directions, and dying down in amplitude as a function of the turbulence in the water. These oscillations have many of the features of intermittant transients so that the usual Fourier procedures miss many of their properties.

There is also the possibility that the time varying ocean currents do

indeed have time to adjust to the driving forces of the locally varying synoptic scale wind.

The data in Kirwan, et al. (1978a) admit of many different interpretations among them those of the authors. For our particular application, just a few features of the buoy paths will be noted from this study.

The day to day motions of the drogued buoys were very irregular with wiggles, loops, bends and turns. The paths of Buoy 1D 1615 was shown from day 106 to day 125, mid March through the first few days in April. Its displacement from day 119 to day 120 was about 9 or 10 km whereas from day 121 to 122 it moved 65 km (times centered on 1200 GMT). Other decelerations and accelerations during the period above were almost as dramatic.

Buoy 1D 1326 was tracked for over 300 days beginning on day 265 of 1976. The time span was from the latter part of September 1976 to mid July 1977 with buoy positions interpolated to each synoptic (6 hourly) period and then smoothed by a 25 point (6 day) running average. This buoy entered the Gulf of Alaska gyre. The buoy velocities do not reflect stronger winds in the winter. The dominant east-west component was eastward and the buoy moved erratically northward until about day 100 of 1977 (early April). Oscillations in the north-south component of the motion were rapid and large during the last third of the period from plus 0.7 m/s to minus 0.8 m/s compared to values between zero and +0.4 earlier. The total speed toward the end of the tracking period oscillated from essentially zero to over 0.8 m/s.

Buoy 1D 0152 was tracked for over a year and entered the main North Pacific gyre. The last part of its path was during the first 120 days of 1977. The oscillations in both velocity and speed were the largest during the period.

These rapid changes in speed and direction could be explained by the eight figures obtained for wind stress and wind stress curl of our study. Extratropical cyclones tend to develop at times in the Pacific around 30° N and move northeastward into the Gulf of Alaska as they deepen and intensify. This intensification as they approach the west coast of North America may be enough to overcome the missing annual variability of a wind effect for the buoy in the Gulf of Alaska gyre, and to explain the rapid changes

from day to day and the general increase and rapid velocity variations as the buoy moves eastward.

Kirwan, et al. (1979) also studied the motions of six drifters from day 290 of 1975 to day 125 of 1976 (Oct. 1975 to May 1976) by combining the gradient current, Stoke's drift and Ekman (u_*^2 law) drift, relaxed so that the current need not be at 45° to the wind. The ratio of the model variance to the actual variance (i.e. that part of the motion that can be predicted from the gradient currents and the wind versus the actual vector buoy motions), designated by R^2, was used as a measure of how well the wind could be used to predict the currents. The model with the most degrees of freedom explained 75% of the variance for a brief interval. The average for 5 day running averages was about 50%, and R^2 at times was as low as 20% to 30%.

The agreement is not too satisfactory. Part of the reason may lie in the quality of the wind fields that were produced by the Fleet Numerical Oceanography Center in 1975 and 1976. These fields cannot be very good for the reasons given in preceding sections. The four passes presented in this study show large gradients in the winds, the wind stress, and localized areas where the curl of the wind stress is large. Otherwise, there are much larger areas of low stress values and extremely weak values of the curl. The movement of drogued buoys may eventually be both explainable and predictable once a combined study of winds from NROSS, sea surface topography from TOPEX and newly deployed drogued buoys becomes possible in the future.

Equations such as (123), (124) and (125), and the many variants that have followed, usually make a number of simplifying assumptions in their derivation. The root mean square variability of surface elevation as in Robinson, et al. (1983) and Cheney, Marsh and Beckley (1983) is, just as in the work of Kirwan, et al. (1978a) and Kirwan, et al. (1979), an effect of rapidly varying winds with large gradients. The actual wind stress is probably the more important quantity for the day by day study of ocean currents.

Additional studies of drogued buoys are those of McNally (1981) and McNally, et al. (1983). McNally (1981) compared the motions of a number of buoys in the Eastern North Pacific over about one month with the average sea level atmospheric isobaric pattern. The drifters move approximately 30° to the right of the surface winds (conventionally obtained) when averaged for 5 days or more.

Over these longer time scales the agreement was quite good.

McNally, et al. (1983) have reviewed the drifting buoy program since 1975. If Japanese buoys drogued to 10 meters (Nitani (1982)) and NORPAX Buoys drogued to 100 m (an exception) in the Kuroshio are counted more than 135 buoys were involved. The buoys in the Kuroshio at 10 and 100 m moved in nearly the same way.

The analysis shows many features of the North Pacific circulation not revealed by present theories and many other features partially confirmed. For example, the North Equatorial current is remarkably steady and non-dispersive. The differences between the various methods to study currents such as dynamic topography referred to a 500 decibar level of no motion as in Wyrtki (1974) and seasonally averaged sea level pressure fields and actual buoy trajectories are at times and places quite small and at other times and places quite large.

Another area of investigation that requires knowledge of the wind stress is the study of the excitation of oscillations in the pycnocline in the equatorial Pacific from 15° N to 11° S as Kelvin and Rossby waves. The only data presently available as described by Busalacchi, et al. (1983) are monthly mean values of the stress gleaned from transient ships from 1961 to 1979 (19 years). Zonal stress obtained this way is coherent from month to month and shows considerable interannual variability. When scatterometry data have been available for a comparable period, it will be interesting to see what kinds of differences are found.

The difficulties involved in calculating the wind stress over times longer than synoptic times and in correcting for air sea temperature differences are treated by Hellerman and Rosenstein (1983) and Thompson, et al. (1983). Both account for a non-constant drag coefficient, but only the latter appears to treat the fluctuations of the wind from one observation to another.

The possible study of the entire ocean circulation as in Wunsch and Gapaschkin (1980) that involves scatterometry and altimetry may also require other data of conventional form as well as drifting buoy data. An example of the use of combined conventional and altimeter data is Bernstein, et al. (1982). The North Atlantic currents are even more complex (Richardson (1981)).

121

DIVERGENCE, VERTICAL VELOCITIES, WATER VAPOR, CLOUDS AND PRECIPITATION

Vertical velocities at 200 m above the sea surface were computed in two different ways. One used equation (117) and (118). The other simply reversed the sign of equation (67), used (68) and multiplied the values obtained by 200. Results were converted to cm/sec. Tables 3, 4, 5 and 6 show the results for REVS 1141, 1212, 1183, and 1298 respectively. Two hundred meters may be pushing the theory too far because the winds may be changing direction at these heights.

The columns from left to right are: (1) latitude, (2) longitude, (3) vertical velocity from (67) (plus is up), (4) its standard deviation, (5) vertical velocity from (117), (6) its standard deviation from (118). The next column shows the ratio of column (5) to (3), and the last column tags whether the ratio is greater or less than one.

A better model for the variation of wind with height would improve equations (117) and (118), but the available data seem to show that the air was nearly neutrally stratified so that the neutral log profile may be good enough. Vertical motions based on the neutral wind profile are in general somewhat higher than those based on the wind at 19.5 meters assumed to be constant with height. Since each of the five grid points involved is treated separately, there are some rather large differences in the vertical velocities. Large ratios such as the 4.43 for REV 1212 and the -3.47 for REV 1298 are the result of negligable values near zero that changed by negligable amounts that nevertheless produced a high ratio. The exception is the -19.61 for REV 1298 for which -0.03 cm/sec changed to 0.51 cm/sec.

The divergence fields as discussed for each revolution located those regions of upward and downward air motion correctly for all REVS except REV 1298 where the direction reversed twelve times. For four of these sign changes, the vertical velocities were negligable.

Katsaros and McMurdie (1983a) have studied the distribution of atmospheric water near extratropical cyclones by means of the SMMR. SEASAT REV 1098 for September 1978 was used. The inherent difficulties in verifying the fields that were produced by means of radiosonde ascents, aircraft, flights and precipitation measurements over the ocean are many times more difficult than

TABLE 3a Vertical Velocities for REV 1141. See Text for meaning of Column Heading Numbers.

(1)	(2)	(3)	(4)	(5)	(6)	(7)	(8)
34.	220.	0.26	0.05	0.27	0.05	1.02	1
34.	221.	0.29	0.05	0.30	0.05	1.04	1
34.	222.	0.17	0.05	0.19	0.10	1.09	1
35.	219.	-0.47	0.13	-0.48	0.10	1.02	1
35.	220.	0.06	0.06	0.06	0.06	1.02	1
35.	221.	0.29	0.06	0.30	0.06	1.03	1
35.	222.	0.03	0.07	0.04	0.07	1.37	1
36.	219.	-0.29	0.09	-0.30	0.09	1.02	1
36.	220.	0.29	0.08	0.30	0.08	1.03	1
36.	221.	0.15	0.07	0.15	0.07	1.01	1
37.	218.	-0.06	0.09	-0.06	0.09	1.01	1
37.	219.	0.50	0.08	0.51	0.08	1.02	1
37.	220.	0.69	0.08	0.71	0.08	1.02	1
38.	218.	0.16	0.07	0.16	0.07	1.01	1
38.	219.	0.50	0.08	0.51	0.08	1.03	1
39.	217.	-0.23	0.07	-0.24	0.07	1.02	1
39.	218.	-0.32	0.06	-0.32	0.06	1.02	1
40.	216.	0.03	0.08	0.03	0.08	1.09	1
40.	217.	-0.24	0.08	-0.25	0.08	1.03	1
40.	218.	-0.30	0.05	-0.31	0.05	1.04	1
41.	216.	-0.28	0.12	-0.29	0.12	1.03	1
41.	217.	-0.16	0.08	-0.17	0.08	1.04	1
41.	218.	0.04	0.11	0.04	0.11	0.92	-1
42.	215.	-0.19	0.09	-0.20	0.09	1.04	1
42.	216.	-0.34	0.05	-0.35	0.05	1.02	1
42.	217.	-0.14	0.08	-0.15	0.08	1.06	1
43.	214.	-0.19	0.07	-0.19	0.07	1.01	1
43.	215.	-0.24	0.04	-0.24	0.04	1.03	1
43.	216.	-0.28	0.05	-0.28	0.05	1.02	1
44.	214.	-0.01	0.04	-0.00	0.04	0.33	-1
44.	215.	-0.13	0.05	-0.13	0.05	1.01	1
44.	216.	-0.22	0.05	-0.22	0.05	1.02	1
45.	213.	0.30	0.04	0.33	0.04	1.09	1
45.	214.	0.07	0.03	0.07	0.03	1.02	1
45.	215.	-0.13	0.04	-0.14	0.04	1.06	1
45.	216.	-0.08	0.04	-0.08	0.05	0.96	-1
46.	212.	0.24	0.05	0.28	0.05	1.17	1
46.	213.	0.04	0.03	0.04	0.03	1.06	1
46.	214.	-0.13	0.03	-0.14	0.03	1.12	1
46.	215.	-0.22	0.03	-0.24	0.03	1.07	1
46.	216.	-0.07	0.05	-0.06	0.05	0.88	-1
47.	212.	0.03	0.02	0.03	0.03	1.25	1
47.	213.	-0.20	0.02	-0.22	0.03	1.11	1
47.	214.	-0.26	0.03	-0.28	0.03	1.08	1
47.	215.	-0.24	0.02	-0.26	0.02	1.06	1
48.	211.	0.16	0.03	0.18	0.03	1.14	1
48.	212.	-0.05	0.02	-0.06	0.02	1.19	1
48.	213.	-0.27	0.03	-0.30	0.03	1.12	1
48.	214.	-0.23	0.02	-0.26	0.03	1.09	1
49.	210.	0.37	0.03	0.41	0.03	1.12	1
49.	211.	0.11	0.02	0.11	0.02	0.97	-1
49.	212.	-0.10	0.04	-0.13	0.04	1.28	1
49.	213.	-0.08	0.04	-0.09	0.04	1.10	1
49.	214.	-0.03	0.05	-0.02	0.05	0.67	-1
50.	209.	0.24	0.03	0.29	0.03	1.18	1
50.	210.	0.04	0.03	0.03	0.03	0.82	-1
50.	211.	-0.08	0.07	-0.11	0.07	1.40	1
50.	212.	-0.14	0.07	-0.17	0.07	1.19	1
50.	213.	0.03	0.07	0.05	0.03	1.59	1
51.	208.	0.21	0.03	0.24	0.03	1.17	1
51.	209.	-0.02	0.03	-0.03	0.03	1.60	1

TABLE 3b. (Table 3a continued.)

(1)	(2)	(3)	(4)	(5)	(6)	(7)	(8)
51.	210.	-0.29	0.05	-0.35	0.06	1.20	1
51.	211.	-0.23	0.09	-0.27	0.09	1.17	1
51.	212.	-0.04	0.09	-0.03	0.09	0.90	-1
51.	213.	-0.07	0.09	-0.06	0.09	0.82	-1
52.	207.	0.17	0.04	0.18	0.04	1.08	1
52.	208.	0.08	0.05	0.08	0.05	0.96	-1
52.	209.	-0.03	0.08	-0.04	0.08	1.63	1
52.	210.	-0.12	0.10	-0.14	0.10	1.17	1
52.	211.	-0.10	0.11	-0.11	0.10	1.10	1
52.	212.	-0.01	0.12	-0.00	0.12	0.48	-1
53.	206.	0.28	0.06	0.29	0.06	1.04	1
53.	207.	0.11	0.06	0.11	0.06	0.99	-1
53.	208.	-0.04	0.07	-0.07	0.07	1.74	1
53.	209.	0.06	0.10	0.07	0.10	1.08	1
53.	210.	0.15	0.13	0.19	0.13	1.31	1
53.	211.	0.20	0.14	0.25	0.14	1.26	1
53.	212.	0.62	0.12	0.73	0.12	1.18	1
54.	205.	0.53	0.06	0.69	0.06	1.30	1
54.	206.	0.24	0.05	0.27	0.05	1.09	1
54.	207.	0.34	0.13	0.38	0.10	1.12	1
54.	208.	0.45	0.09	0.49	0.09	1.10	1
54.	209.	0.54	0.12	0.63	0.12	1.17	1
54.	210.	0.24	0.15	0.31	0.16	1.30	1
54.	211.	-0.17	0.17	-0.18	0.17	1.06	1
55.	207.	1.33	0.11	1.55	0.11	1.16	1
55.	208.	1.47	0.13	1.71	0.14	1.17	1
55.	209.	0.96	0.21	1.05	0.21	1.09	1
55.	210.	0.45	0.22	0.45	0.23	0.99	-1
56.	208.	1.27	0.18	1.51	0.19	1.19	1
56.	209.	0.73	0.20	0.91	0.20	1.24	1
56.	210.	0.50	0.24	0.30	0.25	0.59	-1

TABLE 4a Vertical Velocities for REV 1183. See text for Meaning of Column Heading Numbers.

(1)	(2)	(3)	(4)	(5)	(6)	(7)	(8)
34.	201.	0.08	0.03	0.08	0.03	1.04	1
34.	202.	0.05	0.07	0.05	0.07	1.07	1
34.	203.	-0.19	0.11	-0.20	0.11	1.02	1
34.	204.	-0.33	0.07	-0.34	0.07	1.03	1
34.	212.	0.16	0.03	0.18	0.03	1.09	1
34.	213.	0.26	0.02	0.28	0.02	1.06	1
35.	201.	0.09	0.03	0.09	0.03	1.02	1
35.	202.	0.17	0.03	0.17	0.04	1.04	1
35.	203.	0.18	0.06	0.19	0.06	1.04	1
35.	211.	0.17	0.09	0.19	0.09	1.13	1
35.	212.	0.16	0.02	0.17	0.02	1.11	1
35.	213.	0.29	0.07	0.30	0.07	1.06	1
36.	200.	-0.18	0.04	-0.18	0.04	1.04	1
36.	201.	0.04	0.03	0.04	0.03	1.03	1
36.	202.	0.24	0.04	0.25	0.04	1.04	1
36.	203.	0.63	0.05	0.65	0.05	1.04	1
36.	210.	0.32	0.25	0.36	0.25	1.12	1
36.	211.	0.36	0.09	0.42	0.10	1.14	1
36.	212.	0.01	0.11	0.00	0.11	0.15	-1
36.	213.	0.19	0.14	0.21	0.15	1.15	1
37.	200.	-0.28	0.04	-0.29	0.04	1.05	1
37.	201.	-0.12	0.04	-0.13	0.04	1.05	1
37.	202.	0.17	0.03	0.17	0.03	1.03	1
37.	210.	0.50	0.23	0.54	0.24	1.09	1
37.	211.	0.02	0.18	0.02	0.18	0.91	-1
37.	212.	-0.94	0.20	-1.01	0.21	1.38	1
38.	200.	-0.33	0.05	-0.35	0.05	1.06	1
38.	201.	-0.17	0.04	-0.17	0.04	1.05	1
38.	202.	0.25	0.04	0.26	0.04	1.03	1
38.	209.	0.30	0.19	0.32	0.19	1.05	1
38.	210.	-0.41	0.29	-0.44	0.29	1.08	1
38.	211.	-0.84	0.24	-0.90	0.24	1.07	1
39.	200.	-0.23	0.06	-0.25	0.06	1.10	1
39.	201.	-0.23	0.08	-0.24	0.09	1.06	1
39.	209.	-0.55	0.21	-0.57	0.21	1.03	1
39.	210.	-1.23	0.23	-1.32	0.23	1.07	1
39.	211.	-0.74	0.30	-0.79	0.30	1.07	1
40.	208.	-0.85	0.14	-0.89	0.14	1.05	1
40.	209.	-0.75	0.23	-0.83	0.24	1.11	1
40.	210.	-0.49	0.24	-0.54	0.25	1.11	1
41.	207.	-0.23	0.18	-0.24	0.18	1.05	1
41.	208.	-0.72	0.17	-0.79	0.17	1.11	1
41.	209.	-0.33	0.13	-0.38	0.13	1.15	1
41.	210.	-0.20	0.10	-0.22	0.10	1.09	1
42.	207.	-0.13	0.09	-0.15	0.09	1.15	1
42.	208.	-0.22	0.09	-0.24	0.09	1.13	1
42.	209.	-0.23	0.07	-0.26	0.07	1.12	1
42.	210.	-0.10	0.08	-0.11	0.08	1.09	1
43.	207.	-0.04	0.06	-0.04	0.06	1.20	1
43.	208.	-0.08	0.06	-0.09	0.06	1.21	1
43.	209.	-0.19	0.06	-0.22	0.06	1.14	1
44.	206.	-0.05	0.05	-0.06	0.05	1.06	1
44.	207.	-0.05	0.06	-0.06	0.06	1.18	1
44.	208.	0.08	0.07	0.07	0.07	0.88	-1
44.	209.	0.12	0.09	0.12	0.10	0.95	-1
45.	205.	0.32	0.05	0.33	0.05	1.03	1
45.	206.	0.01	0.05	0.01	0.05	0.99	-1
45.	207.	-0.21	0.07	-0.22	0.07	1.06	1
45.	208.	-0.02	0.11	-0.04	0.11	1.70	1
46.	204.	0.69	0.05	0.72	0.05	1.05	1
46.	205.	0.38	0.05	0.39	0.05	1.03	1
46.	206.	0.04	0.04	0.04	0.05	1.01	1

TABLE 4b   (Table 4a continued).

(1)	(2)	(3)	(4)	(5)	(6)	(7)	(8)
46.	207.	-0.32	0.11	-0.34	0.11	1.06	1
47.	203.	0.61	0.05	0.67	0.05	1.10	1
47.	204.	0.61	0.06	0.65	0.06	1.06	1
47.	205.	0.40	0.05	0.42	0.05	1.04	1
47.	206.	0.09	0.06	0.09	0.06	1.02	1
47.	207.	-0.14	0.08	-0.15	0.08	1.09	1
48.	202.	0.50	0.03	0.55	0.03	1.11	1
48.	203.	0.51	0.04	0.56	0.04	1.09	1
48.	204.	0.54	0.06	0.58	0.06	1.07	1
48.	205.	0.45	0.05	0.48	0.05	1.06	1
48.	206.	0.10	0.06	0.11	0.06	1.06	1
49.	201.	0.30	0.04	0.39	0.04	1.29	1
49.	202.	0.18	0.03	0.21	0.03	1.18	1
49.	203.	0.29	0.04	0.32	0.05	1.12	1
49.	204.	0.38	0.06	0.41	0.06	1.09	1
49.	205.	0.42	0.06	0.45	0.06	1.07	1
50.	201.	-0.27	0.05	-0.27	0.05	1.03	1
50.	202.	0.05	0.04	0.07	0.04	1.50	1
50.	203.	0.08	0.05	0.10	0.05	1.33	1
50.	204.	0.18	0.06	0.21	0.06	1.17	1
50.	205.	0.21	0.08	0.24	0.08	1.11	1
51.	200.	-0.61	0.11	-0.67	0.11	1.10	1
51.	201.	-0.31	0.05	-0.34	0.05	1.10	1
51.	202.	0.04	0.05	0.05	0.05	1.30	1
51.	203.	0.15	0.05	0.17	0.05	1.18	1
51.	204.	0.20	0.09	0.23	0.09	1.16	1
52.	199.	-0.45	0.10	-0.50	0.10	1.10	1
52.	200.	-0.80	0.08	-0.89	0.08	1.12	1
52.	201.	-0.45	0.07	-0.51	0.07	1.14	1
52.	202.	0.10	0.05	0.10	0.05	1.07	1
52.	203.	0.23	0.08	0.27	0.08	1.16	1
52.	204.	0.55	0.11	0.62	0.11	1.13	1
53.	198.	0.12	0.13	0.13	0.14	1.07	1
53.	199.	-0.52	0.10	-0.59	0.10	1.12	1
53.	200.	-0.68	0.09	-0.79	0.09	1.16	1
53.	201.	-0.30	0.11	-0.36	0.11	1.19	1
53.	202.	0.29	0.10	0.34	0.11	1.18	1
53.	203.	0.49	0.12	0.59	0.12	1.19	1
54.	201.	0.85	0.36	0.90	0.37	1.06	1
54.	202.	0.79	0.29	0.87	0.30	1.10	1

TABLE 5 Vertical Velocities for REV 1212. See Text for Meaning
of Column Heading Numbers.

(1)	(2)	(3)	(4)	(5)	(6)	(7)	(8)
3A.	234.	-0.36	0.06	-0.40	0.06	1.09	1
39.	234.	-0.28	0.06	-0.31	0.07	1.09	1
40.	233.	-0.54	0.09	-0.58	0.09	1.08	1
40.	234.	-0.19	0.10	-0.21	0.10	1.12	1
41.	233.	-0.71	0.08	-0.75	0.08	1.06	1
41.	234.	-0.35	0.09	-0.37	0.09	1.08	1
42.	232.	-0.02	0.12	-0.02	0.12	1.08	1
42.	233.	-0.41	0.06	-0.42	0.06	1.03	1
42.	234.	-0.25	0.10	-0.26	0.10	1.00	1
43.	231.	0.15	0.09	0.15	0.09	1.02	1
43.	232.	0.17	0.07	0.17	0.07	1.02	1
43.	233.	-0.04	0.10	-0.04	0.10	0.96	-1
44.	230.	-0.20	0.07	-0.21	0.07	1.03	1
44.	231.	-0.13	0.08	-0.14	0.08	1.04	1
44.	232.	-0.13	0.08	-0.14	0.08	1.04	1
45.	230.	-0.14	0.07	-0.15	0.07	1.07	1
45.	231.	-0.13	0.07	-0.14	0.07	1.10	1
45.	232.	-0.37	0.08	-0.39	0.08	1.05	1
45.	233.	-0.64	0.15	-0.66	0.15	1.03	1
46.	229.	-0.00	0.07	-0.01	0.07	1.83	1
46.	230.	-0.12	0.07	-0.14	0.07	1.16	1
46.	231.	-0.12	0.06	-0.14	0.06	1.16	1
46.	232.	-0.21	0.10	-0.23	0.10	1.11	1
47.	228.	0.16	0.08	0.18	0.08	1.14	1
47.	229.	0.37	0.06	0.40	0.07	1.07	1
47.	230.	-0.02	0.07	-0.04	0.07	1.54	1
47.	231.	-0.10	0.06	-0.12	0.06	1.14	1
47.	232.	0.20	0.14	0.20	0.14	1.00	1
48.	227.	0.99	0.12	1.06	0.12	1.07	1
48.	228.	0.54	0.12	0.58	0.12	1.08	1
48.	229.	0.29	0.09	0.30	0.09	1.04	1
48.	230.	0.12	0.09	0.13	0.09	1.08	1
48.	231.	0.17	0.08	0.18	0.08	1.08	1
49.	227.	1.02	0.11	1.06	0.12	1.05	1
49.	228.	0.88	0.12	0.93	0.12	1.06	1
49.	229.	0.21	0.11	0.20	0.12	0.96	-1
49.	230.	0.19	0.11	0.20	0.11	1.05	1
49.	231.	1.10	0.14	1.17	0.14	1.06	1
50.	226.	0.30	0.06	0.35	0.06	1.14	1
50.	227.	0.79	0.15	0.83	0.15	1.05	1
50.	228.	0.96	0.13	1.00	0.13	1.04	1
50.	229.	0.50	0.19	0.50	0.19	1.00	-1
50.	230.	0.39	0.17	0.37	0.17	0.94	-1
51.	225.	0.16	0.05	0.23	0.05	1.41	1
51.	226.	0.52	0.10	0.60	0.10	1.17	1
51.	227.	0.95	0.19	1.01	0.19	1.06	1
52.	224.	0.06	0.04	0.11	0.04	1.65	1
52.	225.	0.58	0.09	0.69	0.09	1.18	1
52.	226.	1.60	0.18	1.75	0.19	1.10	1
53.	223.	0.01	0.05	0.03	0.05	4.43	1
53.	224.	0.11	0.05	0.15	0.06	1.39	1
53.	225.	1.06	0.26	1.19	0.26	1.13	1
54.	222.	0.12	0.06	0.15	0.06	1.23	1
54.	223.	0.17	0.06	0.21	0.06	1.21	1
54.	224.	0.38	0.09	0.45	0.09	1.18	1
55.	221.	0.31	0.08	0.35	0.08	1.13	1
55.	222.	0.18	0.08	0.21	0.08	1.15	1
55.	223.	0.44	0.10	0.50	0.11	1.14	1
56.	220.	-0.02	0.08	-0.00	0.08	0.13	-1
56.	221.	0.18	0.10	0.20	0.10	1.16	1
56.	222.	0.38	0.11	0.44	0.11	1.15	1
57.	219.	0.78	0.14	0.88	0.14	1.13	1
57.	220.	0.48	0.24	0.53	0.25	1.10	1
57.	221.	0.38	0.33	0.37	0.33	0.97	-1
57.	222.	0.63	0.53	0.26	0.53	0.40	-1
58.	218.	0.51	0.37	0.49	0.37	0.96	-1

TABLE 6   Vertical Velocities for REV 1298.   See Text for Meaning of
Column Heading Numbers.

(1)	(2)	(3)	(4)	(5)	(6)	(7)	(8)
35.	236.	-0.17	0.05	-0.12	0.05	0.69	-1
36.	235.	-0.09	0.03	-0.16	0.03	1.78	1
36.	236.	-0.11	0.06	-0.10	0.06	0.91	-1
36.	237.	-0.40	0.16	-0.20	0.16	0.49	-1
37.	235.	-0.02	0.04	-0.04	0.04	1.88	1
37.	236.	0.24	0.08	-0.18	0.08	-0.74	-1
38.	234.	0.20	0.04	0.13	0.04	0.65	-1
38.	235.	0.19	0.09	0.07	0.09	0.34	-1
39.	234.	0.19	0.04	0.20	0.04	1.02	1
40.	233.	-0.04	0.04	-0.05	0.04	1.04	1
41.	232.	-0.04	0.06	0.04	0.06	-0.96	-1
41.	233.	0.19	0.03	0.16	0.04	0.86	-1
42.	232.	0.04	0.04	0.03	0.04	0.91	-1
42.	233.	0.31	0.02	0.13	0.02	0.42	-1
43.	231.	-0.43	0.05	-0.47	0.05	1.08	1
43.	232.	-0.18	0.04	-0.19	0.04	1.05	1
43.	233.	0.02	0.03	0.12	0.03	5.01	1
44.	231.	-0.40	0.06	-0.42	0.06	1.07	1
44.	232.	-0.10	0.05	-0.11	0.05	1.10	1
44.	233.	0.26	0.05	0.27	0.06	1.02	1
45.	230.	-0.05	0.06	-0.06	0.06	1.28	1
45.	231.	-0.23	0.08	-0.25	0.08	1.12	1
45.	232.	0.12	0.07	0.11	0.07	0.95	-1
45.	233.	0.29	0.06	0.29	0.06	1.02	1
46.	229.	0.50	0.08	0.53	0.08	1.07	1
46.	230.	0.27	0.09	0.29	0.09	1.05	1
46.	231.	0.29	0.08	0.29	0.08	1.00	1
46.	232.	0.19	0.08	0.19	0.08	0.99	-1
46.	233.	0.28	0.05	0.08	0.05	0.29	-1
47.	228.	0.17	0.07	-0.10	0.07	-0.61	-1
47.	229.	0.26	0.07	0.27	0.07	1.03	1
47.	230.	0.39	0.05	0.41	0.05	1.04	1
47.	231.	0.39	0.08	0.40	0.08	1.03	1
47.	232.	0.08	0.07	0.09	0.07	1.10	1
48.	227.	-0.23	0.07	-0.56	0.08	2.40	1
48.	228.	-0.23	0.07	-0.25	0.06	1.05	1
48.	229.	-0.01	0.07	-0.01	0.07	2.37	1
48.	230.	0.07	0.05	0.06	0.05	0.97	-1
48.	231.	0.01	0.07	0.01	0.07	0.78	-1
49.	227.	-0.37	0.08	-0.36	0.08	0.95	-1
49.	228.	-0.11	0.06	-0.13	0.06	1.18	1
49.	229.	0.05	0.06	-0.03	0.06	-0.59	-1
49.	230.	-0.07	0.05	-0.07	0.05	1.03	1
50.	226.	-0.11	0.08	-0.16	0.08	1.40	1
50.	227.	-0.19	0.08	-0.24	0.08	1.24	1
50.	228.	-0.02	0.09	-0.07	0.09	3.24	1
50.	229.	0.14	0.09	0.14	0.09	0.99	-1
50.	230.	-0.02	0.10	0.06	0.10	-3.47	1
51.	225.	-0.03	0.06	0.51	0.06	-19.61	1
51.	226.	0.03	0.05	0.02	0.05	0.75	-1
51.	227.	-0.02	0.07	-0.03	0.08	1.40	1
52.	224.	-0.21	0.06	0.48	0.06	-2.24	1
52.	225.	-0.01	0.05	-0.01	0.05	1.46	1
52.	226.	0.02	0.08	0.02	0.09	0.75	-1
53.	223.	-0.46	0.07	0.21	0.07	-0.45	-1
53.	224.	-0.20	0.05	-0.21	0.05	1.04	1
53.	225.	-0.09	0.05	-0.10	0.05	1.17	1
54.	222.	-0.39	0.08	0.72	0.08	-1.85	1
54.	223.	-0.28	0.05	-0.27	0.06	0.96	-1
54.	224.	-0.18	0.06	-0.19	0.06	1.05	1
55.	221.	-0.11	0.04	0.21	0.04	-1.90	1
55.	222.	-0.13	0.04	-0.15	0.05	1.12	1
55.	223.	-0.15	0.03	-0.16	0.03	1.04	1
56.	220.	-0.09	0.05	0.04	0.05	-0.48	-1
56.	221.	-0.04	0.04	-0.07	0.04	1.60	1
56.	222.	0.00	0.06	-0.01	0.06	-7.35	1
57.	221.	-0.17	0.11	-0.02	0.11	0.13	-1

verifying the SASS winds by means of conventional measurements. The abstract and the introduction of this paper are quoted in full below.

"Abstract. Information on integrated water vapor, cloud liquid water and rain rate obtained by the Scanning Multichannel Microwave Radiometers (SMMR) on the SEASAT and Nimbus 7 polar orbiting satellites have been used to study cyclones crossing the Pacific Ocean. The SMMR's cover swaths about 600 km wide with a resolution of approximately 50 km for the atmospheric water parameters derived from brightness temperatures in the three highest frequencies employed on these radiometers, 18, 21, and 37 GHz.

Many features of the distributions of water vapor, cloud liquid water and mesoscale rainbands are mapped instantly by the SMMR's. New perspectives on frontal instabilities, such as developing waves, are obtained. From a few case studies it is already clear that a passive microwave instrument like SMMR can contribute significantly to accurately locating atmospheric fronts over the ocean and to prediction of coastal rainfall.

Keywords: Passive microwaves, cyclone structure, precipitable water, cloud liquid water, rain rate, locating fronts, frontal rainbands, coastal rainfall".

INTRODUCTION

"In this report we will apply recent passive microwave measurements to study the distribution of atmospheric water in mid-latitude cylones. Integrated water vapor, integrated liquid water and rainfall rate can be deduced from the brightness temperatures at certain microwave frequencies measured by SMMR.

The obvious practical use of locating fronts by the moisture pattern for cyclones over the ocean is illustrated. This is especially valuable when widespread cirrus clouds obscure features in the infrared satellite image, which at present is the main guide in regions of sparse surface data. The relationship between coastal rainfall amounts and the atmospheric water content (as vapor, cloud droplets or rain drops) is also explored. At present, this study does not relate the satellite derived water parameters to the dynamics of a storm. However, with the simultaneous observations of the surface wind by a scatterometer instrument, this may eventually become possible".

Three figures from this study, as re-drafted, are reproduced here as Figures 42, 43 and 44 which show in order integrated water vapor in kilograms per square meter for the atmospheric column above an area, the integrated liquid water in kg per square meter and the rainfall rate in millimeters per hour. Values range from 28 to 44 kg/m^2 for Fig. 42, from zero to 1.2 kg/m^2 for Fig. 43 and from zero to 5 mm/hr for Fig. 44. The high values
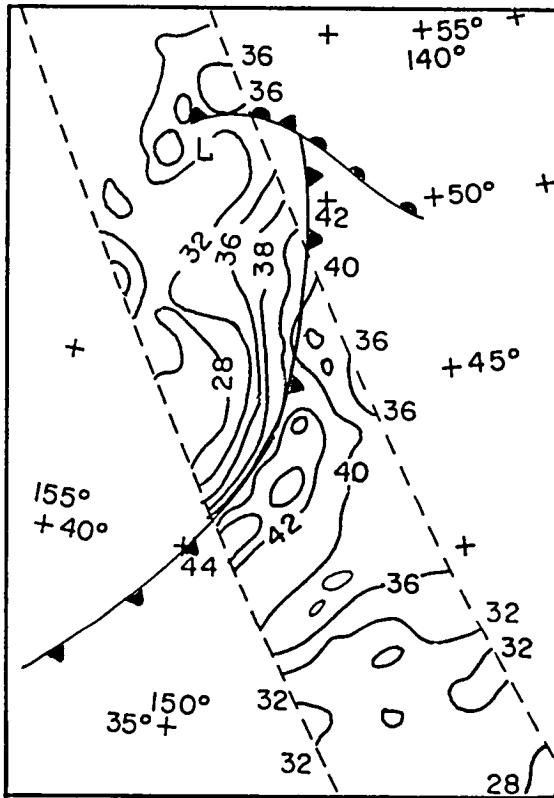
FIG. 42   Integrated Water Vapor in kg/m^2 for REV 1098
from the SMMR.   1840 GMT Sept. 11, 1978. (From
Katsaros and McMurdie (1983a)),
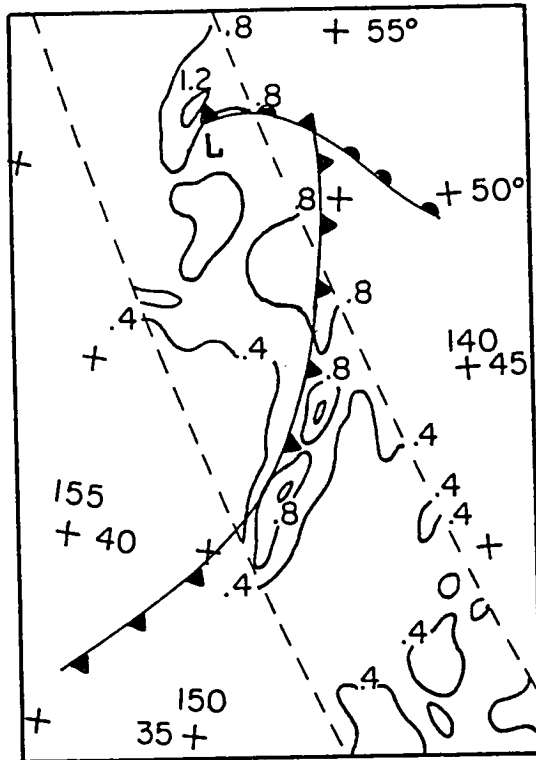
FIG. 43   Integrated Liquid Water for the Same
          Time and Area as Fig. 42.   (From Katsaros
          and McMurdie (1983a)).
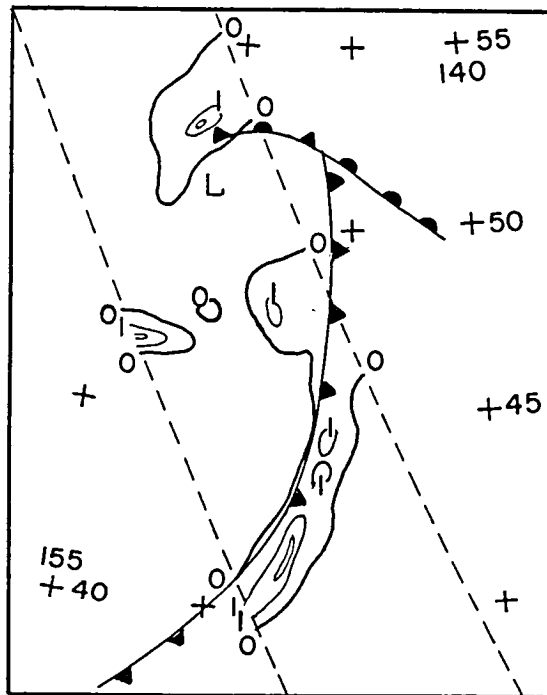
FIG. 44   Rainfall Rate in mm/hr for the Same Time and
Area as Fig. 42.   (From Katsaros and McMurdie
(1983a)).

are concentrated just in advance of the cold front and near the tip of the occlusion. The integrated water vapor decreases smoothly in Fig. 42 into the surface cold air region as the warmer moister air rides up over the sloping frontal surface.

The final report for NOAA, on which the preceding IGARSS '83 report was based, contains three reports, McMurdie (1983) Katsaros and McMurdie (1983b) and McMurdie and Katsaros (1983). This last reference contains an analysis of REV 1212. The details of REV 1212 are given starting on page 100 of our report as far as the winds, stress and its curl. The vertical velocity field is given in Table 5 on page 126.

Three pages from the third of the above cited reports are reproduced herein verbatum with only a change in page number. It should be noted that the SMMR swath is somewhat narrower than the SASS swath and that the different analyses involved were completely independent up to this point. Combined, they produce a coherent integrated analysis of the dynamics of an extratropical cyclone.

INTEGRATED WATER VAPOR (kg/m²)
SEASAT REV 1212

SEPTEMBER 19, 1978
TIME 1808Z
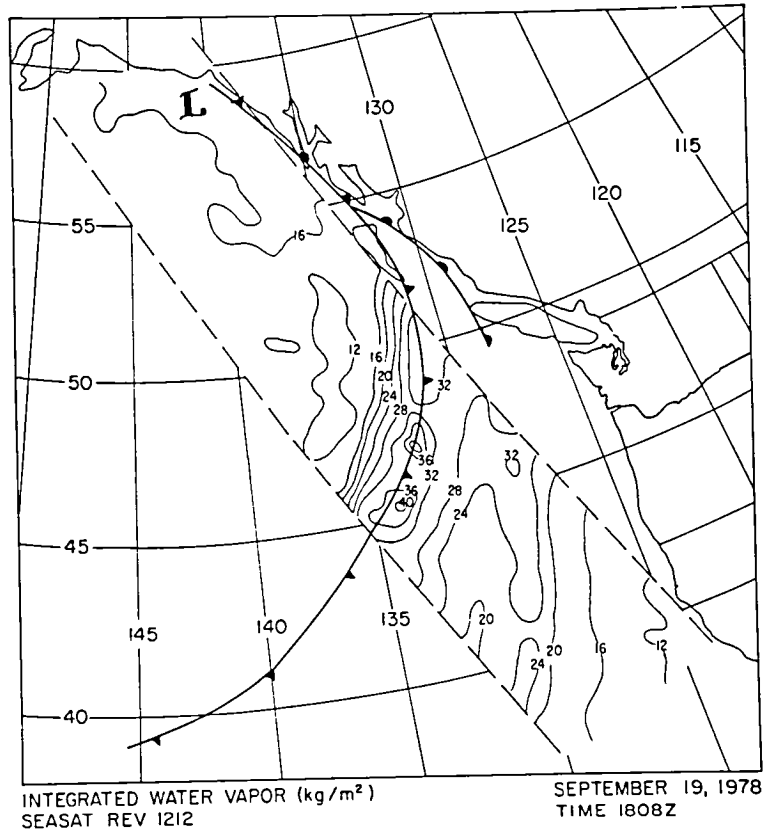
FIGURE 45

Integrated Water Vapor (kg/m²)   September 19, 1978
REV 1212   Analysis time 1800Z
SEASAT time 1808Z   GOES-W 1745Z

When the cyclone is in the mature stage of its development as it is here, the maxima in integrated water vapor seem to occur in the vicinity of the surface front with relatively dry air on both sides. There is a sharp gradient between the maxima and the air behind the front to the north. To the south of the maxima the gradient is not as sharp, yet the air becomes very dry towards the south near the coast. In that region ship and station reports indicate an offshore wind probably bringing dry continental air. (Courtesy of McMurdie and Katsaros (1983)).
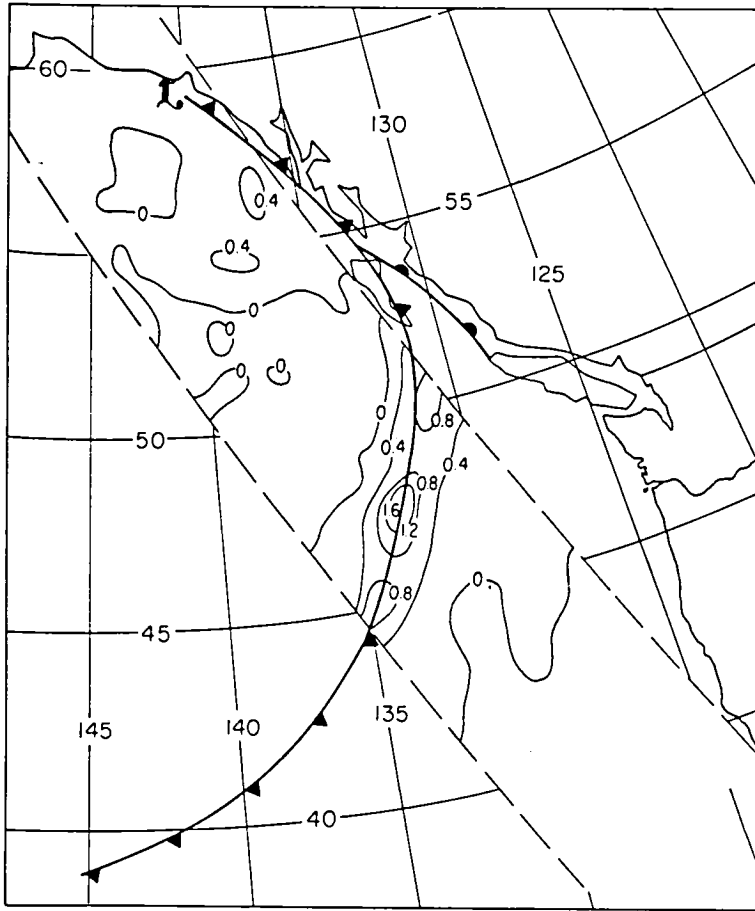
FIGURE 46

Integrated Liquid Water (kg/m^2)
REV 1212
SEASAT time 1808Z

September 19, 1978
Analysis time 1800Z
GOES-W time 1745Z

The maxima in liquid water occurs along the frontal zone in three distinct
bands or cells. Two of these cells show amounts greater than 1.00 kg/m^2.
These are largest amounts seen yet during the development of this storm.
To the north near the surface low pressure center, there are integrated
liquid water amounts greater than 0.2 kg/m^2 that correspond well to enhance-
ment seen on the infrared satellite image. (Courtesy of McMurdie and
Katsaros (1983)).
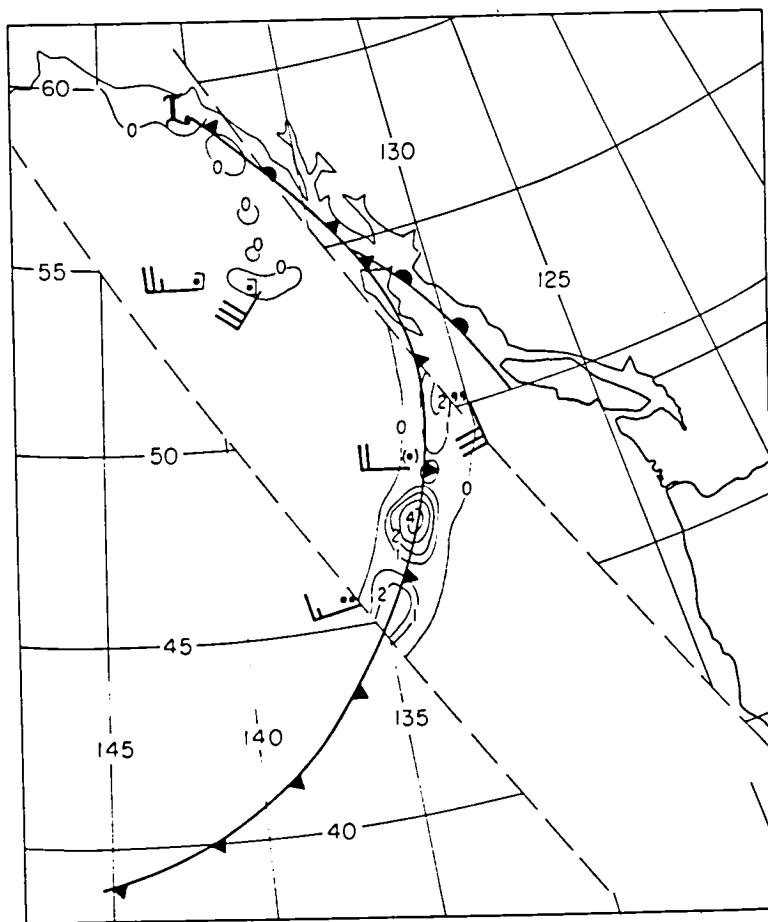
FIGURE 47

Rain Rate (mm/hr)   September 19, 1978
REV 1212   Analysis time 1800Z
SEASAT time 1808Z   GOES-W time 1745Z

Rainfall rates are highest along the front and the rainfall seems to be
distributed again in three distinct bands. The location of the maxima
rainfall rates are the same as the maxima in integrated liquid water.
Although there are no ship reports within the rain cells themselves,
the ship reports that are available do support the rainfall pattern seen
by SMMR. (Courtesy of McMurdie and Katsaros (1983)).

If these SASS winds are an improvement over conventional winds, they imply that wind fields over the ocean have much sharper wind shifts and much stronger winds in some areas of the synoptic pattern than conventional analyses presently explain. These features have been recognized for many years but seem to have been lost in present day analysis methods.

Consider for example some figures from Brunt (1942). An open wave cyclone is shown in Fig 48. Fig 49 shows continuous traces for 16 hours of wind speed, wind direction, air temperature accumulated rainfall and atmospheric pressure at Holyhead, England (52.5^o N 4.8^o W). The highly turbulent flow and the sharp increase in average wind speed in the warm air sector, are reflected in similar SASS and SMMR analyses for REV 1212 by a field of flow over an area at virtually an instant of time, which, if translated in the correct direction with the correct speed, would produce time histories at one point like those in Fig. 49.

The new remote sensing potential capability to define the divergence field, and vertical velocity field and the H_2O fields permits an even deeper understanding of wave cyclones and fronts and the atmospheric field of motion associated with them than was possible four decades ago. The detailed description of this particular weather disturbace during October 21, and 22, 1932 suggests that all these features were known, or inferrable, long ago, but that present numerical models have lost them.

FIG. 48 Conventional Analysis of an Open Wave Cyclone
for Oct. 22, 1932 at 07h (From Brunt (1942)).
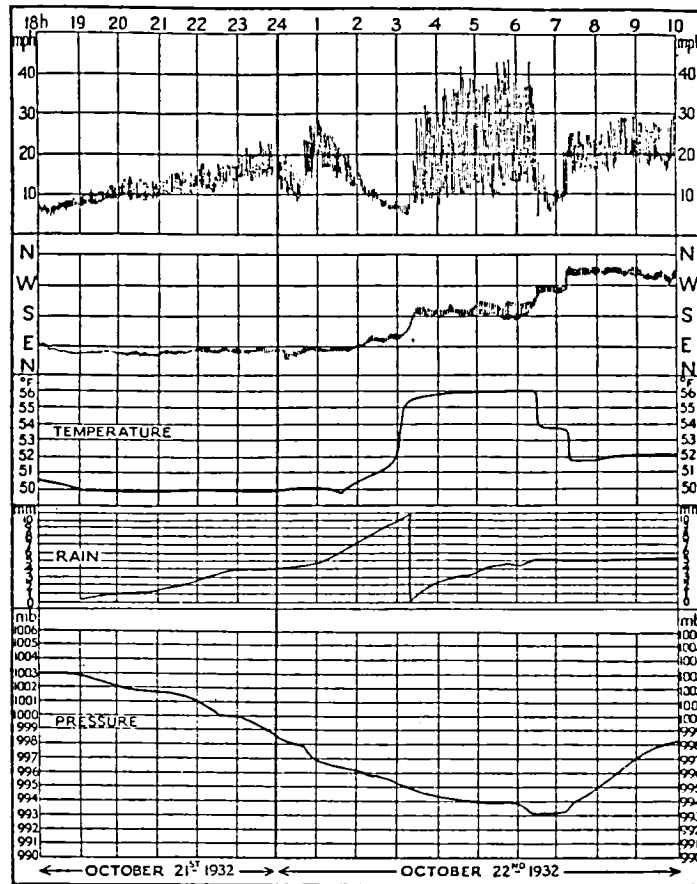
FIG. 49   Time Histories of Wind Speed, Wind Direction, Air
Temperature Integrated Rainfall, and Sea Surface
Pressure at Holyhead England (52.5° N, 4.8° W) During
the Passage of the Wave Cyclone of Fig. 48.   (From
Brunt (1942)).

Conventional meteorological analysis methods would have a great deal of difficulty in explaining the wind and divergence fields of our analyses of four REVS and the results shown in these six figures concerning the various H_2O fields. The question to be answered would be "How did all that H_2O get concentrated into such a narrow strip along the front and at the tips of the occlusions".

Air near the sea surface contains most of the water vapor simply because it is warmest. Since the air toward the Equator is warmer, it contains much of the water vapor. The sources of the water vapor in the air over the ocean are shown in numerous publications with the classical one of Jacobs (1951) (with some figures reproduced in Neumann and Pierson (1966)) serving as an example.

The wind fields of our study show a mechanism capable of producing the fields shown in Figs. 42 to 44 and in the figures for REV 1212. A strong jet-like wind just in advance of a cold front as in REV 1212 is capable of moving H_2O northward more rapidly. The divergence fields and the vertical velocity fields are in the right places to raise the surface air to elevations where clouds can form and rain can occur.

Guymer (1983a) has related vertical velocities at the top of the friction layer (perhaps a kilometer or so) to the curl of the wind stress at the sea surface by means of various assumptions (Ekman pumping). The equation is (126).

$$w_f = \frac{1}{\rho f} \text{ curl } \vec{\tau}_h \tag{126}$$

In the absence of frontal surfaces, this equation may be useful if there is a top of the boundary layer. However, it is clear from the fields of wind stress curl shown in our results that (126) will not produce vertical velocities similar to those at 200 m obtained from the surface wind field.

Guymer (1983b) cites additional studies by Guymer and Taylor (1982) as follows:

"Several more passes during Phase 2 JASIN were analysed in a similar way (Guymer & Taylor 1982), and mean values for the JASIN triangle have been plotted as a time series ----. For comparison, hourly values have also been calculated by applying (2) to ship measurements of the surface wind at the corners of the

JASIN triangle, after removal of interplatform biases based on careful comparison of results. The two sets of values agree within the uncertainty to be expected from errors in the wind measurements; they are also comparable with vertical velocities obtained from the divergence method applied to JASIN radiosonde winds at the triangle corners. This implies that most of the divergence in the atmospheric boundary layer was frictionally induced".

Present conventional analysis of widely separated ship reports and the planetary boundary layer models that are used do not produce fields such as those that have been obtained from the SASS and the SMMR. Some of the predictions on the accuracy of SEASAT data at least, isofar, as its internal consistency and on its potential applications such as those of Pierson (1978) are beginning to verify. Much more is yet to be learned from the combined study of SMMR and SASS data.

SEA SURFACE ATMOSPHERIC PRESSURE FIELDS

For numerical weather prediction, it is extremely important to specify the atmospheric pressure at the ocean surface. Since conventional radiosonde ascents are sparce over the ocean, remote sensing for temperature versus pressure and water vapor versus pressure is used. The remote soundings are not synoptic with the 0000GMT, 0600GMT, 1200GMT and 1800GMT conventional data. The soundings are integrated upward starting with the sea surface atmospheric pressure from a synoptic analysis. Since the air temperature field at the sea surface is not too well known, it is often assumed that the ocean surface temperature corresponds to the air temperature.

An error in the sea surface pressure field, even if the data were synoptic, propagates upward in the specification of the heights of the constant pressure surfaces for all of the atmospheric layers of the numerical model.

It can be estimated that the typical errors in the specification of the sea surface atmospheric pressure account for about half of the root mean square error in the specification of the heights of constant pressure surfaces. This is not too difficult to explain because the atmospheric pressure field at the surface is the most complicated field compared to the constant pressure surfaces, which evolve into smoother planetary wave patterns with height.

Niether the pressure fields given in the previous figures nor the pressure fields of the PBL analyses given in Woiceshyn, et al. (1979) would produce the superobservation wind fields obtained in our results, if presently available models are used. A feature of the SASS winds analysed in both the SEASAT I and II special issues of the Journal of Geophysical Research was that they tended to average about 10° more counter clockwise than the wind fields (produced by PBL analyses) with which they were compared, with the exception of JASIN. Features of our superobservation wind fields are (1) much greater gradients in wind speed, and at times direction, (2) stronger winds in advance of cold fronts and (3) concentrated areas of divergence (or convergence) along with large areas of nearly non-divergent, but nevertheless apparently stronger cross isobar flow.

142

The higher resolution possible from the SASS winds will help to define these fields more accurately over the ocean, but both better boundary layer models and more realistic data assimilation methods especially those that relate atmospheric pressures to winds will be needed so as to utilize scatterometer data optimumly.

It would be interesting to find out whether any of the present boundary layer models could be forced to reproduce the superobservation wind fields that have been obtained, given ship reports of pressure, air temperature, and relative humidity and sea surface temperature fields from remote sensors. The pressure gradients would have to be quite different. A number of terms in the full equations of motion are neglected in these models, which may prove to be a considerable importance.

CONCLUSION

It is always useful to procede to the next steps for the analysis of remotely sensed data so as to illustrate the properties of the data and to demonstrate its potential. This is true even though it may be necessary at times to go back to the raw backscatter data and reprocess the entire data stream so as to make whatever corrections may be required.

This entire analysis has been based on about 36 minutes of SASS data. It demonstrates many of the properties that scatterometer data have and that will still be properties of any portions of those parts of the data processing stream that may require revision, if, indeed, it should turn out that they do. The planned scatterometer on NROSS will have many of the properties of the SASS data from SEASAT. These are exemplified by the analysis of the super-observations of this study.

A cluster of scatterometer winds near a latitude and longitude to be used in a computor based synoptic scale initial value update will be such that each vector wind will be composed of four components. These are (1) the best synoptic scale representation for the wind at a desired grid point, (2) the effects of synoptic scale gradients on the scatterometer wind as a function of its distance from the desired grid point, (3) the inevitable, unresolvable and unpredictable (deterministically) mesoscale variability for the area of the scatterometer cells and (4) the unavoidable communiction noise and attitude error effects that produce an incorrect wind that would differ even from the mesoscale value.

For most applications of scatterometer winds, the reduction of the effects of gradients, mesoscale variability and communication noise can be accomplished by creating superobservations. These superobservations can be generated in such a way that the effects of gradients are reduced and the remaining effects are estimates of the standard deviations of the estimates of the synoptic scale components.

Our results show that superobservations have an inherent accuracy sufficient to yield realistic fields of divergence and vertical velocities in the lower levels of the atmosphere. These in turn correlate exceptionally well with cloud patterns and the fields of water vapor, liquid water and

144

precipitation obtained from the SMMR.

The wind fields that were obtained differ considerably from wind fields obtained from present analysis procedures and present planetary boundary layer models. This suggests that future measurements of winds by scatterometers should only be verified by a larger scale, long lasting program similar to JASIN with some of the inconsistencies of that program eliminated. A better understanding of turbulence for the winds is an a priori requirement for any future program.

The question of whether scatterometers measure more nearly either wind or wind stress can probably be answered along the lines of the analysis given in one of the papers cited herein. A scatterometer measures the roughness of the sea surface at short wavelengths. These short waves are the result of the wind itself close to the surface and of the pressure fluctuations caused by that wind. It is interesting that other authors on the subject have also avoided the question of which of many possible relationships which have been proposed between u_* and $\bar{U}_{10}$ should be used to obtain wind stress.

The question need not really be answered in order to justify scatterometry. An answer satisfactory to those who require wind stress could come later that the next scatterometer and still the scatterometer would be justified. The equations given in this report would probably give more realistic results than any model that used a constant drag coefficient since the recent results that have been cited are quite convincing in that the wind stress varies more strongly than the square of the wind speed for high winds in mid-ocean.

The surface currents of the ocean are undoubtedly caused to vary by synoptic scale variations of the wind. Passing cyclonic systems can cause the wind stress for a given ocean area to vary by several orders of magnitude from one day to the next, and evidently the surface currents respond accordingly. A full study of the ocean circulation will require altimeters, scatterometers, drogued buoys, acoustic tomography, and conventional data.

Scatterometry, as shown herein, has the potential of providing some of the data needed at the density required to permit vastly improved numerical weather predictions and an understanding of the ocean circulation. This report illustrates some of the steps that can be taken to reach these goals.

ACKNOWLEDGEMENTS

146

REFERENCES

Atlas, R. (1981): The effects of varying amounts of satellite data, orography and diabatic processes on the numerical prediction of an intense cyclone. Res. Rev. 1980-81, NASA Tech. Memo. 83907, GSFC, Greenbelt, M.S.

Atlas, R., G. Cole, A. Pursch and C. Long (1981): Interactive processing of SEASAT scatterometer data, Res. Rev. 1980-81. NASA Tech. Memo. 83907, GSFC Greenbelt, M.D.

Barrick, D. E., J. C. Wilkerson, P. M. Woiceshyn, G. B. Born, and D. B. Lame (1979): SEASAT Gulf of Alaska Workshop II, Report Rep. 622-107. Jet. Propul. Lab., Pasadena, Cal.

Bernstein, R. L., G. H. Born, and R. H. Whritner (1982): SEASAT altimeter determination of ocean current variability. J. Geophys. Res. Vol. 87 No. C5, pp. 3261-3268.

Boggs, D. H. (1982): SEASAT geophysical data record (GDR), Users Handbook, Scatterometer. Jet. Propul. Lab. Rep. 622-232, (JPL D-129). Pasadena, Cal.

Born, G. H., J. C. Wilkerson and D. B. Lame (1979): SEASAT Gulf of Alaska Workshop Report, Vol. 1, Rep. 622-101, Jet. Propul. Lab. Pasadena, Cal.

Brown, R. A., V. J. Cardone, T. Guymer, J. Hawkins, J. E. Overland, W. J. Pierson, S. Peteherych, J. C. Wilkerson, P. M. Woiceshyn, and M. Wurtele (1982): Surface wind analyses for SEASAT. J. Geophys. Res., Vol. 87 C5 pp. 3385-3364.

Brown, R. A. (1983): On a satellite scatterometer as an anemometer. J. Geophys. Res., Vol. 88 C3, pp. 1663-1673.

Brown, R. A., and T. Liu (1982): An operational large scale marine planetary boundary layer model. J. Appl. Meteorol., Vol. 21 No. 2.

Brunt, D. (1942): Weather Study. The Roland Press Co. pp. 215.

Busalacchi, A. J., K. Takeuchi and J. J. O'Brien (1983): Interannual variability of the Equatorial Pacific-Revisited. J. Geophys. Res. Vol. 88 C12 pp. 7551-7562.

Cane, M. A., V. J. Cardone, M. Halem and I. Halberstam (1981): On the sensitivity of numerical weather prediction to remotely sensed Marine surface wind data: A Simulation Study. J. Geophys. Res. Vol. 86, No. C5, pp. 8093-8106.

Cheney, R. E. (1982): Comparison data for SEASAT altimetry in the Western North Atlantic. J. Geophys. Res. Vol. 87 C5, pp. 3247-3253.

Cheney, R. E., J. G. Marsh, and B. D. Beckley (1983): Global mesoscale variability from repeat trades of SEASAT altimeter data. J. Geophys. Res. Vol. 88 No. C7. pp. 4343-4354.

Davidson, K. L., G. E. Schacher, G. W. Fairall and J. D. Jarrell (1981): Observational results pertaining to scatterometer interpretation in Gower JFR. ed Oceanography from Space. Plenum Press. pp. 597-606.

Dittmer, K. V. (1977): The hydrodynamic roughness of the sea surface at low wind speeds, "Meteor" Forsch-Ergebnisse, Reihe B No. 12 S10-15.

Ghil, H., M. Halem and R. Atlas (1979): Time-continuous assimilation of remote-sounding data and its effects on weather forecasting. Mon. Wea. Rev. Vol. 107. pp. 140-171.

Guymer, T. H. (1983a): Validation and applications of SASS over JASIN in T. D. Allan (ed) Satellite Microwave Remote Sensing. John Wiley and Sons. pp. 87-106.

Guymer, T. H. (1983): A review of SEASAT scatterometer data. Phil Trans. Roy. Soc. Lond. A Vol. 309, pp. 399-414.

Guymer, T. H., and P. K. Taylor (1983): In Studies of atmospheric water with the SEASAT scanning multichannel microwave radiometer. Final Report to NOAA Cont. NA-81-SAC-60756. U. of Wash. Seattle Cont. No. 671.

Hellerman, S. and M. Rosenstein (1983): Normal monthly wind stress over the World Ocean with error estimates. J. Phys. Oceanogr. Vol. 13 No. 7. pp. 1093-1104.

Jacobs, W. C. (1951): The energy exchange between the sea and the atmosphere and some of its consequences. Bull. Scripps. Inst. of Oceanogr. Univ. of Cal. Vol. 6 pp. 27-122.

Jones, W. L., P. G. Black, D. M. Boggs, E. M. Bracalente, R. A. Brown, G. Dome, J. A. Ernst, I. M. Halberstam, J. E. Overland, S. Peteherych, W. J. Pierson, F. J. Wentz, P. M. Woiceshyn and M. G. Wurtele (1979): SEASAT scatterometer: Results of the Gulf of Alaska. Workshop, Science Vol. 204. No. 4400.

Jones, W. L., L. C. Schroeder, D. H. Boggs, E. M. Bracalente, R. A. Brown, G. J. Dome, W. J. Pierson, and F. J. Wentz (1982): The SEASAT-A satellite scatterometer: The Geophysical Evaluation of Remotely Sensed Wind Vectors Over the Ocean. J. Geophys. Res. Vol. 87 C5. pp. 3297-3317.

Katsaros, K. B., and L. A. McMurdie (1983a): SEASAT Scanning Multichannel Microwave Radiometer (SMMR). Observation of North Pacific cyclones. IGARSS '83. Digest Aug. 31-Sept. 2, 1983. San Francisco, Cal.

Katsaros, K. B., and L. A. McMurdie (1983b): Atmospheric water distribution in cyclones as seen with Scanning Multichannel Microwave Radiometers. in Studies of atmospheric water with the SEASAT Scanning Multichannel Microwave Radiometer. Final Report to NOAA, Cont. NA-81-SAS-00756 U. of Wash. Seattle Contribution No. 671.

Kirwan, A. D., G. McNally, M. S. Chang and R. Molinari (1975): The effect of wind and surface currents on drifters. J. Phys. Oceanogr. Vol. 5, pp. 361-368.

Kirwan, A. D., and M. S. Chang (1978): Effect of sampling rate and random position error on analysis of drifters data. J. Phys. Oceanogr. Vol. 9, pp. 382-387.

Kirwan, A. D., G. J. McNally, E. Reyna and W. J. Merrell Jr. (1978a): The near surface circulation of the Eastern North Pacific. J. Phys. Oceanogr. Vol. 8 No. 6, pp. 937-945.

Kirwan, A. D., G. J. McNally and S. Pazan (1978b): Wind drag and relative separations of undrogued drifters. J. Phys. Oceanogr. Vol. 8, pp. 1146-1150.

Kirwan, A. D., G. J. McNally, S. Pazan and R. Wert (1979): Analysis of surface current response to wind. J. Phys. Oceanogr. Vol. 9, No. 2, pp. 401-412.

Klose, J. C. (1979): SEASAT node tables and osculating orbital elements, 622-215, NASA Jet. Propul. Lab. Pasadena, Cal.

Lame, D. B., and G. H. Born (1982): SEASAT measurement system evaluation: Achievements and Limitations. J. Geophys. Res. Vol. 87 No. C5, pp. 3175-3178.

Large, W. G., and S. Pond (1981): Open ocean momentum flux measurements in moderate to strong winds. J. Phys. Oceanogr. Vol. 11, pp. 324-326.

Madsen, O. S. (1978): Mass transport in deep water waves. J. Phys. Oceanogr. Vol. 8 No. 6, PP. 1009-1015.

McMurdie, L. A. (1983): SEASAT Scanning Multichannel Microwave Radiometer (SMMR) Observation of North Pacific cyclones. in Studies of atmospheric water with the SEASAT Scanning Multichannel Microwave Radiometer. Final Report to NOAA, Cont. NA-81-SAS-00756 U. of Wash. Seattle Contribution No. 671.

McMurdie, L. A., and K. B. Katsaros (1983): Locating synoptic fronts and rain areas using the SEASAT Scanning Multichannel Microwave Radiometer. in Studies of atmospheric water with the SEASAT Scanning Multichannel Microwave Radiometer. Final Report to NOAA, Cont. NA-81-SAS-00756 U. of Wash. Seattle Contribution No. 671.

McNally, G. J. (1981): Satellite-traced drift buoy observations of the near-surface flow in the Eastern Mid-latitude North Pacific. J. Geophys. Res. Vol. 86, No. C3, pp. 8022-8030.

McNally, G. J., E. Reyna, W. J. Merrell Jr. and A. D. Kirwan Jr. (1978): Technical evaluation of ADS I and II drifter performance Rep. 78-3-T. Texas A and M Univ. College Station.

McNally G. J., W. C. Patzert, A. D. Kirwan Jr. and A. C. Vastano (1983): The near-surface circulation of the North Pacific using satellite tracked drifting buoys. J. Geophys. Res. Vol. 88, No. C12, pp. 7507-7518.

Monin, A, S., and A. M. Obukhov (1953): Dimensionless characteristics of the turbulence in layers of the atmosphere near the Earth. Docklady Nat. Acad. USSR. Vol. 93, No. 2.

Moore, R. K., I. J. Birrer, E. M. Bracalente, G. J. Dome and F. J. Wentz (1982): Evaluation of atmospheric attenuation from SMMR brightness temperature for the SEASAT satellite scatterometer. J. Geophys. Res. Vol. 87 C5, pp. 3337-3354.

Munk, W. H. (1950): On the wind driven ocean circulation. J. Meteor. Vol. 7, pp. 79-83.

Munk, W. H. and G. F. Carrier (1950): On the wind driven circulation in ocean basins of various shapes. Tellus, Vol. 2 pp. 158-167.

Neumann, G. and W. J. Pierson (1966): Principles of Physical Oceanography. Prentice Hall. pp. 545.

Nitani, H. (1982): The Kuroshio study drifting buoy experiment. ARGOS, Newslett. Vol. 14, pp. 1-3.

O'Brien, J. J. et al. (1982): Scientific opportunities using satellite wind stress measurements over the ocean. (Report of the Satellite Surface Stress Working Group) Nova Univ./NYIT. Press Ft. Lauderdale. Fla.

Phillips, O. M. (1977): The Dynamics of the Upper Ocean. Cambridge Univ. Press. pp. 336.

Pierson, W. J. (1978): The potential impact of SEASAT-A on the study of the planetary boundary layer over the ocean in Favre, A and K. Hasselmann (Eds) "Turbulent Fluxes Through the Sea Surface, Wave Dynamics and Prediction NATO Conference Series 5, Plenum. pp. 563-571.

Pierson, W. J. (1979): A suggested technique for the assimilation of the SASS winds from SEASAT into National Meteorological Center Operational Numerical Weather Prediction Models. CUNY Institute of Marine and Atmospheric Sciences at the City College. Final Report Prepared for the Spacecraft Oceanography Group of NOAA/NESS.

Pierson, W. J. (1982a): The measurement of the synoptic scale wind over the ocean. NASA Contractor's Report 166041. NASA Langley Research Center Hampton Va.

Pierson, W. J. (1982b): The spectral ocean wave model (SOWM), a Northern Hemisphere computor model for specifying and forecasting ocean wave spectra. DTNSRDC-82/011 (July). 191 pp.

150

Pierson, W. J. (1983a): The measurement of the synoptic scale wind over the ocean. J. Geophys. Res. Vol. 88 No. C3. pp. 1683-1708.

Pierson, W. J. (1983b): Highlights of the SEASAT-SASS program; A Review, in Allan T. D. Satellite Microwave Remote Sensing. John Wiley and Sons. pp. 69-86.

Pierson, W. J. (1983c): The SEASAT Radar Scatterometer: Design and theory for the measurement of vector wind over the ocean. (CUNY Inst. Marine and Atmos. Sci., Prepared for NASA, Contract NAGW-266. Submitted for Publication).

Pierson, W. J. and R. E. Salfi (1982): Monte Carlo studies of ocean wind vector measurements by SCATT: Objective criteria and maximum likelihood estimates for removal of aliases, and effects of cell size in accuracy of vector winds. NASA Contractor Report 165837-1. Langley Research Center Hampton, Va. 23665.

Richardson, P. L. (1981): Gulf Stream trajectories measured with free drifting buoys. J. Phys. Oceanogr. Vol. 11 No. 7. pp. 999-1010.

Robinson, A. R., N. E. Huang, C. D. Leitao and C. G. Parra (1983): A study of the variability of ocean currents in the Nothwestern Atlantic Using Satellite Altimetry. J. Phys. Oceanogr. Vol. 73. No. 4. pp. 565-585.

Schroeder, L. C., D. H. Boggs, G. Dome, I. M. Halberstam, W. L. Jones, W. J. Pierson and F. J. Wentz (1982): The relationship between wind vector and normalized radar cross section used to derive SEASAT-A satellite scatterometer winds. J. Geophys. Res. Vol. 87. C5. pp. 3318-3336.

Smith, S. D. (1980): Wind stress and heat flux over the ocean for Gale Force Winds. J. Phys. Oceanogr. Vol. 10 No. 5. pp. 709-736.

Stommel, H. (1948): The westward intensification of wind-driven ocean currents. Trans. Amer. Geophys. Un. Vol. 29. No. 2.

Strong, A. E. and E. P. McClain (1984): Improved ocean surface temperatures from space-comparisons with drifting buoys. Bull. Amer. Meteor. Soc. (In Press).

Sverdrup, H. U. (1947): Wind driven currents in a baroclinic ocean, with application to the Equatorial currents of the Eastern Pacific. Proc. Nat. Acad. Sci. Vol. 33 No. 11. (Washington, DC).

Sylvester, W. B. (1983): A SEASAT-SASS simulation experiment to quantify the errors related to a ± 3-hour intermittent assimilation technique. CUNY Inst. Mar. Atmos. Sci. Tech Rept. Prepared for NASA Contr. NAGW-266.

Thompson, K. R., R. F. Marsden and D. G. Wright (1983): Estimation of low-frequency wind stress fluctuations over the open ocean. J. Phys. Oceanogr. Vol. 13 No. 6. pp. 1003-1011.

Welander, P. (1959): On the vertically integrated mass transport in the oceans. in The atmosphere and the sea in motion. Sci. Contr. to the Rossby Memorial Volume. B. Bolin ed . The Rockefeller Inst. Press. in Assoc. with Oxford Univ. Press. New York.

Weller, R. A., R. E. Payne, W. G. Large and W. Zenk (1983): Wind measurements from an array of oceanographic mooring and from F/S *meteor* During JASIN 1978. J. Geophys. Res. Vol. 88 No. C14. pp. 9689-9706.

Wentz, F. J. and L. A. Thomas (1983): A model function for ocean radar cross section at 14.6 GHz, Remote Sensing Systems, Sausalito, Cal. 94965. (Contractors Rept. for NASA, Cont. NASW 3606.).

Wilkerson, J. and S. McNutt (1979): SEASAT Gulf of Alaska surface truth data inventory. NOAA. JPL Report 622-99.

Woiceshyn, P. M. ed (1979): SEASAT Gulf of Alaska Workshop Vol II Comparison Data Base: Conventional Marine Meteorological and Sea Surface Temperature Analysis. Appendice A and B. JPL Document 622-101. Jet Propul. Lab. Pasadena, Cal.

Woiceshyn, P. M., M. G. Wurtele, D. H. Boggs, L. F. McGoldrick and S. Peteherych (1984): A new parameterization of a empirical model for wind/ocean scatterometry. Advance copy IURS Conference, Shoresh, Israel May 14-23, 1984.

Wunsch, C. and E. M. Gaposchkin (1980): On using satellite altimetry to determine the general circulation of the oceans with applications to geoid improvement. Rev. Geophys. Space Phys. Vol. 18. No. 4. pp. 725-745.

Wurtele, M. G., P. M. Woiceshyn, S. Peteherych, M. Borowski and W. S. Appleby (1982): Wind direction alias removal studies of SEASAT scatterometer-derived wind fields. J. Geophys. Res. Vol. 87 C5. pp. 3365-3377.

Wyrtki, K. (1974): The dynamic topography of the Pacific Ocean and its fluctuation. Rep. HIG-74-5. Hawaii, Inst. of Geophys. Honolulu, Hawaii.

APPENDIX A

SUPPLEMENTARY GEOSTATIONARY CLOUD IMAGES

Figures A1, A2, A3 and A4 show the infrared cloud images for REVS 1141, 1183, 1212 and 1298. Only portions involved with the swath are retained from the original full disk images. The higher the cloud, the colder the top and the brighter the white of the image. Lower clouds are various shades of gray.

Fig. A1, REV 1141, shows the hook-like cloud system and the front to the north of it to be made up of low clouds and that the front is weak. The surface wind field would, of course, influence the low level clouds first so that the results of the main text are reinforced.

Fig. A2, REV 1183, shows the cumulus clouds in the convergence area of the left portion of the swath and that the main cold front and occlusion to the north have produced clouds with very high cold tops. The clouds to the south at the start of the REV are mostly low.

Fig. A3, REV 1212, shows bright high clouds along the cold front and the occlusion. The features deduced fron SMMR and SASS are again reinforced by this figure.

Fig. A4, REV 1298, shows the triple split features of a low that cannot quite get organized into one simple cyclone. Three centers are trying to dominate the flow with the winner not quite decided. Low and high clouds and a confused partially convective pattern off the coast are indicated. From the partial information in REV 1298, and the present image, one might expect the system in the center to dominate in a half a day, or so, because it is receiving the strongest input from the surface circulation.

Fig. A5, REV 1183, shows a visible image obtained an hour earlier than the one in the main text. The towering cumulus tops showing through the frontal cloud band are particularly striking in this image.

Fig. A6, REV 1212, is for the same image as the one in the main text except that the superimposed geographical data are missing. A comparison with Fig. A3 makes it possible to separate the high and the low clouds and to identify the areas of greatest activity.
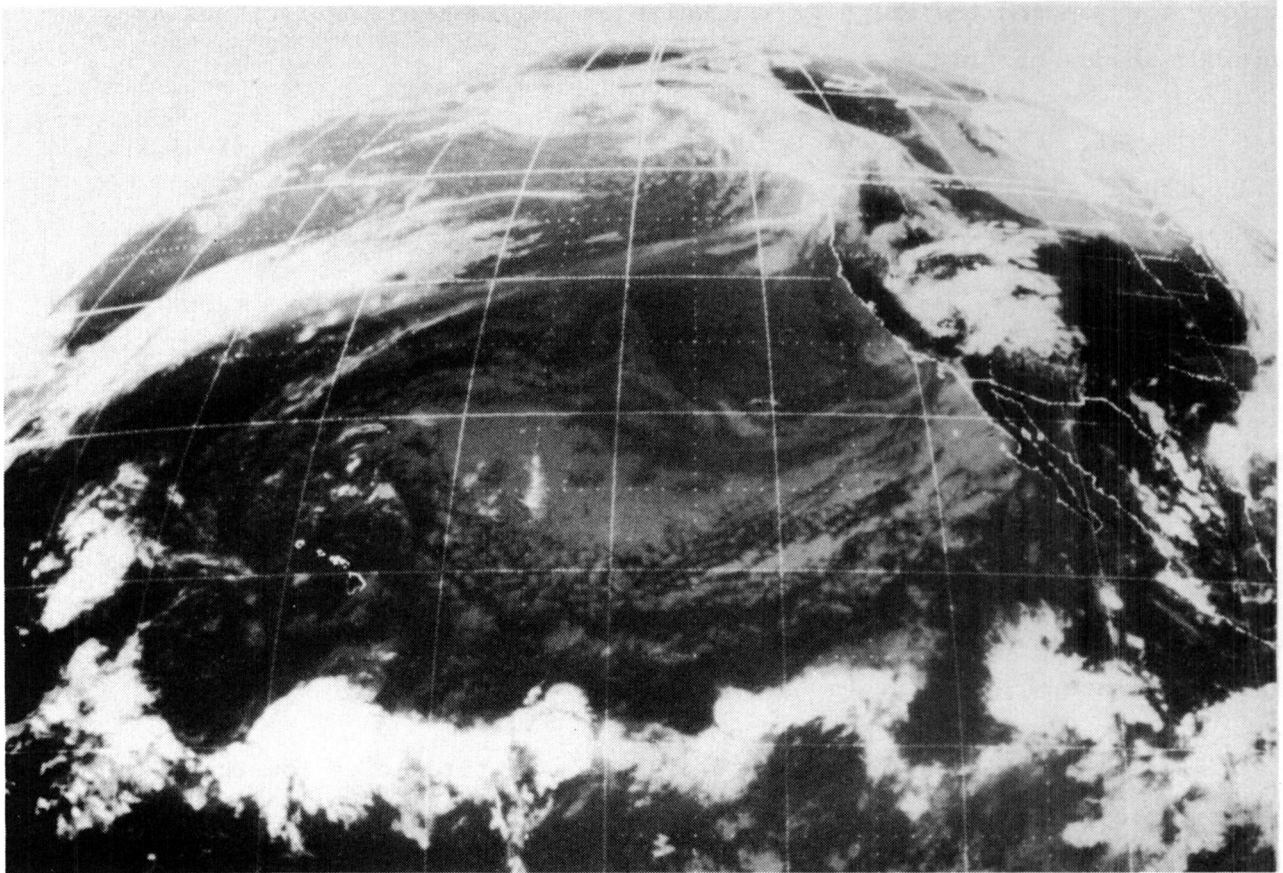
FIG. A1 Infrared Image for REV 1141 Obtained at 1915 GMT.
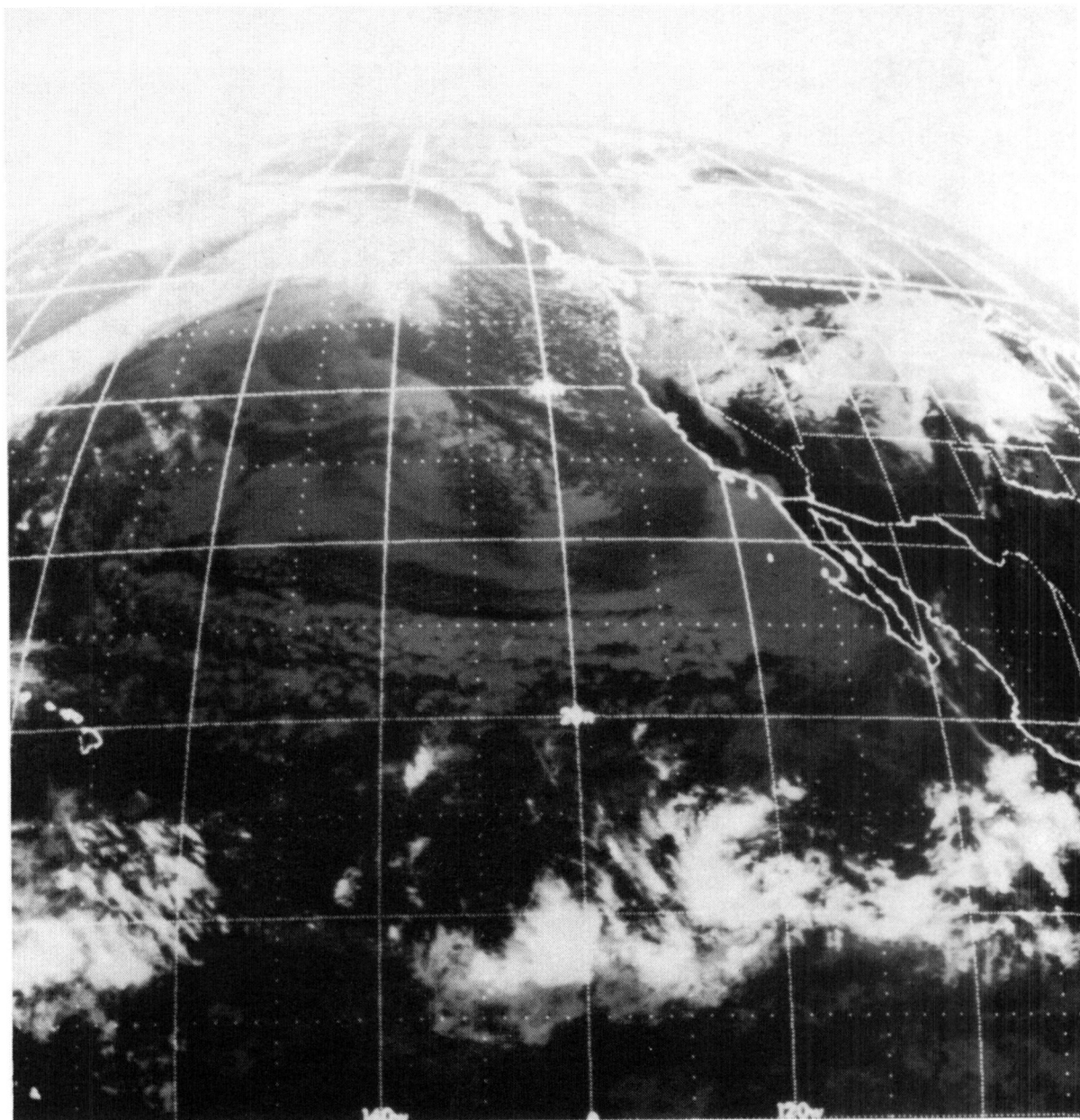
FIG. A2   Infrared Image for REV 1183 Obtained at 1815 GMT.
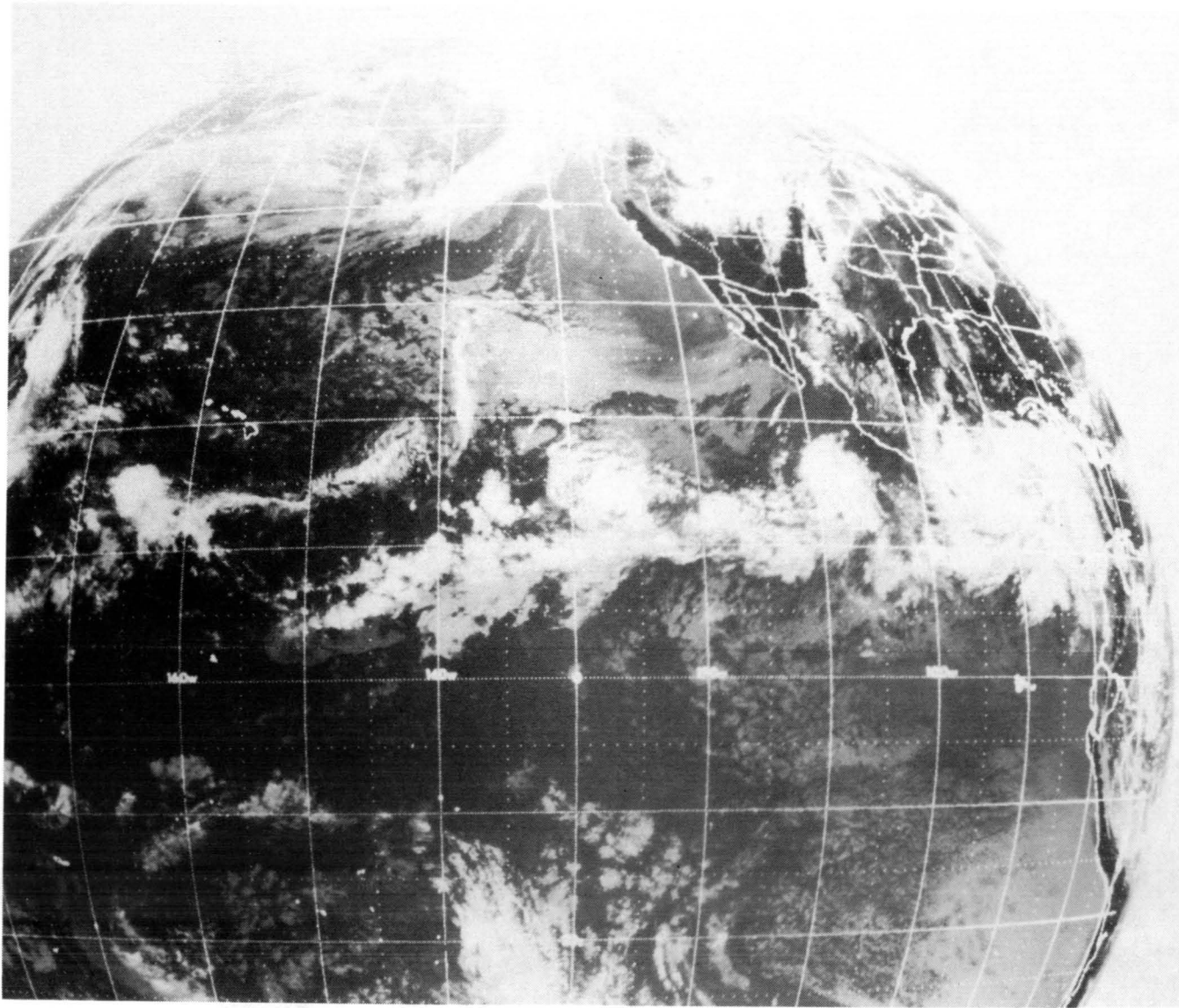
FIG. A3   Infrared Image for REV 1212   Obtained at 1815 GMT.
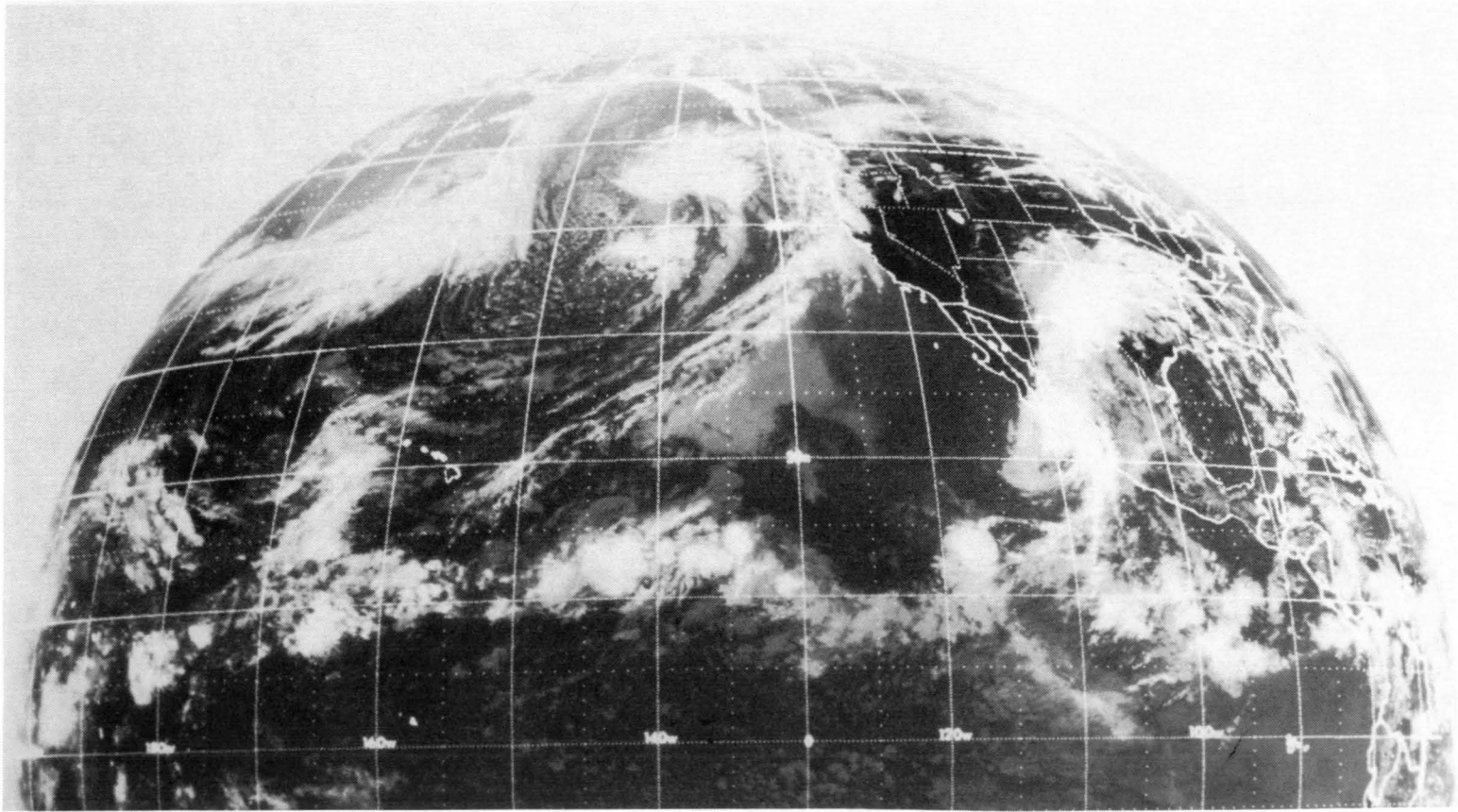
FIG. A4   Infrared Image for REV 1298   Obtained at 1815 GMT.

FIG. A5 Visible Image for REV 1183 Obtained at 1715 GMT.

FIG. A6 Visible Image for REV 1212 Obtained at 1815 GMT.

A, B, C; constants defined by equations (72) and (74).

C_{D10}; the drag coefficient at 10 meters for neutral stability, equal to $u_*^2/\bar{u}_{10}^2$.

C_1, C_2, C_3; constants to be found to correct an edge point.

COV ($\cdot$); the covariance of two random variables.

CURL ($\cdot$); the vertical component of the curl of a vector.

CURL ($\vec{\tau}_h$); the curl of the vector wind stress, (newtons per square meter per meter).

CURL ($\vec{\tau}_h$)$_s$; the desired synoptic scale value at λ_o, θ_o.

$\overline{\text{CURL } (\vec{\tau}_h)}$; the estimate of the synoptic scale value at λ_o, θ_o.

$\text{div}_2\ W_h$; the horizontal divergence of the vector wind on a sphere (sec^{-1}).

$(\text{div}_2\ W_h)_s$; the desired one degree resolution of the divergence.

$\overline{\text{div}_2\ W_h}$; the divergence estimated from the superobservations.

$\mathcal{E}$; the expectation operator.

f ; the Coriolis term (= $2\omega \sin \theta$).

f (u); the probability density function (pdf) of the measurements of u.

$f^*(t)$; the pdf that normalizes. f(u) to a zero mean unit variance random variable as in t = ($u - u_1$)/Δu.

H ; horizontal polarization.

h, h_1, h_2 ; heights above the sea surface.

i ; subscript, summation index.

K ; a constant found from equation (53).

ℓn ; natural logarithm.

M ; generalized sample size.

N ; the number of samples of the SASS dealiased winds used to make $\overline{\Delta\lambda}$ and $\overline{\Delta\theta}$ small.

$N+n$; the number of samples in a two by two degree latitude longitude.

N_4, N_5, N_8, N_9; sample sizes in the one degree squares defined in Fig. 1.

n ; subscript, normal component to $\bar{\chi}$.

p ; subscript, parallel component to $\bar{\chi}$.

Q ; a positive quantity to be minimized.

r ; upper limit of an integral.

R ; gas constant for the atmosphere.

R ; radius of the Earth.

S ; ocean mass transport.

s ; subscript, synoptic.

t ; a normalized random variable as in $t = (u - u_1)/\Delta u$, not necessarily normally distributed.

t_i, t_1, t_2, t_{1i}, t_{4i}, etc. : normalized random variables, not necessarily from the same pdf. Subscripts describe quantites to be summed, or possibly different causes for the variability.

T ; virtual temperature.

u ; a generalized wind for analysis purpose including sources of error in its measurement.

u_1; the first moment of $f(u)$.

$\bar{u}$; mean value of u.

$\bar{U}$; the east-west component (toward which) of the vector sum of $\bar{V}_p$ and $\bar{V}_N$ (similarly for $\bar{V}$).

$\bar{U}$ $(\lambda_o + \overline{\Delta\lambda}, \theta_o + \overline{\Delta\theta})$; a statistic equal to the mean east-west wind component at $\lambda_o + \overline{\Delta\lambda}$, $\theta_o + \overline{\Delta\theta}$ (similarly for north-south $\bar{V}$ $(\cdot, \cdot)$).

$\bar{U}_s(\lambda_o + \overline{\Delta\lambda}, \theta_o + \overline{\Delta\theta})$; the desired synoptic scale wind at a one degree resolution at $\lambda_o + \overline{\Delta\lambda}$, $\theta_o + \overline{\Delta\theta}$ (similarly for $\bar{V}_s$ $(\cdot, \cdot)$)

U_s (λ_o, θ_o) ; error free synoptic scale east-west component of the neutral stability wind at 19.5 m. at λ_o, θ_o. (Similarly for north-south $V_s(\cdot, \cdot)$).

$\bar{U}_p$; the magnitude of the superobservation wind reduced to 10 meters.

u_* ; friction velocity, magnitude.

$\vec{u}_*$; vector friction velocity.

$u_*\,(U_{10})$; friction velocity as a function of the mean wind speed at 10 meters.

$\vec{u}_*^2$; vector u_*^2.

$\bar{U}(z)$, $\bar{V}(z)$, $\Delta U_1(z)$ etc. ; various terms involved in calculating the vertical velocity as a function of height, z.

$<u'\,w'>$; the time averaged eddy fluctuations that define u_*^2 and τ/ρ.

V ; vertical polarization.

V_{Pi} ; the vector component of a SASS wind parallel to $\bar{\chi}$.

V_{Ni} ; the vector component of a SASS wind parallel to $\bar{\chi}$.

$\bar{V}_P$; the average of these N values.

$\bar{V}_N$; the average of these N values.

$|V_i|$; the magnitude of a SASS wind for wind stress calculations.

$VAR\,(\cdot)$; the variance of

$(VAR(CURL(\vec{\tau}_h)))^{\frac{1}{2}}$; the standard deviation of the estimate of the curl of the wind stress.

$(VAR(div_2(\mathbb{W}_h)))^{\frac{1}{2}}$; the standard deviation of the estimate of the horizontal divergence.

W ; vertical velocity as a function of z (or R).

$\mathbb{w}(h)_s$; the synoptic scale vertical velocity at the height, h_1 (meters per second, or cm per second as needed).

$\overline{\mathbb{w}}(200)_s$; the synoptic scale vertical velocity at 200 m at λ_0, θ_0.

$\mathbb{w}(200)$; the estimate of the synoptic scale vertical velocity at λ_0, θ_0.

$\mathbb{w}_f$; vertical velocity at the top of the fraction layer.

z ; height above the sea surface (meters).

α ; a constant to be found in a power law representation for the wind stress (equation (75)).

β ; the power law for the wind stress (equation (75)).

β ; the north-south derivative of the Coriolis term (eqns. (123), (124), (125)).

ΔG_{1i}, ΔG_{2i} ; measurements in degrees of arc along two orthogonal great circles through λ_o, θ_o.

Δu ; the standard deviation of V_p.

Δv ; the standard deviation of V_N.

$(\Delta u)^2$; the variance of u.

Δu_1, Δu_2 ; the components of ΔV_p, ΔV_N in the east-west direction.

Δv_1, Δv_2 ; similar components in the north-south direction.

$\Delta U_1'$, $\Delta U_2'$, $\Delta V_1'$, $\Delta V_2'$; corrected values of $\Delta u_1'$, $\Delta u_2'$, $\Delta v_1'$, $\Delta v_2'$.

ΔU_i, ΔV_i ; standard deviations of V_{pi} and V_{Ni} in local great circle coordinates.

ΔU_m, ΔU_c, ΔV_m, ΔV_c; mesoscale variability and communication noise contributions to ΔU_i and ΔV_i.

$\Delta \overline{w}$ (200) ; the standard deviation of the estimate of the vertical velocity.

$\Delta\lambda$, $\Delta\theta$; the decimal fraction that shows how far a given SASS wind is from λ_o, θ_o; also $\Delta\lambda_i$, $\Delta\theta_i$.

$\overline{V}_p$ (τ/ρ) ; an estimate of the standard deviation of the wind stress $(\vec{u}_*^2)$ in the direction of the superobservation wind.

Δ_N (τ/ρ) ; an estimate of the standard deviation of the wind stress $(\vec{u}_*^2)$ normal to the direction of the superobservation wind.

$$\nabla^2 \psi = \frac{\partial^2 \psi}{\partial x^2} + \frac{\partial^2 \psi}{\partial y^2}$$

$$\nabla^4 \psi = \frac{\partial^4 \psi}{\partial x^4} + \frac{2\partial^2}{\partial x^2}\frac{\partial^2 \psi}{\partial y^2} + \frac{\partial^4 \psi}{\partial y^4}$$

θ ; latitude

θ_o ; latitude at an integer value

θ_o+1, θ_o-1 ; latitudes east and west of θ_o.

λ, λ_o, λ_o+1, λ_o-1 ; for longitude and north-south variations, as for θ.

χ_o ; the pointing direction of the SASS lead radar beam.

χ_i ; wind direction, from which, clock angle, for a SASS wind.

$\overline{\chi}$; average wind direction for N measurements.

κ ; von Karman's constant (0.41 in this study).

ρ ; air density, kilograms per cubic meter.

$\sum$; summation sign, quantities to be summed understood from contents.

τ ; wind stress newtons per square meter.

ψ ; a stream function.

ω ; the angular rotation of the Earth relative to the Stars.

APPENDIX C

TABLES FOR

SUPEROBSERVATION DATA

FOR

REVS 1141, 1183, 1212 AND 1298

(SEE ALSO TABLES 3 TO 6 IN MAIN TEXT)

TABLE 1, REV 1141 VECTOR NEUTRAL WINDS

COLUMN	QUANTITY
1	Latitude
2	Longitude
3	Sample size
4	Wind direction, from which, clock angle
5	Standard deviation normal to mean wind
6	Mean wind
7	$\overline{\Delta\theta}$, before correction
8	$\overline{\Delta\lambda}$, before correction
9	$\sum(\Delta\theta_i)^2$
10	$\sum(\Delta\lambda_i)^2$
11	$\sum(\Delta\theta_i \Delta\lambda_i)$
12	$\Delta U_1'$ (eq. (54))
13	$\Delta U_2'$ (eq. (55))
14	$\Delta V_1'$ (eq. (56))
15	$\Delta V_2'$ (eq. (57))

1	2	3	4	5	6	7	8	9	10	11	12	13	14	15
33	219	10	347	1.0	2.3	0.0	0.0	2.6	0.8	-1.1	0.03	-0.30	-0.16	-0.05
33	220	25	6	1.5	2.3	-0.1	0.1	8.2	7.2	-0.4	-0.02	-0.27	-0.19	0.03
33	221	41	47	1.8	4.2	-0.0	0.1	12.7	11.8	-0.0	-0.14	-0.13	-0.13	0.14
33	222	48	56	1.5	6.5	0.0	-0.0	15.5	17.3	0.4	-0.12	-0.08	-0.08	0.12
33	223	31	53	1.6	8.2	-0.0	-0.1	9.4	4.0	-0.5	-0.07	-0.11	-0.05	0.14
34	219	24	353	0.9	3.4	0.1	0.0	5.4	7.3	-2.6	0.02	-0.11	-0.17	-0.01
34	220	27	16	2.2	2.1	0.1	0.0	8.3	9.3	-2.9	-0.05	-0.35	-0.15	0.11
34	221	36	64	1.3	3.9	-0.0	0.1	12.0	8.0	0.3	-0.29	-0.09	-0.13	0.20
34	222	48	67	1.3	6.3	0.0	-0.0	16.0	16.5	-1.4	-0.15	-0.07	-0.06	0.17
34	223	21	64	1.3	8.2	0.0	0.0	6.6	5.7	-3.5	-0.21	-0.13	-0.11	0.26
35	218	13	344	3.0	3.3	0.0	0.0	2.6	0.9	-1.2	0.26	-0.73	-0.89	-0.22
35	219	36	328	2.9	2.8	-0.0	0.0	11.0	12.6	4.0	0.13	-0.32	-0.20	-0.20
35	220	39	302	2.5	0.9	0.1	0.1	14.3	14.9	-1.4	0.30	-0.10	-0.11	-0.27
35	221	40	92	2.2	3.0	0.0	0.0	12.7	11.4	-2.9	-0.38	0.01	0.01	0.28
35	222	27	80	1.3	5.7	-0.1	0.0	6.1	7.7	-3.4	-0.14	-0.03	-0.03	0.17
35	223	6	71	0.8	6.9	0.0	0.0	2.0	1.6	-1.0	-0.28	-0.06	-0.07	0.24
36	218	24	265	4.2	2.3	0.1	-0.1	7.7	5.2	-1.9	0.47	0.07	0.04	-0.82
36	219	23	242	2.1	3.9	-0.1	0.0	6.1	7.4	-2.0	0.46	0.21	0.25	-0.39
36	220	35	200	3.2	2.9	-0.1	0.1	8.9	12.2	0.6	0.09	0.43	0.26	-0.15
36	221	33	139	2.5	3.7	-0.1	-0.1	11.0	10.2	-2.3	-0.22	0.32	0.27	0.26
36	222	9	115	3.3	3.8	0.0	0.0	3.2	2.3	-2.1	-0.21	0.24	0.10	0.52
37	217	11	357	0.6	3.3	0.0	0.0	3.1	1.0	-0.2	0.09	-0.18	-0.40	-0.04
37	218	16	259	2.8	2.0	-0.0	-0.1	2.7	4.2	-0.2	0.42	0.09	0.08	-0.51
37	219	21	205	2.3	2.8	0.0	0.1	8.0	5.9	2.5	0.19	0.28	0.41	0.13
37	220	34	165	2.7	3.7	0.0	-0.0	9.1	11.4	-0.1	-0.07	0.34	0.28	0.09
37	221	15	147	1.3	4.7	0.0	0.0	3.2	4.8	-2.5	-0.15	0.20	0.25	0.12
38	217	18	1	1.4	1.9	0.1	0.0	4.7	6.0	-2.7	-0.01	-0.31	-0.30	0.01
38	218	15	61	1.7	0.9	0.0	-0.0	7.3	3.6	0.4	-0.24	-0.14	-0.13	0.27
38	219	11	90	1.7	1.9	-0.0	0.1	3.1	3.0	-1.4	-0.22	0.00	0.00	0.30
38	220	13	87	2.4	4.1	0.0	0.0	3.6	3.6	-0.5	-0.40	0.38	0.29	0.52
39	216	25	8	2.0	3.5	0.1	0.0	6.9	5.4	-4.1	-0.07	-0.39	-0.44	0.06
39	217	33	72	1.9	1.2	-0.0	-0.0	9.4	11.8	1.0	-0.22	-0.13	-0.09	0.30
39	218	22	128	1.7	1.5	0.0	-0.1	6.5	4.2	2.8	-0.05	0.14	0.04	0.18
39	219	12	130	1.0	1.8	0.0	0.0	3.5	5.6	-1.2	-0.07	0.21	0.17	0.09
40	215	16	359	1.6	7.2	0.0	0.0	5.2	3.0	-2.8	-0.00	-0.39	-0.36	0.00
40	216	24	3	1.7	3.9	0.0	-0.1	8.7	6.1	-1.9	-0.03	-0.29	-0.65	0.02
40	217	19	188	2.2	1.5	-0.0	0.0	6.7	6.6	0.5	0.04	0.25	0.44	-0.02
40	218	23	185	1.9	3.5	0.0	-0.0	9.4	5.9	1.1	0.03	0.23	0.32	-0.02
40	219	13	179	1.0	3.2	0.0	-0.1	3.9	3.5	1.6	-0.00	0.19	0.21	0.00
41	215	30	355	1.2	6.3	0.1	0.1	9.2	7.5	-3.8	0.01	-0.18	-0.12	-0.02
41	216	30	346	3.3	4.4	0.1	-0.0	8.6	9.8	4.5	0.11	-0.38	-0.45	-0.09
41	217	19	240	3.6	3.4	0.1	0.0	3.0	7.1	0.7	0.77	0.33	0.44	0.58
41	218	22	216	2.3	5.9	0.0	0.0	3.4	7.2	-0.4	0.22	0.27	0.31	-0.20
41	219	20	213	2.2	5.5	0.0	-0.1	4.5	5.1	0.8	0.20	0.28	0.31	-0.19
42	214	17	323	3.6	4.8	0.0	0.0	5.6	4.2	-3.7	0.22	-0.55	-0.31	-0.38
42	215	34	342	0.8	5.6	-0.0	-0.0	9.3	12.0	-0.5	0.02	-0.10	-0.07	-0.03
42	216	39	332	2.8	4.6	0.0	0.0	12.3	12.6	0.7	0.13	-0.29	-0.24	-0.16
42	217	42	268	4.6	4.2	0.0	-0.0	14.5	13.3	0.6	0.20	-0.00	-0.00	-0.41
42	218	36	243	2.3	6.7	0.0	-0.0	11.5	11.5	-0.2	0.09	0.09	0.04	-0.19

1	2	3	4	5	6	7	8	9	10	11	12	13	14	15
42	219	14	248	1.9	7.1	0.0	0.0	3.8	2.5	-2.2	0.16	0.12	0.07	-0.27
43	213	12	253	4.2	5.8	0.0	0.0	2.8	3.4	-1.9	0.39	0.05	0.03	-0.64
43	214	37	287	4.1	4.8	0.1	0.0	11.7	9.5	-1.3	0.09	-0.07	-0.02	-0.26
43	215	35	310	3.3	5.1	0.0	-0.0	10.3	13.8	-2.8	0.06	-0.23	-0.06	-0.27
43	216	26	316	2.0	5.5	-0.0	-0.0	4.9	9.1	0.8	0.07	-0.20	-0.08	-0.19
43	217	26	291	3.2	5.5	-0.1	0.0	4.7	8.8	0.6	0.11	-0.11	-0.04	-0.28
44	213	29	253	1.2	8.3	0.1	0.1	8.2	8.9	-5.3	0.17	0.05	0.05	-0.16
44	214	41	265	2.2	7.1	0.0	-0.0	12.8	13.2	-0.1	0.16	0.02	0.01	-0.21
44	215	34	284	2.5	7.1	0.0	-0.1	12.2	11.7	-1.9	0.17	-0.06	-0.04	-0.24
44	216	23	292	1.9	7.3	-0.1	-0.1	8.5	7.6	-1.3	0.21	-0.10	-0.09	-0.24
44	217	17	281	2.1	7.5	0.0	0.0	5.4	4.2	-0.2	0.24	-0.06	-0.05	-0.32
45	212	19	252	1.3	10.9	0.0	0.0	7.3	4.4	-4.0	0.18	0.06	0.05	-0.20
45	213	39	261	1.8	9.6	0.0	-0.0	12.1	11.6	-0.3	0.10	0.02	0.01	-0.16
45	214	33	269	1.6	9.2	-0.0	-0.0	10.0	10.0	-0.9	0.15	0.00	0.00	-0.18
45	215	31	277	1.4	9.6	-0.0	-0.0	11.4	11.0	1.7	0.15	-0.02	-0.02	-0.17
45	216	23	283	1.3	9.7	0.0	-0.1	9.1	7.8	2.2	0.19	-0.04	-0.04	-0.19
45	217	13	275	2.3	9.2	-0.0	-0.1	5.0	2.5	-2.0	0.22	-0.03	-0.02	-0.35
46	211	11	250	0.7	13.1	0.0	0.0	4.3	3.1	-2.8	0.29	0.06	0.09	-0.17
46	212	36	258	1.2	11.8	0.0	0.1	9.9	10.0	-2.6	0.11	0.02	0.02	-0.13
46	213	40	266	1.6	11.3	-0.0	-0.0	12.2	11.8	-0.3	0.11	0.01	0.01	-0.15
46	214	29	271	1.4	11.4	-0.0	-0.1	9.8	8.4	0.7	0.17	-0.00	-0.00	-0.18
46	215	30	273	1.7	11.8	0.1	0.1	9.1	9.7	0.3	0.11	-0.01	-0.01	-0.16
46	216	29	277	1.6	11.6	0.1	0.0	7.2	7.8	1.3	0.11	-0.02	-0.01	-0.16
46	217	8	273	2.2	10.4	0.0	0.0	1.7	0.9	-0.6	0.31	-0.04	-0.02	-0.45
47	211	30	253	1.2	13.8	0.0	0.1	8.8	8.6	-3.5	0.09	0.04	0.03	-0.13
47	212	40	260	1.2	13.1	-0.0	0.0	14.1	13.6	-2.3	0.08	0.02	0.01	-0.11
47	213	37	264	1.4	13.1	-0.1	-0.0	12.3	11.7	-0.1	0.11	0.01	0.01	-0.14
47	214	35	266	1.6	13.3	0.0	0.0	11.4	12.1	2.2	0.10	0.01	0.01	-0.15
47	215	39	265	1.8	13.1	0.1	0.1	12.3	13.3	-1.1	0.06	0.01	0.00	-0.12
47	216	28	268	2.3	12.8	-0.1	-0.1	8.5	5.6	-3.5	0.06	0.00	0.00	-0.16
48	210	23	250	1.3	15.3	0.0	0.0	6.9	6.6	-4.5	0.07	0.05	0.03	-0.14
48	211	40	256	1.6	14.7	0.0	-0.0	12.6	13.2	-1.2	0.06	0.03	0.01	-0.12
48	212	36	259	1.0	14.5	-0.0	-0.0	13.0	11.9	-0.2	0.11	0.02	0.02	-0.12
48	213	32	260	1.5	14.6	-0.0	-0.0	11.6	9.4	0.5	0.09	0.02	0.01	-0.14
48	214	37	260	2.0	14.7	0.0	0.0	12.9	12.1	0.5	0.06	0.02	0.01	-0.14
48	215	41	259	1.7	14.4	-0.1	-0.1	11.9	13.4	-3.2	0.06	0.02	0.01	-0.13
49	209	17	254	1.5	16.4	0.0	0.0	6.0	4.2	-4.0	0.10	0.05	0.03	-0.18
49	210	41	259	1.9	15.8	0.0	-0.0	12.8	12.7	-2.8	0.05	0.02	0.01	-0.12
49	211	38	261	1.6	15.9	-0.0	-0.1	12.0	11.3	0.1	0.07	0.02	0.01	-0.13
49	212	32	260	1.9	16.2	-0.0	-0.0	9.2	10.8	-1.1	0.10	0.03	0.02	-0.17
49	213	29	255	2.0	16.2	-0.0	-0.0	8.2	9.2	0.1	0.11	0.05	0.03	-0.19
49	214	33	255	2.3	15.9	-0.0	0.0	10.9	9.1	-0.1	0.06	0.04	0.02	-0.16
49	215	19	256	2.7	15.4	0.0	0.0	8.7	4.5	-5.2	0.09	0.06	0.02	-0.24
50	208	10	256	1.1	17.5	0.0	0.0	3.0	2.6	-2.4	0.12	0.04	0.02	-0.19
50	209	32	261	1.6	16.9	-0.0	0.0	9.0	8.6	-1.6	0.07	0.02	0.01	-0.14
50	210	34	265	2.0	16.9	-0.0	0.0	11.1	11.6	-0.2	0.07	0.01	0.01	-0.15
50	211	32	264	3.0	17.3	0.0	-0.0	11.5	9.1	-1.0	0.04	0.01	0.00	-0.14
50	212	31	257	3.0	17.5	0.0	0.0	10.4	10.6	0.3	0.11	0.09	0.02	-0.39
50	213	32	255	2.7	17.2	0.0	0.0	11.3	10.6	0.0	0.11	0.09	0.03	-0.35
50	214	29	255	3.1	16.6	-0.0	-0.1	8.0	6.8	-2.1	0.13	0.13	0.03	-0.49

1	2	3	4	5	6	7	8	9	10	11	12	13	14	15
51	207	8	255	1.2	18.1	0.0	0.0	2.4	2.3	-1.8	0.11	0.04	0.02	-0.20
51	208	25	261	2.3	17.7	0.0	0.1	8.5	6.2	-2.4	0.07	0.03	0.01	-0.18
51	209	35	262	2.2	17.7	0.0	0.0	12.7	11.4	2.0	0.07	0.02	0.01	-0.15
51	210	34	263	2.9	17.9	0.0	0.0	10.7	12.7	1.4	0.06	0.03	0.01	-0.23
51	211	29	261	4.0	18.2	0.0	-0.0	9.7	8.1	0.6	0.13	0.11	0.02	-0.70
51	212	32	253	4.1	18.0	0.0	0.1	11.7	10.3	0.8	0.11	0.22	0.04	-0.69
51	213	38	252	4.1	17.6	0.0	-0.0	12.7	11.4	-3.6	0.14	0.20	0.04	-0.62
51	214	12	251	.4.5	17.0	0.0	0.0	3.9	3.2	-2.0	0.08	0.13	0.02	-0.42
52	206	7	254	1.4	18.6	0.0	0.0	2.2	2.6	-1.3	0.11	0.05	0.02	-0.24
52	207	25	261	2.6	18.6	0.1	0.0	5.5	7.5	-3.2	0.09	0.03	0.01	-0.25
52	208	30	264	2.8	18.8	0.0	0.0	7.5	10.0	1.0	0.09	0.02	0.01	-0.21
52	209	32	262	3.4	18.9	-0.0	0.0	11.0	10.1	2.5	0.09	0.03	0.01	-0.22
52	210	33	257	3.8	18.8	-0.1	0.0	11.8	9.7	0.5	0.15	0.11	0.03	-0.52
52	211	29	253	4.9	18.7	0.0	-0.0	8.1	9.9	1.5	0.14	0.25	0.04	-0.86
52	212	34	249	5.0	18.6	0.0	0.1	10.0	10.6	-0.6	0.14	0.30	0.05	-0.81
52	213	22	247	4.7	18.3	0.0	0.0	7.7	4.8	-3.2	0.18	0.33	0.07	-0.80
53	205	12	261	2.1	19.0	0.0	0.0	2.8	4.7	0.6	0.03	0.01	0.00	-0.14
53	206	22	265	2.4	19.5	0.0	0.1	4.8	5.2	-1.9	0.09	0.02	0.01	-0.25
53	207	33	265	2.8	19.6	-0.0	0.0	11.0	10.5	0.7	0.08	0.02	0.01	-0.26
53	208	27	265	2.9	19.8	-0.0	-0.0	7.0	9.6	-0.7	0.13	0.03	0.01	-0.47
53	209	25	261	4.3	20.1	-0.0	0.0	6.5	6.7	1.1	0.18	0.12	0.03	-0.78
53	210	28	256	5.1	19.7	0.0	-0.0	8.7	8.7	-0.5	0.17	0.22	0.04	-0.92
53	211	34	252	5.3	19.3	0.0	0.0	11.7	11.8	0.4	0.16	0.27	0.05	-0.87
53	212	31	247	4.9	18.8	-0.0	-0.1	9.7	8.2	-2.2	0.18	0.34	0.08	-0.80
53	213	7	234	3.2	18.1	0.0	0.0	1.5	1.7	-1.1	0.21	0.35	0.13	-0.58
54	204	8	247	4.2	22.0	0.0	0.0	3.4	3.3	0.4	0.18	0.00	0.00	-0.50
54	205	14	267	1.9	19.5	-0.0	0.0	3.8	1.8	-1.3	0.15	0.02	0.01	-0.50
54	206	21	267	2.6	19.9	-0.1	0.0	4.7	7.6	-0.2	0.13	0.02	0.01	-0.56
54	207	25	267	2.8	19.9	-0.1	0.0	8.1	8.3	0.8	0.11	0.03	0.01	-0.53
54	208	25	264	4.2	20.1	-0.1	-0.0	8.3	8.0	-0.2	0.12	0.06	0.01	-0.62
54	209	26	261	5.9	20.2	-0.0	0.0	7.8	7.1	0.8	0.17	0.14	0.02	-0.96
54	210	28	255	6.9	19.7	-0.0	0.0	9.1	9.5	-0.8	0.14	0.30	0.04	-1.16
54	211	31	250	6.4	19.4	-0.1	-0.0	8.1	9.7	-0.6	0.15	0.35	0.05	-1.02
54	212	15	251	6.1	19.0	0.0	0.0	3.5	2.0	-2.2	0.12	0.19	0.04	-0.56
55	204	12	283	5.9	17.3	0.0	0.0	2.7	5.5	-1.0	0.08	-0.14	-0.02	-0.50
55	205	10	277	5.2	18.4	-0.0	0.1	2.3	2.1	1.0	0.12	-0.06	-0.02	-0.46
55	206	15	275	5.3	19.1	-0.1	0.0	3.4	4.4	0.3	0.08	-0.03	-0.01	-0.34
55	207	20	277	7.2	19.0	-0.0	0.0	5.3	5.8	0.9	0.29	-0.13	-0.04	-1.03
55	208	23	281	9.7	18.1	-0.0	-0.0	8.7	8.7	-2.5	0.20	-0.13	-0.04	-0.69
55	209	26	273	10.3	17.5	-0.0	0.0	9.3	8.2	1.3	0.37	-0.04	-0.01	-0.88
55	210	25	253	8.8	18.1	-0.0	-0.0	7.3	9.1	-2.3	0.65	0.37	0.19	-1.23
55	211	10	240	5.4	19.4	-0.0	-0.0	2.3	2.0	-1.7	0.53	0.86	0.30	-1.49
56	207	12	308	8.3	19.0	0.0	0.0	4.2	3.7	0.4	0.25	-0.42	-0.11	-0.98
56	208	12	312	6.3	18.3	-0.1	0.0	2.7	4.3	0.9	0.37	-0.84	-0.34	-0.92
56	209	19	297	10.3	15.1	-0.1	0.1	5.3	6.8	-0.7	0.50	-0.71	-0.23	-1.54
56	210	13	264	9.6	14.0	-0.0	-0.1	3.0	4.3	-2.2	0.39	0.07	0.03	-0.99
56	211	7	232	6.7	21.7	0.0	0.0	2.3	2.5	0.1	0.64	0.54	0.27	-1.26
57	208	6	333	2.5	17.6	0.0	0.0	1.7	2.3	-0.1	0.33	-0.57	-0.40	-0.48
57	209	12	313	6.1	15.1	0.0	0.0	3.2	2.9	-0.8	0.35	-0.64	-0.25	-0.89
57	210	9	18	6.7	7.7	0.0	0.0	3.7	3.4	1.1	-0.25	-0.34	-0.10	-0.90

TABLE 2, REV 1141, VECTOR $\vec{u}_*^2$

COLUMN	QUANTITY
16	Latitude
17	Longitude
18	Direction (meteorological)
19	$\tau/\rho \ (U_p + N^{-\frac{1}{2}} \Delta U_{mc}) \ m^2/sec^2$
20	$\Delta_p \ (\tau/\rho)$
21	$\Delta_N \ (\tau/\rho)$
22	$-\Delta_p \ (\tau/\rho) \sin \bar{\chi}$
23	$-\Delta_N \ (\tau/\rho) \cos \bar{\chi}$
24	$-\Delta_p \ (\tau/\rho) \cos \bar{\chi}$
25	$-\Delta_N \ (\tau/\rho) \sin \bar{\chi}$

Note $\vec{u}_*^2 = \tau/\rho \ (U_p + \Delta N^{-\frac{1}{2}} U_{mc}) - \Delta_p(\tau/\rho)$

16	17	18	19	20	21	22	23	24	25
33	219	347	0.0079	0.0007	0.0009	0.0002	-0.0009	-0.0007	-0.0002
33	220	6	0.0082	0.0008	0.0009	-0.0001	-0.0009	-0.0008	0.0001
33	221	47	0.0196	0.0015	0.0008	-0.0011	-0.0006	-0.0010	0.0006
33	222	56	0.0420	0.0019	0.0009	-0.0016	-0.0005	-0.0011	0.0008
33	223	53	0.0664	0.0016	0.0014	-0.0013	-0.0009	-0.0010	0.0011
34	219	353	0.0139	0.0011	0.0004	0.0001	-0.0004	-0.0010	0.0000
34	220	16	0.0073	0.0007	0.0011	-0.0002	-0.0011	-0.0007	0.0003
34	221	64	0.0183	0.0023	0.0009	-0.0021	-0.0004	-0.0010	0.0008
34	222	67	0.0395	0.0020	0.0011	-0.0019	-0.0004	-0.0008	0.0010
34	223	64	0.0700	0.0044	0.0023	-0.0040	-0.0010	-0.0019	0.0021
35	218	344	0.0181	0.0061	0.0028	0.0016	-0.0027	-0.0059	-0.0007
35	219	328	0.0108	0.0013	0.0013	0.0007	-0.0011	-0.0011	-0.0007
35	220	302	0.0035	0.0010	0.0008	0.0009	-0.0004	-0.0005	-0.0007
35	221	.92	0.0125	0.0021	0.0010	-0.0021	0.0000	0.0001	0.0010
35	222	80	0.0322	0.0016	0.0009	-0.0016	-0.0002	-0.0003	0.0009
35	223	71	0.0497	0.0043	0.0016	-0.0041	-0.0005	-0.0013	0.0015
36	218	265	0.0098	0.0023	0.0026	0.0023	0.0002	0.0002	-0.0026
36	219	242	0.0200	0.0039	0.0018	0.0035	0.0008	0.0018	-0.0016
36	220	200	0.0117	0.0015	0.0016	0.0005	0.0015	0.0014	-0.0006
36	221	139	0.0172	0.0024	0.0016	-0.0016	0.0013	0.0019	0.0011
36	222	115	0.0167	0.0016	0.0023	-0.0015	0.0010	0.0007	0.0020
37	217	357	0.0150	0.0026	0.0007	0.0001	-0.0007	-0.0026	0.0000
37	218	259	0.0080	0.0019	0.0016	0.0018	0.0003	0.0003	-0.0015
37	219	205	0.0119	0.0024	0.0010	0.0010	0.0009	0.0022	-0.0004
37	220	165	0.0166	0.0020	0.0014	-0.0005	0.0014	0.0019	0.0003
37	221	147	0.0244	0.0026	0.0011	-0.0014	0.0009	0.0022	0.0006
38	217	1	0.0071	0.0013	0.0009	0.0000	-0.0009	-0.0013	0.0000
38	218	61	0.0031	0.0009	0.0008	-0.0008	-0.0004	-0.0004	0.0007
38	219	90	0.0067	0.0009	0.0009	-0.0009	0.0000	0.0000	0.0009
38	220	87	0.0208	0.0038	0.0027	-0.0038	-0.0001	-0.0002	0.0027
39	216	8	0.0166	0.0030	0.0015	-0.0005	-0.0015	-0.0030	0.0002
39	217	72	0.0041	0.0008	0.0009	-0.0008	-0.0003	-0.0002	0.0009
39	218	128	0.0046	0.0002	0.0006	-0.0002	0.0004	0.0001	0.0005
39	219	130	0.0062	0.0007	0.0007	-0.0006	0.0004	0.0005	0.0005
40	215	359	0.0552	0.0057	0.0027	0.0000	-0.0027	-0.0057	0.0000
40	216	3	0.0211	0.0050	0.0012	-0.0003	-0.0012	-0.0050	0.0001
40	217	188	0.0060	0.0017	0.0007	0.0003	0.0007	0.0017	-0.0001
40	218	185	0.0153	0.0021	0.0009	0.0002	0.0009	0.0021	-0.0001
40	219	179	0.0126	0.0012	0.0007	0.0000	0.0007	0.0012	0.0000
41	215	355	0.0394	0.0015	0.0011	0.0001	-0.0011	-0.0015	-0.0001
41	216	346	0.0228	0.0038	0.0017	0.0009	-0.0016	-0.0037	-0.0004
41	217	240	0.0184	0.0059	0.0025	0.0052	0.0012	0.0029	-0.0021
41	218	216	0.0372	0.0045	0.0019	0.0027	0.0015	0.0037	-0.0011
41	219	213	0.0325	0.0040	0.0018	0.0022	0.0015	0.0033	-0.0010
42	214	323	0.0262	0.0035	0.0031	0.0021	-0.0025	-0.0028	-0.0019
42	215	342	0.0303	0.0008	0.0006	0.0002	-0.0005	-0.0008	-0.0002
42	216	332	0.0234	0.0024	0.0015	0.0011	-0.0014	-0.0021	-0.0007
42	217	268	0.0197	0.0016	0.0017	0.0016	0.0000	0.0000	-0.0017
42	218	243	0.0442	0.0013	0.0013	0.0012	0.0006	0.0006	-0.0012
42	219	248	0.0503	0.0027	0.0020	0.0025	0.0007	0.0010	-0.0018

TABLE 2B, REV 1141, VECTOR $\vec{u}_*^2$

16	17	18	19	20	21	22	23	24	25
43	213	253	0.0367	0.0046	0.0035	0.0044	0.0010	0.0013	-0.0034
43	214	287	0.0232	0.0008	0.0013	0.0008	-0.0004	-0.0002	-0.0012
43	215	310	0.0258	0.0008	0.0018	0.0006	-0.0012	-0.0005	-0.0013
43	216	316	0.0299	0.0011	0.0015	0.0008	-0.0011	-0.0008	-0.0010
43	217	291	0.0297	0.0013	0.0016	0.0012	-0.0006	-0.0005	-0.0015
44	213	253	0.0701	0.0035	0.0013	0.0034	0.0004	0.0010	-0.0013
44	214	265	0.0512	0.0024	0.0014	0.0024	0.0001	0.0002	-0.0014
44	215	284	0.0512	0.0027	0.0017	0.0026	-0.0004	-0.0007	-0.0016
44	216	292	0.0543	0.0036	0.0018	0.0033	-0.0007	-0.0014	-0.0017
44	217	281	0.0577	0.0042	0.0023	0.0041	-0.0004	-0.0008	-0.0023
45	212	252	0.1313	0.0057	0.0024	0.0054	0.0007	0.0017	-0.0023
45	213	261	0.0961	0.0024	0.0015	0.0024	0.0002	0.0003	-0.0015
45	214	269	0.0877	0.0034	0.0017	0.0034	0.0000	0.0000	-0.0017
45	215	277	0.0981	0.0038	0.0017	0.0038	-0.0002	-0.0005	-0.0017
45	216	283	0.1020	0.0050	0.0019	0.0049	-0.0004	-0.0011	-0.0019
45	217	275	0.0909	0.0052	0.0033	0.0052	-0.0003	-0.0005	-0.0033
46	211	250	0.2110	0.0126	0.0028	0.0118	0.0010	0.0043	-0.0026
46	212	258	0.1575	0.0037	0.0017	0.0036	0.0003	0.0008	-0.0017
46	213	266	0.1408	0.0034	0.0018	0.0034	0.0001	0.0002	-0.0018
46	214	271	0.1463	0.0055	0.0022	0.0055	0.0000	-0.0001	-0.0022
46	215	273	0.1559	0.0037	0.0021	0.0037	-0.0001	-0.0002	-0.0021
46	216	277	0.1507	0.0037	0.0021	0.0036	-0.0003	-0.0005	-0.0020
46	217	273	0.1232	0.0088	0.0049	0.0088	-0.0003	-0.0005	-0.0049
47	211	253	0.2317	0.0043	0.0022	0.0041	0.0006	0.0012	-0.0021
47	212	260	0.2019	0.0034	0.0017	0.0033	0.0003	0.0006	-0.0017
47	213	264	0.2033	0.0045	0.0021	0.0044	0.0002	0.0004	-0.0021
47	214	266	0.2102	0.0042	0.0023	0.0042	0.0001	0.0003	-0.0023
47	215	265	0.2035	0.0024	0.0019	0.0024	0.0001	0.0002	-0.0019
47	216	268	0.1922	0.0025	0.0024	0.0025	0.0001	0.0001	-0.0024
48	210	250	0.2981	0.0043	0.0028	0.0040	0.0010	0.0015	-0.0026
48	211	256	0.2698	0.0030	0.0022	0.0029	0.0005	0.0007	-0.0021
48	212	259	0.2655	0.0054	0.0021	0.0054	0.0004	0.0010	-0.0021
48	213	260	0.2689	0.0046	0.0026	0.0045	0.0004	0.0008	-0.0025
48	214	260	0.2696	0.0033	0.0026	0.0032	0.0004	0.0006	-0.0026
48	215	259	0.2560	0.0032	0.0023	0.0031	0.0004	0.0006	-0.0022

TABLE 2C, REV 1141 VECTOR $\vec{u}_*^2$

16	17	18	19	20	21	22	23	24	25
49	209	254	0.3604	0.0063	0.0041	0.0061	0.0011	0.0017	-0.0039
49	210	259	0.3269	0.0028	0.0025	0.0028	0.0005	0.0005	-0.0024
49	211	261	0.3319	0.0043	0.0027	0.0043	0.0004	0.0006	-0.0027
49	212	260	0.3488	0.0062	0.0037	0.0061	0.0006	0.0010	-0.0037
49	213	255	0.3531	0.0067	0.0041	0.0065	0.0010	0.0017	-0.0040
49	214	255	0.3293	0.0035	0.0033	0.0034	0.0008	0.0009	-0.0032
49	215	256	0.3064	0.0050	0.0048	0.0049	0.0011	0.0011	-0.0047
50	208	256	0.4297	0.0083	0.0047	0.0081	0.0011	0.0019	-0.0046
50	209	261	0.3911	0.0046	0.0031	0.0045	0.0005	0.0007	-0.0031
50	210	265	0.3858	0.0047	0.0034	0.0047	0.0003	0.0004	-0.0034
50	211	264	0.4082	0.0026	0.0034	0.0026	0.0003	0.0003	-0.0034
50	212	257	0.4262	0.0079	0.0096	0.0077	0.0021	0.0017	-0.0094
50	213	255	0.4107	0.0079	0.0085	0.0077	0.0022	0.0020	-0.0083
50	214	255	0.3743	0.0088	0.0112	0.0085	0.0028	0.0022	-0.0109
51	207	255	0.4674	0.0084	0.0053	0.0081	0.0013	0.0021	-0.0051
51	208	261	0.4404	0.0052	0.0045	0.0052	0.0007	0.0008	-0.0044
51	209	262	0.4388	0.0047	0.0038	0.0046	0.0005	0.0006	-0.0037
51	210	263	0.4512	0.0046	0.0059	0.0046	0.0006	0.0005	-0.0059
51	211	261	0.4772	0.0095	0.0183	0.0094	0.0029	0.0015	-0.0180
51	212	253	0.4636	0.0087	0.0182	0.0083	0.0053	0.0025	-0.0174
51	213	252	0.4393	0.0104	0.0160	0.0099	0.0049	0.0032	-0.0152
51	214	251	0.3972	0.0053	0.0103	0.0050	0.0032	0.0017	-0.0097
52	206	254	0.5042	0.0087	0.0065	0.0083	0.0018	0.0024	-0.0062
52	207	261	0.5018	0.0069	0.0067	0.0068	0.0010	0.0010	-0.0066
52	208	264	0.5143	0.0071	0.0056	0.0071	0.0005	0.0006	-0.0056
52	209	262	0.5200	0.0069	0.0061	0.0069	0.0008	0.0009	-0.0061
52	210	257	0.5238	0.0122	0.0143	0.0119	0.0030	0.0025	-0.0140
52	211	253	0.5100	0.0115	0.0241	0.0110	0.0068	0.0032	-0.0231
52	212	249	0.5044	0.0119	0.0229	0.0112	0.0079	0.0041	-0.0215
52	213	247	0.4858	0.0147	0.0223	0.0135	0.0087	0.0057	-0.0206
53	205	261	0.5248	0.0025	0.0039	0.0025	0.0006	0.0004	-0.0038
53	206	265	0.5703	0.0075	0.0073	0.0075	0.0006	0.0006	-0.0073
53	207	265	0.5773	0.0065	0.0076	0.0065	0.0006	0.0005	-0.0076
53	208	265	0.5996	0.0116	0.0139	0.0115	0.0010	0.0008	-0.0138
53	209	261	0.6232	0.0167	0.0237	0.0165	0.0036	0.0026	-0.0234

TABLE 2D, REV 1141, VECTOR $\vec{u}_*^2$

16	17	18	19	20	21	22	23	24	25
53	210	256	0.5957	0.0155	0.0279	0.0151	0.0067	0.0037	-0.0271
53	211	252	0.5588	0.0143	0.0256	0.0136	0.0077	0.0043	-0.0244
53	212	247	0.5281	0.0158	0.0236	0.0145	0.0092	0.0061	-0.0217
53	213	234	0.4816	0.0185	0.0174	0.0150	0.0102	0.0109	-0.0141
54	204	247	0.7973	0.0186	0.0175	0.0172	0.0067	0.0072	-0.0162
54	205	267	0.5736	0.0125	0.0143	0.0125	0.0007	0.0006	-0.0142
54	206	267	0.6056	0.0118	0.0168	0.0118	0.0006	0.0005	-0.0168
54	207	267	0.6037	0.0094	0.0157	0.0094	0.0007	0.0004	-0.0157
54	208	264	0.6173	0.0107	0.0187	0.0107	0.0017	0.0010	-0.0187
54	209	261	0.6356	0.0152	0.0297	0.0151	0.0043	0.0022	-0.0294
54	210	255	0.5865	0.0126	0.0349	0.0122	0.0088	0.0032	-0.0338
54	211	250	0.5665	0.0133	0.0308	0.0125	0.0101	0.0044	-0.0290
54	212	251	0.5350	0.0104	0.0164	0.0099	0.0051	0.0033	-0.0155
55	204	283	0.4174	0.0060	0.0124	0.0058	-0.0030	-0.0014	-0.0120
55	205	277	0.4921	0.0096	0.0122	0.0095	-0.0016	-0.0013	-0.0121
55	206	275	0.5413	0.0066	0.0095	0.0066	-0.0009	-0.0006	-0.0095
55	207	277	0.5444	0.0237	0.0284	0.0235	-0.0037	-0.0031	-0.0282
55	208	281	0.4780	0.0153	0.0179	0.0150	-0.0036	-0.0031	-0.0175
55	209	273	0.4453	0.0258	0.0211	0.0258	-0.0014	-0.0017	-0.0210
55	210	253	0.5095	0.0515	0.0325	0.0493	0.0093	0.0147	-0.0311
55	211	240	0.6065	0.0526	0.0490	0.0456	0.0244	0.0262	-0.0425
56	207	308	0.5449	0.0223	0.0293	0.0175	-0.0181	-0.0138	-0.0231
56	208	312	0.5140	0.0387	0.0324	0.0286	-0.0218	-0.0261	-0.0240
56	209	297	0.3172	0.0305	0.0322	0.0270	-0.0149	-0.0141	-0.0285
56	210	264	0.2550	0.0186	0.0167	0.0185	0.0015	0.0017	-0.0166
56	211	232	0.8220.	0.0740	0.0472	0.0589	0.0286	0.0447	-0.0376
57	208	333	0.4615	0.0369	0.0180	0.0166	-0.0161	-0.0330	-0.0081
57	209	313	0.3090	0.0232	0.0208	0.0169	-0.0143	-0.0159	-0.0151
57	210	18	0.0612	0.0047	0.0071	-0.0015	-0.0067	-0.0045	0.0022

TABLE 3, REV 1141, WIND STRESS CURL IN NEWTONS PER SQUARE
METER PER METER (X 10^7).

COLUMN	QUANTITY
26	Latitude
27	Longitude
28	$\overline{\text{CURL } (\vec{\tau}_h)}$
29	$(\text{VAR}(\text{CURL}(\vec{\tau}_h)))^{\frac{1}{2}}$
30	(28) + (29)
31	(28) - (29)

26	27	28	29	30	31
34	220	-1.59	0.17	-1.42	-1.76
34	221	-3.11	0.18	-2.93	-3.29
34	222	-4.18	0.33	-3.85	-4.51
35	219	-1.44	0.28	-1.15	-1.72
35	220	-2.26	0.20	-2.07	-2.46
35	221	-3.56	0.20	-3.37	-3.76
35	222	-3.66	0.36	-3.30	-4.02
36	219	-1.50	0.24	-1.26	-1.74
36	220	-3.00	0.31	-2.69	-3.31
36	221	-2.44	0.21	-2.23	-2.65
37	218	0.44	0.12	0.57	0.32
37	219	-0.31	0.21	-0.10	-0.51
37	220	-0.60	0.27	-0.33	-0.88
38	218	-0.55	0.10	-0.45	-0.65
38	219	-0.91	0.31	-0.60	-1.22
39	217	-0.81	0.17	-0.64	-0.98
39	218	-1.00	0.15	-0.85	-1.14
40	216	0.35	0.34	0.69	0.01
40	217	-0.39	0.26	-0.13	-0.65
40	218	-1.57	0.24	-1.34	-1.81
41	216	0.88	0.51	1.39	0.37
41	217	1.55	0.31	1.87	1.24
41	218	-0.06	0.47	0.41	-0.53
42	215	-1.66	0.31	-1.35	-1.98
42	216	0.72	0.26	0.98	0.46
42	217	3.29	0.26	3.56	3.03
43	214	-2.63	0.41	-2.22	-3.05
43	215	-1.06	0.19	-0.87	-1.25
43	216	0.61	0.24	0.85	0.37
44	214	-1.82	0.36	-1.45	-2.18
44	215	-0.30	0.35	0.06	-0.65
44	216	0.58	0.42	1.00	0.17
45	213	-2.29	0.53	-1.76	-2.83
45	214	0.56	0.40	0.96	0.16
45	215	0.78	0.51	1.29	0.28
45	216	-0.64	0.54	-0.10	-1.19
46	212	-4.27	1.01	-3.26	-5.28
46	213	-0.92	0.56	-0.36	-1.48
46	214	0.52	0.45	0.96	0.07
46	215	-1.39	0.55	-0.83	-1.94
46	216	-4.27	0.80	-3.47	-5.07
47	212	-2.40	0.53	-1.87	-2.93
47	213	-1.08	0.49	-0.60	-1.57
47	214	-2.71	0.46	-2.25	-3.17
47	215	-4.55	0.44	-4.11	-4.99
48	211	-0.45	0.62	0.16	-1.07

26	27	28	29	30	31
48	212	-0.94	0.54	-0.40	-1.49
48	213	-3.43	0.63	-2.81	-4.06
48	214	-4.89	0.53	-4.36	-5.42
49	210	2.60	0.71	3.30	1.89
49	211	3.42	0.64	4.06	2.78
49	212	-1.33	1.01	-0.32	-2.34
49	213	-5.37	0.90	-4.46	-6.27
49	214	-6.21	1.13	-5.09	-7.34
50	209	-0.43	0.88	0.45	-1.32
50	210	2.56	0.66	3.21	1.90
50	211	1.27	1.65	2.91	-0.38
50	212	-4.97	1.58	-3.40	-6.55
50	213	-7.06	1.61	-5.44	-8.67
51	208	1.47	0.96	2.43	0.51
51	209	0.87	0.79	1.66	0.07
51	210	-1.14	1.48	0.34	-2.63
51	211	-6.15	2.09	-4.06	-8.24
51	212	-8.93	2.18	-6.76	-11.11
51	213	-10.26	1.96	-8.30	-12.23
52	207	6.83	1.19	8.02	5.65
52	208	3.15	1.42	4.57	1.73
52	209	-2.10	2.27	0.17	-4.37
52	210	-7.41	2.55	-4.86	-9.96
52	211	-8.46	2.58	-5.88	-11.04
52	212	-7.28	2.58	-4.70	-9.87
53	206	11.84	1.50	13.34	10.35
53	207	5.30	1.80	7.09	3.50
53	208	3.40	2.25	5.65	1.14
53	209	-2.93	3.01	0.08	-5.93
53	210	-9.55	3.45	-6.10	-13.00
53	211	-10.54	3.22	-7.32	-13.76
53	212	-12.53	2.57	-9.96	-15.10
54	205	-4.63	2.31	-2.32	-6.94
54	206	8.43	1.68	10.11	6.75
54	207	7.38	2.72	10.10	4.66
54	208	10.54	2.25	12.78	8.29
54	209	2.75	2.44	5.19	0.30
54	210	-8.77	3.39	-5.38	-12.16
54	211	-12.70	4.11	-8.60	-16.81
55	207	13.42	2.59	16.01	10.83
55	208	12.92	4.20	17.12	8.71
55	209	15.39	5.68	21.07	9.71
55	210	15.41	5.83	21.24	9.59
56	208	1.91	4.47	6.38	-2.55
56	209	-2.84	4.34	1.50	-7.18
56	210	49.11	7.33	56.45	41.78

TABLE 4, REV 1141, DIVERGENCE (X 10^5), SEC^{-1}

COLUMN	QUANTITY
32	Latitude
33	Longitude
34	$DIV_2\ \vec{W}_h$
35	Standard deviation
36	(34) + (35)
37	(34) - (35)

TABLE 4A, REV 1141, DIVERGENCE

32	33	34	35	36	37
34	220	-1.31	0.24	-1.07	-1.54
34	221	-1.46	0.26	-1.20	-1.72
34	222	-0.86	0.23	-0.62	-1.09
35	219	2.35	0.51	2.86	1.84
35	220	-0.28	0.32	0.05	-0.60
35	221	-1.46	0.28	-1.18	-1.73
35	222	-0.13	0.36	0.23	-0.50
36	219	1.45	0.43	1.88	1.02
36	220	-1.47	0.40	-1.07	-1.87
36	221	-0.77	0.35	-0.42	-1.12
37	218	0.31	0.45	0.76	-0.15
37	219	-2.49	0.40	-2.09	-2.89
37	220	-3.46	0.38	-3.08	-3.85
38	218	-0.80	0.33	-0.47	-1.12
38	219	-2.49	0.41	-2.08	-2.91
39	217	1.17	0.34	1.51	0.82
39	218	1.59	0.28	1.86	1.31
40	216	-0.14	0.40	0.25	-0.54
40	217	1.21	0.42	1.63	0.80
40	218	1.52	0.26	1.78	1.26
41	216	1.39	0.60	2.00	0.79
41	217	0.81	0.41	1.22	0.39
41	218	-0.22	0.56	0.35	-0.78
42	215	0.97	0.43	1.40	0.54
42	216	1.72	0.26	1.98	1.46
42	217	0.71	0.41	1.12	0.30
43	214	0.95	0.37	1.32	0.58
43	215	1.18	0.19	1.37	0.99
43	216	1.39	0.25	1.64	1.14
44	214	0.06	0.21	0.27	-0.16
44	215	0.67	0.23	0.90	0.44
44	216	1.09	0.23	1.33	0.86
45	213	-1.52	0.18	-1.34	-1.70
45	214	-0.34	0.17	-0.17	-0.51
45	215	0.66	0.21	0.86	0.45
45	216	0.40	0.22	0.62	0.18
46	212	-1.21	0.23	-0.99	-1.44
46	213	-0.19	0.16	-0.03	-0.35
46	214	0.64	0.14	0.79	0.50
46	215	1.12	0.16	1.28	0.96
46	216	0.33	0.24	0.57	0.09
47	212	-0.13	0.12	0.00	-0.25
47	213	0.99	0.12	1.12	0.87
47	214	1.28	0.13	1.41	1.15
47	215	1.21	0.12	1.34	1.09
48	211	-0.78	0.13	-0.66	-0.91

32	33	34	35	36	37
48	212	0.27	0.12	0.39	0.15
48	213	1.33	0.14	1.47	1.19
48	214	1.17	0.12	1.30	1.05
49	210	-1.83	0.13	-1.70	-1.96
49	211	-0.57	0.12	-0.46	-0.69
49	212	0.51	0.21	0.72	0.30
49	213	0.41	0.19	0.60	0.22
49	214	0.16	0.26	0.41	-0.10
50	209	-1.22	0.15	-1.07	-1.37
50	210	-0.20	0.13	-0.07	-0.33
50	211	0.41	0.34	0.75	0.07
50	212	0.72	0.34	1.06	0.39
50	213	-0.16	0.34	0.17	-0.50
51	208	-1.04	0.16	-0.88	-1.20
51	209	0.10	0.14	0.24	-0.04
51	210	1.45	0.27	1.72	1.17
51	211	1.16	0.43	1.59	0.72
51	212	0.19	0.46	0.65	-0.26
51	213	0.35	0.45	0.80	-0.10
52	207	-0.85	0.19	-0.66	-1.03
52	208	-0.40	0.24	-0.15	-0.64
52	209	0.13	0.39	0.52	-0.26
52	210	0.60	0.48	1.09	0.12
52	211	0.52	0.57	1.09	-0.06
52	212	0.03	0.59	0.61	-0.56
53	206	-1.40	0.28	-1.12	-1.68
53	207	-0.55	0.29	-0.26	-0.84
53	208	0.21	0.34	0.55	-0.14
53	209	-0.32	0.50	0.19	-0.82
53	210	-0.74	0.64	-0.09	-1.38
53	211	-0.98	0.70	-0.28	-1.68
53	212	-3.10	0.59	-2.51	-3.70
54	205	-2.65	0.28	-2.37	-2.93
54	206	-1.22	0.24	-0.99	-1.46
54	207	-1.71	0.50	-1.21	-2.21
54	208	-2.25	0.42	-1.83	-2.67
54	209	-2.71	0.59	-2.11	-3.30
54	210	-1.21	0.77	-0.44	-1.98
54	211	0.84	0.85	1.69	0.00
55	207	-6.67	0.54	-6.13	-7.21
55	208	-7.34	0.65	-6.69	-7.98
55	209	-4.80	1.03	-3.78	-5.83
55	210	-2.26	1.08	-1.17	-3.34
56	208	-6.34	0.91	-5.44	-7.25
56	209	-3.65	0.99	-2.67	-4.64
56	210	-2.49	1.19	-1.30	-3.69

TABLE 5A, REV 1183, VECTOR WINDS, COLUMNS AS IN TABLE 1.

1	2	3	4	5	6	7	8	9	10	11	12	13	14	15
33	201	13	159	0.4	5.8	0.0	0.0	4.0	3.6	-0.4	-0.06	-0.06	0.10	-0.03
33	202	16	143	2.2	4.2	0.1	-2.0	4.2	6.7	1.3	-0.26	-0.46	0.37	-0.31
33	203	14	86	4.5	3.6	0.0	-0.0	3.6	3.6	0.3	-0.41	0.01	-0.00	-1.11
33	204	18	62	2.5	5.9	0.0	0.1	4.9	5.9	0.3	-0.42	0.26	-0.21	-0.51
33	205	17	72	2.1	6.8	0.0	-0.0	6.3	5.0	-3.6	-0.32	0.15	-0.11	-0.43
33	211	11	69	1.6	13.6	-0.0	0.1	3.5	2.3	-1.9	-0.11	0.13	-0.04	-0.35
33	212	20	76	1.4	13.5	0.0	0.0	6.4	6.9	0.3	-0.09	0.06	-0.02	-0.28
33	213	20	82	1.4	13.5	-0.0	-0.0	5.7	6.4	-0.4	-0.10	0.03	-0.01	-0.25
33	214	20	84	1.4	13.1	-0.0	-0.0	6.1	6.9	1.6	-0.14	0.03	-0.01	-0.27
33	215	8	91	1.3	12.8	-0.0	-0.1	2.3	1.2	-0.9	-0.06	-0.00	0.00	-0.15
34	200	8	157	0.6	5.5	0.0	0.0	1.5	2.1	-0.3	-0.06	-0.12	0.09	-0.09
34	201	14	148	0.4	3.6	0.0	-0.0	3.5	4.6	1.2	-0.06	-0.09	0.09	-0.06
34	202	15	151	0.6	4.5	0.0	-0.0	4.5	4.4	-0.5	-0.11	-0.13	0.21	-0.07
34	203	16	146	2.6	4.6	-0.0	-0.0	5.9	4.0	0.1	-0.25	-0.50	0.37	-0.33
34	204	22	118	4.9	4.8	-0.0	0.0	5.5	7.3	-1.1	-0.25	-0.47	0.13	-0.92
34	205	13	112	5.4	7.2	0.0	0.0	3.9	4.4	-0.6	-0.07	-0.10	0.02	-0.40
34	211	19	70	1.5	13.2	-0.0	0.0	5.0	6.6	-0.5	-0.10	0.11	-0.04	-0.31
34	212	21	75	0.8	13.4	-0.0	0.0	6.9	6.6	-1.5	-0.07	0.03	-0.02	-0.12
34	213	21	73	1.4	13.5	-0.0	0.0	7.2	7.3	1.8	-0.04	0.04	-0.01	-0.12
34	214	16	76	2.0	12.9	-0.0	0.0	5.5	4.6	-1.9	-0.10	0.10	-0.02	-0.43
34	215	17	75	1.6	23.1	0.0	0.0	3.8	3.5	1.0	-0.03	0.01	-0.00	-0.13
35	200	9	154	0.7	4.7	0.0	0.0	2.8	2.8	-0.6	-0.10	-0.17	0.13	-0.13
35	201	15	145	0.4	3.5	0.0	0.1	4.9	4.6	0.2	-0.08	-0.09	0.12	-0.06
35	202	15	149	0.4	4.3	0.1	0.0	4.0	4.2	0.3	-0.07	-0.10	0.12	-0.06
35	203	19	150	0.8	5.4	0.0	0.0	6.4	6.5	-1.1	-0.10	-0.14	0.17	-0.08
35	204	14	147	1.3	7.0	-0.0	-0.1	5.2	3.0	-2.4	-0.11	-0.22	0.16	-0.15
35	210	15	76	5.4	11.1	0.0	0.1	5.9	2.9	-2.4	-0.70	0.22	-0.17	-0.87
35	211	21	71	1.0	13.0	-0.0	0.0	8.0	7.0	1.1	-0.12	0.07	-0.04	-0.21
35	212	14	71	1.1	13.4	-0.0	0.0	5.2	4.9	0.2	-0.08	0.07	-0.03	-0.22
35	213	20	66	1.2	13.5	0.0	0.0	6.5	5.8	-0.2	-0.05	0.05	-0.02	-0.12
35	214	9	70	1.9	13.2	-0.0	-0.0	3.3	1.2	-1.0	-0.05	0.08	-0.02	-0.23
36	199	12	148	0.8	4.9	0.1	0.0	1.9	3.9	-1.2	-0.13	-0.13	0.21	-0.08
36	200	14	141	0.6	3.6	0.0	0.0	4.6	2.5	-1.3	-0.13	-0.11	0.16	-0.09
36	201	17	139	0.5	3.0	-0.0	-0.0	5.1	5.4	0.3	-0.10	-0.08	0.12	-0.07
36	202	20	144	0.6	3.7	0.0	-0.0	5.6	7.3	-0.1	-0.12	-0.11	0.16	-0.08
36	203	19	142	1.1	5.1	-0.0	-0.0	4.6	6.1	-1.7	-0.17	-0.18	0.22	-0.14
36	204	10	156	1.5	13.3	0.0	0.0	3.0	3.3	0.1	-0.23	-0.24	0.25	-0.22
36	209	13	152	9.6	10.4	0.0	0.0	5.2	3.8	-1.9	-0.51	-1.51	0.43	-1.81
36	210	20	94	8.2	9.5	0.0	0.0	6.1	6.8	-0.6	-0.70	-0.13	0.05	-1.77
36	211	18	71	0.5	12.9	-0.0	0.0	5.6	6.1	-0.5	-0.09	0.03	-0.03	-0.08
36	212	20	67	1.5	13.4	0.0	0.0	6.4	6.2	0.5	-0.05	0.06	-0.02	-0.14
36	213	20	51	5.5	12.5	0.0	-0.1	5.9	5.6	-0.9	-0.35	0.48	-0.26	-0.64
36	214	17	21	6.3	23.5	0.0	0.0	3.1	3.5	0.4	-0.53	0.86	-0.45	-1.03
37	199	20	152	0.8	6.2	-0.1	0.0	6.1	5.2	0.8	-0.14	-0.16	0.28	-0.08
37	200	17	144	0.6	4.5	-0.0	-0.0	6.5	4.5	0.1	-0.20	-0.10	0.28	-0.07
37	201	17	138	0.5	3.3	0.0	0.0	5.7	6.3	1.0	-0.11	-0.07	0.12	-0.06
37	202	21	136	0.8	3.5	-0.0	0.0	7.6	6.7	0.5	-0.12	-0.12	0.12	-0.12
37	203	7	116	0.6	3.8	-0.1	-0.0	1.7	0.8	-1.0	-0.17	-0.08	0.09	-0.15
37	209	15	157	5.7	11.9	0.0	0.0	4.8	3.8	-1.9	-0.31	-0.86	0.76	-0.35
37	210	18	108	9.2	9.4	0.0	-0.0	5.5	5.9	1.3	-0.21	-0.65	0.08	-1.77
37	211	18	68	3.2	12.3	0.1	-0.0	4.8	6.0	-0.2	-0.43	0.19	-0.17	-0.48

TABLE 5B, REV 1183, VECTOR WINDS, COLUMNS AS IN TABLE 1.

1	2	3	4	5	6	7	8	9	10	11	12	13	14	15
37	212	22	43	8.2	12.5	-2.0	0.0	7.9	5.8	-1.9	-0.25	0.96	-0.28	-0.87
37	213	8	351	5.3	12.5	0.0	-0.1	1.9	1.4	-0.9	0.13	1.60	-0.92	0.23
38	199	11	160	1.1	6.1	-0.0	0.1	3.8	1.7	1.3	-0.08	-0.22	0.21	-0.08
38	200	19	152	0.9	5.8	0.0	0.0	6.5	6.8	0.8	-0.16	-0.16	0.31	-0.09
38	201	19	146	0.5	4.1	0.0	0.0	6.0	6.8	-2.0	-0.13	-0.11	0.20	-0.07
38	202	14	140	1.0	3.8	-0.0	-0.0	3.4	3.5	-1.7	-0.09	-0.14	0.10	-0.13
38	203	7	159	1.3	12.5	0.0	0.0	2.3	2.3	0.5	-0.13	-0.20	0.10	-0.25
38	208	12	171	0.7	20.9	0.0	0.0	3.9	3.1	-0.8	-0.03	-0.15	0.11	-0.04
38	209	18	160	0.7	12.9	0.0	0.0	5.6	5.6	-0.2	-0.03	-0.12	0.09	-0.04
38	210	19	126	8.6	6.6	0.0	0.0	6.2	7.0	-0.5	-1.06	-0.82	0.79	-1.11
38	211	18	25	9.8	7.3	-0.0	-0.0	6.3	6.5	0.2	-0.51	1.65	-1.06	-0.79
38	212	14	348	5.5	11.6	-0.0	0.0	2.8	4.1	-0.6	0.16	1.16	-0.85	0.21
38	213	8	339	1.4	40.7	0.0	0.0	1.8	2.5	0.7	0.05	0.41	-0.15	0.15
39	199	10	174	1.3	16.4	0.0	0.0	3.3	3.4	-0.2	-0.06	-0.31	0.26	-0.07
39	200	17	165	1.3	7.0	-0.0	-0.0	4.8	5.0	1.1	-0.07	-0.20	0.25	-0.05
39	201	17	153	1.1	4.6	-0.1	0.0	4.8	5.5	-0.9	-0.09	-0.16	0.17	-0.08
39	202	10	171	0.5	8.3	0.0	0.0	2.9	3.1	0.0	-0.28	-0.09	0.12	-0.06
39	208	16	163	0.9	11.8	0.0	0.0	5.0	5.1	-2.0	-0.04	-0.14	0.14	-0.04
39	209	16	171	5.7	11.0	-0.0	-0.0	5.4	4.0	-1.2	-0.14	-1.14	0.80	-0.20
39	210	17	218	10.1	7.8	0.0	-0.0	4.1	5.5	0.4	0.71	-1.43	0.91	1.12
39	211	18	307	10.0	8.2	0.0	0.0	4.3	5.3	0.4	0.67	0.96	-0.52	1.23
39	212	10	338	1.6	12.9	-0.0	-0.1	2.4	1.9	-1.1	0.26	0.43	-0.14	0.17
40	200	13	186	2.6	8.5	-0.0	0.0	4.5	1.5	0.7	0.04	-0.64	0.33	0.28
40	201	9	187	2.8	6.6	0.0	0.0	3.3	1.8	-2.3	0.05	-0.83	0.86	0.05
40	207	13	162	0.8	13.1	0.0	0.0	4.0	3.1	-1.8	-0.05	-0.12	0.18	-0.03
40	208	17	192	7.9	9.2	-0.0	0.0	5.4	5.6	2.1	0.08	-1.78	0.31	0.44
40	209	17	221	7.7	12.6	0.1	-0.0	5.3	5.6	0.0	0.39	-0.97	0.41	0.92
40	210	17	236	4.1	13.5	-0.0	-0.0	5.3	4.7	-1.1	0.35	-0.36	0.23	0.54
40	211	16	260	9.2	9.2	-0.1	-2.0	3.7	5.0	-1.7	1.30	-0.37	0.23	2.09
40	212	11	322	10.1	20.8	0.0	0.0	3.8	3.8	1.2	0.61	1.60	-0.45	2.16
41	206	11	185	5.3	15.2	0.0	0.0	3.7	3.9	-0.3	0.14	-1.30	0.30	0.59
41	207	14	201	5.9	7.1	0.0	-0.0	3.7	3.9	-0.2	0.11	-1.32	0.28	0.53
41	208	14	230	4.4	12.1	0.0	0.0	4.3	3.8	-1.0	0.43	-0.51	0.35	0.63
41	209	17	235	2.5	13.0	-0.0	0.0	4.9	5.6	0.7	0.14	-0.31	0.10	0.45
41	210	22	227	3.0	13.7	-0.1	0.1	8.5	6.7	0.2	0.07	-2.30	0.07	0.32
41	211	12	230	3.1	13.6	0.0	-0.0	4.1	1.3	-0.9	0.20	-0.56	0.17	0.68
42	206	11	237	2.2	5.0	0.0	0.0	4.0	1.6	-1.3	0.37	-0.25	0.24	0.39
42	207	19	233	2.0	7.7	0.1	-0.0	7.6	6.8	0.0	0.24	-0.18	0.17	0.26
42	208	21	228	1.9	9.7	0.1	-0.0	6.3	7.2	-1.4	0.18	-0.19	0.16	0.22
42	209	23	223	2.5	11.8	0.0	0.0	4.4	7.0	0.8	0.13	-0.28	0.14	0.26
42	210	24	218	2.6	13.2	0.1	-0.1	7.2	7.8	-2.0	0.07	-0.30	0.09	0.24
42	211	8	207	2.3	18.0	0.0	0.0	3.4	2.4	-1.8	0.09	-0.44	0.10	0.40
43	206	15	242	0.8	4.8	0.0	0.1	4.0	3.0	-0.3	0.35	-0.08	0.18	0.16
43	207	25	231	1.6	6.7	0.0	0.1	5.5	8.9	-0.7	0.16	-0.14	0.13	0.17
43	208	33	221	2.0	6.7	0.0	0.0	9.3	10.7	-1.2	0.14	-0.18	0.16	0.16
43	209	36	215	2.1	11.1	-0.1	-0.1	11.8	10.6	-1.9	0.10	-0.21	0.13	0.15
43	210	16	209	1.9	15.0	0.0	0.0	5.7	5.3	-3.2	0.13	-0.29	0.18	0.20
44	204	9	196	1.5	6.6	0.0	0.0	2.8	1.6	0.7	0.38	-0.20	0.25	0.31
44	205	14	241	1.3	3.0	0.0	0.0	3.4	7.1	-3.1	0.20	-0.11	0.18	0.22
44	206	18	238	1.2	3.3	0.0	0.0	5.4	2.9	0.0	0.20	-0.10	0.12	0.17

TABLE 5C, REV 1183, VECTOR WINDS, COLUMNS AS IN TABLE 1.

1	2	3	4	5	6	7	8	9	10	11	12	13	14	15
44	207	25	233	1.5	5.1	-0.1	0.0	7.5	8.5	-0.1	0.19	-0.13	0.14	0.17
44	208	33	220	2.3	7.6	-0.0	0.0	9.6	8.5	1.6	0.24	-0.30	0.28	0.25
44	209	24	211	1.7	10.9	0.0	-0.1	7.1	3.9	-0.9	0.11	-0.30	0.17	0.19
44	212	6	198	1.7	18.9	0.0	0.0	1.8	1.5	-0.9	0.14	-0.49	0.22	0.30
45	204	22	237	1.3	4.9	0.0	0.0	6.6	4.8	-3.2	0.31	-0.11	0.20	0.18
45	205	18	249	1.2	2.6	-0.0	-0.0	6.5	8.6	-1.1	0.23	-0.10	0.09	0.27
45	206	18	249	0.9	2.4	-0.0	0.1	7.5	2.8	1.5	0.13	-0.07	0.05	0.20
45	207	22	241	1.1	3.8	-0.1	-0.0	7.0	7.4	-2.2	0.20	-0.09	0.11	0.16
45	208	24	234	3.0	6.2	-0.1	0.1	6.3	7.1	0.9	0.32	-0.37	0.24	0.48
45	209	13	218	3.3	9.0	0.0	0.0	4.1	2.3	-2.6	0.25	-0.50	0.28	0.44
46	203	13	237	0.8	8.4	0.0	0.0	5.2	3.3	-3.7	0.26	-0.09	0.17	0.14
46	204	29	245	1.4	5.2	0.0	-0.0	10.1	7.9	1.2	0.25	-0.08	0.12	0.18
46	205	22	262	1.3	2.7	0.0	-0.1	6.1	6.6	1.5	0.18	-0.02	0.01	0.16
46	206	17	264	0.9	2.6	-0.1	0.0	5.8	5.5	-0.9	0.10	-0.01	0.01	0.13
46	207	13	246	1.1	3.6	-0.0	-0.0	5.7	3.4	0.2	0.22	-0.12	0.09	0.27
46	208	11	248	2.9	6.0	-0.1	-0.0	2.6	3.6	-1.5	0.65	-0.32	0.25	0.82
47	202	11	232	0.8	11.8	0.0	0.0	3.8	2.7	-2.7	0.26	-0.10	0.15	0.17
47	203	25	246	1.4	8.6	0.0	0.0	7.4	7.2	-2.1	0.23	-0.08	0.10	0.20
47	204	26	257	1.3	6.3	-0.0	0.1	8.1	6.8	3.0	0.21	-0.04	0.04	0.19
47	205	19	274	0.8	3.9	-0.0	-0.1	6.0	2.5	-1.7	0.36	0.01	-0.03	0.17
47	206	13	275	0.9	3.2	-0.0	-0.0	3.2	4.7	2.4	0.24	0.04	-0.04	0.24
47	207	12	253	1.9	3.6	0.0	0.0	2.2	2.9	-1.4	0.07	-0.05	0.02	0.20
47	208	7	217	1.9	8.6	0.0	0.0	3.0	2.4	-0.3	0.42	-0.20	0.19	0.46
48	201	12	230	0.5	14.1	0.0	0.0	2.9	3.0	-1.7	0.26	-0.04	0.03	0.09
48	202	33	247	0.8	12.9	0.1	0.0	8.8	8.9	-4.4	0.29	-0.04	0.04	0.09
48	203	30	254	1.2	9.3	0.1	-0.1	9.0	8.5	2.5	0.12	-0.04	0.03	0.14
48	204	29	260	1.1	7.4	0.0	0.0	10.2	10.1	-4.1	0.23	-0.03	0.04	0.16
48	205	19	266	0.9	4.9	-0.0	-0.1	5.5	4.3	1.7	0.38	-0.01	0.03	0.18
48	206	13	276	1.0	3.1	-0.0	0.0	4.1	2.8	-1.2	0.19	0.02	-0.02	0.19
48	207	11	0	1.8	4.0	0.0	0.0	3.9	3.0	0.6	0.10	-0.00	0.00	0.22
49	200	12	231	1.4	36.1	0.0	0.0	3.5	4.5	1.4	0.19	-0.15	0.12	0.23
49	201	27	244	1.6	12.0	0.0	0.1	7.2	8.0	-4.4	0.16	-0.13	0.08	0.28
49	202	41	252	1.0	11.2	-0.0	-0.0	15.1	12.4	-0.9	0.07	-0.03	0.02	0.10
49	203	39	258	1.6	9.9	-0.0	-0.1	13.6	11.3	2.6	0.10	-0.03	0.02	0.14
49	204	25	259	1.5	8.4	0.0	-0.0	7.6	8.4	-1.7	0.22	-0.04	0.04	0.21
49	205	21	260	1.6	6.0	-0.0	-0.0	6.0	6.4	1.4	0.34	-0.05	0.06	0.27
49	206	13	275	1.4	4.1	0.0	-0.1	3.2	3.0	-0.7	0.24	0.02	-0.02	0.26
50	200	22	229	2.2	12.8	0.1	0.1	7.7	5.8	-4.6	0.17	-0.21	0.15	0.24
50	201	37	242	1.7	12.9	0.0	-0.0	11.6	12.2	0.2	0.19	-0.10	0.05	0.19
50	202	37	252	1.4	11.9	0.0	-0.0	11.4	11.7	0.7	0.28	-0.04	0.03	0.12
50	203	36	253	2.1	10.7	-0.0	-0.1	12.3	12.7	-1.6	0.20	-0.09	0.06	0.30
50	204	30	251	2.4	9.0	0.0	-0.1	10.0	11.3	3.9	0.25	-0.14	0.09	0.42
50	205	24	251	2.5	6.8	0.0	-0.1	8.0	6.8	-3.0	0.28	-0.13	0.09	0.39
50	206	7	272	1.9	5.3	0.0	0.0	1.5	1.1	-1.0	0.31	0.01	-0.01	0.43
51	199	17	222	2.3	8.3	0.0	0.0	4.9	5.5	-4.5	0.63	-0.27	0.57	0.30
51	200	39	231	2.5	11.8	0.0	0.0	13.3	11.3	-2.2	0.23	-0.21	0.18	0.26
51	201	38	242	1.4	13.0	-0.0	-0.0	13.4	11.0	-1.0	0.07	-0.07	0.04	0.14
51	202	35	247	1.1	12.7	0.0	-0.0	12.0	9.9	-2.0	0.06	-0.04	0.02	0.10
51	203	34	241	1.9	11.7	-0.0	-0.0	12.0	11.9	1.0	0.18	-0.14	0.09	0.27
51	204	37	237	1.7	10.1	0.0	0.0	12.1	12.7	0.2	0.15	-0.12	0.10	0.18
51	205	18	239	2.2	8.4	0.0	0.0	6.1	3.4	-3.6	0.40	-0.23	0.21	0.44

TABLE 5D, REV 1183, VECTOR WINDS, COLUMNS AS IN TABLE 1.

1	2	3	4	5	6	7	8	9	10	11	12	13	14	15
52	198	13	246	1.4	4.5	0.0	0.0	4.2	3.5	-3.7	0.28	-0.10	0.10	0.27
52	199	30	231	2.2	6.3	0.0	0.0	11.9	11.2	-1.7	0.38	-0.22	0.30	0.29
52	200	38	236	2.4	12.6	-0.0	0.0	11.8	12.2	-3.2	0.34	-0.22	0.23	0.32
52	201	36	245	1.7	13.3	-0.0	0.0	12.4	10.6	1.3	0.09	-0.07	0.04	0.15
52	202	33	244	2.4	13.3	0.0	-0.0	10.9	10.1	-1.0	0.13	-0.14	0.06	0.29
52	203	32	237	2.3	12.6	0.0	0.1	10.0	11.8	-0.4	0.17	-0.21	0.11	0.33
52	204	36	238	2.8	11.0	-0.0	0.0	11.7	10.0	-1.6	0.29	-0.23	0.18	0.37
52	205	12	226	4.1	9.2	0.0	0.0	5.8	1.8	-2.0	0.38	-0.38	0.23	0.63
53	197	7	220	2.4	7.6	0.0	0.0	0.9	1.1	-0.9	0.41	-0.63	0.38	0.67
53	198	25	239	0.8	4.3	-0.0	0.1	6.5	6.1	1.4	0.20	-0.06	0.12	0.10
53	199	37	240	1.8	5.8	0.0	0.0	12.4	10.6	-0.3	0.35	-0.14	0.19	0.26
53	200	35	242	2.1	12.6	-0.0	-0.0	10.4	11.4	-1.1	0.45	-0.16	0.24	0.31
53	201	31	244	2.1	14.1	-2.0	-0.0	9.6	9.6	0.3	0.12	-0.10	0.06	0.21
53	202	31	242	2.9	14.2	0.0	0.0	9.5	11.3	1.2	0.11	-0.13	0.06	0.25
53	203	32	232	4.4	12.4	-0.0	0.0	9.0	9.6	-0.2	0.25	-0.31	0.19	0.41
53	204	21	230	5.8	12.0	-0.1	-0.0	4.8	6.3	-3.5	0.36	-0.54	0.29	0.66
54	198	9	242	2.0	2.8	0.0	0.0	3.6	2.8	2.3	0.45	-0.12	0.12	0.45
54	199	19	265	2.7	4.5	-0.1	0.0	2.1	6.7	0.3	0.44	-0.03	0.03	0.44
54	200	23	263	5.1	8.4	-0.1	-0.0	5.3	7.1	1.7	0.39	-0.07	0.05	0.59
54	201	23	249	5.7	12.7	-0.0	-0.0	6.1	6.1	-0.3	2.97	-0.31	0.36	0.83
54	202	27	224	7.3	12.7	-0.0	0.1	10.0	10.5	-0.3	0.50	-0.72	0.53	0.69
54	203	25	194	7.6	11.5	-0.2	-0.1	8.9	6.3	-3.6	0.09	-1.30	0.21	0.53
54	204	13	165	7.6	51.8	0.0	0.0	5.3	5.0	1.6	0.16	-1.66	0.31	0.82
55	201	6	343	7.0	1.3	0.0	0.0	-0.2	1.7	0.1	3.40	1.89	-2.98	2.15
55	202	13	162	6.2	8.9	-0.1	0.0	1.1	4.2	0.6	-2.49	-1.47	1.52	-0.47
55	203	6	160	0.7	19.9	0.0	0.0	1.4	1.3	-1.0	-0.02	-0.24	0.11	-0.05

16	17	18	19	20	21	22	23	24	25
33	201	159	0.0331	0.0014	0.0004	-0.0005	0.0004	0.0013	0.0001
33	202	143	0.0196	0.0034	0.0023	-0.0022	0.0018	0.0027	0.0013
33	203	86	0.0170	0.0028	0.0043	-0.0028	-0.0003	-0.0002	0.0043
33	204	62	0.0390	0.0257	0.0032	-0.0052	-0.0015	-0.0027	0.0028
33	205	70	0.0495	0.0051	0.0030	-0.0048	-0.0010	-0.0017	0.0028
33	211	69	0.2262	0.0254	0.0061	-0.0251	-0.0022	-0.0019	0.0057
33	212	76	0.2179	0.0041	0.0045	-0.0040	-0.0010	-0.0009	0.0044
33	213	82	0.2203	0.0046	0.0041	-0.0046	-0.0006	-0.0006	0.0040
33	214	84	0.2048	0.0057	0.0041	-0.0057	-0.0004	-0.0006	0.0041
33	215	91	0.1897	0.0023	0.0023	-0.0023	0.0000	0.0000	0.0023
34	200	157	0.0301	0.0012	0.0008	-0.0005	0.0007	0.0011	0.0003
34	201	146	0.0148	0.0007	0.0004	-0.0004	0.0004	0.0006	0.0002
34	202	151	0.0218	0.0022	0.0007	-0.0009	0.0006	0.0018	0.0003
34	203	146	0.0246	0.0040	0.0027	-0.0022	0.0022	0.0033	0.0015
34	204	116	0.0248	0.0025	0.0048	-0.0022	0.0023	0.0012	0.0042
34	205	112	0.0508	0.0011	0.0029	-0.0012	0.0011	0.0004	0.0026
34	211	72	0.2065	0.0045	0.0050	-0.0042	-0.0017	-0.0015	0.0047
34	212	75	0.2139	0.0032	0.0020	-0.0029	-0.0005	-0.0008	0.0019
34	213	73	0.2155	0.0017	0.0024	-0.0016	-0.0006	-0.0005	0.0019
34	214	76	0.1955	0.0041	0.0066	-0.0047	-0.0015	-0.0010	0.0064
34	215	75	0.8654	0.0044	0.0052	-0.0238	-0.0013	-0.0010	0.0050
35	200	154	0.0228	0.0014	0.0010	-0.0006	0.0009	0.0012	0.0004
35	201	145	0.0143	0.0009	0.0004	-0.0005	0.0003	0.0007	0.0002
35	202	149	0.0193	0.0011	0.0005	-0.0006	0.0004	0.0009	0.0002
35	203	150	0.0373	0.0021	0.0008	-0.0010	0.0007	0.0018	0.0004
35	204	147	0.0496	0.0029	0.0018	-0.0016	0.0015	0.0024	0.0010
35	210	76	0.1565	0.0237	0.0107	-0.0230	-0.0026	-0.0057	0.0104
35	211	71	0.2023	0.0052	0.0033	-0.0048	-0.0011	-0.0016	0.0032
35	212	71	0.2135	0.0035	0.0036	-0.0033	-0.0012	-0.0011	0.0034
35	213	66	0.2192	0.0023	0.0021	-0.0021	-0.0008	-0.0009	0.0020
35	214	70	0.2052	0.0022	0.0037	-0.0021	-0.0013	-0.0007	0.0035
36	199	148	0.0257	0.0023	0.0007	-0.0012	0.0006	0.0019	0.0004
36	200	141	0.0150	0.0014	0.0005	-0.0009	0.0004	0.0011	0.0003
36	201	139	0.0117	0.0009	0.0004	-0.0006	0.0003	0.0007	0.0002
36	202	144	0.0160	0.0014	0.0005	-0.0008	0.0004	0.0011	0.0003
36	203	142	0.0278	0.0028	0.0011	-0.0017	0.0009	0.0022	0.0007
36	204	156	0.2224	0.0149	0.0051	-0.0062	0.0047	0.0137	0.0020
36	209	152	0.1338	0.0196	0.0258	-0.0091	0.0228	0.0173	0.0120
36	210	94	0.1483	0.0177	0.0170	-0.0176	0.0014	0.0014	0.0170
36	211	71	0.1968	0.0037	0.0013	-0.0035	-0.0004	-0.0012	0.0012
36	212	67	0.2148	0.0022	0.0025	-0.0021	-0.0009	-0.0008	0.0023
36	213	51	0.1946	0.0173	0.0113	-0.0136	-0.0070	-0.0107	0.0089
36	214	21	1.0116	0.0851	0.0530	-0.0312	-0.0493	-0.0792	0.0194
37	199	152	0.0405	0.0040	0.0011	-0.0018	0.0010	0.0035	0.0005
37	200	144	0.0230	0.0030	0.0006	-0.0017	0.0005	0.0024	0.0003
37	201	138	0.0132	0.0010	0.0004	-0.0007	0.0003	0.0007	0.0002
37	202	136	0.0141	0.0011	0.0006	-0.0007	0.0005	0.0008	0.0004
37	203	116	0.0163	0.0013	0.0007	-0.0012	0.0003	0.0006	0.0006
37	209	157	0.1890	0.0306	0.0124	-0.0115	0.0114	0.0283	0.0046
37	210	198	0.0952	0.0053	0.0180	-0.0050	0.0057	0.0017	0.0170

16	17	18	19	20	21	22	23	24	25
37	211	68	0.1893	0.0176	0.0071	-0.0164	-0.0026	-0.0065	0.0066
37	212	43	0.1266	0.0108	0.0143	-0.0074	-0.0194	-0.0079	0.0098
37	213	351	0.2141	0.0377	0.0229	0.0053	-0.0226	-0.0373	-0.0032
38	199	160	0.0675	0.0042	0.0019	-0.0014	0.0017	0.0040	0.0006
38	200	152	0.0355	0.0040	0.0010	-0.0019	0.0009	0.0036	0.0005
38	201	146	0.0191	0.0018	0.0006	-0.0010	0.0005	0.0015	0.0003
38	202	140	0.0163	0.0009	0.0008	-0.0006	0.0006	0.0007	0.0005
38	203	159	0.1821	0.0063	0.0245	-0.0022	0.0043	0.0059	0.0016
38	208	171	0.6913	0.0114	0.0250	-0.0017	0.0049	0.0112	0.0008
38	209	160	0.1954	0.0039	0.0018	-0.0013	0.0017	0.0036	0.0006
38	210	126	0.0652	0.0215	0.0089	-0.0173	0.0053	0.0128	0.0072
38	211	25	0.0720	0.0229	0.0128	-0.0090	-0.0115	-0.0189	0.0055
38	212	348	0.1792	0.0310	0.0150	0.0062	-0.0147	-0.0303	-0.0030
38	213	339	4.3281	0.0522	0.0457	0.0183	-0.0428	-0.0489	-0.0160
39	199	174	0.3743	0.0169	0.0269	-0.0016	0.0069	0.0168	0.0007
39	200	165	0.0513	0.0042	0.0014	-0.0012	0.0013	0.0038	0.0003
39	201	153	0.0228	0.0017	0.0008	-0.0007	0.0007	0.0015	0.0004
39	202	171	0.0706	0.0028	0.0009	-0.0004	0.0009	0.0028	0.0001
39	208	163	0.1589	0.0052	0.0020	-0.0015	0.0019	0.0050	0.0006
39	209	171	0.1574	0.0266	0.0137	-0.0038	0.0136	0.0264	0.0020
39	210	218	0.0822	0.0228	0.0138	0.0141	0.0108	0.0179	-0.0085
39	211	307	0.0821	0.0171	0.0124	0.0135	-0.0076	-0.0105	-0.0098
39	212	335	0.1962	0.0062	0.0065	0.0023	-0.0064	-0.0057	-0.0026
40	200	186	0.0780	0.0065	0.0054	0.0008	0.0054	0.0068	-0.0006
40	201	187	0.0537	0.0128	0.0052	0.0016	0.0051	0.0127	-0.0007
40	207	162	0.2457	0.0077	0.0019	-0.0024	0.0018	0.0074	0.0006
40	208	192	0.0933	0.0075	0.0170	0.0015	0.0166	0.0073	-0.0037
40	209	221	0.1361	0.0169	0.0150	0.0112	0.0112	0.0126	-0.0100
40	210	236	0.2337	0.0189	0.0102	0.0157	0.0057	0.0105	-0.0085
40	211	262	0.1178	0.0334	0.0196	0.0329	0.0034	0.0058	-0.0193
40	212	322	1.4435	0.1186	0.1331	0.0719	-0.1056	-0.0943	-0.0806
41	206	185	0.3178	0.0183	0.0274	0.0017	0.0273	0.0179	-0.0026
41	207	201	0.0530	0.0248	0.0097	0.0017	0.0290	0.0044	-0.0035
41	208	230	0.1197	0.0152	0.0084	0.0116	0.0054	0.0097	-0.0064
41	209	235	0.2420	0.0070	0.0081	0.0257	0.0046	0.0040	-0.0067
41	210	227	0.2277	0.0043	0.0071	0.0032	0.0048	0.0029	-0.0052
41	211	232	0.2303	0.0117	0.0141	0.0090	0.0090	0.0074	-0.0109
42	206	237	0.0289	0.0043	0.0023	0.0037	0.0012	0.0024	-0.0019
42	207	233	0.0629	0.0053	0.0024	0.0043	0.0014	0.0031	-0.0019
42	208	226	0.1027	0.0062	0.0029	0.0047	0.0019	0.0041	-0.0022
42	209	223	0.1609	0.0069	0.0050	0.0047	0.0036	0.0050	-0.0034
42	210	216	0.2090	0.0246	0.0059	0.0029	0.0046	0.0036	-0.0037
42	211	207	0.4613	0.0094	0.0150	0.0043	0.0133	0.0084	-0.0069
43	206	242	0.0257	0.0036	0.0008	0.0032	0.0004	0.0017	-0.0007
43	207	231	0.0457	0.0030	0.0014	0.0023	0.0009	0.0019	-0.0011
43	208	221	0.0796	0.0044	0.0021	0.0029	0.0016	0.0033	-0.0014
43	209	215	0.1385	0.0053	0.0031	0.0031	0.0025	0.0043	-0.0018
43	210	209	0.2907	0.0114	0.0266	0.0056	0.0057	0.0099	-0.0032
44	204	196	0.0481	0.0065	0.0023	0.0018	0.0022	0.0062	-0.0006
44	205	241	0.0117	0.0012	0.0009	0.0011	0.0004	0.0006	-0.0007

16	17	18	19	20	21	22	23	24	25
44	206	238	0.0135	0.0014	0.0007	0.0012	0.0004	0.0007	-0.0006
44	207	233	0.0270	0.0023	0.0010	0.0018	0.0006	0.0013	-0.0008
44	208	220	0.0624	0.0064	0.0029	0.0042	0.0022	0.0048	-0.0019
44	209	211	0.1320	0.0063	0.0041	0.0033	0.0035	0.0053	-0.0021
44	210	198	0.5335	0.0207	0.0156	0.0265	0.0148	0.0197	-0.0049
45	204	237	0.0267	0.0035	0.0010	0.0029	0.0005	0.0018	-0.0029
45	205	249	0.0047	0.0012	0.0009	0.0011	0.0003	0.0004	-0.0009
45	206	249	0.0065	0.0007	0.0007	0.0006	0.0002	0.0002	-0.0006
45	207	241	0.0168	0.0015	0.0007	0.0014	0.0003	0.0007	-0.0006
45	208	234	0.0422	0.0052	0.0036	0.0043	0.0021	0.0030	-0.0029
45	209	218	0.1396	0.0099	0.0067	0.0062	0.0052	0.0077	-0.0042
46	203	237	0.0757	0.0063	0.0014	0.0053	0.0007	0.0034	-0.0011
46	204	245	0.0245	0.0028	0.0010	0.0025	0.0004	0.0011	-0.0009
46	205	262	0.0046	0.0005	0.0006	0.0005	0.0001	0.0001	-0.0005
46	206	264	0.0051	0.0005	0.0004	0.0005	0.0000	0.0002	-0.0004
46	207	246	0.0153	0.0015	0.0011	0.0014	0.0004	0.0006	-0.0010
46	208	248	0.0434	0.0090	0.0050	0.0084	0.0018	0.0032	-0.0047
47	202	232	0.1647	0.0106	0.0025	0.0084	0.0015	0.0065	-0.0020
47	203	246	0.0778	0.0052	0.0018	0.0047	0.0007	0.0020	-0.0016
47	204	257	0.0403	0.0027	0.0011	0.0027	0.0003	0.0006	-0.0011
47	205	274	0.0187	0.0026	0.0007	0.0026	0.0000	-0.0002	-0.0007
47	206	278	0.0128	0.0014	0.0009	0.0014	-0.0001	-0.0002	-0.0009
47	207	253	0.0156	0.0005	0.0008	0.0004	0.0002	0.0001	-0.0008
47	208	217	0.0837	0.0099	0.0043	0.0061	0.0034	0.0078	-0.0026
48	201	230	0.2436	0.0029	0.0017	0.0022	0.0011	0.0018	-0.0013
48	202	247	0.1309	0.0030	0.0011	0.0028	0.0004	0.0011	-0.0010
48	203	254	0.0925	0.0028	0.0014	0.0027	0.0004	0.0008	-0.0013
48	204	260	0.0568	0.0039	0.0011	0.0038	0.0002	0.0006	-0.0011
48	205	266	0.0269	0.0036	0.0009	0.0036	0.0001	0.0002	-0.0009
48	206	276	0.0124	0.0011	0.0007	0.0011	-0.0001	-0.0001	-0.0007
48	207	0	0.0174	0.0007	0.0009	0.0002	-0.0009	-0.0007	0.0000
49	200	201	3.1097	0.0587	0.0230	0.0211	0.0214	0.0548	-0.0083
49	201	244	0.1671	0.0064	0.0042	0.0057	0.0018	0.0027	-0.0038
49	202	252	0.1365	0.0025	0.0012	0.0023	0.0004	0.0007	-0.0012
49	203	258	0.1031	0.0026	0.0015	0.0025	0.0003	0.0005	-0.0015
49	204	259	0.0736	0.0045	0.0018	0.0044	0.0023	0.0008	-0.0018
49	205	260	0.0380	0.0042	0.0015	0.0041	0.0003	0.0007	-0.0015
49	206	275	0.0189	0.0018	0.0011	0.0018	-0.0001	-0.0002	-0.0011
50	200	229	0.1971	0.0092	0.0047	0.0072	0.0031	0.0060	-0.0036
50	201	242	0.1907	0.0047	0.0032	0.0042	0.0015	0.0021	-0.0028
50	202	252	0.1611	0.0029	0.0017	0.0027	0.0006	0.0010	-0.0016
50	203	253	0.1260	0.0061	0.0035	0.0059	0.0010	0.0018	-0.0034
50	204	251	0.0866	0.0060	0.0040	0.0057	0.0013	0.0019	-0.0037
50	205	251	0.0482	0.0043	0.0026	0.0041	0.0008	0.0013	-0.0025
50	206	272	0.0364	0.0032	0.0022	0.0032	-0.0001	-0.0001	-0.0022
51	199	222	0.0854	0.0177	0.0033	0.0119	0.0024	0.0131	-0.0022
51	200	231	0.1629	0.0102	0.0044	0.0079	0.0028	0.0064	-0.0034
51	201	242	0.1995	0.0234	0.0024	0.0030	0.0011	0.0015	-0.0021
51	202	247	0.1859	0.0223	0.0016	0.0022	0.0006	0.0009	-0.0015
51	203	241	0.1562	0.0069	0.0039	0.0061	0.0019	0.0032	-0.0035

TABLE 6D, REV 1183, VECTOR $\vec{u}_*^2$, COLUMNS AS IN TABLE 2.

16	17	18	19	20	21	22	23	24	25
51	204	237	0.1115	0.0248	0.0023	0.0041	0.0012	0.0026	-0.0019
51	205	239	0.0744	0.0093	0.0041	0.0087	0.0021	0.0047	-0.0035
52	196	246	0.0227	0.0025	0.0013	0.0023	0.0005	0.0010	-0.0012
52	199	231	0.0435	0.0064	0.0022	0.0050	0.0013	0.0040	-0.0017
52	202	236	0.1294	0.0119	0.0043	0.0099	0.0024	0.0066	-0.0036
52	201	245	0.2105	0.0044	0.0026	0.0042	0.0011	0.0018	-0.0024
52	202	244	0.2124	0.0064	0.0051	0.0057	0.0022	0.0028	-0.0046
52	203	237	0.1872	0.0079	0.0056	0.0067	0.0030	0.0042	-0.0047
52	204	238	0.1390	0.0107	0.0050	0.0091	0.0026	0.0056	-0.0043
52	205	226	0.0951	0.0104	0.0068	0.0076	0.0047	0.0071	-0.0049
53	197	222	0.0658	0.0099	0.0067	0.0064	0.0051	0.0075	-0.0044
53	198	234	0.0206	0.0018	0.0005	0.0016	0.0003	0.0009	-0.0000
53	199	240	0.2373	0.0048	0.0016	0.0042	0.0008	0.0023	-0.0014
53	200	242	0.1339	0.0152	0.0039	0.0135	0.0018	0.0070	-0.0034
53	201	244	0.2461	0.0064	0.0039	0.0058	0.0017	0.0028	-0.0035
53	202	242	0.2503	0.0058	0.0049	0.0052	0.0022	0.0026	-0.0043
53	203	232	0.1658	0.0119	0.0072	0.0095	0.0044	0.0072	-0.0057
53	204	230	0.1159	0.0126	0.0088	0.0098	0.0055	0.0079	-0.0068
54	198	242	0.0121	0.0025	0.0016	0.0023	0.0007	0.0012	-0.0014
54	199	265	0.0237	0.0038	0.0020	0.0038	0.0001	0.0003	-0.0020
54	202	263	0.0776	0.0079	0.0049	0.0079	0.0006	0.0009	-0.0048
54	201	249	0.1536	0.0327	0.0101	0.0307	0.0035	0.0114	-0.0094
54	202	224	0.1429	0.0224	0.0112	0.0157	0.0082	0.0160	-0.0079
54	203	194	0.1525	0.0277	0.0176	0.0022	0.0170	0.0075	-0.0045
54	204	165	8.6585	0.1857	0.3033	-0.0474	0.2933	0.1796	0.0775
55	201	343	0.0340	0.0305	0.0079	0.0088	-0.0075	-0.0292	-0.0023
55	202	162	0.1175	0.0395	0.0136	-0.0127	0.0130	0.0376	0.0041
55	203	163	0.6015	0.0100	0.0072	-0.0034	0.0068	0.0094	0.0025

26	27	28	29	30	31
33	203	-5.25	0.57	-4.68	-5.82
33	204	-4.43	0.51	-3.92	-4.95
33	212	-0.29	0.51	0.22	-0.80
33	213	3.11	0.50	3.61	2.61
33	214	3.82	0.62	4.44	3.20
34	201	1.20	0.13	1.32	1.07
34	202	-0.42	0.27	-0.16	-0.69
34	203	-2.31	0.25	-2.05	-2.56
34	204	-5.60	0.32	-5.28	-5.92
34	212	0.19	0.43	0.63	-0.24
34	213	4.29	0.39	4.68	3.90
35	201	0.23	0.10	0.33	0.13
35	202	-0.09	0.15	0.06	-0.24
35	203	-1.24	0.28	-0.96	-1.51
35	211	-3.96	1.61	-2.35	-5.57
35	212	0.86	0.42	1.28	0.44
35	213	3.89	0.98	4.87	2.92
36	200	0.53	0.19	0.72	0.35
36	201	0.12	0.11	0.23	0.01
36	202	-0.28	0.16	-0.12	-0.44
36	203	-4.41	0.55	-3.86	-4.95
36	210	-12.50	2.22	-10.28	-14.72
36	211	-6.05	1.40	-4.65	-7.44
36	212	3.58	1.41	5.00	2.17
36	213	-5.12	4.58	-0.54	-9.69
37	200	-0.38	0.27	-0.11	-0.64
37	201	-0.11	0.17	0.06	-0.28
37	202	-0.38	0.13	-0.24	-0.51
37	210	-9.00	1.88	-7.13	-10.88
37	211	0.34	1.56	1.90	-1.21
37	212	19.64	2.65	22.28	16.99
38	200	-0.82	0.31	-0.51	-1.13
38	201	-0.12	0.19	0.07	-0.31
38	202	-7.04	0.39	-6.65	-7.43
38	209	5.09	2.56	7.65	2.53
38	210	0.62	1.61	2.23	-0.99
38	211	5.10	2.01	7.12	3.09
39	200	-0.70	0.68	-0.03	-1.38
39	201	-1.94	0.73	-1.20	-2.67
39	209	11.87	1.69	13.56	10.18
39	210	1.32	1.90	3.22	-0.59
39	211	-3.26	2.34	-0.92	-5.61
40	208	15.77	1.43	17.19	14.34
40	209	15.27	2.35	17.62	12.91
40	210	-2.94	2.91	-0.03	-5.85
40	211	38.91	9.54	48.45	29.37
41	207	13.78	2.30	16.08	11.48
41	208	12.42	1.01	13.42	11.41
41	209	5.00	1.32	6.33	3.68

26	27	28	29	30	31
41	210	-2.75	1.29	0.54	-2.05
42	207	5.27	0.56	5.83	4.71
42	208	5.58	0.81	6.39	4.76
42	209	4.39	0.67	5.36	3.72
42	210	2.47	1.31	3.78	1.15
43	207	3.51	0.41	3.92	3.10
43	208	4.73	0.53	5.26	4.20
43	209	7.41	0.80	8.21	6.61
44	206	1.41	0.20	1.62	1.21
44	207	3.47	0.40	3.88	3.07
44	208	5.78	0.53	6.30	5.25
44	209	11.64	1.45	13.09	10.19
45	205	-0.91	0.25	-0.67	-1.16
45	206	0.81	0.15	0.96	0.65
45	207	2.67	0.40	3.07	2.27
45	208	6.12	0.82	6.94	5.30
46	204	-4.07	0.46	-3.61	-4.52
46	205	-1.10	0.22	-0.88	-1.32
46	206	0.65	0.14	0.79	0.50
46	207	2.76	0.70	3.46	2.06
47	203	-6.55	0.77	-5.77	-7.32
47	204	-4.20	0.46	-3.74	-4.66
47	205	-2.23	0.26	-1.97	-2.49
47	206	-0.18	0.22	0.05	-0.40
47	207	4.51	0.59	5.10	3.92
48	202	-4.97	0.49	-4.48	-5.46
48	203	-4.85	0.43	-4.42	-5.28
48	204	-5.28	0.41	-4.87	-5.69
48	205	-4.11	0.36	-3.75	-4.47
48	206	-2.27	0.32	-1.95	-2.60
49	202	-4.41	0.58	-3.83	-4.99
49	203	-5.54	0.52	-5.02	-6.05
49	204	-6.48	0.52	-5.96	-7.00
49	205	-5.32	0.46	-4.86	-5.78
50	201	-2.69	0.75	0.06	-1.44
50	202	-6.25	0.67	-5.58	-6.91
50	203	-9.06	0.66	-8.40	-9.72
50	204	-9.14	0.67	-8.46	-9.81
50	205	-6.36	0.70	-5.66	-7.06
51	200	14.13	1.26	15.39	12.87
51	201	4.28	0.81	5.09	3.47
51	202	-5.54	0.75	-4.78	-6.29
51	203	-10.30	0.63	-9.67	-10.93
51	204	-8.63	1.05	-7.58	-9.68
52	199	10.53	1.22	11.74	9.31
52	200	16.87	0.85	17.72	16.02
52	201	7.09	1.13	8.22	5.96
52	202	-5.11	0.86	-4.25	-5.97
52	203	-8.59	1.21	-7.38	-9.80
52	204	-8.71	1.28	-7.43	-9.98
53	198	-2.74	0.87	0.14	-1.61
53	199	10.93	1.31	12.24	9.62
53	200	21.43	0.87	22.30	20.55
53	201	11.89	1.70	13.59	10.19
53	202	-7.23	1.58	-5.65	-8.81
53	203	-14.82	1.32	-13.50	-16.14
54	201	10.11	2.49	12.59	7.62
54	202	-9.63	4.00	-5.63	-13.64

TABLE 8A, REV 1183, DIVERGENCE, COLUMNS AS IN TABLE 4.

32	33	34	34	36	37
34	202	-0.25	0.35	0.10	-0.61
34	203	0.97	0.56	1.53	0.40
34	204	1.63	0.37	2.00	1.26
34	212	-0.81	0.14	-0.67	-0.95
34	213	-1.32	0.12	-1.20	-1.43
35	201	-0.44	0.15	-0.29	-0.59
35	202	-0.83	0.17	-0.65	-1.00
35	203	-0.92	0.30	-0.62	-1.22
35	211	-0.83	0.43	-0.39	-1.26
35	212	-0.78	0.12	-0.66	-0.90
35	213	-1.43	0.33	-1.10	-1.75
36	200	0.89	0.20	1.08	0.69
36	201	-0.19	0.16	-0.04	-0.35
36	202	-1.20	0.19	-1.01	-1.39
36	203	-3.15	0.24	-2.91	-3.39
36	210	-1.59	1.26	-0.33	-2.84
36	211	-1.82	0.47	-1.35	-2.29
36	212	-0.07	0.54	0.47	-0.60
36	213	-0.93	0.71	-0.22	-1.64
37	200	1.40	0.21	1.61	1.19
37	201	0.61	0.19	0.81	0.42
37	202	-0.84	0.17	-0.67	-1.01
37	210	-2.50	1.16	-1.34	-3.66
37	211	-0.11	0.90	0.80	-1.01
37	212	4.69	1.02	5.72	3.67
38	200	1.66	0.24	1.89	1.42
38	201	0.83	0.19	1.02	0.64
38	202	-1.27	0.19	-1.08	-1.47
38	209	-1.51	0.94	-0.58	-2.45
38	210	2.04	1.43	3.47	0.62
38	211	4.21	1.20	5.42	3.01
39	200	1.14	0.29	1.43	0.85
39	201	1.14	0.42	1.56	0.72
39	209	2.74	1.03	3.78	1.71
39	210	6.13	1.16	7.29	4.97
39	211	3.70	1.48	5.18	2.23
40	208	4.24	0.70	4.94	3.54
40	209	3.73	1.17	4.90	2.57
40	210	2.45	1.20	3.66	1.25
41	207	1.13	0.89	2.02	0.25
41	208	3.59	0.86	4.46	2.73
41	209	1.63	0.64	2.27	0.99
41	210	0.99	0.50	1.49	0.49
42	207	0.67	0.43	1.09	0.24
42	208	1.08	0.43	1.51	0.65

32	33	34	35	36	37
42	209	1.15	0.33	1.49	0.82
42	210	0.52	0.38	0.90	0.14
43	207	0.18	0.31	0.49	-0.14
43	208	0.39	0.29	0.67	0.10
43	209	0.97	0.30	1.27	0.67
44	206	0.27	0.25	0.52	0.03
44	207	0.25	0.31	0.56	-0.05
44	208	-0.41	0.36	-0.05	-0.77
44	209	-0.61	0.47	-0.14	-1.08
45	205	-1.62	0.27	-1.35	-1.88
45	206	-0.06	0.24	0.17	-0.30
45	207	1.05	0.36	1.41	0.69
45	208	0.12	0.57	0.69	-0.45
46	204	-3.43	0.24	-3.18	-3.67
46	205	-1.91	0.24	-1.67	-2.15
46	206	-0.21	0.22	0.01	-0.44
46	207	1.62	0.53	2.15	1.09
47	203	-3.06	0.26	-2.80	-3.32
47	204	-3.06	0.31	-2.75	-3.37
47	205	-1.99	0.24	-1.75	-2.23
47	206	-0.45	0.29	-0.15	-0.74
47	207	0.68	0.39	1.06	0.29
48	202	-2.48	0.15	-2.33	-2.62
48	203	-2.57	0.21	-2.37	-2.78
48	204	-2.71	0.30	-2.41	-3.01
48	205	-2.25	0.25	-2.00	-2.51
48	206	-0.52	0.31	-0.21	-0.83
49	201	-1.52	0.20	-1.32	-1.72
49	202	-0.89	0.17	-0.72	-1.06
49	203	-1.44	0.22	-1.22	-1.67
49	204	-1.88	0.32	-1.56	-2.20
49	205	-2.09	0.30	-1.79	-2.38
50	201	1.33	0.24	1.57	1.09
50	202	-0.23	0.19	-0.04	-0.42
50	203	-0.38	0.26	-0.12	-0.64
50	204	-0.88	0.30	-0.58	-1.18
50	205	-1.06	0.39	-0.67	-1.45
51	200	3.03	0.54	3.57	2.49
51	201	1.53	0.26	1.79	1.28
51	202	-0.21	0.23	0.02	-0.44
51	203	-0.74	0.25	-0.48	-0.99
51	204	-1.00	0.46	-0.54	-1.46
52	199	2.25	0.49	2.73	1.76
52	200	3.99	0.41	4.40	3.59
52	201	2.25	0.35	2.60	1.90
52	202	-0.49	0.25	-0.24	-0.74
52	203	-1.14	0.39	-0.76	-1.53
52	204	-2.74	0.55	-2.19	-3.29
53	198	-0.61	0.67	0.06	-1.29
53	199	2.62	0.48	3.09	2.14
53	200	3.40	0.44	3.84	2.96
53	201	1.49	0.56	2.05	0.92
53	202	-1.43	0.52	-0.91	-1.95
53	203	-2.47	0.58	-1.89	-3.05
54	201	-4.25	1.81	-2.44	-6.07
54	202	-3.95	1.46	-2.50	-5.41

TABLE 9A, REV 1212, VECTOR WINDS,COLUMNS AS IN TABLE 1.

1	2	3	4	5	6	7	8	9	10	11	12	13	14	15
36	234	5	19	1.7	14.6	0.0	0.0	0.9	0.8	-0.2	-0.05	-0.67	-0.22	0.16
37	234	27	9	1.6	13.0	0.1	0.1	8.1	6.5	-3.6	-0.03	-0.25	-0.17	0.04
37	235	18	4	1.9	11.9	0.0	-0.1	5.7	4.8	4.6	-0.04	-0.45	-0.53	0.04
38	233	13	13	1.5	12.3	0.0	0.0	3.7	2.3	-2.1	-0.03	-0.37	-0.16	0.08
38	234	35	8	1.6	12.4	0.0	0.0	10.3	10.3	2.2	-0.02	-0.26	-0.12	0.04
38	235	29	2	1.9	11.3	0.0	-0.1	8.7	5.5	-2.2	-0.01	-0.32	-0.25	0.01
39	233	26	9	1.4	12.1	0.1	0.0	9.6	8.4	-5.7	-0.02	-0.23	-0.14	0.04
39	234	35	8	1.7	12.4	-0.0	0.1	11.6	11.2	-0.9	-0.02	-0.29	-0.13	0.04
39	235	15	1	2.2	11.8	0.0	0.0	5.2	4.0	-2.8	-0.02	-0.49	-0.30	0.03
40	232	19	21	3.7	9.1	0.0	0.0	5.2	4.1	-3.6	-0.17	-0.63	-0.45	0.23
40	233	34	8	2.0	11.1	0.0	-0.0	9.6	12.4	-0.7	-0.03	-0.29	-0.19	0.04
40	234	34	8	1.9	11.8	-0.0	0.0	10.7	10.3	1.2	-0.02	-0.30	-0.13	0.04
40	235	9	9	2.7	11.8	0.0	0.0	3.8	0.4	0.0	-0.05	-0.80	-0.36	0.11
41	232	34	41	2.5	6.7	0.1	0.0	8.5	10.1	-0.8	-0.30	-0.32	-0.35	0.28
41	233	35	22	3.2	9.1	0.0	0.0	11.5	11.1	-1.6	-0.11	-0.41	-0.26	0.16
41	234	36	17	2.7	10.7	0.0	0.0	13.5	10.5	-1.3	-0.06.	-0.36	-0.21	0.11
41	235	10	18	2.1	11.0	0.0	0.0	1.4	1.0	-0.4	-0.07	-0.57	-0.22	0.17
42	231	11	65	1.3	0.9	0.0	0.1	5.4	3.5	-1.7	-0.84	-0.14	-0.37	0.32
42	232	32	56	1.1	4.0	0.0	0.0	11.0	10.4	4.5	-0.26	-0.09	-0.20	0.12
42	233	38	39	2.0	6.7	-0.0	-0.0	13.9	11.0	0.7	-0.22	-0.22	-0.26	0.19
42	234	36	31	2.6	9.6	-0.0	-0.0	11.3	10.9	-0.8	-0.15	-0.26	-0.25	0.16
42	235	9	31	2.9	12.3	0.0	0.0	3.6	1.0	-0.1	-0.16	-0.67	-0.25	0.41
43	230	9	231	1.1	3.5	0.0	0.0	1.5	1.0	-0.7	0.36	0.18	0.34	-0.19
43	231	14	227	1.3	1.3	0.1	0.0	4.3	6.7	-0.3	0.26	0.17	0.25	-0.18
43	232	14	73	1.0	1.0	-0.1	0.0	5.4	3.2	-0.9	-0.49	-0.08	-0.19	0.21
43	233	15	54	0.8	3.2	-0.1	-0.0	2.8	5.2	1.7	-0.30	-0.10	-0.22	0.13
43	234	19	43	1.6	6.7	-0.1	0.0	2.9	4.9	-0.1	-0.37	-0.18	-0.39	0.17
44	229	11	210	1.5	8.8	0.0	0.0	4.5	3.3	-2.4	0.27	0.24	0.44	-0.14
44	230	34	217	1.4	6.5	0.1	0.1	9.5	9.5	-1.9	0.16	0.13	0.22	-0.10
44	231	26	214	1.8	3.7	0.1	-0.0	6.9	8.4	4.3	0.15	0.21	0.23	-0.14
44	232	9	233	1.8	1.4	0.0	0.0	2.3	2.8	1.4	0.18	0.43	0.24	-0.33
44	233	10	121	2.7	0.5	-0.0	0.0	4.1	4.0	-2.8	-0.33	0.29	0.20	0.47
45	229	25	207	1.5	11.0	0.0	0.1	9.1	6.3	-4.6	0.19	0.26	0.37	-0.13
45	230	34	209	2.2	9.0	-0.0	0.0	11.2	12.0	1.9	0.12	0.33	0.21	-0.19
45	231	36	204	2.3	7.0	0.0	0.0	11.3	12.3	-0.0	0.13	0.31	0.31	-0.13
45	232	24	195	2.0	4.8	0.0	-0.1	7.5	6.2	2.3	0.12	0.37	0.44	-0.10
45	233	13	198	1.9	2.4	0.0	0.0	4.2	4.3	-0.4	0.16	0.43	0.53	-0.13
45	234	4	298	2.6	3.2	0.0	0.0	2.3	1.3	-0.8	0.73	0.56	0.34	-1.19
46	228	18	202	0.8	14.6	0.0	0.0	5.5	4.3	-3.6	0.07	0.11	0.16	-0.05

TABLE 9B, REV 1212, VECTOR WINDS, COLUMNS AS IN TABLE 1.

1	2	3	4	5	6	7	8	9	10	11	12	13	14	15
46	229	33	202	2.2	12.7	0.1	-0.0	9.1	10.4	0.1	0.11	0.35	0.26	-0.15
46	230	30	200	2.3	10.8	-0.0	0.0	7.7	9.9	-0.3	0.08	0.35	0.21	-0.13
46	231	35	198	1.8	9.7	0.0	0.0	10.3	13.0	1.2	0.06	0.23	0.17	-0.08
46	232	31	193	1.5	8.3	0.0	-0.0	10.0	9.6	1.9	0.05	0.16	0.21	-0.04
46	233	13	193	2.4	5.4	-0.0	-0.0	3.6	2.1	0.2	0.16	0.63	0.65	-0.15
47	227	14	200	1.3	15.5	0.0	0.0	4.2	3.9	-3.1	0.07	0.25	0.16	-0.11
47	228	38	209	2.6	15.2	0.0	0.0	12.1	10.4	-3.2	0.06	0.30	0.11	-0.17
47	229	38	202	3.1	14.0	0.0	0.0	12.6	12.8	0.7	0.09	0.45	0.21	-0.18
47	230	33	196	1.7	12.8	0.0	-0.1	9.9	9.4	-2.6	0.07	0.25	0.23	-0.07
47	231	29	199	1.3	11.4	-0.1	0.0	6.8	9.7	0.9	0.04	0.18	0.11	-0.06
47	232	30	196	1.8	10.3	-0.0	-0.0	8.7	8.8	-0.3	0.07	0.29	0.24	-0.09
47	233	8	184	2.9	7.8	0.0	0.0	2.8	1.1	-1.5	0.10	0.99	0.98	-0.11
48	226	10	239	5.0	10.8	0.0	0.0	1.8	2.5	-0.1	0.18	0.55	0.13	-0.77
48	227	27	220	4.4	13.1	0.0	0.1	5.9	7.4	-3.3	0.23	0.48	0.28	-0.40
48	228	38	211	4.0	14.7	0.0	-0.0	14.5	14.4	1.4	0.16	0.54	0.25	-0.34
48	229	32	201	3.6	15.0	0.0	0.0	12.5	9.3	0.3	0.06	0.54	0.16	-0.21
48	230	34	198	1.7	13.9	-0.0	0.0	12.2	11.1	2.2	0.06	0.21	0.18	-0.07
48	231	35	199	1.8	12.3	0.1	0.0	12.6	11.1	1.8	0.05	0.24	0.13	-0.08
48	232	26	193	3.1	11.1	0.0	-0.1	7.4	4.7	-0.9	0.04	0.54	0.19	-0.13
49	226	19	257	1.8	11.0	0.0	0.0	6.2	5.3	-3.5	0.07	0.04	0.01	-0.19
49	227	37	237	4.7	11.8	0.0	-0.0	12.3	14.3	-0.1	0.24	0.35	0.15	-0.56
49	228	36	210	5.4	14.0	0.0	-0.0	11.0	13.7	2.7	0.22	0.68	0.37	-0.41
49	229	28	196	3.2	15.8	0.1	0.0	6.3	8.4	-0.8	0.05	0.53	0.18	-0.16
50	225	13	260	1.8	12.7	0.0	0.0	3.0	2.8	-2.5	0.29	0.06	0.05	-0.33
50	226	35	260	1.4	11.3	0.0	-0.0	10.5	11.3	-2.7	0.12	0.02	0.02	-0.15
50	227	39	245	5.0	11.0	0.0	-0.0	14.7	14.1	-1.2	0.18	0.18	0.08	-0.39
50	228	35	207	7.1	13.1	-0.0	-0.0	11.5	9.9	1.7	0.24	0.87	0.47	-0.45
50	229	32	191	4.1	16.5	0.0	-0.0	10.5	10.9	0.7	0.06	0.63	0.33	-0.12
50	230	35	186	5.7	15.1	0.0	0.0	11.9	10.4	0.2	0.05	0.83	0.46	-0.09
50	231	15	173	4.1	14.1	0.0	0.0	4.3	2.6	-2.0	-0.04	0.85	0.64	0.06
51	224	13	253	1.2	15.2	0.0	0.0	4.7	3.7	-4.0	0.17	0.06	0.05	-0.21
51	225	33	255	1.3	13.7	0.0	0.0	11.0	9.7	-1.6	0.15	0.04	0.04	-0.15
51	226	36	255	1.6	11.9	-0.0	-0.0	10.9	10.3	-0.7	0.10	0.04	0.03	-0.15
51	227	33	230	7.1	9.0	-0.1	-0.1	8.8	12.1	-1.5	0.30	0.43	0.20	-0.63
51	228	23	185	6.8	12.6	-0.1	-0.0	4.4	7 9	-1.2	0.07	1.15	0.79	-0.10
51	229	20	178	7.6	17.0	-0.1	-0.0	3.4	6.7	2.4	-0.02	1.59	0.75	0.04
51	230	22	171	8.1	17.5	-0.1	-0.0	2.7	6.2	-0.3	-0.12	1.69	0.77	0.26
51	231	5	171	2.9	19.2	0.0	0.0	0.3	0.6	-0.3	-0.13	1.28	0.75	0.22
52	223	10	248	1.1	16.3	0.0	0.0	3.8	3.5	-3.3	0.13	0.07	0.05	-0.19
52	224	34	249	1.3	15.7	0.1	0.1	9.9	12.3	-1.6	0.13	0.08	0.05	-0.21

TABLE 9C, REV 1212, VECTOR WINDS, COLUMNS AS IN TABLE 1.

1	2	3	4	5	6	7	8	9	10	11	12	13	14	15
52	225	37	248	1.4	14.4	0.0	-0.0	11.2	12.0	-0.5	0.15	0.07	0.06	-0.19
52	226	34	233	6.3	10.6	-0.0	-0.0	10.9	9.9	-1.2	0.37	0.40	0.26	-0.58
52	227	15	171	5.4	10.8	-0.0	-0.1	5.7	5.4	-4.7	-0.13	1.11	0.80	0.17
53	222	7	244	1.5	16.8	0.0	0.0	0.9	0.6	-0.4	0.19	0.15	0.10	-0.30
53	223	23	245	1.4	16.5	0.0	0.0	6.5	7.4	-1.9	0.06	0.06	0.03	-0.13
53	224	30	244	1.4	16.1	-0.1	0.0	7.9	10.1	2.6	0.07	0.06	0.03	-0.13
53	225	33	239	2.9	14.8	-0.1	-0.0	9.3	11.8	-0.3	0.20	0.16	0.11	-0.28
53	226	18	204	8.9	10.9	-0.1	-0.0	4.9	5.5	-3.7	0.17	1.69	0.37	-0.78
54	221	13	244	1.8	15.5	0.0	0.0	4.6	4.8	-4.0	0.22	0.14	0.10	-0.29
54	222	29	241	1.8	15.6	0.1	0.1	7.2	9.4	-1.0	0.17	0.11	0.09	-0.20
54	223	28	243	2.0	15.9	0.0	-0.0	8.3	9.3	-0.1	0.11	0.10	0.06	-0.20
54	224	28	237	3.6	15.5	-0.0	0.1	9.8	6.8	-0.5	0.12	0.22	0.08	-0.33
54	225	23	226	4.2	15.1	-0.0	-0.1	6.2	6.1	-3.7	0.18	0.42	0.17	-0.44
54	226	10	239	6.5	18.7	0.0	0.0	3.0	3.6	1.8	0.50	1.20	0.54	-1.11
55	220	15	251	1.5	12.7	0.0	0.0	3.1	3.9	-3.0	0.33	0.09	0.11	-0.28
55	221	33	244	1.9	12.6	0.1	0.0	10.4	10.6	-1.4	0.24	0.10	0.11	-0.22
55	222	37	242	2.2	13.0	0.0	0.0	13.6	13.5	-1.1	0.24	0.12	0.12	-0.23
55	223	33	242	2.6	13.2	-0.0	0.0	10.2	10.2	0.4	0.27	0.15	0.14	-0.28
55	224	21	228	4.0	13.1	-0.0	0.0	5.0	6.2	-3.4	0.23	0.40	0.20	-0.44
56	219	15	252	1.2	11.6	0.0	0.0	5.2	5.7	-5.1	0.10	0.05	0.03	-0.17
56	220	31	252	1.5	11.0	0.0	0.0	7.6	11.2	-0.5	0.04	0.04	0.01	-0.11
56	221	32	248	2.4	11.4	0.1	0.0	10.0	10.7	-0.5	0.07	0.08	0.03	-0.19
56	222	35	239	4.3	10.4	-0.0	0.0	12.9	10.6	0.4	0.36	0.25	0.21	-0.43
56	223	28	231	6.0	9.2	-0.1	-0.1	7.2	7.9	-2.7	0.39	0.48	0.31	-0.60
57	218	17	251	1.2	12.4	0.0	0.1	5.0	3.7	-3.2	0.14	0.06	0.05	-0.18
57	219	31	247	4.1	10.2	-0.0	0.0	10.6	9.1	-2.2	0.60	0.21	0.25	-0.51
57	220	34	225	8.5	7.4	0.0	0.0	11.4	14.1	0.6	0.32	0.73	0.32	-0.73
57	221	30	211	9.4	7.5	0.0	-0.0	8.1	9.7	0.3	0.17	1.25	0.28	-0.74
57	222	22	177	8.8	8.1	-0.1	0.0	5.1	6.5	-2.8	0.05	1.80	0.41	-0.23
57	223	8	149	8.7	8.6	0.0	0.0	3.1	2.7	-1.7	0.11	2.92	0.66	-0.48
58	216	12	252	7.4	15.8	0.0	0.0	3.2	4.2	0.1	1.42	1.23	1.00	-1.74
58	217	17	233	7.9	9.1	-0.0	0.1	4.7	4.6	-2.8	0.84	0.79	0.63	-1.05
58	218	27	193	11.9	7.0	-0.0	0.0	8.5	7.8	-1.8	0.05	2.15	0.19	-0.53
58	219	30	186	10.2	7.1	0.0	0.0	10.3	9.1	-0.8	0.04	1.79	0.51	-0.13
58	220	26	161	6.3	9.0	-0.1	-0.1	8.1	7.8	-4.0	-0.25	0.89	0.73	0.30
58	221	11	147	1.7	12.9	0.0	0.0	0.6	3.9	-0.8	-0.10	0.36	0.19	0.20
59	218	5	132	2.0	16.1	0.0	0.0	0.3	1.7	0.1	-0.58	0.64	0.64	0.59
59	219	7	142	3.4	13.4	0.0	0.0	0.5	1.9	0.3	-0.39	1.12	0.73	0.60

TABLE 10A, REV 1212, VECTOR $\vec{u}_*^2$. COLUMNS AS IN TABLE 2.

16	17	18	19	20	21	22	23	24	25
36	234	19	0.2754	0.0113	0.0124	-0.0037	-0.0117	-0.0107	0.0041
37	234	9	0.2035	0.0069	0.0038	-0.0011	-0.0038	-0.0068	0.0006
37	235	4	0.1780	0.0196	0.0060	-0.0016	-0.0060	-0.0196	0.0005
38	233	13	0.1768	0.0061	0.0052	-0.0014	-0.0051	-0.0059	0.0012
38	234	8	0.1800	0.0046	0.0037	-0.0007	-0.0036	-0.0046	0.0005
38	235	2	0.1479	0.0083	0.0040	-0.0003	-0.0040	-0.0083	0.0002
39	233	9	0.1695	0.0051	0.0032	-0.0008	-0.0032	-0.0050	0.0005
39	234	8	0.1792	0.0049	0.0041	-0.0007	-0.0041	-0.0048	0.0006
39	235	1	0.1647	0.0104	0.0064	-0.0003	-0.0064	-0.0104	0.0002
40	232	21	0.0933	0.0111	0.0061	-0.0041	-0.0056	-0.0103	0.0022
40	233	8	0.1399	0.0061	0.0035	-0.0009	-0.0034	-0.0060	0.0005
40	234	8	0.1576	0.0045	0.0039	-0.0007	-0.0039	-0.0045	0.0006
40	235	9	0.1665	0.0128	0.0105	-0.0020	-0.0104	-0.0127	0.0016
41	232	41	0.0501	0.0068	0.0027	-0.0045	-0.0021	-0.0051	0.0018
41	233	22	0.0885	0.0064	0.0040	-0.0024	-0.0037	-0.0059	0.0015
41	234	17	0.1266	0.0064	0.0043	-0.0019	-0.0041	-0.0061	0.0012
41	235	18	0.1354	0.0071	0.0070	-0.0022	-0.0066	-0.0068	0.0022
42	231	65	0.0055	0.0032	0.0009	-0.0029	-0.0004	-0.0013	0.0008
42	232	56	0.0192	0.0025	0.0006	-0.0021	-0.0004	-0.0014	0.0005
42	233	39	0.0472	0.0048	0.0018	-0.0031	-0.0014	-0.0037	0.0012
42	234	31	0.0998	0.0071	0.0030	-0.0037	-0.0025	-0.0060	0.0016
42	235	31	0.1800	0.0111	0.0108	-0.0058	-0.0092	-0.0095	0.0056
43	230	231	0.0164	0.0033	0.0010	0.0026	0.0006	0.0021	-0.0008
43	231	227	0.0049	0.0013	0.0007	0.0010	0.0005	0.0009	-0.0005
43	232	73	0.0046	0.0018	0.0006	-0.0017	-0.0002	-0.0005	0.0006
43	233	54	0.0140	0.0022	0.0006	-0.0018	-0.0003	-0.0013	0.0005
43	234	43	0.0502	0.0078	0.0016	-0.0054	-0.0011	-0.0056	0.0011
44	229	210	0.0882	0.0114	0.0024	0.0057	0.0021	0.0098	-0.0012
44	230	217	0.0441	0.0037	0.0010	0.0022	0.0008	0.0029	-0.0006
44	231	214	0.0164	0.0018	0.0010	0.0010	0.0008	0.0015	-0.0006
44	232	233	0.0051	0.0011	0.0015	0.0009	0.0009	0.0007	-0.0012
44	233	121	0.0023	0.0011	0.0013	-0.0010	0.0007	0.0006	0.0012
45	229	207	0.1432	0.0133	0.0034	0.0061	0.0031	0.0118	-0.0016
45	230	209	0.0870	0.0055	0.0034	0.0027	0.0029	0.0048	-0.0017
45	231	204	0.0512	0.0051	0.0022	0.0021	0.0020	0.0047	-0.0009
45	232	195	0.0266	0.0043	0.0018	0.0011	0.0017	0.0041	-0.0005
45	233	198	0.0104	0.0027	0.0014	0.0009	0.0014	0.0026	-0.0005
45	234	298	0.0165	0.0051	0.0047	0.0045	-0.0022	-0.0024	-0.0042
46	228	202	0.2729	0.0089	0.0022	0.0034	0.0021	0.0082	-0.0009
46	229	202	0.1970	0.0112	0.0055	0.0044	0.0051	0.0103	-0.0022
46	230	200	0.1317	0.0067	0.0043	0.0023	0.0040	0.0062	-0.0015
46	231	198	0.1017	0.0046	0.0024	0.0014	0.0023	0.0043	-0.0008
46	232	193	0.0711	0.0042	0.0014	0.0010	0.0013	0.0041	-0.0003
46	233	193	0.0350	0.0074	0.0034	0.0017	0.0033	0.0072	-0.0008
47	227	200	0.3168	0.0098	0.0055	0.0035	0.0051	0.0091	-0.0020
47	228	209	0.2962	0.0070	0.0066	0.0035	0.0057	0.0061	-0.0033
47	229	202	0.2475	0.0109	0.0082	0.0042	0.0076	0.0101	-0.0031
47	230	196	0.1963	0.0095	0.0038	0.0026	0.0037	0.0091	-0.0010
47	231	199	0.1452	0.0040	0.0024	0.0013	0.0023	0.0038	-0.0008
47	232	196	0.1173	0.0070	0.0032	0.0020	0.0031	0.0067	-0.0009
47	233	184	0.0784	0.0190	0.0076	0.0013	0.0075	0.0190	-0.0005
48	226	239	0.1298	0.0068	0.0109	0.0058	0.0055	0.0035	-0.0094
48	227	220	0.2130	0.0151	0.0095	0.0098	0.0072	0.0115	-0.0061
48	228	211	0.2813	0.0154	0.0115	0.0081	0.0098	0.0131	-0.0060
48	229	201	0.2883	0.0091	0.0108	0.0034	0.0101	0.0085	-0.0040
48	230	198	0.2406	0.0086	0.0036	0.0027	0.0034	0.0081	-0.0012
48	231	199	0.1739	0.0051	0.0036	0.0017	0.0034	0.0048	-0.0012
48	232	193	0.1391	0.0061	0.0066	0.0014	0.0065	0.0059	-0.0015

TABLE 10B, REV 1212, VECTOR $\vec{u}_*^2$.   COLUMNS AS IN TABLE 2.

16	17	18	19	20	21	22	23	24	25
49	226	257	0.1313	0.0021	0.0023	0.0020	0.0005	0.0004	-0.0023
49	227	237	0.1636	0.0098	0.0085	0.0083	0.0045	0.0052	-0.0072
49	228	210	0.2573	0.0208	0.0134	0.0105	0.0116	0.0180	-0.0067
49	229	196	0.3314	0.0109	0.0112	0.0031	0.0107	0.0105	-0.0032
49	230	198	0.2618	0.0111	0.0050	0.0035	0.0048	0.0105	-0.0016
49	231	190	0.1831	0.0071	0.0064	0.0012	0.0063	0.0070	-0.0011
49	232	157	0.1897	0.0118	0.0124	-0.0046	0.0115	0.0108	0.0048
50	225	260	0.1953	0.0118	0.0048	0.0117	0.0008	0.0020	-0.0048
50	226	260	0.1429	0.0038	0.0019	0.0038	0.0003	0.0006	-0.0019
50	227	245	0.1345	0.0062	0.0050	0.0057	0.0021	0.0026	-0.0046
50	228	207	0.2237	0.0226	0.0150	0.0104	0.0133	0.0201	-0.0069
50	229	191	0.3792	0.0211	0.0139	0.0041	0.0137	0.0207	-0.0027
50	230	186	0.3131	0.0253	0.0158	0.0028	0.0157	0.0251	-0.0018
50	231	173	0.2709	0.0312	0.0144	-0.0034	0.0143	0.0310	0.0016
51	224	253	0.2999	0.0097	0.0041	0.0093	0.0012	0.0028	-0.0040
51	225	255	0.2323	0.0072	0.0026	0.0070	0.0007	0.0019	-0.0025
51	226	255	0.1598	0.0037	0.0021	0.0036	0.0005	0.0009	-0.0020
51	227	230	0.0882	0.0081	0.0069	0.0063	0.0044	0.0052	-0.0053
51	228	185	0.2117	0.0324	0.0165	0.0029	0.0165	0.0323	-0.0015
51	229	178	0.4420	0.0518	0.0365	-0.0012	0.0365	0.0517	0.0008
51	230	171	0.4791	0.0562	0.0412	-0.0087	0.0407	0.0555	0.0064
51	231	171	0.6008	0.0647	0.0364	-0.0100	0.0360	0.0639	0.0056
52	223	248	0.3591	0.0083	0.0043	0.0077	0.0016	0.0030	-0.0040
52	224	249	0.3238	0.0079	0.0045	0.0074	0.0016	0.0028	-0.0042
52	225	248	0.2607	0.0081	0.0036	0.0075	0.0013	0.0030	-0.0033
52	226	233	0.1312	0.0133	0.0079	0.0106	0.0047	0.0079	-0.0063
52	227	171	0.1505	0.0258	0.0129	-0.0040	0.0127	0.0255	0.0020
53	222	244	0.3905	0.0139	0.0076	0.0125	0.0033	0.0060	-0.0069
53	223	245	0.3649	0.0040	0.0032	0.0037	0.0013	0.0017	-0.0030
53	224	244	0.3422	0.0047	0.0030	0.0042	0.0013	0.0020	-0.0027
53	225	239	0.2847	0.0118	0.0060	0.0102	0.0030	0.0060	-0.0051
53	226	204	0.1407	0.0128	0.0218	0.0054	0.0198	0.0117	-0.0091
54	221	244	0.3192	0.0135	0.0063	0.0122	0.0027	0.0057	-0.0057
54	222	241	0.3204	0.0109	0.0044	0.0096	0.0021	0.0052	-0.0039
54	223	243	0.3354	0.0075	0.0046	0.0067	0.0021	0.0034	-0.0041
54	224	237	0.3143	0.0079	0.0078	0.0067	0.0042	0.0042	-0.0066
54	225	226	0.2977	0.0134	0.0115	0.0097	0.0080	0.0093	-0.0083
54	226	239	0.5627	0.0596	0.0440	0.0514	0.0223	0.0302	-0.0380
55	220	251	0.1995	0.0140	0.0042	0.0133	0.0013	0.0044	-0.0040
55	221	244	0.1915	0.0103	0.0034	0.0092	0.0015	0.0044	-0.0031
55	222	242	0.2076	0.0111	0.0039	0.0099	0.0018	0.0051	-0.0035
55	223	242	0.2157	0.0129	0.0049	0.0114	0.0023	0.0061	-0.0043
55	224	228	0.2127	0.0130	0.0090	0.0097	0.0060	0.0087	-0.0067
56	219	252	0.1500	0.0037	0.0022	0.0035	0.0007	0.0011	-0.0021
56	220	252	0.1314	0.0014	0.0014	0.0014	0.0004	0.0004	-0.0014
56	221	248	0.1432	0.0024	0.0025	0.0022	0.0009	0.0009	-0.0023
56	222	239	0.1261	0.0122	0.0054	0.0105	0.0027	0.0061	-0.0047
56	223	231	0.0958	0.0116	0.0070	0.0091	0.0044	0.0072	-0.0055
57	218	251	0.1806	0.0055	0.0026	0.0053	0.0008	0.0018	-0.0025
57	219	247	0.1269	0.0184	0.0058	0.0170	0.0023	0.0071	-0.0054
57	220	225	0.0609	0.0077	0.0074	0.0055	0.0052	0.0054	-0.0052
57	221	211	0.0590	0.0055	0.0104	0.0029	0.0089	0.0047	-0.0054
57	222	177	0.0709	0.0079	0.0142	-0.0004	0.0142	0.0079	0.0007
57	223	149	0.0883	0.0145	0.0253	-0.0074	0.0217	0.0125	0.0129
58	216	252	0.4310	0.1108	0.0432	0.1055	0.0132	0.0339	-0.0412
58	217	233	0.1087	0.0257	0.0119	0.0205	0.0072	0.0154	-0.0095
58	218	193	0.0501	0.0030	0.0149	0.0007	0.0145	0.0029	-0.0034
58	219	186	0.0556	0.0080	0.0121	0.0009	0.0120	0.0080	-0.0014
58	220	161	0.0980	0.0180	0.0084	-0.0057	0.0080	0.0170	0.0027
58	221	147	0.1997	0.0087	0.0061	-0.0047	0.0051	0.0073	0.0033
59	218	132	0.3917	0.0540	0.0182	-0.0398	0.0123	0.0365	0.0134
59	219	142	0.2471	0.0376	0.0199	-0.0229	0.0158	0.0299	0.0121

TABLE 11A, REV 1212, WIND STRESS CURL,   COLUMNS AS IN TABLE 3.

26	27	28	29	30	31
38	234	0.96	0.67	1.62	0.29
39	234	0.14	0.64	0.77	-0.50
40	233	-4.23	0.74	-3.49	-4.97
40	234	-3.88	0.93	-2.95	-4.81
41	233	-6.20	0.65	-5.55	-6.84
41	234	-4.82	0.76	-4.06	-5.58
42	232	-3.97	0.45	-3.52	-4.42
42	233	-6.96	0.51	-6.45	-7.47
42	234	-9.70	0.98	-8.71	-10.68
43	231	-2.20	0.27	-1.93	-2.48
43	232	-1.93	0.21	-1.72	-2.14
43	233	-4.46	0.50	-3.96	-4.96
44	230	-6.36	0.58	-5.77	-6.94
44	231	-4.19	0.35	-3.84	-4.54
44	232	-2.39	0.27	-2.11	-2.66
45	230	-8.37	0.72	-7.65	-9.08
45	231	-7.42	0.44	-6.98	-7.86
45	232	-5.05	0.36	-4.70	-5.41
45	233	-1.22	0.59	-0.62	-1.81
46	229	-10.18	1.03	-9.14	-11.21
46	230	-9.71	0.83	-8.88	-10.54
46	231	-7.28	0.53	-6.75	-7.80
46	232	-6.67	0.58	-6.08	-7.25
47	228	-0.36	1.33	0.97	-1.68
47	229	-11.99	1.05	-10.94	-13.05
47	230	-9.30	0.95	-8.35	-10.25
47	231	-5.16	0.61	-4.55	-5.77
47	232	-6.99	0.79	-6.20	-7.77
48	227	15.11	1.51	16.62	13.60
48	228	-0.21	1.81	1.60	-2.02

TABLE 11B, REV 1212, WIND STRESS CURL, COLUMNS AS IN TABLE 3.

26	27	28	29	30	31
48	229	-10.36	1.42	-8.94	-11.78
48	230	-6.94	1.24	-5.71	-8.18
48	231	-5.89	0.81	-5.08	-6.70
49	227	6.29	1.55	7.84	4.74
49	228	-1.05	1.92	0.87	-2.97
49	229	-9.21	1.92	-7.29	-11.13
49	230	-9.38	1.85	-7.53	-11.24
49	231	-18.83	2.13	-16.70	-20.95
50	226	-6.73	1.17	-5.56	-7.90
50	227	-1.47	1.63	0.15	-3.10
50	228	-3.17	2.49	-0.68	-5.66
50	229	-12.06	3.60	-8.46	-15.66
50	230	-20.95	3.68	-17.27	-24.64
51	225	-15.22	0.96	-14.26	-16.17
51	226	-17.00	1.15	-15.85	-18.14
51	227	-17.27	2.11	-15.16	-19.38
52	224	-11.57	1.04	-10.53	-12.61
52	225	-22.53	1.38	-21.16	-23.91
52	226	-29.03	1.71	-27.32	-30.74
53	223	-4.82	1.34	-3.48	-6.17
53	224	-10.77	1.22	-9.55	-11.99
53	225	-29.15	2.14	-27.01	-31.29
54	222	5.64	1.47	7.11	4.17
54	223	1.69	1.30	3.00	0.39
54	224	-7.28	1.56	-5.72	-8.84
55	221	4.40	1.68	6.09	2.72
55	222	7.08	1.57	8.66	5.51
55	223	2.85	1.62	4.47	1.23
56	220	0.23	0.71	0.94	-0.49
56	221	0.35	1.24	1.59	-0.88
56	222	-4.27	1.17	-3.10	-5.45
57	219	-13.60	1.07	-12.53	-14.66
57	220	-11.74	2.24	-9.50	-13.98
57	221	-11.15	1.73	-9.42	-12.88
58	218	-20.02	3.51	-16.51	-23.53

TABLE 12, REV 1212, DIVERGENCE, COLUMNS AS IN TABLE 4.

32	33	34	35	36	37
38	234	1.82	0.30	2.12	1.52
39	234	1.41	0.32	1.74	1.09
40	233	2.68	0.45	3.13	2.24
40	234	0.93	0.52	1.44	0.41
41	233	3.55	0.38	3.93	3.17
41	234	1.73	0.45	2.18	1.28
42	232	0.09	0.60	0.69	-0.51
42	233	2.03	0.31	2.34	1.72
42	234	1.27	0.50	1.78	0.77
43	231	-0.74	0.47	-0.28	-1.21
43	232	-0.83	0.35	-0.48	-1.17
43	233	0.21	0.48	0.69	-0.27
44	230	1.02	0.35	1.37	0.67
44	231	0.66	0.38	1.04	0.28
44	232	0.65	0.40	1.05	0.26
45	230	0.71	0.33	1.04	0.38
45	231	0.65	0.36	1.01	0.28
45	232	1.86	0.42	2.28	1.44
45	233	3.19	0.74	3.93	2.45
46	229	0.02	0.33	0.35	-0.31
46	230	0.60	0.33	0.92	0.27
46	231	0.62	0.30	0.93	0.32
46	232	1.04	0.51	1.54	0.53
47	228	-0.81	0.41	-0.41	-1.22
47	229	-1.86	0.32	-1.54	-2.18
47	230	0.12	0.36	0.48	-0.24
47	231	0.51	0.28	0.79	0.23
47	232	-1.02	0.68	-0.34	-1.71
48	227	-4.93	0.61	-4.32	-5.54
48	228	-2.70	0.58	-2.12	-3.28
48	229	-1.46	0.44	-1.02	-1.89
48	230	-0.58	0.43	-0.16	-1.01
48	231	-0.83	0.41	-0.42	-1.23
49	227	-5.08	0.57	-4.51	-5.65
49	228	-4.39	0.58	-3.81	-4.97
49	229	-1.03	0.56	-0.46	-1.59
49	230	-0.97	0.53	-0.44	-1.49
49	231	-5.52	0.70	-4.83	-6.22
50	226	-1.51	0.30	-1.22	-1.81
50	227	-3.93	0.75	-3.18	-4.68
50	228	-4.79	0.65	-4.15	-5.44
50	229	-2.52	0.93	-1.59	-3.44
50	230	-1.94	0.83	-1.11	-2.77
51	225	-0.81	0.23	-0.58	-1.04
51	226	-2.59	0.49	-2.10	-3.08
51	227	-4.75	0.93	-3.82	-5.68
52	224	-0.32	0.20	-0.12	-0.52
52	225	-2.89	0.44	-2.45	-3.33
52	226	-7.98	0.91	-7.07	-8.89
53	223	-0.04	0.23	0.20	-0.27
53	224	-0.54	0.27	-0.27	-0.81
53	225	-5.29	1.30	-3.99	-6.58
54	222	-0.60	0.29	-0.31	-0.89
54	223	-0.87	0.29	-0.58	-1.15
54	224	-1.92	0.43	-1.49	-2.36
55	221	-1.56	0.38	-1.18	-1.93
55	222	-0.92	0.39	-0.52	-1.31
55	223	-2.21	0.52	-1.69	-2.73
56	220	0.10	0.40	0.50	-0.30
56	221	-0.88	0.52	-0.36	-1.39
56	222	-1.91	0.56	-1.35	-2.46
57	219	-3.88	0.72	-3.17	-4.60
57	220	-2.40	1.22	-1.17	-3.62
57	221	-1.90	1.63	-0.27	-3.54
58	218	-2.57	1.85	-0.72	-4.42
58	219	-0.97	2.05	1.09	-3.02

TABLE 13A, REV 1298, VECTOR WINDS, COLUMNS AS IN TABLE 1.

1	2	3	4	5	6	7	8	9	10	11	12	13	14	15
33	229	13	222	0.9	6.6	0.0	0.0	3.5	3.8	0.3	0.22	0.17	0.21	0.18
33	230	15	232	0.7	4.7	-0.0	-0.0	5.2	3.0	-1.2	0.30	0.11	0.23	0.15
34	229	7	216	0.9	8.2	0.0	0.0	2.6	2.1	-0.7	0.24	0.26	0.27	0.23
34	230	9	220	0.9	5.8	0.0	0.0	2.2	1.5	0.6	0.22	0.22	0.23	0.21
34	235	7	262	0.5	3.5	0.0	0.0	1.3	2.0	0.4	0.36	0.02	0.04	0.20
34	236	10	265	0.7	4.1	0.0	0.0	1.8	3.2	-0.1	0.28	0.02	0.03	0.21
35	235	13	257	0.5	3.6	0.0	0.0	4.8	2.8	-0.8	0.17	0.03	0.03	0.14
35	236	18	268	0.8	4.1	0.1	0.0	7.6	6.4	1.7	0.18	0.01	0.01	0.18
35	237	8	272	1.0	5.2	0.0	0.0	1.7	2.6	1.7	0.45	0.01	0.02	0.36
36	234	7	254	0.3	3.9	0.0	0.0	3.7	2.1	-2.3	0.19	0.03	0.05	0.11
36	235	19	258	0.9	4.1	0.1	0.0	6.4	4.9	-0.2	0.11	0.04	0.02	0.21
36	236	20	267	0.9	4.3	0.0	0.0	5.6	6.0	-3.5	0.14	0.01	0.01	0.21
36	237	16	263	1.8	3.6	-0.0	-0.0	4.1	3.8	-2.1	0.60	0.05	0.07	0.44
36	238	6	269	1.5	3.9	0.0	_0.0	1.3	1.6	0.8	1.30	0.00	0.00	0.61
37	234	22	252	0.7	3.6	0.0	0.1	5.6	5.4	-3.6	0.17	0.04	0.06	0.14
37	235	29	253	1.4	3.7	0.0	0.0	6.9	7.9	-0.1	0.18	0.07	0.05	0.25
37	236	20	235	2.7	3.2	-0.0	-0.1	4.3	6.7	-2.9	0.27	0.30	0.16	0.52
37	237	10	158	3.3	5.1	0.0	0.0	2.4	3.1	0.7	0.24	0.79	0.29	0.66
38	233	12	249	0.9	3.9	0.0	0.0	4.1	2.3	-2.2	0.20	0.10	0.09	0.24
38	234	30	237	1.2	2.6	0.0	-0.1	8.8	10.4	-0.8	0.20	0.11	0.12	0.19
38	235	24	212	2.2	2.3	-0.1	-0.0	7.6	6.3	-2.1	0.13	0.36	0.16	0.28
38	236	7	170	2.1	4.4	0.0	0.0	3.3	2.7	-2.7	0.01	0.78	0.31	0.02
39	233	24	213	1.9	2.6	0.0	0.0	6.1	5.3	-2.5	0.08	0.33	0.13	0.22
39	234	21	191	1.7	2.0	-0.1	0.0	5.0	9.0	-1.8	0.02	0.36	0.11	0.08
39	235	8	162	0.7	2.8	-0.0	-0.0	1.4	1.0	-1.3	0.10	0.23	0.30	0.07
40	232	11	173	1.0	4.6	0.0	0.0	2.9	1.4	-1.8	0.05	0.29	0.43	0.03
40	233	19	183	1.4	3.0	0.0	-0.1	6.8	4.8	0.6	0.01	0.32	0.24	0.02
40	234	10	163	0.7	2.4	-0.0	0.0	4.9	4.2	-3.5	0.07	0.20	0.23	0.06
41	231	8	169	1.2	7.4	0.0	0.0	3.4	2.6	-2.3	0.04	0.41	0.32	0.05
41	232	25	179	0.9	4.8	0.0	-0.0	8.0	6.1	-1.0	0.00	0.18	0.27	0.00
41	233	21	173	0.8	3.0	-0.0	-0.0	6.2	7.2	0.4	0.03	0.18	0.25	0.02
41	234	11	152	0.6	1.8	0.0	0.0	2.4	3.4	0.6	0.06	0.18	0.20	0.06
42	231	25	163	1.4	6.6	0.1	0.1	6.8	5.5	-2.9	0.11	0.27	0.38	0.08
42	232	27	174	0.9	4.0	-0.0	-0.1	9.1	8.6	0.8	0.03	0.16	0.29	0.02
42	233	14	160	0.5	2.2	-0.0	-0.0	4.0	4.5	-2.9	0.04	0.12	0.12	0.04
42	234	7	123	0.4	2.7	0.0	0.0	2.6	2.0	0.5	0.06	0.14	0.12	0.07
43	230	15	143	2.0	9.8	0.0	0.0	6.1	2.2	-2.6	0.14	0.41	0.20	0.30
43	231	33	150	1.7	6.2	0.0	-0.0	12.3	9.7	-0.4	0.18	0.25	0.31	0.14
43	232	24	157	1.0	3.3	-0.1	-0.1	7.9	7.1	-0.0	0.10	0.20	0.25	0.08
43	233	11	162	0.4	2.2	-0.0	-0.1	3.6	1.4	0.8	0.04	0.11	0.11	0.04
43	234	6	174	0.3	3.2	0.0	0.0	2.2	3.9	-0.5	0.04	0.10	0.08	0.05
44	230	25	138	1.3	9.0	-0.1	0.0	5.6	8.5	-2.2	0.26	0.20	0.29	0.17
44	231	32	139	1.3	6.6	0.0	0.1	9.8	10.0	1.4	0.15	0.18	0.18	0.15

TABLE 13B, REV 1298, VECTOR WINDS, COLUMNS AS IN TABLE 1.

1	2	3	4	5	6	7	8	9	10	11	12	13	14	15
44	232	26	140	1.7	3.6	0.1	-0.0	6.6	7.1	-0.2	0.27	0.26	0.31	0.22
44	233	20	103	2.1	2.5	0.1	0.0	6.3	4.9	2.0	0.33	0.11	0.08	0.45
44	234	8	82	2.7	2.0	0.0	-0.0	2.4	2.5	0.8	0.55	0.12	0.07	0.94
45	229	19	138	1.6	10.5	0.0	-0.0	6.0	4.6	-3.0	0.15	0.28	0.17	0.24
45	230	16	134	1.3	9.0	-0.0	-0.0	6.3	6.7	1.8	0.28	0.23	0.27	0.24
45	231	19	132	2.0	7.3	-0.0	0.1	6.3	3.3	0.9	0.17	0.30	0.15	0.34
45	232	34	111	3.4	4.6	-0.0	0.0	10.9	12.7	1.1	0.32	0.22	0.13	0.55
45	233	30	72	1.5	4.3	0.0	0.0	8.7	8.3	0.0	0.29	0.08	0.09	0.26
45	234	10	54	1.3	5.4	0.0	0.0	2.3	0.9	-1.3	0.36	0.23	0.24	0.34
46	228	16	132	3.2	8.4	0.0	0.0	4.6	3.5	-2.4	0.36	0.53	0.33	0.58
46	229	22	131	1.8	8.1	-0.0	-0.0	8.6	3.8	-3.1	0.28	0.26	0.24	0.30
46	230	11	132	1.0	8.0	-0.0	0.0	4.0	5.9	-0.0	0.30	0.19	0.27	0.21
46	231	15	128	2.7	7.4	0.0	0.1	4.3	1.5	-0.6	0.21	0.42	0.16	0.55
46	232	34	86	3.4	5.4	0.0	-0.0	11.4	12.5	-2.6	0.26	0.03	0.01	0.59
46	233	31	63	1.0	5.6	-0.0	-0.0	8.3	7.0	-2.1	0.19	0.08	0.09	0.16
46	234	6	54	0.6	7.6	0.0	0.0	1.1	1.6	-0.4	0.32	0.14	0.21	0.22
47	227	8	106	3.2	8.5	0.0	0.0	3.3	2.3	-2.2	0.52	0.27	0.13	1.10
47	228	28	101	3.0	6.9	-0.0	0.1	7.4	7.3	-1.8	0.19	0.13	0.04	0.56
47	229	28	111	2.6	6.2	0.0	-0.1	8.9	7.8	4.1	0.13	0.17	0.05	0.47
47	230	15	119	2.1	6.0	0.1	0.0	3.1	6.0	1.0	0.27	0.27	0.15	0.48
47	231	25	100	3.4	5.6	0.0	0.1	7.3	8.1	-3.4	0.24	0.12	0.04	0.67
47	232	24	71	2.6	5.1	-0.1	-0.0	7.1	7.0	-2.3	0.22	0.17	0.08	0.49
47	233	12	57	0.9	6.1	0.0	0.0	4.7	2.2	-2.9	0.34	0.13	0.20	0.23
48	226	6	92	1.0	10.7	0.0	0.0	1.8	2.5	-1.2	0.37	0.01	0.01	0.41
48	227	25	91	1.6	8.9	0.0	-0.0	7.9	7.9	-4.3	0.22	0.01	0.01	0.32
48	228	10	93	1.5	6.9	-0.0	-0.0	3.2	4.0	-2.8	0.33	0.03	0.02	0.46
48	229	17	92	1.0	6.2	-0.1	0.0	5.1	6.2	2.7	0.14	0.01	0.01	0.25
48	230	28	97	1.5	5.4	0.0	-0.0	9.3	8.9	1.6	0.19	0.04	0.02	0.29
48	231	22	86	2.0	4.7	-0.0	-0.1	7.9	5.6	-0.7	0.22	0.02	0.01	0.42
48	232	12	65	1.2	4.4	-0.0	-0.0	2.3	2.2	-1.0	0.22	0.14	0.10	0.31
49	226	22	81	2.2	11.1	0.1	0.1	7.3	5.9	-3.8	0.45	0.07	0.07	0.46
49	227	28	84	2.1	8.5	0.0	-0.1	8.8	7.6	3.4	0.30	0.04	0.03	0.39
49	228	14	90	1.5	5.7	0.0	0.0	3.3	3.8	2.7	0.39	0.02	0.02	0.41
49	229	20	88	1.0	5.3	0.1	-0.0	4.8	8.8	-1.6	0.17	0.01	0.01	0.23
49	230	27	88	0.9	4.9	0.0	0.0	6.6	8.9	0.4	0.17	0.01	0.01	0.16
49	231	13	74	0.8	4.0	0.0	-0.1	3.9	3.8	-2.5	0.24	0.06	0.07	0.21
50	225	16	70	1.6	13.8	0.1	0.0	5.8	4.8	-4.3	0.42	0.14	0.15	0.38
50	226	34	72	1.1	12.7	0.1	0.0	10.7	11.0	-0.3	0.28	0.06	0.09	0.18
50	227	36	71	1.2	11.0	0.1	0.0	10.6	12.0	-0.7	0.42	0.07	0.15	0.19
50	228	35	68	1.4	8.5	0.0	-0.1	11.0	9.0	-1.0	0.53	0.09	0.21	0.22
50	229	28	75	1.9	6.5	0.0	-0.1	9.1	9.9	-1.6	0.50	0.10	0.14	0.34
50	230	29	81	1.2	5.2	-0.0	-0.0	10.1	9.5	-0.4	0.30	0.03	0.04	0.22
50	231	8	76	1.2	3.9	0.0	0.0	3.2	0.8	-0.3	0.58	0.09	0.13	0.43

TABLE 13C, REV 1298, VECTOR WINDS, COLUMNS AS IN TABLE 1.

1	2	3	4	5	6	7	8	9	10	11	12	13	14	15
51	224	14	58	2.0	14.0	0.0	0.0	4.8	4.8	-4.3	0.30	0.27	0.18	0.45
51	225	36	65	1.3	12.5	0.0	0.0	12.0	10.6	-1.4	0.27	0.09	0.13	0.21
51	226	35	67	1.2	12.0	-0.0	-0.0	11.8	10.5	-1.3	0.30	0.08	0.12	0.19
51	227	31	64	1.6	12.2	-0.1	0.0	8.5	10.8	-2.5	0.28	0.12	0.13	0.26
51	228	20	57	1.9	11.6	-0.1	0.0	4.5	5.6	-2.7	0.43	0.22	0.27	0.35
51	229	19	51	3.1	9.8	-0.1	0.0	3.0	5.8	0.5	0.52	0.45	0.41	0.57
51	230	20	57	3.4	7.1	-0.1	0.0	3.4	7.4	-1.5	0.48	0.42	0.31	0.65
51	231	11	106	2.0	4.9	0.0	0.0	2.5	3.1	1.5	0.53	0.17	0.15	0.57
52	223	10	47	1.0	12.2	0.0	0.0	2.3	2.4	-2.2	0.31	0.21	0.28	0.23
52	224	33	50	1.6	11.2	0.0	0.0	10.3	10.7	-2.0	0.19	0.18	0.16	0.22
52	225	35	55	1.9	10.1	-0.0	0.0	11.1	12.4	-1.2	0.19	0.19	0.13	0.27
52	226	30	59	1.3	9.3	-0.0	-0.0	9.0	9.1	-1.3	0.28	0.12	0.16	0.20
52	227	13	55	1.0	9.8	-0.0	-0.1	4.5	4.8	-4.1	0.63	0.16	0.43	0.23
53	222	10	46	1.0	8.9	0.0	0.0	3.2	2.9	-2.9	0.50	0.21	0.46	0.22
53	223	22	45	0.9	8.6	0.0	0.1	7.8	3.9	-0.3	0.34	0.13	0.33	0.14
53	224	37	45	1.1	9.0	0.0	-0.0	13.6	12.4	-1.0	0.22	0.13	0.21	0.13
53	225	32	47	1.2	9.3	-0.0	0.0	8.8	10.5	-0.1	0.14	0.14	0.13	0.15
53	226	15	51	1.1	8.5	-0.1	-0.1	4.7	4.6	-3.3	0.24	0.17	0.19	0.22
54	221	10	54	0.8	5.2	0.0	0.0	3.7	4.1	-3.4	0.54	0.16	0.39	0.22
54	222	25	51	0.6	5.2	0.1	-0.0	6.3	7.3	-0.4	0.24	0.08	0.19	0.09
54	223	29	49	0.8	5.6	0.0	0.1	8.8	10.6	-1.7	0.25	0.09	0.21	0.11
54	224	33	51	0.9	6.3	-0.0	0.0	10.6	9.2	1.8	0.28	0.10	0.22	0.12
54	225	25	50	0.8	7.4	-0.1	-0.1	8.1	5.9	-4.1	0.36	0.10	0.30	0.12
55	220	9	56	0.8	2.8	0.0	0.0	1.8	2.3	-1.7	0.17	0.14	0.11	0.22
55	221	19	59	0.6	3.1	-0.1	-0.0	5.3	5.0	-3.2	0.22	0.07	0.13	0.12
55	222	16	55	0.4	3.3	-0.0	0.0	2.7	4.6	1.2	0.13	0.05	0.09	0.08
55	223	25	59	0.5	3.5	-0.1	-0.1	7.6	8.9	0.7	0.14	0.05	0.09	0.08
55	224	18	57	0.5	3.9	-0.0	0.0	4.5	5.5	-3.1	0.18	0.06	0.12	0.10
55	225	5	37	0.6	5.1	0.0	0.0	2.6	1.7	-1.0	0.82	0.19	0.74	0.21
56	219	10	66	1.0	2.8	0.0	0.0	1.3	1.7	-1.3	0.15	0.14	0.07	0.30
56	220	30	58	0.7	3.0	0.1	0.0	7.8	10.7	-0.9	0.17	0.07	0.11	0.11
56	221	18	62	0.5	2.5	0.0	-0.0	5.1	5.4	2.7	0.16	0.06	0.08	0.12
56	222	17	62	0.5	2.5	-0.0	0.0	6.7	4.4	-1.1	0.11	0.06	0.06	0.11
56	223	15	67	0.5	2.8	-0.0	-0.1	2.4	3.2	-1.2	0.18	0.05	0.07	0.12
57	219	10	57	1.2	1.3	-0.0	0.0	4.5	0.8	0.9	0.36	0.21	0.23	0.33
57	220	14	44	1.3	1.8	-0.1	0.0	4.1	7.1	-4.0	0.26	0.24	0.26	0.23
57	221	11	38	1.1	2.2	0.0	0.0	1.5	2.9	0.9	0.23	0.26	0.27	0.22
57	222	6	37	1.6	1.5	0.0	0.0	1.2	2.4	-1.2	0.31	0.47	0.33	0.44
58	217	7	327	0.6	4.2	0.0	0.0	2.7	1.9	2.0	0.17	0.13	0.14	0.17
58	219	10	308	0.4	1.9	0.0	0.0	2.7	3.1	-0.2	0.14	0.07	0.10	0.09
58	221	4	90	1.4	1.0	0.0	0.0	0.8	0.7	-0.3	0.33	0.61	0.63	0.32
59	217	7	162	0.6	3.2	0.0	0.0	2.7	1.9	-0.4	0.17	0.13	0.14	0.17
59	218	9	201	0.5	1.3	0.0	0.0	1.9	2.6	0.1	0.18	0.11	0.13	0.15
59	219	7	304	0.4	2.8	0.0	0.0	2.0	2.9	-0.4	0.17	0.09	0.12	0.13

TABLE 14A, REV 1298, VECTOR $\vec{u}_*^2$.   COLUMNS AS IN TABLE 2.

16	17	18	19	20	21	22	23	24	25
33	229	222	0.0448	0.0042	0.0015	0.0028	0.0011	0.0030	-0.0011
33	230	232	0.0250	0.0034	0.0009	0.0027	0.0005	0.0021	-0.0007
34	229	216	0.0721	0.0070	0.0028	0.0041	0.0022	0.0057	-0.0016
34	230	220	0.0355	0.0037	0.0017	0.0024	0.0013	0.0028	-0.0011
34	235	262	0.0158	0.0024	0.0008	0.0024	0.0001	0.0003	-0.0007
34	236	265	0.0192	0.0021	0.0009	0.0021	0.0001	0.0002	-0.0009
35	235	257	0.0150	0.0011	0.0006	0.0011	0.0001	0.0002	-0.0006
35	236	268	0.0184	0.0013	0.0007	0.0013	0.0000	0.0000	-0.0007
35	237	272	0.0305	0.0046	0.0018	0.0046	-0.0001	-0.0002	-0.0018
36	234	254	0.0170	0.0014	0.0005	0.0013	0.0001	0.0004	-0.0005
36	235	258	0.0179	0.0008	0.0009	0.0008	0.0002	0.0002	-0.0009
36	236	267	0.0199	0.0011	0.0009	0.0011	0.0000	0.0000	-0.0009
36	237	263	0.0182	0.0042	0.0017	0.0042	0.0002	0.0005	-0.0017
36	238	269	0.0265	0.0108	0.0025	0.0108	0.0000	0.0002	-0.0025
37	234	252	0.0147	0.0012	0.0006	0.0011	0.0002	0.0004	-0.0005
37	235	253	0.0159	0.0013	0.0010	0.0012	0.0003	0.0004	-0.0010
37	236	235	0.0137	0.0019	0.0022	0.0016	0.0012	0.0011	-0.0018
37	237	158	0.0287	0.0037	0.0051	-0.0014	0.0047	0.0034	0.0019
38	233	249	0.0174	0.0016	0.0010	0.0015	0.0004	0.0006	-0.0010
38	234	237	0.0100	0.0012	0.0007	0.0010	0.0004	0.0006	-0.0006
38	235	212	0.0084	0.0009	0.0015	0.0005	0.0012	0.0008	-0.0008
38	236	170	0.0218	0.0025	0.0034	-0.0004	0.0034	0.0025	0.0006
39	233	213	0.0095	0.0007	0.0013	0.0004	0.0011	0.0006	-0.0007
39	234	191	0.0064	0.0004	0.0011	0.0001	0.0011	0.0004	-0.0002
39	235	162	0.0114	0.0017	0.0008	-0.0005	0.0008	0.0016	0.0003
40	232	173	0.0249	0.0039	0.0013	-0.0004	0.0013	0.0038	0.0001
40	233	183	0.0119	0.0013	0.0011	0.0001	0.0011	0.0013	-0.0001
40	234	163	0.0089	0.0011	0.0007	-0.0003	0.0006	0.0011	0.0002
41	231	169	0.0581	0.0054	0.0030	-0.0009	0.0029	0.0053	0.0005
41	232	179	0.0250	0.0025	0.0008	0.0000	0.0008	0.0025	0.0000
41	233	173	0.0121	0.0014	0.0006	-0.0002	0.0006	0.0014	0.0001
41	234	152	0.0062	0.0008	0.0006	-0.0004	0.0005	0.0007	0.0003
42	231	163	0.0462	0.0055	0.0018	-0.0015	0.0017	0.0053	0.0005
42	232	174	0.0183	0.0021	0.0007	-0.0002	0.0007	0.0021	0.0001
42	233	160	0.0073	0.0005	0.0004	-0.0002	0.0004	0.0005	0.0001
42	234	123	0.0096	0.0007	0.0005	-0.0006	0.0003	0.0004	0.0004
43	230	143	0.1035	0.0062	0.0050	-0.0037	0.0040	0.0050	0.0030
43	231	150	0.0412	0.0046	0.0017	-0.0023	0.0015	0.0040	0.0008
43	232	157	0.0139	0.0016	0.0008	-0.0006	0.0007	0.0015	0.0003
43	233	162	0.0075	0.0005	0.0004	-0.0002	0.0004	0.0005	0.0001
43	234	174	0.0123	0.0005	0.0004	-0.0001	0.0004	0.0005	0.0000
44	230	138	0.0897	0.0088	0.0023	-0.0058	0.0018	0.0066	0.0015
44	231	139	0.0452	0.0033	0.0015	-0.0021	0.0011	0.0025	0.0009
44	232	140	0.0167	0.0028	0.0013	-0.0018	0.0010	0.0021	0.0008

16	17	18	19	20	21	22	23	24	25
44	233	103	0.0097	0.0016	0.0015	-0.0016	0.0004	0.0004	0.0015
44	234	82	0.0084	0.0024	0.0029	-0.0024	-0.0004	-0.0003	0.0028
45	229	138	0.1230	0.0064	0.0041	-0.0042	0.0031	0.0048	0.0027
45	230	134	0.0891	0.0087	0.0029	-0.0063	0.0020	0.0060	0.0021
45	231	132	0.0550	0.0037	0.0032	-0.0027	0.0021	0.0025	0.0023
45	232	111	0.0235	0.0030	0.0027	-0.0027	0.0010	0.0011	0.0025
45	233	72	0.0211	0.0024	0.0012	-0.0023	-0.0003	-0.0007	0.0011
45	234	54	0.0325	0.0047	0.0021	-0.0038	-0.0012	-0.0027	0.0017
46	228	132	0.0792	0.0101	0.0065	-0.0074	0.0044	0.0069	0.0048
46	229	131	0.0707	0.0071	0.0031	-0.0053	0.0020	0.0047	0.0023
46	230	132	0.0694	0.0076	0.0022	-0.0056	0.0015	0.0051	0.0017
46	231	128	0.0566	0.0042	0.0049	-0.0033	0.0031	0.0027	0.0038
46	232	86	0.0302	0.0027	0.0030	-0.0027	-0.0002	-0.0002	0.0030
46	233	63	0.0318	0.0023	0.0010	-0.0021	-0.0004	-0.0010	0.0009
46	234	54	0.0621	0.0066	0.0019	-0.0054	-0.0011	-0.0038	0.0016
47	227	106	0.0814	0.0111	0.0094	-0.0106	0.0026	0.0031	0.0090
47	228	101	0.0486	0.0030	0.0038	-0.0029	0.0008	0.0006	0.0037
47	229	111	0.0383	0.0018	0.0029	-0.0017	0.0010	0.0006	0.0027
47	230	119	0.0380	0.0038	0.0032	-0.0033	0.0015	0.0018	0.0028
47	231	100	0.0324	0.0027	0.0036	-0.0027	0.0007	0.0005	0.0036
47	232	71	0.0275	0.0023	0.0026	-0.0021	-0.0008	-0.0007	0.0024
47	233	57	0.0400	0.0050	0.0015	-0.0042	-0.0008	-0.0026	0.0013
48	226	92	0.1335	0.0111	0.0047	-0.0111	0.0002	0.0005	0.0047
48	227	91	0.0836	0.0047	0.0028	-0.0047	0.0001	0.0002	0.0028
48	228	93	0.0508	0.0050	0.0031	-0.0050	0.0002	0.0003	0.0031
48	229	92	0.0385	0.0018	0.0015	-0.0018	0.0001	0.0001	0.0015
48	230	97	0.0294	0.0019	0.0015	-0.0019	0.0002	0.0002	0.0015
48	231	86	0.0233	0.0019	0.0019	-0.0019	-0.0001	-0.0001	0.0019
48	232	65	0.0215	0.0020	0.0015	-0.0018	-0.0006	-0.0008	0.0014
49	226	81	0.1468	0.0145	0.0055	-0.0143	-0.0008	-0.0022	0.0055
49	227	84	0.0763	0.0062	0.0033	-0.0062	-0.0003	-0.0006	0.0032
49	228	90	0.0359	0.0045	0.0022	-0.0045	0.0000	0.0000	0.0022
49	229	88	0.0286	0.0017	0.0012	-0.0017	0.0000	0.0000	0.0012
49	230	88	0.0245	0.0016	0.0008	-0.0016	0.0000	0.0000	0.0008
49	231	74	0.0183	0.0018	0.0009	-0.0018	-0.0002	-0.0005	0.0009
50	225	70	0.2459	0.0208	0.0066	-0.0195	-0.0022	-0.0070	0.0062
50	226	72	0.1955	0.0117	0.0027	-0.0112	-0.0008	-0.0035	0.0026
50	227	71	0.1427	0.0139	0.0023	-0.0131	-0.0007	-0.0045	0.0022
50	228	68	0.0830	0.0119	0.0020	-0.0111	-0.0007	-0.0044	0.0019
50	229	75	0.0475	0.0073	0.0022	-0.0070	-0.0006	-0.0019	0.0021
50	230	81	0.0289	0.0030	0.0011	-0.0030	-0.0002	-0.0004	0.0011
50	231	76	0.0203	0.0045	0.0018	-0.0044	-0.0004	-0.0010	0.0017
51	224	58	0.2514	0.0167	0.0089	-0.0142	-0.0047	-0.0088	0.0075
51	225	65	0.1880	0.0117	0.0032	-0.0106	-0.0013	-0.0049	0.0029
51	226	67	0.1722	0.0118	0.0028	-0.0110	-0.0010	-0.0045	0.0026

TABLE 14C, REV 1298, VECTOR $\vec{u}_*^2$.   COLUMNS AS IN TABLE 2.

16	17	18	19	20	21	22	23	24	25
51	227	64	0.1800	0.0117	0.0039	-0.0106	-0.0017	-0.0051	0.0035
51	228	57	0.1664	0.0180	0.0053	-0.0152	-0.0029	-0.0096	0.0045
51	229	51	0.1159	0.0176	0.0072	-0.0138	-0.0045	-0.0109	0.0057
51	230	57	0.0577	0.0092	0.0052	-0.0077	-0.0028	-0.0050	0.0044
51	231	106	0.0290	0.0054	0.0028	-0.0051	0.0008	0.0015	0.0027
52	223	47	0.1826	0.0156	0.0042	-0.0114	-0.0029	-0.0107	0.0031
52	224	50	0.1422	0.0078	0.0034	-0.0060	-0.0022	-0.0050	0.0026
52	225	55	0.1126	0.0063	0.0034	-0.0052	-0.0020	-0.0036	0.0028
52	226	59	0.0954	0.0078	0.0022	-0.0067	-0.0011	-0.0039	0.0019
52	227	55	0.1199	0.0207	0.0028	-0.0170	-0.0016	-0.0117	0.0023
53	222	46	0.0949	0.0155	0.0027	-0.0113	-0.0019	-0.0106	0.0020
53	223	45	0.0827	0.0099	0.0016	-0.0071	-0.0011	-0.0070	0.0012
53	224	45	0.0880	0.0069	0.0016	-0.0049	-0.0011	-0.0048	0.0012
53	225	47	0.0918	0.0044	0.0019	-0.0033	-0.0013	-0.0030	0.0014
53	226	51	0.0777	0.0063	0.0023	-0.0049	-0.0015	-0.0040	0.0018
54	221	54	0.0331	0.0071	0.0013	-0.0057	-0.0008	-0.0041	0.0011
54	222	51	0.0294	0.0031	0.0006	-0.0024	-0.0004	-0.0019	0.0005
54	223	49	0.0335	0.0036	0.0007	-0.0028	-0.0005	-0.0023	0.0006
54	224	51	0.0418	0.0046	0.0009	-0.0036	-0.0006	-0.0029	0.0007
54	225	50	0.0607	0.0080	0.0011	-0.0061	-0.0007	-0.0051	0.0009
55	220	56	0.0105	0.0010	0.0009	-0.0009	-0.0005	-0.0006	0.0007
55	221	59	0.0124	0.0014	0.0005	-0.0012	-0.0002	-0.0007	0.0004
55	222	55	0.0133	0.0010	0.0003	-0.0008	-0.0002	-0.0005	0.0003
55	223	59	0.0146	0.0011	0.0004	-0.0009	-0.0002	-0.0005	0.0003
55	224	57	0.0174	0.0015	0.0005	-0.0013	-0.0003	-0.0008	0.0004
55	225	37	0.0370	0.0120	0.0014	-0.0073	-0.0011	-0.0095	0.0008
56	219	66	0.0106	0.0009	0.0011	-0.0008	-0.0004	-0.0004	0.0010
56	220	58	0.0114	0.0011	0.0004	-0.0009	-0.0002	-0.0006	0.0004
56	221	62	0.0088	0.0008	0.0004	-0.0007	-0.0002	-0.0004	0.0004
56	222	62	0.0088	0.0006	0.0004	-0.0005	-0.0002	-0.0003	0.0004
56	223	67	0.0108	0.0010	0.0004	-0.0009	-0.0002	-0.0004	0.0004
57	219	57	0.0050	0.0015	0.0011	-0.0013	-0.0006	-0.0008	0.0009
57	220	44	0.0069	0.0015	0.0010	-0.0010	-0.0007	-0.0011	0.0007
57	221	38	0.0083	0.0016	0.0011	-0.0010	-0.0008	-0.0013	0.0007
57	222	37	0.0059	0.0017	0.0018	-0.0010	-0.0014	-0.0013	0.0011
58	217	327	0.0199	0.0017	0.0009	0.0009	-0.0008	-0.0015	-0.0005
58	219	308	0.0063	0.0007	0.0003	0.0005	-0.0002	-0.0004	-0.0003
58	221	90	0.0051	0.0025	0.0018	-0.0025	0.0000	0.0000	0.0018
59	217	162	0.0128	0.0013	0.0008	-0.0004	0.0007	0.0012	0.0002
59	218	201	0.0043	0.0008	0.0005	0.0003	0.0005	0.0007	-0.0002
59	219	304	0.0109	0.0011	0.0006	0.0009	-0.0003	-0.0006	-0.0005

TABLE 15A, REV 1298, WIND STRESS CURL, COLUMNS AS IN TABLE 3.

26	27	28	29	30	31
35	236	1.13	0.33	1.46	0.80
36	235	0.18	0.15	0.32	0.03
36	236	-0.36	0.34	-0.03	-0.70
36	237	-1.10	0.79	-0.31	-1.90
37	235	-0.38	0.18	-0.20	-0.56
37	236	-2.97	0.39	-2.58	-3.35
38	234	-0.93	0.15	-0.78	-1.08
38	235	-1.20	0.27	-0.93	-1.48
39	234	-0.81	0.13	-0.68	-0.94
40	233	-0.20	0.14	-0.06	-0.35
41	232	1.07	0.34	1.41	0.74
41	233	0.10	0.11	0.21	-0.01
42	232	1.50	0.24	1.74	1.26
42	233	-0.17	0.11	-0.06	-0.28
43	231	4.94	0.54	5.48	4.40
43	232	1.70	0.28	1.98	1.42
43	233	0.58	0.15	0.73	0.44
44	231	3.81	0.60	4.41	3.21
44	232	1.82	0.32	2.14	1.50
44	233	0.94	0.27	1.21	0.67
45	230	4.51	0.70	5.21	3.81
45	231	3.38	0.68	4.06	2.70
45	232	2.49	0.42	2.91	2.07
45	233	0.55	0.40	0.95	0.15
46	229	5.06	0.91	5.97	4.15
46	230	3.28	0.72	4.00	2.56
46	231	3.56	0.61	4.17	2.95
46	232	2.25	0.45	2.70	1.80
46	233	-0.84	0.53	-0.31	-1.37
47	228	6.36	1.02	7.39	5.34
47	229	3.74	0.48	4.23	3.26
47	230	2.77	0.42	3.19	2.35
47	231	2.68	0.41	3.09	2.26

TABLE 15B, REV 1298, WIND STRESS CURL, COLUMNS AS IN TABLE 3.

26	27	28	29	30	31
47	232	0.20	0.44	0.64	-0.24
48	227	8.61	1.07	9.68	7.54
48	228	4.35	0.46	4.81	3.89
48	229	2.62	0.46	3.08	2.16
48	230	2.36	0.25	2.61	2.11
48	231	1.40	0.24	1.64	1.16
49	227	12.09	1.32	13.42	10.77
49	228	5.96	0.62	6.58	5.34
49	229	1.74	0.46	2.19	1.28
49	230	1.37	0.23	1.60	1.14
50	226	10.71	2.10	12.81	8.62
50	227	13.48	1.44	14.92	12.04
50	228	12.74	1.45	14.20	11.29
50	229	8.23	1.26	9.50	6.97
50	230	4.01	0.85	4.86	3.16
51	225	3.59	1.73	5.32	1.85
51	226	0.06	1.39	1.45	-1.34
51	227	2.74	1.85	4.59	0.89
52	224	-0.48	1.32	0.84	-1.80
52	225	1.34	0.92	2.26	0.42
52	226	-1.59	1.68	0.10	-3.27
53	223	-5.35	1.32	-4.03	-6.67
53	224	-4.63	0.82	-3.81	-5.45
53	225	-1.35	0.76	-0.59	-2.11
54	222	-3.15	0.86	-2.30	-4.01
54	223	-3.81	0.58	-3.23	-4.39
54	224	-5.01	0.70	-4.31	-5.71
55	221	-1.10	0.27	-0.83	-1.36
55	222	-1.01	0.19	-0.82	-1.19
55	223	-1.36	0.20	-1.16	-1.57
56	220	0.13	0.15	0.27	-0.02
56	221	0.19	0.15	0.34	0.04
56	222	-0.38	0.17	-0.22	-0.55
57	221	-0.12	0.26	0.14	-0.38

32	33	34	35	36	37
35	236	0.56	0.23	0.79	0.33
36	235	0.78	0.14	0.92	0.65
36	236	0.47	0.32	0.79	0.15
36	237	0.92	0.77	1.70	0.15
37	235	0.21	0.21	0.41	-0.00
37	236	0.87	0.39	1.25	0.48
38	234	-0.63	0.20	-0.42	-0.83
38	235	-0.33	0.45	0.12	-0.78
39	234	-0.97	0.22	-0.75	-1.19
40	233	0.22	0.22	0.44	-0.01
41	232	-0.20	0.29	0.09	-0.49
41	233	-0.80	0.19	-0.61	-0.98
42	232	-0.16	0.20	0.03	-0.36
42	233	-0.63	0.12	-0.52	-0.75
43	231	2.25	0.26	2.51	2.00
43	232	0.89	0.19	1.08	0.70
43	233	-0.60	0.17	-0.43	-0.77
44	231	1.96	0.30	2.26	1.66
44	232	0.52	0.23	0.75	0.29
44	233	-1.31	0.31	-1.01	-1.62
45	230	0.24	0.28	0.52	-0.05
45	231	1.14	0.38	1.51	0.76
45	232	-0.60	0.35	-0.25	-0.95
45	233	-1.43	0.28	-1.15	-1.70
46	229	-2.49	0.41	-2.08	-2.90
46	230	-1.37	0.45	-0.92	-1.82
46	231	-1.47	0.38	-1.09	-1.84
46	232	-0.98	0.39	-0.58	-1.37
46	233	-0.38	0.27	-0.10	-0.65
47	228	0.41	0.37	0.77	0.04
47	229	-1.31	0.33	-0.98	-1.64
47	230	-1.95	0.27	-1.67	-2.22
47	231	-1.95	0.39	-1.56	-2.35
47	232	-0.44	0.37	-0.07	-0.81
48	227	2.51	0.37	2.88	2.14
48	228	1.11	0.32	1.43	0.78
48	229	0.03	0.34	0.37	-0.31
48	230	-0.33	0.26	-0.07	-0.59
48	231	-0.06	0.34	0.28	-0.39
49	227	1.54	0.41	1.95	1.13
49	228	0.56	0.29	0.85	0.27
49	229	0.11	0.31	0.43	-0.20
49	230	0.35	0.25	0.60	0.10
50	226	0.57	0.41	0.98	0.16
50	227	0.97	0.41	1.38	0.57
50	228	0.24	0.45	0.68	-0.21
50	229	-0.72	0.44	-0.28	-1.15
50	230	-0.29	0.49	0.20	-0.78
51	225	-2.31	0.31	-2.00	-2.62
51	226	-0.15	0.26	0.11	-0.41
51	227	0.10	0.37	0.48	-0.27
52	224	-2.33	0.28	-2.04	-2.61
52	225	-0.07	0.24	0.17	-0.31
52	226	-0.11	0.42	0.31	-0.53
53	223	-1.01	0.35	-0.66	-1.36
53	224	0.97	0.25	1.21	0.72
53	225	0.44	0.25	0.70	0.19
54	222	-3.49	0.41	-3.08	-3.89
54	223	1.26	0.28	1.54	0.98
54	224	0.90	0.28	1.19	0.62
55	221	-1.00	0.22	-0.79	-1.22
55	222	0.73	0.22	0.95	0.50
55	223	0.76	0.17	0.93	0.58
56	220	-0.22	0.24	0.02	-0.45
56	221	0.32	0.19	0.52	0.13
56	222	0.07	0.28	0.35	-0.21
57	221	0.11	0.57	0.68	-0.45

16. Abstract

Dealiased SEASAT SASS vector winds obtained during the GOASEX program have been processed to obtain superobservations centered on a one degree by one degree grid. The results provide values for the combined effects of mesoscale variability and communication noise on the individual SASS winds. Each grid point of the synoptic field provides the mean synoptic east-west and north-south wind components with the effects of synoptic scale gradients removed plus estimates of the standard deviations of these means. These superobservations winds are then processed further to obtain estimates of synoptic scale vector winds stress fields, the horizontal divergence of the wind, the curl of the wind stress and the vertical velocity at 200 m above the sea surface, each with appropriate standard deviations of the estimates for each grid point value. The resulting fields appear to be consistent over large distances and to agree with, for example, geostationary cloud images obtained concurrently. They also explain the concentration of water vapor, liquid water and precipitation found by means of the SMMR at fronts and occlusions in terms of strong warm, moist air advection in the warm air sector accompanied by convergence in the friction layer. Their quality is far superior to that of analyses based on conventional data, which are shown to yield many inconsistencies.

National Aeronautics and
Space Administration

Washington, D.C.
20546

SPECIAL FOURTH CLASS MAIL
BOOK

U.S.MAIL

NASA

POSTMASTER: If Undeliverable (Section 158
Postal Manual) Do Not Return